Developing Viral Vectored Vaccines for MAGE-expressing Tumours



James McAuliffe

Wolfson College

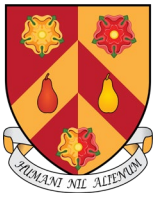
University of Oxford

A thesis submitted for the degree of

Doctor of Philosophy

Michaelmas 2019
Word Count ≈49,000

LUDWIG CANCER RESEARCH



Developing Viral Vectored Vaccines for MAGE-expressing Tumours

James McAuliffe, Wolfson College

Thesis submitted for the degree of Doctor of Philosophy, Michaelmas Term 2019

Abstract

The MAGE-type antigen family represent excellent targets for a therapeutic cancer vaccine. However, numerous attempts to develop effective MAGE-targeting cancer vaccines to date have shown poor induction of specific CD8+ T-cell responses and little clinical efficacy. In this study, a novel vaccination strategy based on a heterologous prime-boost with recombinant Chimpanzee Adenovirus (ChAdOx1) and Modified vaccinia Ankara (MVA) viral vectors was assessed for its potential in targeting MAGE-expressing tumours. The immunogenicity and anti-tumour efficacy of vaccination with ChAdOx1/MVA encoding the murine MAGE-type antigen P1A was evaluated in pre-clinical murine models. Heterologous prime-boost with ChAdOx1/MVA encoding P1A induced a very strong P1A-specific CD8+ T-cell response in DBA/2 and BL/6 mice and demonstrated good therapeutic efficacy in the P1A-expressing 15V4T3 tumour model. Many tumours are poorly infiltrated by tumour-specific CD8+ T-cells, which is believed to underlie the unresponsiveness of many patients to recently developed immunotherapies such as immune checkpoint blockade. Vaccination was seen to greatly increase the magnitude of P1A-specific CD8+ T-cell infiltrate into the tumour and synergised with anti-PD-1 blockade to provide improved control of tumour growth and increased survival. ChAdOx1/MVA vectors encoding the human MAGE-type antigens MAGE-A3 and NY-ESO-1 were also constructed and their immunogenicity evaluated in mice with the view to translation of this strategy to the clinical setting. A prime with ChAdOx1 encoding a dual-antigen MAGE-A3/NY-ESO-1 fusion construct was seen to induce high magnitude CD8+ T-cells to both antigens, which could be boosted further still against either antigen of choice with an MVA vector encoding either MAGE-A3 or NY-ESO-1 alone. Overall, these results strongly indicate that ChAdOx1/MVA is an efficient vaccination strategy for generating MAGE-type antigen-specific CD8+ T-cell responses and that vaccination in combination with PD-1 blockade has high therapeutic potential for treating cancer patients with MAGE-expressing tumours.

Acknowledgements

Firstly, I would like to thank my supervisors, Professor Benoit Van den Eynde, Dr Carol Leung and Professor Chris Pugh. In particular to Benoit and Carol for giving me the opportunity to work on this project and for their guidance and tutelage. Furthermore to Chris for first providing me with the chance to undertake research in Oxford. My time as a DPhil student has been immensely enjoyable and I feel forever grateful having been given this opportunity to learn and develop as a scientist.

I would also like to thank all of the members of the Oxford Van Den Eynde lab, past and present, with special thanks to Laurine, Vinnycius, Vineeth, Andrei, and Yaxuan. Thank you for your assistance with mouse work, bleeds and tissue harvests during long hours spent in the FGF, and for thoughtful discussions outside of it. Furthermore to everyone in the wider LICR - such a stimulating environment of which I feel privileged to have been a member. I would also like to give thanks to members of the Brussels Van den Eynde lab for their support particularly when the lab was first being established in Oxford and to this day. I extend my gratitude to the technicians at the FGF, for their professionalism and care of the mice needed to undertake this work.

I give special thanks to my parents for their constant encouragement, unwavering belief and without whose support none of my achievements would have been possible. To Sian, for being a constant source of light, and for making this chapter the most enjoyable so far. Lastly to everyone from Wolfson, Argyle St and further back home for their friendship and contribution to making the time what it was.

Table of Contents

List of Tables ..... **viii**

List of figures ..... **x**

List of abbreviations ..... **xiv**

Chapter 1. Introduction **1**

1.1 Immunotherapy **2**

1.1.1 The burden of cancer and conventional therapy 2

1.1.2 Immunotherapy, the 4th pillar of cancer treatment 3

1.1.3 Drawbacks of current immunotherapeutic approaches 6

1.1.4 The need for new immunotherapeutic agents 8

1.2 Tumour immunology **10**

1.2.1 Immune responses to cancer 10

1.2.2 Innate immunity and the generation of adaptive anti-tumour adaptive immune responses 11

1.2.3 DC subsets important for anti-tumour immunity 13

1.2.4 Adaptive anti-tumour immunity 14

1.2.5 NK cells – cytotoxic cells of the innate immune system 19

1.2.6 Tumour immune evasion 20

1.3 Therapeutic cancer vaccines **29**

1.3.1 Therapeutic cancer vaccines 29

1.3.2 Viral vectored vaccines 34

1.3.3 ChAdOx1/MVA heterologous prime-boost 35

1.3.4 Classes of tumour associated antigen 38

1.3.5 MAGE-type antigens 40

1.3.7 MAGE-targeting cancer vaccines 47

1.3.8 Next generation MAGE-targeting cancer vaccines 49

1.4 Aims of the thesis **50**

Chapter 2. Materials and Methods **51**

2.1 Materials **52**

2.1.1 Reagents and kits 52

2.1.2 Chemicals 53

2.1.3 Cytokines 53

2.1.4 Buffers and media 53

2.1.5 Consumables 56

2.1.6 Instruments 57

2.1.7 Software 57

2.1.8 Cell lines 57
2.1.9 Flow cytometry antibodies 58
2.1.10 MHC-class I multimers 59
2.1.11 Vaccines 59
2.1.12 Therapeutic monoclonal antibodies 60
2.1.13 Peptides 60
2.1.14 Mice 60
2.2 Methods 62
2.2.1 ChAdOx1 and MVA viral vector construction 62
2.2.2 Cell culture 62
2.2.3 In vitro studies 63
2.2.4 In vivo mouse studies 66
2.2.5 Flow cytometric analysis 68
2.2.6 Flow cytometry data analysis 74
2.2.7 Gene expression analysis 78
2.2.8 Statistical analysis 81
Chapter 3. Immunogenicity of ChAdOx1/MVA prime-boost vaccination encoding MAGE-A3 and NY-ESO-1 82
3.1 Introduction 83
3.2 Chapter aims 89
3.3 Results 90
3.3.1 Measuring T-cell responses induced by heterologous prime-boost vaccination with ChAdOx1/MVA vectors encoding MAGE-A3 and NY-ESO-1 90
3.3.2 ChAdOx1-MAGE-A3-NY-ESO-1 vaccination primes a strong antigen-specific CD8+ T-cell response to both encoded antigens 93
3.3.3 Fusion of htPA or hIi sequences to the antigen coding sequence in the ChAdOx1 vector does not increase the magnitude of the MAGE-A3 or NY-ESO-1-specific CD8+ T-cell response 94
3.3.4 Both MAGE-A3 and NY-ESO-1-specific CD8+ T-cell responses induced by ChAdOx1 vaccination are polyfunctional 97
3.3.5 ChAdOx1-MAGE-A3-NY-ESO-1 vaccination induces an antigen-specific CD4+ T-cell response 98
3.3.6 Boost vaccination with either MVA-MAGE-A3 or MVA-NY-ESO-1 greatly increases the magnitude of the CD8+ response against either of the encoded antigens 101
3.3.7 MAGE-A3 and NY-ESO-1-specific CD4+ T-cell responses after MVA boost vaccination 109
3.3.8 Simultaneous vs alternate MVA boosts 113
3.3.9 ChAdOx1 + MVA + MVA prime-boost-boost vaccinations 114

3.3.10 Antigen specific T-cell responses induced by ChAdOx1-Ii-M-NY prime vaccination 116

3.3.11 Fusion of the tPA signal sequence to the antigen in the MVA vector does not increase the magnitude of the antigen-specific CD8+ and CD4+ T-cell responses post-boost 119

3.3.12 MAGE-A3 and NY-ESO-1-specific CD8+ T-cell responses can be boosted simultaneously or alternately with MVA vectors encoding a single antigen 122

3.3.13 Vaccination induces CD8+ T-cell responses against epitopes covering a broad range of sites in MAGE-A3 but against a narrow region of NY-ESO-1. 128

3.4 Discussion 131

Chapter 4. Immunogenicity and anti-tumour therapeutic efficacy of ChAdOx1/MVA P1A vaccination 141

4.1 Introduction 142

4.2 Results 148

4.2.1 Evaluating T-cell responses induced by heterologous prime-boost vaccination with ChAdOx1/MVA vectors encoding P1A 148

4.2.2 Heterologous prime-boost vaccination with ChAdOx1/MVA encoding P1A induces a high magnitude multifunctional P1A-specific CD8+ T-cell response 150

4.2.3 Fusion of invariant chain to the P1A antigen sequence in the ChAdOx1 vector increases the magnitude of P1A-specific CD8+ T-cells induced by vaccination 152

4.2.4 Heterologous prime-boost vaccination with ChAdOx1/MVA encoding P1A does not induce a P1A-specific CD4+ T-cell response 153

4.2.5 ChAdOx1/MVA P1A prime-boost vaccination confers good protection against P1A-expressing tumours in the prophylactic setting 155

4.2.6 Tumour immune escape in the P815 model results from loss of P1A antigen expression, but not in 15V4T3 164

4.2.7 Fusion of tPA to P1A in the MVA vector does not increase the magnitude or improve multifunctionality of the vaccine-induced P1A-specific CD8+ T-cell response 166

4.2.8 Therapeutic ChAdOx1/MVA P1A vaccination exhibits moderate control of growth of established 15V4T3 tumours when administered at early time-points 169

4.2.9 ChAdOx1/MVA P1A vaccine therapeutic efficacy correlates very strongly with the magnitude of vaccine induced P1A-specific CD8+ T-cell response 176

4.2.10 15V4T3 tumours express surface PD-L1 which is further up-regulated by IFN-γ stimulation 178

4.2.11 Therapeutic ChAdOx1/MVA P1A vaccination treatment synergises with anti-PD-1 blockade to promote improved control of established 15V4T3 tumours and increased survival 181

4.2.12 Therapeutic ChAdOx1/MVA P1A vaccination increases P1A-specific CD8+ T-cell infiltration into the tumour 187

4.2.13 Therapeutic ChAdOx1/MVA P1A vaccination promotes an increased inflammatory tumour microenvironment 202
4.3 Discussion 206
Chapter 5. Investigating P1A-specific T-cell responses in the C57BL/6 mouse strain 223
5.1 Introduction 224
5.2 Aims 228
5.3 Results 229
5.3.1 ChAdOx1/MVA P1A heterologous prime-boost vaccination induces a high magnitude P1A-specific CD8+ T-cell response in C57BL/6 mice 229
5.3.2 ChAdOx1/MVA P1A heterologous prime-boost vaccination does not induce a P1A-specific CD4+ T-cell response in C57BL/6 mice 233
5.3.3 P1A-specific CD8+ T-cells in C57BL/6 recognize a single immunogenic 9-amino acid MHC-class I restricted epitope – $P1A_{43-51}$ FAVVTTSFL 234
5.3.4 MHC-class I restriction of the $P1A_{43-51}$-FAVVTTSFL epitope 240
5.3.6 P1A-specific CD8+ T-cell responses can be detected in C57BL/6 mice using a fluorescently labelled H-$2D^b$ $P1A_{43-51}$-FAVVTTSFL multimer 243
5.3.7 Determining the sequence of P1A-specific CD8+ T-cell TCRs recognizing the $P1A_{43-51}$-FAVVTTSFL epitope 245
5.3.8 Generating P1A-expressing C57BL/6 derived murine cancer cell lines 249
5.3.9 P1A expression can be induced in a range of C57BL/6 cancer lines following treatment with the DNMTi, 5-aza-2′-deoxycytidine 252
5.3.10 Tumour P1A expression can be induced in MC38 tumour-bearing C57BL/6 mice treated with 5-aza-2′-deoxycytidine. 254
5.3.11 ChAdOx1/MVA P1A vaccination provides moderately improved control of growth of MC38 tumours formed from cells pre-treated in vitro with 5-aza-2′-deoxycytidine 257
5.3.12 Combined 5-aza-2′-deoxycytidine treatment with ChAdOx1/MVA P1A vaccination is not sufficient to control tumour growth in mice bearing MC38 or EL4 tumours 259
5.4 Discussion 261
Chapter 6. Conclusions and future work 271
6.1 Conclusions and future work 272
References 287
Appendix 306

List of Tables

Table 1.1. Proportion of patients with different cancer types bearing tumours with detectable MAGE-A3 or NY-ESO-1 expression. 43

Table 1.2. MAGE-A3 epitopes experimentally confirmed to be recognized by T-cells from human cancer patients. 44

Table 1.3. NY-ESO-1 epitopes experimentally confirmed to be recognized by T-cells from human cancer patients. 46

Table 2.1. List of reagents and kits 52

Table 2.2. Details of recombinant cytokines 53

Table 2.3. Base media used as primary components of media and buffers for cell culture and tissue processing 53

Table 2.4. Composition of in-house ACK lysis buffer formulated for mouse blood 54

Table 2.5. Composition of tumour digestion and dissociation buffer 54

Table 2.6. Composition of complete RPMI 1640 medium 55

Table 2.7. Composition of complete DMEM 55

Table 2.8. Composition of complete IMDM 55

Table 2.9 Composition of FACS buffer 56

Table 2.10. List of consumables 56

Table 2.11. List of instruments 57

Table 2.12. List of software 57

Table 2.13. Details of antibodies used in T-cell ICS panel 58

Table 2.14. Details of antibodies used in effector T-cell panel 58

Table 2.15. Details of viral vectored vaccines used in this study 59

Table 2.16. List of therapeutic monoclonal antibodies 60

Table 2.17. List of primer sequences used in rt-qPCR assays 80

Table 3.1 Combinations of ChAdOx1 and MVA viral vectors encoding MAGE-A3 and NY-ESO-1 tested in heterologous prime-boost vaccinations. 92

Table 3.2. Proportion of mice that generated a positive MAGE-A3 or NY-ESO-1 specific CD8+ T-cell response following ChAdOx/MVA MAGE-A3/NY-ESO-1 prime-boost vaccination* 106

Table 3.3. Experimental groupings for ChAdOx1-MVA-MVA prime-boost-boost study 116

Table 4.1 Combinations of ChAdOx1 and MVA viral vectors encoding P1A tested in heterologous prime-boost vaccinations. 149

Table 5.1 Combinations of ChAdOx1 and MVA viral vectors encoding P1A tested in heterologous prime-boost vaccinations. 230

Table 5.2. Highest affinity 9mer/10mer epitope sequences from $P1A_{37-51}$-YLGWLVFAVVTTSFL predicted by Net-MHC 4.0 algorithm for binding to H-$2D^b$ 238

Table 5.3. Highest affinity 9mer/10mer epitope sequences from $P1A_{37-51}$-YLGWLVFAVVTTSFL predicted by Net-MHC 4.0 algorithm for binding to H-$2K^b$..... 238

Table 5.4. Highest affinity 9mer/10mer epitope sequences from $P1A_{41-55}$-LVFAVVTTSFLALQM predicted by Net-MHC 4.0 algorithm for binding to H-$2D^b$ 238

Table 5.5. Highest affinity 9mer/10mer epitope sequences from $P1A_{41-55}$-LVFAVVTTSFLALQM predicted by Net-MHC 4.0 algorithm for binding to H-$2K^b$ 238

Table 8.1. Peptide sequences in P1A Pepset library used for T-cell stimulation assays 306

Table 8.2. Peptide sequences in MAGE-A3 Pepset library used for T-cell stimulation assays 307

Table 8.3. Peptide sequences in NY-ESO-1 Pepset library used for T-cell stimulation assays 310

List of figures

Figure 1.1. Schematic of 3 signal paradigm of naïve T-cell activation by interaction with DCs in secondary lymphoid organs. 16

Figure 1.2. Schematic of CTL displaying effector function towards a tumour cell following recognition of cognate antigen presented via MHC-class I. 18

Figure 1.3. Schematic of CD8+ T-cell inhibition by immune checkpoint signalling in the TME and reactivation of suppressed T-cells by CPIs. 24

Figure 1.4. Mechanism of therapeutic cancer vaccines. 33

Figure 2.1. Map of pEF4/V5 hisA P1A plasmid used for stable transfection of murine cancer cell lines. 65

Figure 2.2. Flow cytometry intracellular cytokine staining gating strategy. 75

Figure 2.3. Flow cytometry effector T-cell / P1A tetramer panel staining gating strategy. 77

Figure 3.1 Schematic showing the design of ChAdOx1 viral vectors encoding the human MAGE-A3 and NY-ESO-1 antigens. 86

Figure 3.2. Schematic showing the design of MVA vectors encoding MAGE-A3 and NY-ESO-1 antigens. 87

Figure 3.3. Timeline of ChAdOx1/MVA heterologous prime-boost vaccination scheme with vectors encoding MAGE-A3 and NY-ESO-1. 92

Figure 3.4. MAGE-A3 and NY-ESO-1-specific CD8+ T-cell response induced by ChAdOx1 prime vaccination. 96

Figure 3.5 Cytokine profiles of antigen-specific CD8+ T-cells after ChAdOx1-M-NY prime vaccination. 98

Figure 3.6. MAGE-A3 and NY-ESO-1-specific CD4+ T-cell responses after ChAdOx1 prime vaccination. 100

Figure 3.7. Kinetics of the MAGE-A3-specific and the NY-ESO-1-specific CD8+ T-cell response in the blood. 103

Figure 3.8. IFN-γ response by MAGE-A3-specific and NY-ESO-1-specific CD8+ T-cells after MVA boost vaccination. 105

Figure 3.9. TNF-α and IL-2 response by MAGE-A3-specific and NY-ESO-1-specific CD8+ T-cells after MVA boost vaccination. 107

Figure 3.10. Cytokine profiles of CD8+ T-cells after heterologous prime-boost vaccination with ChAdOx1/MVA encoding MAGE-A3 and NY-ESO-1. 109

Figure 3.11. Kinetics of the MAGE-A3-specific and the NY-ESO-1-specific CD4+ T-cell response in the blood. 111

Figure 3.12. IFN-γ response by MAGE-A3-specific and NY-ESO-1-specific CD4+ T-cells after MVA boost vaccination. 112

Figure 3.13. Timeline of the ChAdOx1-MVA-MVA prime-boost-boost vaccination scheme with vectors encoding MAGE-A3 and NY-ESO-1. 116

Figure 3.14. MAGE-A3 and NY-ESO-1-specific T-cell responses in the blood after ChAdOx1-Ii-M-NY vaccination. 118

Figure 3.15. MAGE-A3 and NY-ESO-1-specific T-cell response in the blood after the first MVA boost vaccination. 121

Figure 3.16. MAGE-A3 and NY-ESO-1-specific T-cell response in the blood after the second MVA boost vaccination. 125

Figure 3.17. MAGE-A3 and NY-ESO-1-specific T-cell response in the spleen after second MVA vaccinations. 126

Figure 3.18. Kinetics of MAGE-A3 and NY-ESO-1-specific CD8+ T-cell response in the blood. 127

Figure 3.19. Breadth of the MAGE-A3 and NY-ESO-1-specific CD8+ T-cell responses induced by ChAdOx1/MVA/MVA vaccination. 130

Figure 4.1. Schematic showing the design of ChAdOx1 viral vectors encoding P1A. 145

Figure 4.2. Schematic showing the design of MVA viral vectors encoding P1A. 146

Figure 4.3 ChAdOx1/MVA heterologous prime-boost vaccination scheme with vectors encoding P1A. 149

Figure 4.4. P1A-specific CD8+ T-cell response induced by prime-boost vaccination with ChAdOx1/MVA encoding P1A. 151

Figure 4.5. Cytokine profiles of P1A-specific CD8+ T-cells induced by prime-boost vaccination with ChAdOx1/MVA encoding P1A. 152

Figure 4.6. P1A-specific CD4+ T-cell response induced by prime-boost vaccination with ChAdOx1/MVA encoding P1A. 154

Figure 4.7. Timeline of vaccination followed by P815 tumour challenge. 156

Figure 4.8. Protective efficacy of ChAdOx1/MVA P1A vaccination against P815 tumour growth in the prophylactic setting. 159

Figure 4.9. Assessment of ChAdOx1/MVA P1A vaccination protective efficacy against P815 tumour challenge. 160

Figure 4.10. Timeline of vaccination followed by 15V4T3 tumour challenge. 161

Figure 4.11. Protective efficacy of ChAdOx1/MVA P1A vaccination against 15V4T3 tumour challenge. 163

Figure 4.12. Tumour expression of P1A at the mRNA level in naive and vaccinated mice. 165

Figure 4.13. The effect of tPA linkage to P1A in MVA on P1A-specific CD8+ T-cell responses induced by ChAdOx1/MVA P1A vaccination. 168

Figure 4.14. Timeline of therapeutic vaccination schedules following 15V4T3 tumour implantation. 171

Figure 4.15. Therapeutic efficacy of ChAdOx1/MVA P1A vaccination against 15V4T3 tumours. 174

Figure 4.16. Individual 15V4T3 tumour growth curves for control and ChAdOx1/MVA P1A vaccinated mice. 175

Figure 4.17. P1A-specific CD8+ T-cell responses in 15V4T3 tumour bearing mice following ChAdOx1/MVA P1A vaccination. 177

Figure 4.18. Surface PD-L1 expression on 15V4T3 cells. 180

Figure 4.19. Timeline of therapeutic ChAdOx1-Ii-P1A/MVA-P1A vaccination in combination with CPI antibody treatment. 183

Figure 4.20. Therapeutic efficacy of ChAdOx1/MVA P1A vaccination in combination with immune checkpoint blockade in the 15V4T3 tumour model. 186

Figure 4.21. Timeline of 15V4T3 tumour harvest study to assess tumour T-cell infiltrate following ChAdOx1-Ii-P1A/MVA vaccination in combination with anti-PD-1 treatment. 189

Figure 4.22. Harvesting 15V4T3 tumours for analysis of T-cell infiltrate. 190

Figure 4.23. P1A-specific CD8+ T-cell responses induced in the blood and spleen of 15V4T3 tumour-bearing mice following treatment with ChAdOx1-Ii-P1A/MVA-tPA-P1A vaccination, with or without αPD-1. 192

Figure 4.24 T-cell infiltrate in 15V4T3 tumours from mice treated with ChAdOx1-Ii-P1A/MVA-tPA-P1A and anti-PD-1 blockade. 195

Figure 4.25. P1A-specific CD8+ T-cell infiltrate in 15V4T3 tumours from mice treated with ChAdOx1-Ii-P1A/MVA-tPA-P1A and anti-PD-1 blockade. 197

Figure 4.26. IFN-γ production by CD8+ TILs in 15V4T3 tumours from mice treated with ChAdOx1-Ii-P1A/MVA-tPA-P1A and anti-PD-1 blockade. 199

Figure 4.27. Central/effector memory phenotype of CD8+ T-cells in 15V4T3 tumour bearing mice. 200

Figure 4.28. PD-1 expression on CD8+ T-cells in 15V4T3 tumour-bearing mice. 202

Figure 4.29. Expression or pro- and anti-inflammatory mediators in the 15V4T3 tumour microenvironment. 205

Figure 5.1. ChAdOx1/MVA heterologous prime-boost vaccination scheme with vectors encoding P1A. 230

Figure 5.2. P1A-specific CD8+ T-cell response induced by prime-boost vaccination with ChAdOx1/MVA encoding P1A in C57BL/6 mice. 232

Figure 5.3. P1A-specific CD4+ T-cell response induced by prime-boost vaccination with ChAdOx1/MVA encoding P1A. 233

Figure 5.4. Identifying immunogenic P1A CTL epitopes in C57BL/6 mice. 236

Figure 5.5 Characterization of the optimal 9-amino-acid P1A CTL epitope within the $P1A_{37-51}$ and $P1A_{41-55}$ peptides. 240

Figure 5.6. Validating the MHC-class I restriction of the $P1A_{43-51}$ epitope. 242

Figure 5.7 Detection of P1A-specific CD8+ T-cell responses in C57BL/6 mice via staining with a PE-labelled H-$2D^b$ $P1A_{43-51}$ tetramer. 244

Figure 5.8. Determining $P1A_{43-51}$-specific TCR sequences from C57BL/6 mice. 248

Figure 5.9. Screening of MC38 and B16F10 clones stably transfected with a P1A-expression plasmid for P1A mRNA expression by qPCR..... 251

Figure 5.10. Assessing P1A expression in murine cancer cell lines following treatment with 5-aza-dC..... 254

Figure 5.11 Assessing P1A expression level by rt-qPCR in tissues of MC38 tumour-bearing C57BL/6 mice following treatment with 5-aza-2′-deoxycytidine..... 256

Figure 5.12 Therapeutic efficacy ChAdOx1-Ii-P1A/MVA-P1A againt tumours formed from 5-aza-2′-deoxycytidine pre-treated MC38 cells. 258

Figure 5.13 Threapeutic efficacy of 5-aza-2′-deoxycytidine treatment combined with ChAdOx1-Ii-P1A/MVA-P1A vaccination against MC38 and EL4 tumours..... 260

List of abbreviations

5-aza-dC	5-aza-2'deoxycytidine
Ab	Antibody
ACK buffer	Ammonium-Chloride-Potassium buffer
ALL	Acute lymphoblastic leukaemia
ANOVA	Analysis of variance
APC	Antigen-presenting cell
ACT	Adoptive cell transfer
CAR	Chimeric antigen receptor
CDR	Complementarity determining region
ChAdOx1	Chimpanzee adenovirus Oxford 1
CPI	Checkpoint inhibitor
CTL	Cytotoxic T-lymphocyte
CTLA-4	Cytotoxic T-lymphocyte-associated protein 4
DAMP	Damage associated molecular pattern
DC	Dendritic cell
DMEM	Dulbecco's modified Eagle's medium
DNA	Deoxyribonucleic acid
DNMTi	DNA methyl transferase inhibitor
ERV	Endogenous retroviral element
FACS	Fluorescence activated cell sorting
FDA	U.S. Food & Drug Administration
g	Gram
HLA	Human leukocyte antigen
i.m.	Intramuscular
i.p.	Intraperitoneal
ICB	Immune checkpoint blockade
ICS	Intracellular cytokine staining
IDO	Indoleamine 2,3-dioxygenase
IFN	Interferon
IHC	Immuno-histochemistry
Ii	Invariant chain
IL	Interleukin
IMDM	Iscove's modified Dulbecco's medium
IRAE	Immune-related adverse event
IU	Infectious units
M. tb	Mycobacterium tuberculosis
MAGE	melanoma-associated antigen
MFI	Mean fluorescence intensity
mg	Milligram
MHC	Major histocompatibility complex
MVA	Modified vaccinia Ankara

NK cells	Natural killer cells
NSCLC	Non-small-cell lung cancer
NY-ESO-1	New York esophageal squamous cell carcinoma 1
ORR	Overall response rate
PAMP	Pathogen associated molecular pattern
PBMC	Peripheral blood mononuclear cells
PBS	Phosphate buffered saline
PCR	Polymerase chain reaction
PD-1	Programmed cell death protein 1
PD-L1	Programmed death ligand 1
PFU	Plaque forming units
PRR	Pattern recognition receptor
RNA	Ribonucleic acid
RPMI 1640	Roswell Park Memorial Institute 1640
RSV	Respiratory syncytial virus
s.c	Subcutaneous
SEM	Standard error of the mean
T_{CM}	Central memory T-cell
TCR	T-cell receptor
T_{EM}	Effector T-cell
Tet	Tetramer
TIL	Tumour infiltrating lymphocyte
TMD	Transmembrane domain
TME	Tumour microenvironment
TNF	Tumour necrosis factor
tPA	Tissue plasminogen activator
T_{reg}	Regulatory T-cell
WHO	World Health Organization

Chapter 1. Introduction

1.1 Immunotherapy

1.1.1 The burden of cancer and conventional therapy

Cancer is a global health issue, being the second leading cause of death globally [1]. In 2018, the World Health Organisation's (WHO) International Agency for Research on Cancer (IARC) estimated that cancer accounted for 9.6 million deaths worldwide, or 17% of total mortalities [2]. Cancer is a proliferative cellular disorder, whereby tumours are formed through uncontrolled cell division. The majority of cancer deaths result from metastasis, the dissemination of cancer cells and formation of tumours distal to that of the primary original tumour. For much of the 20th century, cancer was treated and managed through one or a combination of three different methods - either surgical removal of tumours, chemotherapy, or radiotherapy. These therapeutic interventions formed the "three pillars" of cancer treatment.

As a result of continuous improvements in cancer diagnosis and treatment, survival rates for cancer have greatly improved both globally and in the UK over the last 40 years. For example in the UK, 5-year survival rates following diagnosis from all cancers combined for both men and women almost doubled between 1971-2011, increasing from 30% to 54% [3]. 10-year survival has improved similarly, rising from 24% to 50%. However, survival rates in many types of cancers such as those of the lung, oesophagus and pancreas, termed cancers of unmet clinical need [4], have budged little throughout this time [3]. This is due to the advanced stage at which these cancer types are frequently diagnosed, as

advanced metastasized cancers have proven largely refractory to conventional treatments.

1.1.2 Immunotherapy, the 4th pillar of cancer treatment

This stasis had seemed intractable until recent advances in the field of cancer immunotherapy, which have brought about previously unprecedented improvements in outcomes for difficult to treat advanced cancers [5]. Immunotherapy for cancer, i.e. harnessing the cytotoxic function of the immune system to resolve tumours, is an old concept with much held promise, but until recently one which has failed to deliver in the clinic despite many attempted strategies. However, numerous successes have been achieved in the last decade.

This has been most typified through the development of immune checkpoint blockade (ICB) therapy [6]. These are generally monoclonal antibodies, which block receptor-ligand interactions ("immune checkpoints") between T-cells and other cell types that govern T-cell activation and suppress their effector function [7]. They exhibit anti-tumour activity through the reactivation of suppressed tumour-specific T-cells. Collectively these are termed immune checkpoint inhibitors (CPIs). In clinical trials treatment with CPIs has brought about potent and durable tumour regression in substantial proportions of advanced cancer patients. The strongest results so far have come from treatments combining the inhibitors ipilimumab and nivolumab, targeting the T-cell surface receptors cytotoxic T-lymphocyte-associated protein 4 (CTLA-4) and programmed cell death protein 1 (PD-1) respectively [8]. The highest efficacy and response rates

have been seen in advanced melanoma. In the ongoing CheckMate 067 trial overall survival from the combination treatment has remained above 50% at 3 and 4 years follow-up [9] [10]. Recently, this was extended to 5-years, with 52% of patients still alive following combination treatment [11]. By comparison, historical 5-year survival rates for advanced melanoma have been around 10% [12]. Lesser so, but still improved outcomes have been seen from this approach in other cancers such as non-small cell lung cancer (NSCLC) [13, 14], renal-cell carcinoma (RCC) [15] and colorectal cancers with confirmed DNA mismatch repair or microsatellite instability high tumours [16, 17] amongst others. Since 2011, results such as these have led to the approval by the U.S. Food and Drug Administration (FDA) of 7 different immune checkpoint inhibitors targeting either CTLA-4 or the PD-L1/PD-1 axis for use in the US as treatment for a wide range of cancer indications [8], with similar approvals following in many other countries.

Antibodies blocking the PD-1 and CTLA-4 signalling axes are the most clinically advanced, however much research is being undertaken into the therapeutic potential of targeting of other immune checkpoints [18, 19]. These include the targeting of other inhibitory immune checkpoint pathways, such as drugs blocking signalling through inhibitory T-cell receptors such as lymphocyte activation gene-3 (LAG-3), T cell immunoglobulin and mucin-domain containing-3 (TIM-3), T cell immunoglobulin and ITIM domain (TIGIT) and V-domain Ig suppressor of T cell activation (VISTA). Agonists of stimulatory T-cell receptors are also being evaluated, as a means of boosting anti-tumour T-cell function through the targeting of such receptors as OX40, ICOS, and 4-1BB (CD137). The

therapeutic targeting of many of these pathways has shown promising anti-tumour efficacy in a range of pre-clinical studies and many potential new drugs are at varying stages of clinical testing and development [19].

Adoptive cellular based therapies have provided similar breakthroughs in certain haematological cancers. In particular chimeric antigen receptor T-cell (CAR T-cell) therapy [20]. This involves autologous T-cells isolated from patients, modified ex vivo to express CARs [21]. The extracellular portion of the CAR is derived from the variable region of a monoclonal antibody with specificity for a cell surface antigen expressed by the cancer. The intracellular portion contains downstream signalling components of a normal TCR, such as CD3ζ, and costimulatory molecules [22]. Modified CAR T-cells are reinfused to the patient, where binding of the extracellular domain to its target initiates intracellular signalling and T-cell activation, resulting in destruction of the target cancer cells. Striking results have been obtained using this approach in B-cell malignancies by targeting the cell surface receptor CD19 [21]. B-cell acute lymphoblastic leukaemia (ALL) is one of the highest incidence paediatric cancers, but also affects adults. Many cases can be cured by conventional chemotherapy, however some individuals are refractory to treatment or have cancers that relapse. In these latter cases, historically no further treatment options were available, and the median survival for adult refractory relapsed ALL (r/r ALL) patients was 7.7 months. Clinical trials using CAR T-cells targeting CD19 in paediatric patients with r/r ALL, have achieved complete remission, meaning no detectable signs of disease, in above 90% of subjects following a single round of treatment [23, 24]. Furthermore, upon longer term

follow up these responses were shown to be durable in a significant proportion of patients [25, 26]. Impressive results have also been obtained in large B-cell lymphoma [27-29]. These results have led to approval initially in the United State (U.S.) and later in several other countries [30, 31].

Together these results demonstrate the robust ability of the immune system, in particular CD8+ T-cells to resolve tumours in human patients and more than confirm the validity of immunotherapy as an approach toward treating cancer. Immunotherapy has therefore in a short space of time come to be considered a 4th pillar of cancer treatment, prompting a rapid expansion in the field and interest in developing new immunotherapeutic modalities.

1.1.3 Drawbacks of current immunotherapeutic approaches

Despite the enthusiasm brought about by the undoubted successes achieved with therapies such as ICB and CAR T-cells, both have significant limitations. Although some patients experience profound anti-tumour efficacy and improved outcomes, CPIs have low response rates in the majority of cancer types. Clinical data has shown that in most cancers, the overall response rate (ORR) to ICB, i.e. the proportion of patients who experience either partial or complete tumour regressions, is well below 50% of those treated. Combination therapy targeting both PD-1 and CTLA-4 simultaneously has generally been seen to produce better ORRs than monotherapy with either single agent. The best case has been in advanced melanoma, where ORRs of above 50% have been observed with combined anti-PD-1 and anti-CTLA-4 treatment - in the CheckMate067 trial 57%

for the combination vs 43% nivolumab monotherapy and 19% ipilimumab monotherapy [32]. However, for the majority of cancers the ORRs of either combined or monotherapy have fallen short of this. ORRs of 45% and 42% for combined therapy, and 20% and 26% for nivolumab monotherapy have been seen in NSCLC and RCC respectively [13-15, 33].

Furthermore, whilst these new treatments are associated with a lower degree of toxicity than conventional chemotherapeutic agents, they still induce side-effects in a very high proportion of patients. Many patients treated with CPIs experience what are termed, immune related adverse events (IRAEs) [34]. The receptors targeted by CPIs have regulatory functions to suppress inappropriate or overexuberant T-cell responses in the body. As CPIs act systemically and non-specifically, treatment induced toxicity can occur from excessive inflammation resulting from the undesired activation of T-cells of non-tumour specificities. This toxicity may also be autoimmune in nature, by activating normally suppressed or tolerized autoreactive T-cells. IRAEs effect a wide range of tissues, but most commonly the skin, liver, gastrointestinal tract and endocrine system, leading to organ damage. The incidence of IRAEs is high – experienced by 90% and 70% of patients treated with anti-CTLA-4 and anti-PD-1 respectively [35]. Whilst, combination therapy targeting two immune checkpoints has been more effective clinically than with monotherapy, unsurprisingly it has also been associated with a higher occurrence of IRAEs. Most cases are mild, but can be severe in nature requiring management with intensive care interventions, and have resulted in death in some cases. Similarly the majority of CAR T-cell treated patients

experience toxicity resulting from cytokine release syndrome (CRS) [36]. CAR T-cells activated in the body after reinfusion secrete cytokines, which leads to systemic inflammation and multi-organ failure in severe cases. Patients therefore require careful monitoring and management of symptoms.

Furthermore, whilst these treatments have undoubtedly proven more effective than previously existing options, they currently come with a correspondingly high monetary cost. Relative to standard therapy, the price of a course of treatment with immune-checkpoint inhibitors is high. Given the current rates of patients who respond, this clearly raises cost-effectiveness concerns [37]. One study estimated that as of 2018, 43% of all cancer patients in the U.S. were eligible for treatment with an FDA approved CPI. This is in contrast to 13% of all patients who will respond and derive clinical benefit [38]. Furthermore, the production of transgenically modified T-cells such as CAR T-cells for adoptive transfer is technically demanding [39, 40]. The result of this is that a single round of treatment with the CD19-targeting CAR T-cell therapy Tisagenlecleucel as of 2018 carried a list price of $475,000 USD, making it the single most expensive oncologic treatment available [39].

1.1.4 The need for new immunotherapeutic agents

Given the limited response rates, toxicity, and the cost, improvements to current immunotherapeutic options are needed. This could take the form of determining biomarkers that better predict responses. Better still novel therapies are required that further increase response rates, or function alone to improve treatment in

cases where responses are not observed. Both the successes and limitations underscore the need to improve and develop new immunotherapeutic agents.

1.2 Tumour immunology

1.2.1 Immune responses to cancer

Cancer immunotherapy utilizes the ability of the immune system to recognize and eliminate foreign bodies, and is therefore underpinned by the ability of the immune system to discriminate cancer cells as non-self. For the most part, this relies on the specialized function of the adaptive immune system, which consists of B and T lymphocytes. B cells produce antibodies, whilst T-cells are responsible for cell mediated immunity. Cellular immunity in particular is considered to be key to mediating tumour clearance. T-cells possess unique surface T-cell receptors (TCRs), which recognize specific peptide antigens (epitopes) bound and presented by major histocompatibility (MHC) molecules. During T-cell development in the thymus, recombination of the V(D)J genes that encode the TCR-alpha and TCR-beta subunit chains generates a pool of T-cells with a TCR repertoire capable of recognizing a vast array of peptide epitopes. T-cells can broadly be further divided into two subtypes based on whether they express a CD8 or CD4 co-receptor. CD8+ T-cells are considered to be the critical effectors of the anti-tumour cell-mediated response, through their recognition of tumour antigens presented on the surface of cancer cells in the context of MHC-class I molecules, and ability to directly kill and lyse target cancer cells through cytotoxic effector function. For this reason, most immunotherapeutic strategies for cancer currently under development focus on the generation or augmentation of anti-tumour CD8+ T-cell responses. In order to generate tumour-specific adaptive T-cell responses however, a complex series of cellular events must first take place, starting with the

capture of tumour-specific antigens by innate immune cells and subsequent presentation to T-cells. This dynamic process has been conceptualized as a paradigm termed the "cancer-immunity cycle" by Chen and colleagues [41].

1.2.2 Innate immunity and the generation of adaptive anti-tumour adaptive immune responses

Classically, in the context of infection, cells of the innate immune system such as macrophages, dendritic cells (DCs) and natural killer (NK) cells act as immune sentinels. They either reside within or are recruited to peripheral tissues where they sense and detect pathogenic threats, for example from viruses and bacteria. Innate immune cells are the first responders of the immune system. They detect pathogens that breach the body's epithelial barriers through pathogen recognition receptors (PRRs) - specialized receptors that bind to shared hallmark molecular features of microbes known as pathogen associated molecular patterns (PAMPs). They can also detect tissue damage in the form of damage associated molecular patterns (DAMPs), for example DNA and other intracellular components released from dying cells. Upon detection of pathogens or tissue damage, they act as the body's first line of defence by initiating an inflammatory response and exhibiting anti-microbial functions. Macrophages and DCs are also considered to be professional antigen presenting cells (APCs), and act to form a bridge between the innate and adaptive immune systems to facilitate the generation of antigen-specific T and B cell responses. DCs in particular are the most specialized in terms of antigen-presentation function.

DCs primarily function to uptake antigens from the extracellular environment, process them into short peptide sequences and present them to T-cells in the context of MHC molecules [42]. Antigen uptake in peripheral tissues by DCs in an inflammatory context leads to changes in gene expression whereby DCs transition from an immature to a mature state. In the context of cancer, this could result from tumour antigens released from dying tumour cells alongside pro-inflammatory cytokines or DAMPs. Expression of MHC molecules and costimulatory ligands are further upregulated on mature DCs, along with lymph node (LN) homing receptors. This shift in gene expression pattern enables them to migrate to the LNs where they can present MHC-bound antigen to T-cells.

Through the expression of both MHC-class I and MHC-class II molecules on the cell-surface, DCs are able to present antigens to both CD8+ and CD4+ T-cells respectively. Protein antigens taken up from the extracellular space by the endocytic pathway are typically processed and presented by most APCs via MHC-class II. Here they are degraded in lysosomes into short peptide sequences, and associate with MHC-class II molecules. However, DCs are also able to efficiently present antigens uptaken via endocytosis in the context of MHC-class I to CD8+ T-cells through their specialized cross-presentation capability. In the cross-presentation pathway, antigens leave the endocytic pathway and enter the cytosol for degradation into short peptides by the proteasome, and subsequent loading onto MHC-class I molecules [43].

1.2.3 DC subsets important for anti-tumour immunity

There are considered to be two main DC subsets, conventional DCs (cDCs) and plasmacytoid DCs (pDCs). cDCs are considered to be the most important in terms of generating CD8+ T-cell responses. cDCs can be further broken down into two subsets – cDC1s and cDC2s [44]. Recent work has shown that the presence in tumours of cDC1s in particular is vital for the development of effective anti-tumour CTL responses [45]. cDC1s are characterized by expression of CD8α and the cell surface integrin CD103 and have been shown to be dependent on the transcription factor Batf3 for development [46]. The human equivalent is the CD141+ subset [47, 48]. CD8α+/ CD103+ cDC1s have been found to be particularly adept at cross-presenting exogenous antigen via MHC-class I to CD8+ T-cells. They are further specialized to acquire antigen from necrotic or dying cells [49]. cDC1s are activated to stimulate immune responses against tumours via the cyclic-GMP-AMP synthase (cGAS) - stimulator of interferon genes complex (STING) pathway of PRRs [50, 51]. Through the cGAS-STING pathway cDC1s sense tumour-derived cytosolic DNA, leading to the production of type I interferons (IFN-α/IFN-β). In the tumour microenvironment (TME), they take up tumour antigens from dying tumour cells and migrate to the lymph nodes for antigen presentation to naïve T-cells. In this way, they play a crucial role in priming anti-tumour CD8+ T-cells responses. DCs from *Batf3*$^{-/-}$ mice, which lack the CD8α+/ CD103+ cDC1 subset are unable to cross-present antigens and cannot control growth of normally rejected highly immunogenic tumours [46]. Furthermore, the presence of CD8α+/ CD103+ cDC1s in the tumour is associated

with better responses to immunotherapy and subsequently longer patient survival [52, 53].

1.2.4 Adaptive anti-tumour immunity

(I) T-cell activation

The basis of adaptive anti-cancer immunity is the recognition by CD8+ T-cells of immunogenic tumour-specific peptide antigens presented on the surface of cancer cells in the context of MHC-class I molecules, enabling the discrimination of malignantly transformed cells from healthy ones. In the LNs, the presentation of MHC-bound tumour antigens by DCs to naïve CD8+ and CD4+ T-cells bearing specific cognate TCRs drives activation of naïve T-cells into effector T-cells (Figure 1.1). Three signals are thought to be required for full T-cell activation to occur. The primary signal is recognition by a T-cell of its cognate antigen though its TCR binding MHC/peptide (signal 1). However, DCs are required to provide additional signals. Mature DCs express CD80 and CD86 molecules, which bind the costimulatory receptor CD28 on the surface of T-cells (signal 2) [54, 55]. This interaction serves to amplify intracellular signalling cascades initiated by TCR binding to specific peptide-MHC complexes. Furthermore DCs must provide further differentiation and proliferation signals to activate T-cells in the form of pro-inflammatory secreted cytokines (signal 3) [56] . The exact cytokine skews the differentiation programme of the T-cell. Which signal that the DC secretes is determined by the nature of the PAMPs/DAMPs and other inflammatory cues detected by the DC. Type 1 T-helper (Th1) immunity is considered key for anti-

tumour responses, where naïve CD4+ T-cells differentiate to Th1 cells and naïve CD8+ T-cells acquire cytotoxic effector function to become cytotoxic T-lymphocytes (CTLs). Th1 immune responses for example are regulated by IL-12 secretion, which binds to and signals through IL-12 receptors (IL-12R) on the surface of T-cells. Without IL-12 signalling, antigen-stimulated CD8+ T-cells proliferate but are unable to acquire cytolytic function [57-59]. The integration of all three signals within the T-cell drives a specific activation and differentiation gene expression protocol, and the acquisition of effector functions. This is mediated by specific transcription factors, for example T-bet in the instance of Th1 immunity [60-62]. Additional signals from the DC such as from the ligands OX40L and 4-1BBL that interact with the T-cell surface receptors OX40 and 4-1BB respectively deliver further proliferation and survival cues to activated T-cells [63-68]. Following activation, T-cells undergo rapid clonal expansion. This is driven by T-cell proliferation signals and cytokines such as IL-2 in both an autocrine and paracrine manner.

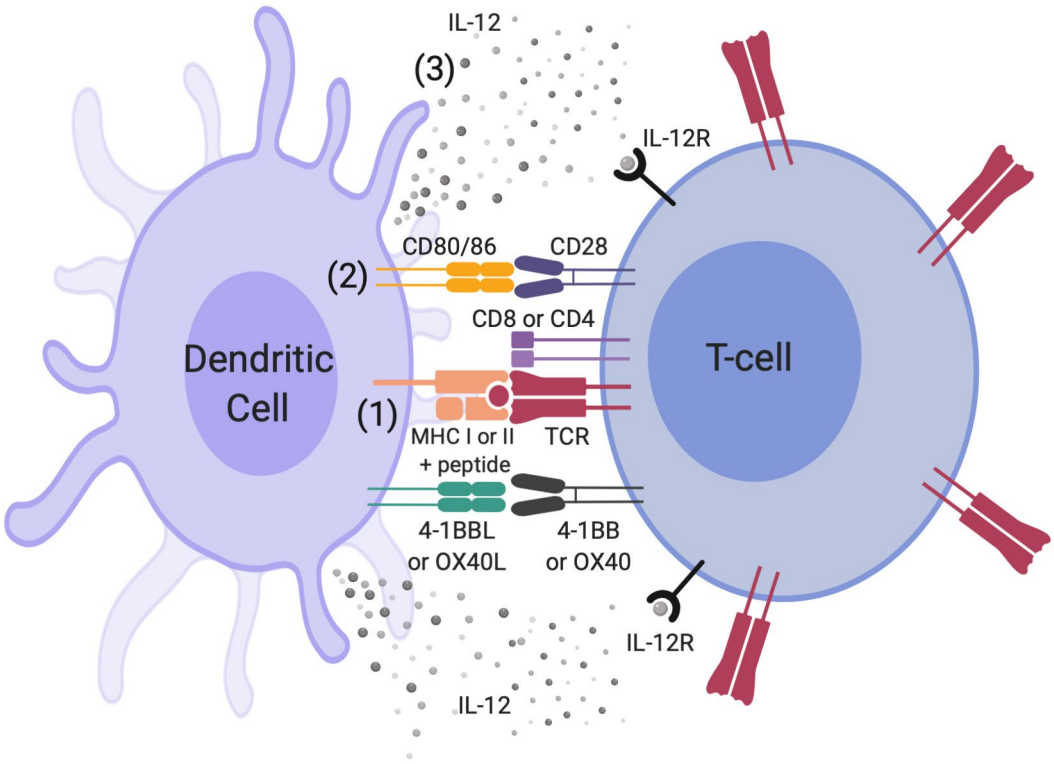


Figure 1.1. Schematic of 3 signal paradigm of naïve T-cell activation by interaction with DCs in secondary lymphoid organs. T-cells are required to receive 3 signals from antigen presenting cells such as DCs in order for activation to occur. (1) The TCR of the T-cell binds its cognate antigen presented by the DC in the context of MHC class I (CD8+ T-cells) or MHC class II (CD4+ T-cells). This leads to intracellular signalling inside the T-cell that drives activation. The CD8 and CD4 co-receptors stabilize the interaction between the TCR and MHC by binding to the constant regions of the MHC-class I and MHC-class II molecules respectively. (2) Co-stimulatory ligands such as CD80 and CD86 are expressed at elevated levels on mature DCs that have taken up antigen in an inflammatory context. CD80 and CD86 bind to the costimulatory receptor CD28 on the surface of the T-cell to amplify intracellular signalling cascades initiated by TCR signalling. (3) Inflammatory cytokines secreted by the DC drive a specific gene programme by the T-cell skewing its differentiation into different effector cell subtypes. Further survival cues also provided by the DC in the form of signalling through the OX40L/OX40 or 4-1BBL/4-1BB axes. Image drawn with BioRender.

(II) Effector T-cell function and cell-mediated immunity

Tumour-specific T-cells activated in the LNs follow inflammatory cues in the form of chemokine homing signals to sites in the periphery to locate target tumour cells. It is now well accepted that anti-tumour immunity is mediated primarily by CTLs, as they exhibit a range of cytotoxic functions that can mediate efficient killing of tumour cells [69]. CTLs recognise endogenous antigen processed intracellularly generated through proteasomal processing in the cytosol and presented by cells in

the context of MHC-class I molecules. MHC-class I is expressed by all nucleated cells. Activated CTLs that have trafficked to the tumour site encounter tumour-specific cognate antigens presented by MHC-class I on the surface of cancer cells, and display cytotoxic effector functions towards them, resulting in their destruction (Figure 1.2) [69]. This involves the secretion of major Th1 pro-inflammatory cytokines such as IFN-γ and TNF-α and production of cytotoxic mediators such as perforin and Granzyme B that kill and lyse target tumour cells. IFN-γ has anti-proliferative effects on cancer cells, can induce apoptosis and increase cancer cell immunogenicity through upregulation of MHC-class I molecules [70, 71]. CTLs can also kill directly through the expression of FasL, which induces apoptosis upon binding the Fas receptor expressed on target tumour cells. Key studies in humans and murine tumour models have demonstrated the importance of these CTL effector mechanisms for bringing about tumour regression. Tumour-antigen specific CD8+ T-cells from IFN-γ-knockout (KO) or perforin-KO mice are much less able to reject immunogenic tumours expressing cognate antigen compared to WT controls [72-75]. Similarly, neutralizing IFN-γ and TNF-α in vivo by administering tumour-bearing mice with anti-IFN-γ and anti-TNF-α antibodies has been shown to inhibit the anti-tumour effectiveness of adoptively transferred CD8+ TILs [71, 76].

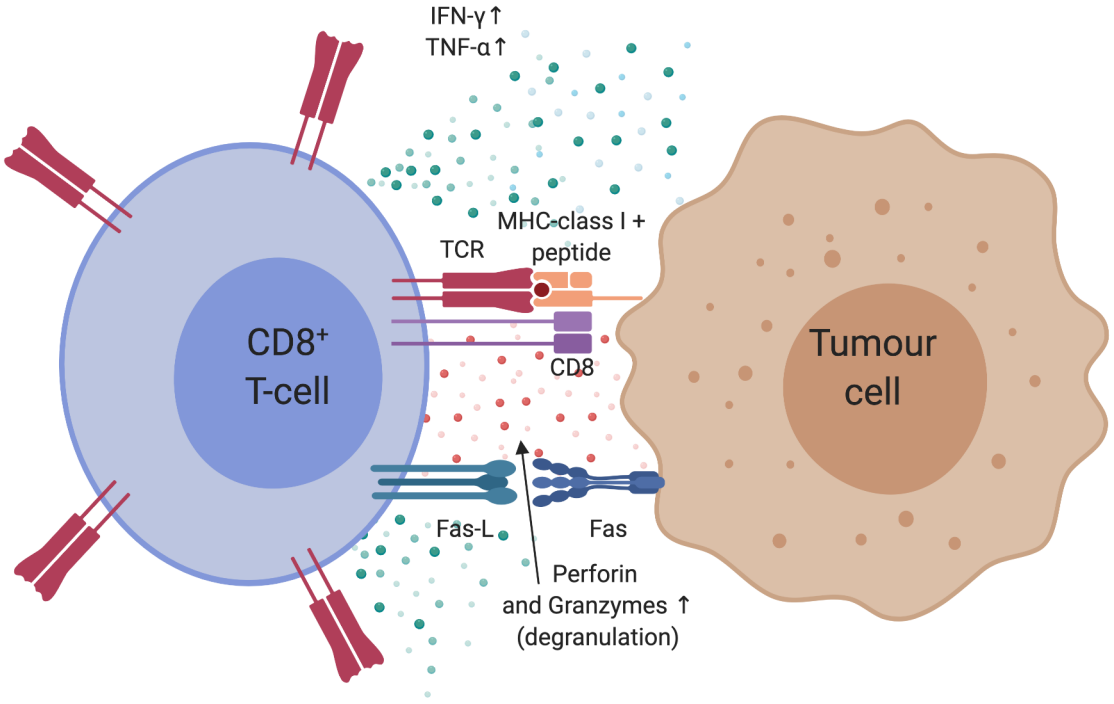


Figure 1.2. Schematic of CTL displaying effector function towards a tumour cell following recognition of cognate antigen presented via MHC-class I. Activated CTLs follow chemokine signalling cues to traffic and infiltrate into tumours. In the tumour site, tumour antigen-specific CTLs recognize their cognate antigen presented on the surface of the cancer cells in the context of MHC-class I. An immunological synapse is formed between the T-cell and the target tumour cells, a spatial concentration of immune-related signalling molecules, where binding of the TCR to its specific antigen/MHC-class I complex and other receptor-ligand interactions occur. Following recognition of specific cell targets, CTLs mediate killing of the tumour cell through cytotoxic effector functions. CTLs secrete inflammatory cytokines such as IFN-γ and TNF-α into the extracellular environment to initiate and augment a local inflammatory immune response. Cytotoxic effector molecules such as perforin and granzymes contained with cytotoxic granules are secreted from the CTL into the spatially contained immunological synapse into the target tumour cell, which induce cell death. Cell death can also be mediated directly through death receptor signalling, for example through the engagement of Fas-ligand on the surface of CD8+ T-cells with the Fas receptor on the surface of tumour cells, which activates apoptotic signalling pathways. Image drawn with BioRender.

CD4+ T-cells recognise exogenous antigen presented via MHC-class II molecules by APCs. They differentiate into T helper cells – termed for their role in supporting other aspects of the immune response. As such, they are believed to predominantly aid in the anti-tumour immune response by facilitating proper activation of CD8+ T-cells. CD4+ T_H cells interact with both DCs and CD8s. Through 'DC licensing, CD4+ T_H cells provide signals to the DCs via CD40-CD40L interactions that enhance DC antigen presentation and co-stimulation capabilities

[77]. In turn this enables DCs to deliver a more potent activation signal to CD8+ T-cells. CD4+ T-cells also help to activate CD8+ T-cells by providing additional proliferation and survival signals in the form of cytokines. This prolongs the duration of the cytotoxic response, prevents CD8+ T-cell exhaustion and induces the development of CD8+ T-cell memory.

1.2.5 NK cells – cytotoxic cells of the innate immune system

NK cells of the innate immune system play a key role alongside T-cells in carrying out cell-mediated cytolytic responses, and are highly important in anti-tumour immunity [78]. They are one of the earliest cell types to respond to viral infection, and play a key role in the surveillance and killing of malignantly transformed cells [79]. NK cells recognize a 'loss of self' and their activation is regulated via signalling through a variety of cell surface receptors. NK cells recognize classical MHC-class I molecules expressed on the surface of nucleated cells in the periphery, which delivers an inhibitory signal to NK cells [80]. This is mediated through killer-cell immunoglobulin-like receptors (KIRs). Another inhibitory NK signal is the detection of non-classical HLA molecules such as HLA-E through the NKG2A receptor. HLA-E presents a 9-amino acid epitope derived from the signal sequence of classical MHC-class I molecules, and is therefore dependent on expression of classical MHC-class I molecules at the cell surface. Loss of surface MHC-class I is therefore an activating signal for NK cells. Downregulation of MHC-class I is frequently induced by many viruses when they infect cells as a mechanism to escape CTL mediated immunity. Similarly, immune selection

pressure combined with genetic instability of malignantly transformed cells frequently drives loss of MHC-class I expression in tumours. NK cells also respond to activating signals through receptors such as NKG2D and Nkp46, which recognize molecules that are absent from the surface of healthy cells, but are upregulated by events of cellular stress such as viral infection, malignant transformation and DNA damage [81, 82].

The detection of general features of stress by NK cells enables a rapid cell mediated response to take place before an adaptive antigen-specific response develops. NK cells kill target cells using a cytolytic mechanism analogous to CTLs through the secretion of granules containing cytotoxic mediators such as granzymes and perforin. NK cells are also important mediators of the inflammatory response, and contribute to the production of cytokines in the TME such as IFN-γ that drive inflammation and recruit and activate other immune cells at the effector site [83]. For example studies have found NK cells to play a key role in the recruitment of CD103+ cDC1s into the TME through production of CCL5 and Xcl1 [84, 85]. They also provide a key link to the adaptive immune response through the production of IFN-γ which stimulates the production of CXCL9 and CXCL10 by cDC1s, promoting T-cell recruitment into tumours [85].

1.2.6 Tumour immune evasion

That tumours grow despite the potential of the immune system to mount anti-tumour immune responses is due to immune evasion by the cancer. This can be

achieved broadly through two strategies – directly through immune suppression by tumours or indirectly through immune ignorance [86].

(I) Immunosuppression

Cancer cells co-opt many in-built immune-regulatory mechanisms to suppress anti-tumour T-cell responses. Typically, these serve a physiological function of dampening inflammatory responses following the resolution of pathogen infection to limit excessive damage to healthy tissue. Through the expression of these factors, a highly immunosuppressive tumour microenvironment is formed, whereby tumours are able to inhibit the effector function of anti-tumour T-cells. This leads to the development of adaptive-immune-resistance by tumours. Recent studies have elucidated many of the mechanisms by which tumours achieve this [87].

A major strategy through which this is achieved is by the expression of immune checkpoint ligands of the B7 family. B7 family ligands play a key role in regulating immune cell function. Many of these serve to deliver negative inhibitory signals to effector T-cells. The most studied of the inhibitory ligands in this family is programmed death-ligand 1 (PD-L1) (also B7-H1). This ligand is expressed constitutively by many epithelial cells. However, it is upregulated by many tumour cells and immune cells in the tumour-microenvironment and delivers inhibitory signals to tumour-specific T-cells by binding to the inhibitory PD-1 receptor expressed on the T-cell surface (Figure 1.3 A). The engagement of PD-1 with PD-L1 inhibits T-cell proliferation, cytokine secretion and induces T-cell

apoptosis [88, 89]. PD-1 itself is highly upregulated by TILs in the TME, and its expression correlates with an exhausted phenotype and impairment of effector T-cell function [90]. Studies in murine tumour models have shown mechanistically that PD-L1 expression can directly inhibit anti-tumour CTL responses and prevent tumour rejection [91]. The inhibitory receptor CTLA-4 is also upregulated on the surface of activated T-cells. CTLA-4 is a homologue of the costimulatory receptor CD28 and competes with CD28 for binding to the ligands CD80 and CD86 on APCs (Figure 1.3 A). CTLA-4 binds with higher affinity to CD80/CD86 than CD28, outcompeting it, preventing costimulatory signalling and further T-cell activation [92]. The success of immune checkpoint inhibitors has so far been built on combatting these immunosuppressive pathways utilized by cancer cells [93]. CPIs are monoclonal antibodies that interfere with the ligand-receptor interactions and serve to re-activate suppressed anti-tumour effector T-cells in the TME to overcome tumour adaptive immune resistance (Figure 1.3 B) [93, 94].

There are numerous other mechanisms through which an immunosuppressive TME is generated. Tumour cells frequently express indoleamine 2,3-dioxygenase (IDO), an enzyme that catabolizes tryptophan. Tryptophan is a key metabolite for T-cells, and its depletion in the TME inhibits T-cell proliferation and effector function [95]. Furthermore, suppressive immune cell subsets such regulatory T-cells (T_{reg}) and myeloid derived suppressor cells (MDSCs) are frequently found to be recruited to tumours [96, 97]. These cells are frequently found within the TME, and express a range of inhibitory molecules such as PD-L1, IL-10, nitric oxide and TGF-β that further suppress T-cell effector functions [98, 99]. CTLA-4 can also be

expressed by cancer cells and T_{regs} to inhibit co-stimulation. Of note, T_{regs} express high levels of CTLA-4 and anti-CTLA-4 blockade has also been demonstrated to exert anti-tumour function through the depletion of T_{regs} from the TME [100, 101].

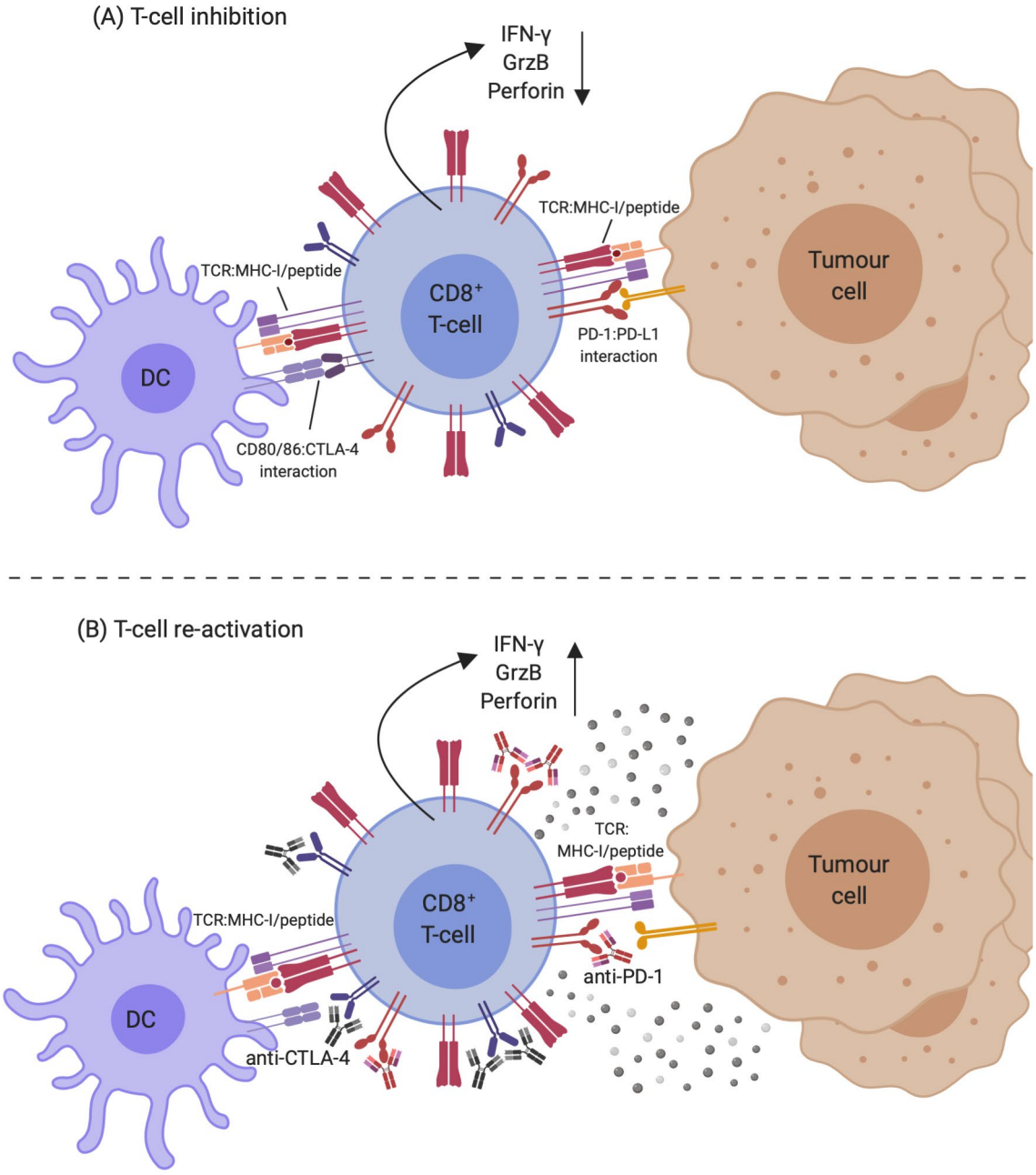


Figure 1.3. Schematic of CD8+ T-cell inhibition by immune checkpoint signalling in the TME and reactivation of suppressed T-cells by CPIs. Receptors on the surface of CD8+ T-cells such as CTLA-4 and PD-1 deliver inhibitory signals to suppress activation and effector function. CTLA-4 competes with CD28 for binding the costimulatory ligands CD80/DC86 during DC-T-cell crosstalk, inhibiting the priming of CD8+ T-cells. PD-1 expressed on activated CD8+ T-cells binds to PD-L1 expressed by either tumour or suppressive immune cell subsets, delivering signals that induce either inhibition of effector function or apoptosis. (B) Immune checkpoint inhibitors in the form of monoclonal antibodies targeting the T-cell surface receptors CTLA-4 and PD-1 have proven highly successful in the clinic. These reinvigorate or promote the effector function of tumour-specific CD8+ T-cells by acting at different stages of CD8+ T-cell activation [94]. Image drawn with Biorender.

(II) Tumour immune infiltration - cold tumours, hot tumours

Another reason why anti-tumour immunity is not effective in many cancer patients is believed to be due to a lack of spontaneous priming of anti-tumour CTL responses, resulting in immune ignorance to tumour growth [87]. Tumours from such patients therefore lack infiltrating CTLs altogether and associated T-cell driven inflammation, and have thus been termed "cold tumours" or non-T-cell inflamed tumours [102]. The presence of tumour infiltrating lymphocytes (TILs) in tumours has been shown to be associated with improved prognoses in several cancer types [103].

Defective priming of anti-tumour CTL responses and subsequent absence of TILs in many patients is also considered to be a key reason underlying sub-optimal response rates to immune checkpoint blockade treatment [104]. CPIs function in a non-specific capacity to reactivate tumour-specific T-cells that have become inhibited or exhausted in the TME. Such an approach is therefore unlikely to work in cases where patients have not spontaneously mounted a T-cell response against their tumour.

Indeed, response to immune checkpoint blockade has become highly associated with patients bearing 'hot' T-cell inflamed tumours. These tumours contain higher levels of CD8+ T-cell infiltrate, and possess a T-cell inflamed gene expression signature showing upregulation of IFN-γ and IFN-γ regulated genes [104, 105]. Studies in mice have shown that the expression by tumours of immunosuppressive mechanisms is itself caused by CD8+ T-cell driven

inflammation, rather than being tumour intrinsic [106]. The expression of genes for many immunosuppressive factors such as PD-L1 and IDO is IFN-γ inducible. Their upregulation therefore follows the production of IFN-γ by activated CD8+ T-cells in response to antigen-recognition in the TME, rather than precedes it. RNA-sequencing studies of tumours from cancer patients has shown that a T-cell inflamed tumour microenvironment bearing a IFN-γ-associated gene expression profile is likely necessary for response to anti-PD-1 blockade [105]. Furthermore studies of melanoma patients have shown that the magnitude of CD8 T-cell tumour infiltrate and degree of PD-L1 expression are strongly correlated with a positive clinical response to anti-PD-1 blockade, and may have predictive value for determining those individuals likely to benefit from treatment [93]. Similar observations have been made with response to anti-CTLA-4 blockade [107].

Failure to prime anti-tumour CTL responses can result from defects at several steps of the 'cancer-immunity cycle'. At the first step, tumours may not be sufficiently immunogenic, lacking expression of antigens to induce a specific T-cell response. Due to the mutator phenotype of cancerous cells, tumours are often highly heterogeneous. Immunoediting may occur where immunogenic tumour cell variants in the tumour are progressively destroyed by anti-tumour immune responses [108]. Through the progressive elimination of these cells, the tumour loses expression of immunogenic tumour-specific antigens and less immunogenic tumour cell variants are selected for survival that do not elicit an anti-tumour response [109, 110]. In some cases tumours have been seen to lose expression of MHC-class I altogether [111]. T-cell inflamed tumours have been associated with

having a high mutational burden, and thus increased generation and expression of immunogenic neoantigens, offering a wider array of prospective targets against which anti-tumour T-cell responses can be mounted. Mutational burden is also somewhat predictive of response to immune checkpoint blockade. However, studies have shown that many T-cell non-inflamed tumours have abundant expression of tumour-specific antigens, suggesting that this may be not be the primary underlying reason [112].

In the second instance, it is feasible that tumour cells may undergo non-immunogenic cell death, releasing no DAMPs, therefore failing to activate APCs. Processing of tumour antigen by DCs and presentation to T-cells in a non-inflammatory context can lead to induction of T-cell tolerance to tumour antigens [113].

Alternatively, anti-tumour T-cells may be generated, but the tumour can lack the necessary inflammatory signals for their recruitment to and infiltration into the tumour site. CXCL9/CXCL10 are the key chemokines regulating infiltration of CD8+ T-cells into tumours [114]. Studies on human melanoma biopsies showed that the CD8+ T-cells do not accumulate in the tumour in the absence of these chemokines [115]. CXCL9/CXCL10 are chemoattractants for activated CTLs expressing the chemokine receptor CXCR3. The surface expression of CXCR3 on tumour-specific CTLs therefore is necessary for their trafficking to the tumour bed [116]. Studies have shown that intratumoural CD8a+/CD103+ cDC1s are the main cells in the TME that express and secrete the CXCL9/CXCL10 T-cell homing

signals [117]. CD103+ cDC1s therefore play a highly critical role in the tumour microenvironment (TME) through orchestrating T-cell infiltration into the tumour and generating a T-cell inflamed environment [45]. The absence of cDC1s and deficiency of T-cell chemokine expression in many tumours therefore underlies the 'cold' tumour phenotype. Recent studies have shown the importance of activation of the CXCL9/CXCR3 axis for response to anti-PD-1 treatment [118, 119].

1.3 Therapeutic cancer vaccines

1.3.1 Therapeutic cancer vaccines

The successes and limitations of immunotherapy highlight the need for alternative and complementary approaches. Therapeutic cancer vaccines represent a promising approach. Conversely to the classically understood concept of vaccination as a prophylactic agent given to immunize against the development of disease, the aim of therapeutic cancer vaccination is to treat those with already established disease [120]. The idea of a therapeutic cancer vaccination is a fairly simple one (Figure 1.4). A patient is vaccinated with tumour-specific antigens delivered in a platform that provides an immunogenic context to stimulate the development of tumour-specific T-cells, helping to overcome deficiencies at the priming step of the cancer-immunity cycle.

The induction of sufficiently high tumour-antigen specific CD8+ tumour cells by a vaccine could act therapeutically for cancer patients in isolation, or more likely in concert with other therapies such as immune checkpoint blockade. In particular, a cancer vaccine might hold much promise in expanding the proportion of patients who respond to immune checkpoint blockade monotherapy. This would work by generating a source of tumour-specific CD8+ T-cells de novo in patients that haven't mounted spontaneous anti-tumour responses, and increase T-cell infiltrate, promoting the generation of a T-cell-inflamed TME.

Therapeutic cancer vaccination however is not a new idea and has been tried many times in the past. However almost all therapeutic cancer vaccine attempts to date have failed in the clinic. Varying different vaccine platforms have been trialled such as recombinant proteins, synthetic long peptides, autologous DCs loaded with antigen and viral vectors [121]. Sipuleucel-T (trade name – Provenge) is currently the only vaccine that has been approved for use therapeutically in any cancer indication [122]. Provenge is an autologous cellular vaccine used to treat prostate cancer. Provenge consists of peripheral blood mononuclear cells (PBMCs) enriched from the blood of patients, then incubated ex vivo with a recombinant fusion protein consisting of a prostate cancer antigen, prostatic acid phosphatase (PAP), fused to granulocyte–macrophage colony-stimulating factor (GM-CSF) to activate dendritic cells [122]. The PBMCs, including the activated DC fraction, are reinfused to patients to generate PAP-specific T-cell responses. Provenge was shown in phase III clinical trials to provide a significant increase in overall survival for patients with metastatic castration resistant prostate cancer (mCRPC) [123]. The improvement was however modest, with median survival 4.1 months longer in the treated group (25.8 months) compared to the placebo (21.7 months). However other than Provenge, no therapeutic vaccination has demonstrated significant enough efficacy for approval for use in the clinic. For example, PROSTVAC is another recent high-profile therapeutic vaccine that has also been evaluated for use as treatment for mCRPC. PROSTVAC is based on vaccinia / fowlpox viral vectors and targets the prostate-specific antigen (PSA). This showed promise in phase II clinical trials, but failed to demonstrate an improvement in

overall survival in larger phase III settings, typifying the experience seen with many candidate therapeutic cancer vaccines [124, 125].

The reasons for these failures is likely to have been due to several limitations of the approaches used of which we now have greater knowledge. Given recent developments in the understanding of the regulation of T-cell effector function, it could be because the anti-tumour activity of any T-cell responses induced by vaccination were blunted by the immunosuppressive tumour microenvironment. On this basis, the failed PROSTVAC vaccine is now being tested in clinical trials in combination with checkpoint inhibitors, to see if the combination improves therapeutic efficacy over the vaccine alone [126, 127]. A more fundamental reason still, and perhaps more crucial given data accumulated during those trials, is vaccine design. Most of the vaccine platforms used to date have been suboptimal for inducing high magnitude tumour-specific CD8+ T-cell responses, the primary effectors of the anti-tumour response. Classical vaccine platforms have been developed for the generation of B-cell-mediated antibody responses, which provide the neutralizing response necessary for protective immunity against infectious disease agents [128]. Induced T-cell responses tended to predominantly involve the CD4+ compartment, where CD4+ T-cell help supports B-cell activation and generation of antibody responses. Therefore, classical vaccination approaches have failed in settings such as cancer therapy where CD8+ T-cell immunity is considered to be critical for disease control.

Despite this poor track record, recent advances in both vaccine platform and technology and immunotherapeutic agents that can act in a complementary manner to target suppression in the TME mean that the development of an effective cancer vaccine still represents a promising therapeutic approach [121].

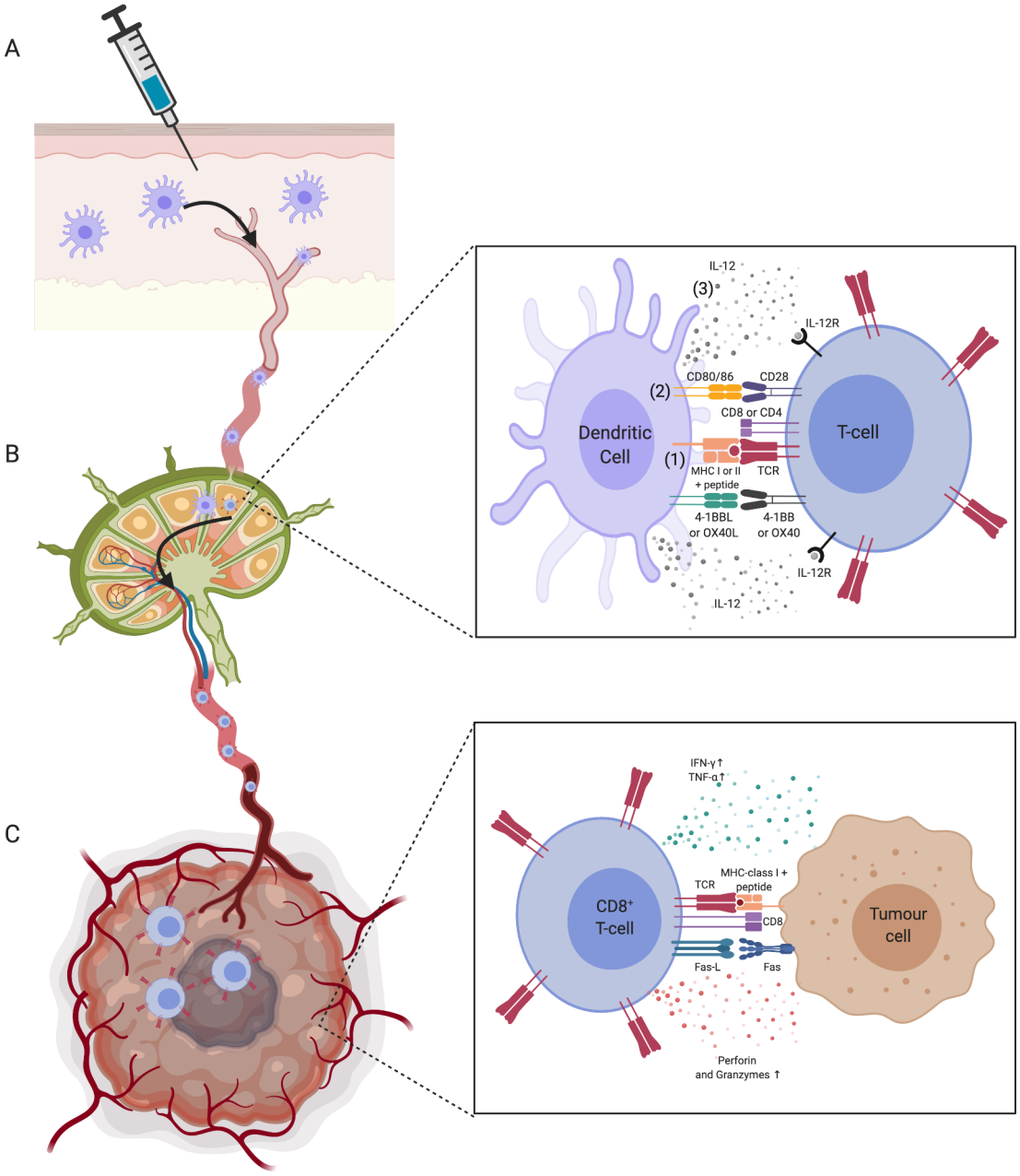


Figure 1.4. Mechanism of therapeutic cancer vaccines. An effective cancer vaccine should function through the generation of tumour-antigen-specific CD8+ T-cells. A) Vaccination delivers a tumour-specific antigen in an inflammatory context, promoting processing of the antigen by APCs at the vaccination site. B) Activated DCs migrate to the lymph nodes where they present processed peptide tumour antigens to naïve CD8+ T-cells via MHC-class I molecules, promoting activation of naïve CD8+ T-cells into CTL effectors. C) Activated CTLs leave the lymph nodes and follow chemokine homing signals to infiltrate the tumour site. Upon recognition of cognate antigen presented on the surface of cancer cells in the context of MHC-class I, CTLs mediate tumour regression by killing target cancer cells through the secretion of effector cytokines such as IFN-γ and TNF-α and cytotoxic molecules such as perforin and Granzyme B. Figure adapted from [121]

1.3.2 Viral vectored vaccines

Vaccines based on recombinant viral vectors are a relatively recent approach that have been developed and tested for efficacy in a range of disease settings where cell-mediated immunity is considered essential for protection [129]. A key advantage of viral vectors is that viruses are naturally immunogenic and stimulate potent CD8+ T-cell driven immune responses though their mechanism of infection. They are highly adaptable, and recombinant viral vectors can be constructed where the target antigen of interest is cloned into the viral genome. Upon vaccination, recombinant viral vectors can infect cells at the injection site such as muscle cells and antigen-presenting DCs and express the recombinant viral transgene intracellularly leading to its accumulation in the cytosol of cells. Importantly viral vectors are 'self adjuvanting', in that by their nature they express a range of PAMPs and therefore stimulate inflammation at the infection site that leads to the necessary activation of innate immune cells such as DCs required to initiate CD8+ T-cell responses. This makes them ideal vectors for vaccines where CD8+ T-cell immunity is required.

The exact mechanism by which viral-vectored vaccination stimulates a CTL response is not completely understood, but potentially proceeds through two routes [130]. It is possible that direct infection of tissue-resident DCs by virus occurs, where intracellular expression and processing in the proteasome of the target antigen and subsequent presentation of peptide epitopes in the context of MHC-class I leads to the generation of antigen-specific CTL responses. However, given the relative rarity of DCs as a cell type in the periphery and the fact that

many viruses that infect DCs are known to impair DC function, this is perhaps not the most prominent pathway [130]. Many viruses induce death of infected muscle and epithelial cells at the infection site, leading to the release of viral transgene encoded antigen into the extracellular space along with DAMPs. Uptake of antigen released by dying or apoptotic cells by DCs recruited to the site of inflammation and subsequent processing/presentation of antigen by the cross-presentation pathway is therefore likely to play a bigger role [131, 132]. DCs can also acquire MHC-class I/peptide complexes from the surfaces of infected cells by a capture mechanism termed cross-dressing [133].

Many different viral vectors from different viral genera have been evaluated for their use as recombinant viral-vectored vaccines – these include adenoviruses (Ad), avian poxviruses - e.g. fowlpox (Fp) and canarypox (ALVAC), mammalian poxviruses – e.g. vaccinia virus (VV) and Modified vaccinia Ankara (MVA), live attenuated yellow fever 17D flavivirus [134, 135], and cytomegaloviruses [136] amongst others. Many of these have been tested in humans, both for infectious disease and in the cancer setting [137]. However, a strategy based on chimpanzee adenovirus (ChAd) and MVA vectors has been shown to be particularly promising based on its highly efficient ability of inducing CD8+ T-cell responses.

1.3.3 ChAdOx1/MVA heterologous prime-boost

Much research has been devoted to determining the most potent vaccination strategy for inducing antigen-specific CD8+ T-cell responses. However, heterologous prime-boost vaccination strategies consisting of a prime vaccination

with recombinant adenoviral vectors and a boost with a recombinant MVA vector have proven the most highly efficient [138]. The use of these vectors was first explored in the infectious disease field to develop vaccines against pathogens where the CD8+ T-cell responses are believed to be the key mechanisms providing effective protective immunity, such as malaria and mycobacterium tuberculosis (*M.tb*). The lack of vaccine platforms capable of generating strong CD8+ T-cell responses in humans has thus far meant that the development effective vaccines against these diseases has proved elusive.

The use of two different recombinant vectors, both encoding the same transgene, as part of a heterologous prime-boost strategy generates higher magnitude responses than either the single use of the vector alone or as part of homologous prime-boost vaccinations [139]. Using two different vectors circumvents neutralizing antibody responses to antigens in the viral capsid that develop following an initial vaccination. Neutralizing antibodies (NAb) blunt much of the infective capability of the vector, preventing delivery of the viral transgene and therefore limiting vaccine potency upon re-use.

Ad vectors have been shown to be highly efficient at priming antigen-specific CD8+ T-cell responses [140, 141]. Conversely, MVA vectors on their own have been seen to be comparatively poor at priming CD8+ T-cell responses but have proven to be exceptional boosting agents [142]. MVA vectors can enhance the magnitude, breadth and duration of CD8+ T-cells responses when administered after an Ad prime vaccination [143]. In murine malaria models, MVA in particular

has been seen to more efficiently boost the magnitude and polyfunctionality of malaria antigen-specific CD8+ T-cells compared to other vectors [142]. The enhanced duration of the responses from Ad/MVA prime-boost was seen to lengthen the window of protection against disease.

Early work with adenoviral vector vaccines focused on human serotype Ad vectors, such as the commonly used human adenovirus serotype 5 (hAd5). In preclinical models, these proved highly effective as part of prime-boost vaccination with MVA [139]. However, NAbs to human Ad vectors are highly prevalent in a large proportion of the human population due to pre-exposure to these viruses in the natural environment [144, 145]. Pre-existing neutralizing immunity is likely to greatly limit the immunogenicity of hAd vectors in humans and thus reduce vaccine efficacy in many individuals. To circumvent this, ChAd vectors have been assessed for use as vaccines, as there is far lower seroprevalence of neutralizing antibodies to these vectors present in most human populations [138, 146]. Screening of different serotypes enabled the identification of vectors that generate very high magnitude CD8+ T-cell responses, with equivalent or superior immunogenicity to hAd vectors [147-149]. ChAd/MVA heterologous prime-boost vaccinations have been shown to induce some of the highest magnitude CD8+ T-cell responses in humans to date of any platform evaluated. ChAd63, a species E ChAd, was the first simian adenovirus to be tested in humans in the setting of Plasmodium falciparum malaria [150, 151]. A prime-boost vaccine with ChAd63/MVA vectors encoding the blood-stage malaria antigen, merozoite surface protein 1 (MSP1) induced the highest MSP1-specific T-cell response as

measured by IFN-γ enzyme-linked immunospot assay (ELISpot) of PBMCs of any vaccine regime tested in clinical trials [151]. Similar results were obtained in clinical trials with the P. falciparum antigen multi-epitope construct, ME-TRAP [150]. ChAd63 /MVA ME-TRAP vaccination provided protection against disease in controlled human malaria infection trials, which correlated with vaccine induced ME-TRAP-specific CD8 IFN-γ responses [152]. ChAdY25 (ChAdOx1), is another type E chimpanzee adenovirus, that has recently been developed and demonstrated comparable immunogenicity to ChAd63 [153]. ChAdOx1/MVA encoding the *M.tb* antigen Ag85A has shown promise in combination with BCG vaccine for improving protection against the development of tuberculosis [154]. Heterologous ChAdOx1/MVA prime-boost vaccination has also been shown to be promising for anti-tumour therapeutic efficacy in a prostate cancer setting for targeting prostate cancer antigens. ChAdOx1/MVA vaccination strategies targeting the tumour-associated antigens STEAP1 and 5T4 have shown high promise as treatment for prostate cancer in both pre-clinical and early stage clinical trial settings [155-157].

1.3.4 Classes of tumour associated antigen

Alongside vaccine platform, the choice of target antigen for a therapeutic cancer vaccine is critical to its effective design [121]. Adaptive anti-cancer immunity relies on the recognition of immunogenic tumour-specific antigens presented on the cell surface in the context of MHC-class I to distinguish malignantly transformed cells from healthy ones. Chosen target antigen(s) must therefore

ideally be both immunogenic and have an expression pattern restricted to cancer cells. There are considered to four broad classes of tumour-antigens; neoantigens, MAGE-type antigens, viral antigens and over-expressed or tissue differentiation antigens [158]. These types of antigens differ hugely in their suitability for use as targets in a cancer vaccine. Overexpressed differentiation antigens are tissue-specific self-antigens that are over-expressed by a tumour. As a result, they are not truly tumour-specific and frequently not very immunogenic due to mechanisms of central tolerance to self-antigens that removes self-reactive T-cells from the T-cell repertoire during T-cell development. Over-expressed antigens can also be aberrantly post-translationally modified by cancer cells to produce new tumour-specific antigens. For example, the cell-surface glycoprotein Mucin-1 (MUC1) is overexpressed in many cancers, but is aberrantly glycosylated within tumour cells leading to its processing in the proteasome [159]. This leads to the generation of novel T-cell epitopes, where aberrantly glycosylated MUC-1 peptides can be loaded onto MHC molecules and recognized by specific T-cell clones [160, 161]. Similar observations have been made regarding the generation of citrullinated proteins [162]. Viral antigens are expressed in cancers that have a viral component to their tumorigenesis such as those induced by HPV or HBV and originate from viral genes expressed in the cancers. These are both truly tumour specific and immunogenic as they are foreign antigens. However, most cancer cases are not virally induced. Neoantigens result from mutations that occur in cancer to the coding regions of genes. Mutations that result in amino acid substitutions and are subsequently expressed can lead to the generation of novel neoepitopes. These are

both specific to the cancer and have been shown to be immunogenic. However, outside of common hotspot mutations, the mutational signature of tumours from different patients are almost completely individual. Furthermore, the targeting of neoantigens with a cancer vaccine, whilst a promising approach, relies on technically complex, personalized pipelines. The remaining class of antigens are the MAGE-type (melanoma-antigen gene) antigens. This family of antigens have a range of properties that make them ideal targets for a cancer vaccine [163], and form the basis of the approach evaluated in this study.

1.3.5 MAGE-type antigens

MAGE-type antigens were amongst the first discovered tumour-specific antigens [158]. MAGE-type antigens result from the expression of genes known as cancer germline (CG) genes. Many CG genes are X-chromosome linked. Under physiological circumstances they have a highly specific tissue expression pattern. In the physiological state they are only expressed in male germline cells, the placenta and cells of the developing trophoblast [164]. This expression pattern would suggest the role they play is largely developmental in function. However, they are aberrantly re-expressed by many cancers. To date, 276 MAGE-type antigens have been defined, with most grouped into larger gene families [165].

Expression of CG genes is primarily regulated by methylation at the gene promoter site [166, 167]. In the majority of adult somatic tissues, CpG islands are methylated, repressing gene expression. However, in cancerous cells, aberrant DNA methylation patterns that arise progressively through the course of tumour

evolution cause their re-expression [168]. There is a strong association of oncogenesis with MAGE gene re-expression. Re-expression of MAGE genes is tightly linked to tumour development and progression. It is believed that their expression in cancer might fulfil a function of helping cells survive in a foreign and hostile tissue environment [169].

The cells of the male germline, placenta and trophoblast are immune privileged sites, and therefore do not express classical MHC-class I genes. This means that whilst CG genes are expressed in these cell types, antigenic peptides from them are not presented to CD8+ T-cells. Most cancer cells do however express MHC-class I genes, and therefore peptides can be loaded onto MHC-class I molecules and recognized by antigen-specific T-cells. Collectively these are termed MAGE-type antigens. By this metric they are ideal antigens to target with a cancer vaccine as it means that they have an effective tumour-specific expression pattern.

Furthermore, many members of the MAGE-type antigen family have been shown to be highly immunogenic. Spontaneous MAGE-type-antigen specific T-cells can be readily detected in the blood and tumours of many cancer patients. Indeed, MAGE-type antigens were amongst the first discovered human tumour-specific antigens against which it could be shown that cytotoxic CTL responses are directed [170, 171]. Experimental evidence using a murine equivalent of the human MAGE-type antigens has shown that CTL responses directed against these antigens can mediate tumour regression [172]. Crucially, antigenic peptides from many MAGE-type antigens have been comprehensively characterized and their

suitability for use in tumour-antigen-specific immunotherapy fully validated [173]. The sequences of antigenic peptide epitopes from many MAGE-type antigens have been defined, and the HLA-restriction of the peptides determined. Furthermore, experimental evidence has shown that peptides are naturally processed and presented by cancer cells in the context of HLA-molecules, enabling their recognition and lysis by isolated stable CTL clones specific for the defined peptide.

This study focuses on two MAGE-type antigens – MAGE-A3 and NY-ESO-1, which are ideal targets for a cancer vaccine strategy [174] [175]. MAGE-A3 and NY-ESO-1 are two of the most highly expressed members of the MAGE-type antigen family in human tumours and have well demonstrated immunogenic properties. Expression of both can be detected in tumours from a high proportion of patients in many different cancers (Table 1.1). Furthermore, gene expression studies have shown that their presence is typically associated with more advanced and aggressive forms of disease [176-179]. Expression of MAGE-A3 and NY-ESO-1 in particular has been shown to be a marker of poor prognosis in NSCLC [176, 180].

Table 1.1. Proportion of patients with different cancer types bearing tumours with detectable MAGE-A3 or NY-ESO-1 expression. Table adapted from [158].

Cancer	MAGEA3 (%)	CTAG1B (NY-ESO-1) (%)
Metastatic melanoma	74	35
Lung carcinoma	47	27
Colorectal carcinoma	17	0
Breast carcinoma	13	23
Prostate carcinoma	18	27

(I) MAGE-A3

MAGE-A3 is part of a larger family of 12 MAGE-A genes located in the q-region of chromosome X [181]. MAGE-A3 expression can be detected in a high proportion of tumours from several cancer types, but particularly in metastatic melanoma and NSCLC (Table 1.1). The gene coding for MAGE-A3 was one of the very first described genes coding for a tumour-specific antigen that could be recognized by autologous CTLs [182]. Spontaneous T-cell responses are not very frequently detected [183] , but MAGE-A3 is expressed in a high proportion of patients of many cancer types. MAGE-A3 specific T-cell responses can be induced and a large number of CD4+ and CD8+ T-cell epitopes presented by common HLA-types have been defined (Table 1.2). A search of the NIH clinical trials database (https://clinicaltrials.gov/) for the terms 'MAGE-A3' and 'cancer' reveals that a total of 44 clinical studies assessing MAGE-A3-based immunotherapeutics were initiated between 1st Jan 2000 and 1st October 2019, indicating its attractiveness as a tumour-specific target.

Table 1.2. MAGE-A3 epitopes experimentally confirmed to be recognized by T-cells from human cancer patients. Information retrieved from [165, 184, 185]

HLA	HLA Frequency (%)	Peptide	Position
A1	26	EVDPIGHLY	168-176
A2	44	FLWGPRALV	271-279
A2	44	KVAELVHFL	112-120
A24	20	TFPDLESEF	97-105
A24	20	VAELVHFLL	113-121
B18	6	MEVDPIGHLY	167-176
B35	20	EVDPIGHLY	168-176
B37	3	REPVTKAEML	127-136
B40	6	AELVHFLLL	114-122
B44	21	MEVDPIGHLY	167-176
B52	5	WQYFFPVIF	143-151
Cw7	41	EGDCAPEEK	212-220
DP4	75	KKLLTQHFVQENYLEY	243-258
DQ6	63	KKLLTQHFVQENYLEY	243-258
DR1	18	ACYEFLWGPRALVETS	267-282
DR4	24	VIFSKASSSLQL	149-160
DR7	25	VIFSKASSSLQL	149-160
DR11	25	GDNQIMPKAGLLIIV	191-205
DR11	25	TSYVKVLHHMVKISG	281-295
DR13	19	AELVHFLLLKYRAR	114-127
DR13	19	LLKYRAREPVTKAE	121-134

(II) NY-ESO-1

NY-ESO-1 was also one of the earliest described MAGE-type antigens [186]. It is expressed in many cancer types, although generally in a lower proportion of patients than MAGE-A3 (Table 1.1). It is considered to be highly immunogenic based on the high-frequency of spontaneous anti-NY-ESO-1 immune responses that can be detected in cancer patients bearing NY-ESO-1+ tumours [179, 187-189]. The majority of cancer patients with NY-ESO-1+ tumours will develop spontaneous NY-ESO-1-specific antibody, CD4+ T-cell and CD8+ T-cell responses [190, 191]. Since its discovery as a tumour antigen, many NY-ESO-1 derived epitopes recognized by human CD4+ and CD8+ T-cells have now been defined (Table 1.3). Like MAGE-A3, many NY-ESO-1-directed immunotherapeutics and cancer vaccines have been evaluated in the clinic. A search of https://clinicaltrials.gov/ for the terms 'NY-ESO-1' and 'cancer' reveals that a total of 136 clinical studies were initiated between 1st Jan 2000 and 1st October 2019. It has been demonstrated that NY-ESO-1 directed CD8+ T-cell responses can provide clinical benefit. Treatment of patients bearing confirmed NY-ESO-1+ metastatic synovial cell sarcomas or metastatic melanomas with an adoptive transfer of autologous T-cells transduced to express an affinity-enhanced TCR recognizing the HLA-A*0201 restricted NY-ESO-$1_{157\text{-}165}$- SLLMWITQC epitope has been shown to produce complete and partial clinical responses in in small scale pilot trials [192, 193]. Similarly promising clinical results have been seen from this same approach in trials involving multiple myeloma patients [194]. Furthermore, detectable anti-tumour CD8+ T-cell responses against NY-ESO-1 correlate with response rates to anti-CTLA-4 blockade in melanoma patients. [195, 196].

Numbers of functional NY-ESO-1 specific CD8+ and CD4+ T-cells have been observed to expand in the blood of patients throughout the course of anti-CTLA-4 treatment [195]. Taken together, this data indicates the importance of CD8+ T-cell responses against these antigens for effective anti-tumour immunity.

Table 1.3. NY-ESO-1 epitopes experimentally confirmed to be recognized by T-cells from human cancer patients. Information retrieved from [165, 184, 185].

HLA	HLA Frequency (%)	Peptide	Position
A2	44	SLLMWITQC	157-165
A2	44	MLMAQEALAFL	ORF2
A31	5	ASGPGGGAPR	53-62
A31	5	LAAQERRVPR	ORF2
B35	20	MPFATPMEA	94-102
B51	12	MPFATPMEA	94-102
Cw3	17	LAMPFATPM	92-100
Cw6	18	ARGPESRLL	80-88
DP4	75	SLLMWITQCFLPVF	157-170
DP4	75	LLEFYLAMPFATPMEAELARRSLAQ	87-111
DR1	18	LLEFYLAMPFATPMEAELARRSLAQ	87-111
DR1	18	EFYLAMPFATPM	89-100
DR2	25	RLLEFYLAMPFA	86-97
DR3	21	QGAMLAAQERRVPRAAEVPR	ORF2
DR4	24	PGVLLKEFTVSGNILTIRLT	119-138
DR4	24	VLLKEFTVSG	121-130
DR4	24	AADHRQLQLSISSCLQQL	139-156
DR4	24	LLEFYLAMPFATPMEAELARRSLAQ	87-111
DR7	25	PGVLLKEFTVSGNILTIRLTAADHR	119-143
DR7	25	LLEFYLAMPFATPMEAELARRSLAQ	87-111
DR15	20	AGATGGRGPRGAGA	37-50

1.3.7 MAGE-targeting cancer vaccines

Given their essentially tumour-specific expression pattern and high immunogenicity, MAGE-type antigens are ideal candidate targets for a cancer vaccine. As they belong to the class of shared tumour-antigens they are expressed by tumours from multiple different patients. This would enable the development of an 'off the shelf' cancer vaccine, circumventing the need for costly and technically challenging personalized approaches.

However, like all attempts to develop effective cancer vaccines, MAGE-targeting vaccines have had a chequered history characterised largely by failure in large-scale clinical trials. Smaller isolated cases however have shown the therapeutic potential of targeting MAGE-type antigens, including MAGE-A3 and NY-ESO-1. In larger clinical trials involving higher numbers of patients however, significant clinical benefit has not been observed. Recently GSK evaluated a MAGE-A3 vaccine in some of the largest clinical trials to date of any therapeutic agent in melanoma and lung cancer [197]. These trials were named DERMA [198] and MAGRIT [199] respectively. In these trials, the therapeutic efficacy of a recombinant MAGE-A3 protein vaccine (rec-MAGE-A3) in combination with an adjuvant AS015 was evaluated as an adjuvant therapy following tumour resection in patients who were pre-screened for tumour MAGE-A3 expression. Both trials measured disease-free survival as the primary endpoint for the study. However, no increase in disease-free survival was observed for patients who received rec-MAGE-A3 + AS015 compared to placebo groups.

As with therapeutic cancer vaccines targeting other antigens, the reason for this is largely believed to be due to the inability of the vaccine platforms designed to consistently induce antigen-specific CD8+ T-cell responses in human patients. In previous clinical work that laid the grounding for the MAGRIT and DERMA trials, CD4+ T-cell and antibody responses against MAGE-A3 were induced in patients following vaccination, but no MAGE-A3-specific CD8+ T-cell responses were observed [200, 201]. Other studies of NSCLC patients have clearly demonstrated that recombinant MAGE-A3 vaccination combined with adjuvant preferentially induces antibody and CD4 responses [202]. Recombinant NY-ESO-1 vaccines administered with adjuvants have also been to induce predominantly CD4+ T-cell and antibody responses [203-205]. What is clear from these trials is that the induction of CD4+ T-cell responses alone is not sufficient for effective anti-tumour immunity against solid tumours such as those of the lung or melanomas. Many other attempts have been made utilizing a wide range of different vaccination platforms. NY-ESO-1 vaccines based on short peptides (corresponding to known epitopes) administered with adjuvant, recombinant vaccinia/fowlpox viral vectors and DC receptor targeting antibodies such as DEC-205 have also been tried in a range of cancers [206-209]. However, like the rec-MAGE-A3 trials, these have also failed to demonstrate clinical efficacy. On the basis, of these findings there is the need to develop more effective MAGE-targeting vaccines.

1.3.8 Next generation MAGE-targeting cancer vaccines

The development of an effective vaccine targeting MAGE-type antigens holds much promise as an effective cancer treatment [210]. A cancer vaccine that induces high magnitude CD8+ T-cell responses could be a highly effective therapy. Given past vaccine failures, there is therefore the need to develop cancer vaccines that induce more potent MAGE-type-antigen specific CD8+ T-cell responses. This could work either alone, or more likely in combination with other immunotherapies. By generating de novo T-cell responses, such an approach could increase the percentage of patients responding to immune checkpoint blockade therapy. Given the excellent results obtained assessing ChAdOx1/MVA vaccination for eliciting CD8+ T-cell responses in human trials for infectious diseases, the platform is ideal for translation to the cancer setting. On the basis of promising data obtained with the platform so far, the evaluation of the platform for inducing MAGE-specific T-cell responses and subsequent extension to other antigens and cancer types is warranted.

The overall aim of this project therefore was to develop and evaluate a vaccination strategy based on a heterologous prime-boost with recombinant ChAdOx1/MVA viral vectors for inducing a high magnitude CD8+ T-cell response against MAGE-type antigens. A further aim was to evaluate in a pre-clinical setting the therapeutic anti-tumour potential of such an approach, alone and in combination with other novel therapeutic agents.

1.4 Aims of the thesis

The specific aims addressed by this study were therefore;

- ➔ To design, develop and test immunogenicity of a vaccination strategy based on ChAdOx1/MVA viral vectors for inducing CD8+ T-cell immunity to MAGE-type antigens – specifically MAGE-A3 and NY-ESO-1

- ➔ To evaluate the therapeutic efficacy of ChAdOx1/MVA vaccine targeting MAGE-type antigens against MAGE-expressing tumours in a pre-clinical setting using murine tumour models.

- ➔ Explore and evaluate the combination of ChAdOx1/MVA vaccine targeting MAGE-type antigens with other novel therapeutics to improve anti-tumour efficacy.

Chapter 2. Materials and Methods

2.1 Materials

2.1.1 Reagents and kits

Table 2.1. List of reagents and kits

Reagent	Supplier	Catalogue No.
ACK (Ammonium-Chloride-Potassium) lysing buffer	Gibco™, ThermoFisher Scientific	A10492-01
Anti-Mouse CD28 (37.51 clone)	Tonbo Biosciences	70-0281-U100
Brefeldin A	Abcam	ab193369
Collagenase type I	Gibco™, Thermo Fisher Scientific	17100017
Cytofix/Cytoperm™ solution	BD Biosciences	554722
Desoxyribonuclease I (DNase I)	Roche	10-104-159-001
EDTA, 0.5M solution	VWR	E522-100ML
Isoflourane	Zoetis, IsoFlo®	50019100
LIVE/DEAD™ Fixable Aqua Dead Cell Stain Kit	Thermo Fisher Scientific	L34965
Perm/Wash™ buffer	BD Biosciences	554723
RNeasy Mini Kit (RNA isolation)	Qiagen	74104
SuperScript™ III Reverse Transcriptase	Invitrogen™, ThermoFisher Scientific	18080044
Oligo(dT)$_{12-18}$ Primer	Invitrogen™, ThermoFisher Scientific	18418012
QuantiTect SYBR® Green qPCR Kit	Qiagen	204143
Takyon ROX Probe Core Kit dTTP	Eurogentec	UF-RPCT-C0201
Trypsin-EDTA (0.05%)	Gibco™, Thermo Fisher Scientific	25300054
Lipofectamine® 2000	Invitrogen™, ThermoFisher Scientific	11668019

2.1.2 Chemicals

Chemical	Supplier	Catalogue No.
5-Aza-2′-deoxycytidine	MP Biomedicals	A3656
Dimethyl Sulfoxide (DMSO)	Sigma Aldrich	D2650-100ML
$KHCO_3$	VWR	0899-500G
NH_4Cl	Sigma Aldrich	A9434
Tetrasodium EDTA (Ethylenediaminetetraacetic acid)	Flourochem	239931

2.1.3 Cytokines

Table 2.2. Details of recombinant cytokines

Cytokine	Supplier	Catalogue No.
rmIL-3	Tonbo	1-8031-U002
rmIFN-γ	Peprotech	315-05

2.1.4 Buffers and media

2.1.4.1 Base media

Table 2.3. Base media used as primary components of media and buffers for cell culture and tissue processing

Reagent	Supplier	Catalogue No.
Dulbecco's Phosphate Buffered Saline (DPBS), 1x	Gibco™, ThermoFisher Scientific	14190-094
Dulbecco's Modified Eagle Medium (DMEM)	Gibco™, ThermoFisher Scientific	31966-021
Iscove's Modified Dulbecco's Medium (IMDM)	Gibco™, ThermoFisher Scientific	21980-032
RPMI 1640 medium	Gibco™, ThermoFisher Scientific	21875-034

2.1.4.2 ACK lysis buffer for mouse blood

ACK lysis buffer was prepared as a 10x stock solution by dissolving 89.9g NH_4Cl, 10.0g $KHCO_3$ and 370mg Tetrasodium EDTA in 1L of double distilled water (ddH_2O) and adjusting the pH to 7.3. The 10x stock was stored for up to 6 months at room temperature (RT) or longer term at -20°C. A 1x solution of working concentration ACK lysis buffer (Table 2.4) was prepared prior to use by diluting 1-part 10x stock in 9-parts ddH_2O.

Table 2.4. Composition of in-house ACK lysis buffer formulated for mouse blood

Reagent	Concentration	Supplier
ddH_2O	-	-
NH_4Cl	0.15M	Sigma Aldrich
$KHCO_3$	1mM	VWR
Tetrasodium EDTA	0.1mM	Flourochem

2.1.4.3 Tumour dissociation buffer

To make tumour dissociation buffer, an appropriate amount of DNaseI and collagenase type I was dissolved in RPMI 1640 medium according to the concentrations given in Table 2.5. Tumour dissociation buffer was freshly prepared for each use.

Table 2.5. Composition of tumour digestion and dissociation buffer

Reagent	Concentration	Supplier
RPMI 1640 medium	-	Gibco™, ThermoFisher Scientific
DNase I	20μg/ml	Roche
Collagenase type I	175U/ml	Gibco™, ThermoFisher Scientific

2.1.4.4 Cell culture media

(I) Complete RPMI medium

Table 2.6. Composition of complete RPMI 1640 medium

Reagent	Concentration	Supplier
Roswell Park Memorial Institute (RPMI) 1640 medium	-	Gibco™, Thermo Fisher Scientific
Foetal Bovine Serum (FBS)	10%	Labtech
L-glutamine (100x)	2mM	Gibco™, Thermo Fisher Scientific
Penicillin-Streptomycin	100U/ml	Gibco™, ThermoFisher Scientific

(II) Complete DMEM

Table 2.7. Composition of complete DMEM

Reagent	Concentration	Supplier
Dulbecco's Modified Eagle Medium (DMEM)	-	Gibco™, ThermoFisher Scientific
FBS	10%	Labtech
L-glutamine (100x)	2mM	Gibco™, ThermoFisher Scientific
Penicillin-Streptomycin	100U/ml	Gibco™, ThermoFisher Scientific

(III) Complete IMDM

Table 2.8. Composition of complete IMDM

Reagent	Concentration	Supplier
Iscove's Modified Dulbecco's Medium (IMDM)	-	Gibco™, ThermoFisher Scientific
FBS	10%	Labtech
L-glutamine (100x)	2mM	Gibco™, ThermoFisher Scientific
Penicillin-Streptomycin	100U/ml	Gibco™, ThermoFisher Scientific

2.1.4.5 FACS buffer

Table 2.9 Composition of FACS buffer

Reagent	Concentration	Supplier
DPBS	-	Gibco™, ThermoFisher Scientific
FBS	2%	Labtech
EDTA	2mM	VWR

2.1.5 Consumables

Table 2.10. List of consumables

Consumable	Supplier	Catalogue No.
BD PlastiPak™ Luer Slip Syringe	BD Biosciences	303172
Cell strainers, 70µm	Falcon, Corning®	352350
Centrifuge tubes, 50ml	Falcon, Corning®	352070
FACS tubes, Polystyrene, 5ml	Sarstedt	55-1579
gentleMACS™ C-tubes	Miltenyi Biotec	130-096-334
Glass slides		
Insulin syringes (29G x 12.7mm), 0.5ml	BD Biosciences	324892
Microcentrifuge tubes, 1.5ml	Eppendorf®	T9661
Scalpel blades, No. 11	Swann-Morton	0203
Syringe needles (23G x 16mm)	Agani, Terumo	AN2316R1

2.1.6 Instruments

Table 2.11. List of instruments

Instrument	Supplier
BD Fortessa flow cytometer	BD Biosciences
Countess™ II cell counter	Thermo Fisher Scientific
gentleMACS dissociator	Miltenyi Biotec, Surrey, UK
StepOnePlus™ Real-Time PCR System	Thermo Fisher Scientific
SH800z FACS sorter	Sony
NanoDrop 2000	ThermoFisher Scientific

2.1.7 Software

Table 2.12. List of software

Software	Supplier
FlowJo version 10	Tree Star, Ashland, OR, UDA
GraphPad Prism version 8	GraphPad software, CA, USA
Net-MHC version 4	Department of Bio and Health Informatics, Technical University of Denmark, Lyngby
Pestle version 2	National Institutes of Health, Bethesda
Simplified Presentation of Incredibly Complex Evaluations (SPICE) version 6	National Institutes of Health, Bethesda

2.1.8 Cell lines

P815, V4D6, 15V4T3 and EL4 cell lines were provided by Prof. Benoit Van den Eynde's lab, Ludwig Institute for Cancer Research (LICR) Brussels branch, Université catholique de Louvain. MC38 cells were a kind gift from Prof. Xin Lu's lab, Ludwig Institute for Cancer Research, Oxford branch, University of Oxford. B16F10 cells were a kind gift from Prof. Adrian Hill's group, Jenner Institute, University of Oxford.

2.1.9 Flow cytometry antibodies

(I) T-cell ICS panel

Table 2.13. Details of antibodies used in T-cell ICS panel

Antigen	Fluorophore	Dilution Factor	Supplier	Clone
anti-mouse CD16/CD32 (Fc block)	N/A	1:100	BD	2.4G2
CD8	FITC	1:200	BioLegend	53-6.7
CD4	Pacific Blue	1:200	BioLegend	GK1.5
IFN-γ	APC	1:200	BioLegend	XMG1.2
TNF-α	BV650	1:250	BioLegend	MP6-XT22
IL-2	PE	1:200	BioLegend	JES6-5H4

(II) Effector T-cell panel

Table 2.14. Details of antibodies used in effector T-cell panel

Antigen	Fluorophore	Dilution Factor	Supplier	Clone
anti-mouse CD16/CD32 (Fc block)	N/A	1:100	BD	2.4G2
CD3	APC	1:100	BioLegend	17A2
CD8	FITC	1:200	BioLegend	53-6.7
CD4	AlexaFluor 700	1:200	BioLegend	GK1.5
CD62L	APC-Cy7	1:200	BioLegend	MEL-14
CD44	BV650	1:200	BioLegend	IM7
PD-1	PE-Cy7	1:200	BioLegend	29F.1A12
CXCR3	BV421	1:100	BioLegend	CXCR3-173
MHC-class I tetramer	PE	1:200	LICR, Brussels	N/A

2.1.10 MHC-class I multimers

H-2L^{d}/P1A$_{35-43}$- LPYLGWLVF and H-2Db/P1A$_{43-51}$-FAVVTTSFL MHC-class I multimers were produced and provided by the Ludwig Institute for Cancer Research Brussels branch.

2.1.11 Vaccines

ChAdOx1 and MVA viral vectors were produced by the Viral Vector Core Facility (VVCF) at the Jenner Insitute, University of Oxford, UK.

Table 2.15. Details of viral vectored vaccines used in this study

Vector	Insert
ChAdOx1	MAGE-A3-NY-ESO-1
	htPA-MAGE-A3-NY-ESO-1
	hIi-MAGE-A3-NY-ESO-1
	P1A
	mIi-P1A
MVA	MAGE-A3
	htPA-MAGE-A3
	NY-ESO-1
	htPA-NY-ESO-1
	P1A
	mtPA-P1A

2.1.12 Therapeutic monoclonal antibodies

Table 2.16. List of therapeutic monoclonal antibodies

Antigen	Clone	Supplier
CTLA-4	9H10	BioXcell
PD-1	RMPI-14	BioXcell
Rat IgG2a isotype control	2A3	BioXcell
Syrian Hamster isotype control	N/A	BioXcell

2.1.13 Peptides

Peptide libraries (PepSets™) for the MAGE-A3, NY-ESO-1 and P1A proteins used for T-cell stimulations were synthesised by Mimotopes (UK). The libraries for each protein consisted of 15-mer peptides overlapping by 10 amino acids and spanning the whole length of the protein. Individual peptides were initially dissolved in DMSO at a concentration of 50mg/ml and then grouped together into pools used for stimulations. Details of the peptide sequences contained in each of the MAGE-A3, NY-ESO-1 and P1A pools can be found in the appendix (Tables).

2.1.14 Mice

Six-8 week-old CD1, C57BL/6 and DBA/2 mice used in this study were purchased from Envigo, UK and housed in the Functional Genomics Facility (FGF), University of Oxford. For the majority of studies presented in this thesis, experimental procedures were carried out in accordance with the terms of the UK Animals (Scientific Procedures) Act Project License (PPL) (P0D369534). This is with the exception of studies involving the use of 5-aza-2'-deoxycytidine

treatment which were carried out under PPL PABB93399. Experimental group sizes were calculated by performing power calculations to determine the numbers of mice needed, taking into account minimum effect sizes to be detected, standard deviation of the data type (using in-house data or that in published literature), thresholds for statistical significance, and the desired power of the experiment [211, 212].

2.2 Methods

2.2.1 ChAdOx1 and MVA viral vector construction

Transgene insert sequences were cloned into ChAdOx1 and MVA viral vectors by Dr Carol Leung and Emily Pollock. Viruses were produced by the VVCF, Jenner Institute, University of Oxford.

2.2.2 Cell culture

P815, MC38, B16F10 and EL4 cell lines were cultured in complete DMEM (Table 2.7). 15V4T3 cell lines were cultured in complete IMDM (Table 2.8). Cell cultures were maintained in an incubator set at 37°C 5% CO_2. To promote recovery from cryostorage, 15V4T3 cells were thawed into complete IMDM medium containing 25U/ml of recombinant mouse IL-3 (rmIL-3).

Cells were passaged before reaching confluency to maintain cell growth in the log-phase. When approaching confluency, suspension cell lines were passaged by diluting the cell suspension in pre-warmed complete medium to the desired splitting ratio and transferred to fresh tissue culture flasks. Adherent cell lines were passaged by first washing cells with PBS to remove residual cell culture medium, and then incubating with trypsin-EDTA (0.05%) at 37°C to detach cells from the surface of the tissue culture flask. Trypsinisation was terminated by the addition of cell culture medium and detached cells were then seeded in fresh tissue culture flasks at the desired density for downstream applications.

2.2.3 In vitro studies

2.2.3.1 Assessment of cell surface PD-L1 expression level on cancer cell lines

To analyse PD-L1 expression on the surface of murine cancer cell lines, cells were first seeded in cell culture flasks, then treated with either 20ng/ml or 100ng/ml of rmIFN-γ for 24-48 hours. Cells were harvested and $1x10^6$ cells were then stained in 5ml FACS tubes with anti-PD-L1-PE (clone 10F.9G2, BioLegend) or a rat IgG2b isotype control antibody (clone RTK4530, BioLegend) at a concentration of 1:200 and viability dye (LIVE/DEAD Aqua, Invitrogen) for 30 minutes at 4°C in 50µl staining buffer (1x PBS). Cells were then washed with 3ml ice-cold PBS, centrifuged at 500g for 5 mins at 4°C and resuspended in 100µl FACS buffer. Samples were analyzed by flow cytometry on a BD Fortessa instrument and PD-L1 expression level determined by measuring geometric mean fluorescence intensity (MFI).

2.2.3.2 5-aza-2′-deoxycytidine (5-aza-dC) treatment of cell lines

5-aza-dC stock was prepared at a concentration of 220mM by diluting powdered compound in DMSO, and stored at -20°C. Further dilutions to achieve a working concentration stock of 1mM were carried out by diluting in 1x PBS. Cells were seeded at a density of 0.1×10^6 cells per well of a 6-well dish. 5-aza-dC was added to cell culture medium at a concentration of 0.1-10µM. Cells were cultured with 5-aza-dC for 48 hours and then for a further 24 hours with fresh media. Cells were then harvested for RNA isolation and assessment of P1A expression by rt-qPCR.

2.2.3.3 Generation of P1A-expressing murine cancer cell lines

(I) Lipofectamine 2000 transfection

MC38 or B16F10 cells were seeded in 6-well plates overnight to achieve 70-80% confluency the following day. Cells were then transfected with a pEF4/V5 His A plasmid (Figure 2.1) containing a P1A gene expression cassette under the control of a human elongation factor-1 alpha promoter (EF-1a) using Lipofectamine 2000 reagent, according to the manufacturer's protocol. Briefly, for each well transfected, 2.5µg pEF4/V5 His A P1A DNA (or control vector) was diluted in 150µl Opti-MEM® Medium and 6µl Lipofectamine® 2000 reagent was diluted in 150µl Opti-MEM® Medium. Diluted DNA was then added to diluted lipofectamine at a 1:1 ratio and reagents incubated together for 5 minutes at room temperature. To transfect cells, 250µl pDNA lipid complex mixture was then added drop-wise into the cell medium of the tissue culture plate wells. Cells were incubated with pDNA-lipid mixture for 8 hours, before the cell medium was replaced with fresh cell culture medium.

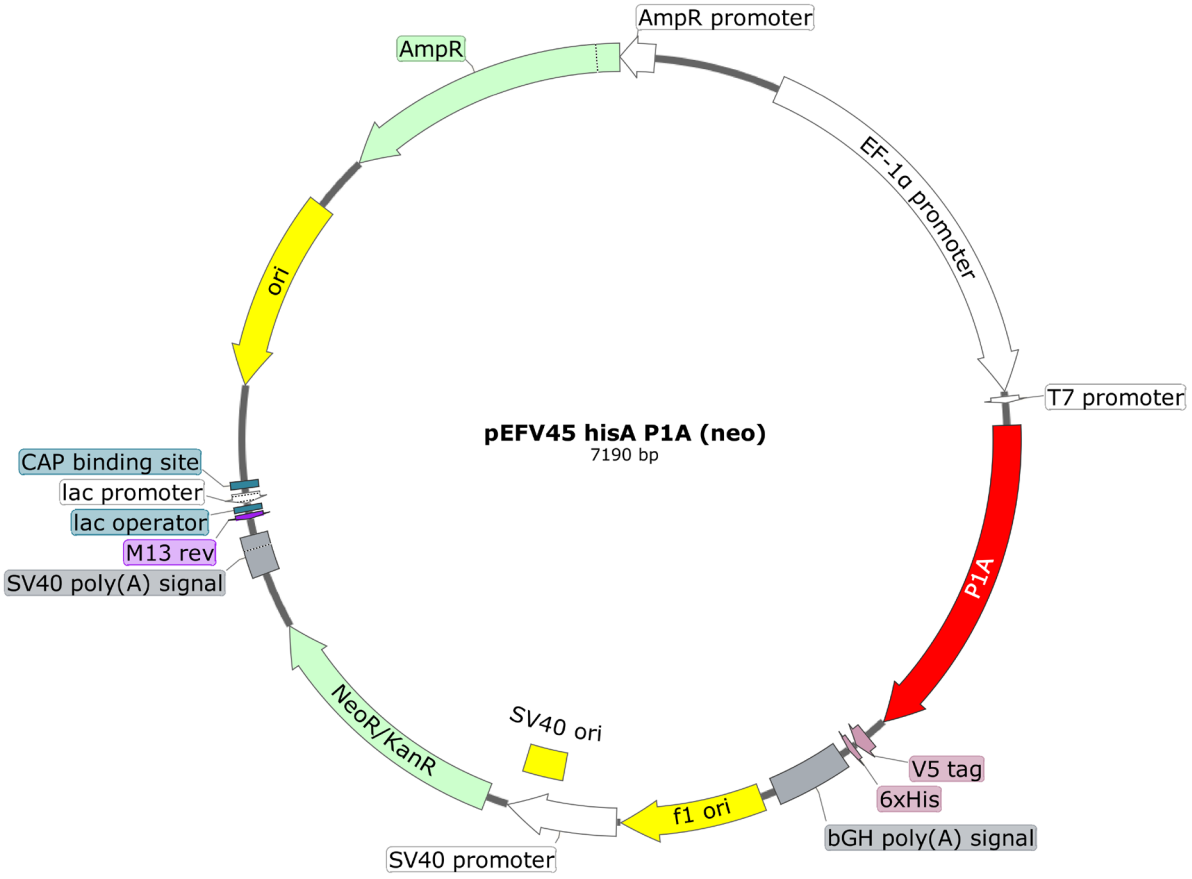


Figure 2.1. Map of pEF4/V5 hisA P1A plasmid used for stable transfection of murine cancer cell lines.

(II) Neomycin selection and P1A+ clone isolation via single-cell sorting

The pEF4/V5 His A P1A plasmid also encoded a neomycin resistance gene, and stable transfectants were selected through continued culture with neomycin-containing cell culture medium for 4 weeks. Following selection, single cells were isolated into 96-well plates via FACS sorting using a Sony SH800z. Clones generated by single-cell sorting were then expanded, and cells harvested for screening of P1A-expression of qPCR. Select P1A+ clones were cryogenically stored for further applications.

2.2.4 In vivo mouse studies

2.2.4.1 Immunisation

To assess vaccine immunogenicity, CD1, C57BL/6 and DBA/2 mice were vaccinated with ChAdOx1 and MVA viral vectors encoding either MAGE-A3, NY-ESO-1 or P1A antigens. Vaccinations were performed under inhalational anaesthesia, using isofluorane as the anaesthetic agent. A dose of either 10^8 or 10^7 infectious units (IU) of ChAdOx1 virus and 10^7 or 10^6 plaque forming units (PFU) of MVA virus was given via intramuscular injection (i.m.) into the thigh in a total volume of 50µl per animal. The vehicle used for all vaccinations was sterile DPBS. Vaccinations were performed at varying intervals indicated in the scheme for each study. Immunizations with L1210.P1A.B7-1 cells were performed by i.p injection, with $1x10^6$ L1210.P1A.B7-1 cells in 200µl DMEM without supplements. Antigen-specific immune responses in the blood, spleen or tumour were measured at the indicated time-points for each study post vaccination.

2.2.4.2 CPI treatment

To assess the therapeutic effect of combined ChAdOx1/MVA vaccination and CPI treatment, mice were administered with monoclonal antibodies against either PD-1, CTLA-4 or the relevant isotype control via intraperitoneal injection (i.p.). These were administered at a dose of 100µg per mouse in 100µl total volume and a total of 3 doses were given, each 3 days apart at the indicated time-points for each study. The vehicle used for all CPI antibody injections was sterile DPBS. Diluted CPIs were made up immediately prior to use kept on ice until administration.

2.2.4.3 5-aza-2'-deoxycytidine treatment

To assess the therapeutic effect of combined ChAdOx1/MVA vaccination and 5-aza-dC treatment, mice were administered with 5-aza-dC at a dose of 0.5-1.0mg/kg body weight given via i.p. injection once per day at the indicated time-points for each study. Stock 5-aza-dC (220mM) was first diluted in DPBS to the desired working concentration. Diluted 5-aza-dC was made up immediately prior to use and kept on ice until administration.

2.2.4.4 Syngeneic tumour models

(I) Tumour implantation

To assess the protective and therapeutic efficacy of ChAdOx1/MVA P1A vaccinations in syngeneic tumour models, mice were injected subcutaneously (s.c.) in the right flank with either 1 x 10^6 P815, 1 x 10^6 15V4T3 cells or 1 x 10^5 MC38 cells suspended in 100ul of cell culture medium without added supplements (minimal culture medium). Prior to injection, cells were washed with minimal culture medium to remove traces of FCS present in the complete growth medium. The procedure to wash cells was to harvest them from their culture flask as a single cell suspension and transfer to a 50ml Falcon tube, spin the cell suspension at 400g for 5 mins to obtain a cell pellet, aspirate off the cell culture medium, then resuspend the cell pellet in 45ml of minimal culture medium. Three washes were carried out. After the third wash cells were manually counted using a haemocytometer and the degree of viability assessed using the Trypan blue

exclusion method. The cells were then resuspended at the required concentration for implantation.

(II) Tumour study

Following s.c. injection, mice were then monitored for tumour growth. Upon the development of palpable tumours, measurements of tumour length and width were carried out 2-3 times per week using digital callipers. The volume of tumour masses (V) was calculated according to the formula: $V = ((\text{length (mm)} \times \text{width}^2 \text{ (mm)}) \times 0.52)$. Mice were sacrificed via cervical dislocation when tumour size reached 12mm in any direction, and this maximal tumour burden was defined as the end-point of tumour studies. In some studies, further analysis was carried out on tumour tissue. Tumour masses were surgically excised, weighed and then divided into portions for RNA/gene expression analysis and flow cytometry. Samples for RNA extraction were immediately snap frozen in liquid nitrogen, then transferred to -80°C freezer for storage. Samples for flow cytometric analysis were stored briefly in RPMI 1640 and kept on ice for processing.

2.2.5 Flow cytometric analysis

2.2.5.1 Collection of tissues and tissue processing

The methods for processing mouse tissues to obtain single cell suspensions for flow cytometric analysis are described in this section. Samples were kept cold on ice during all stages of processing with the exception of steps requiring incubation at a specified temperature. All centrifugations were performed at 4°C.

(I) Blood sampling

To obtain murine PBMCs for ex vivo assessment of vaccine induced T-cell responses, blood was collected from mice via a tail vein bleed. Mice were first warmed in a heat box for 15 minutes at 38°C to promote vasodilation and then a small incision was made in the lateral tail vein using a scalpel blade. Blood was then collected into 1.5ml Eppendorf tubes containing 200µl of 12.5mM EDTA in PBS to inhibit coagulation. Typically 150µl of blood would be collected. No more than 10% of a mouse's total blood volume was collected at any one time and no more than 15% of total blood volume was collected within a month as stipulated in the terms of the PPL. Following blood collection, red blood cells were lysed to enrich for the PBMC fraction by incubating samples in an in-house ACK buffer formulated for use with mouse blood (Table 2.4). This step was performed as follows: 500µl of ACK lysis buffer was added to the collected blood samples after which they were transferred to 5ml FACS tubes. The blood was then incubated with ACK buffer for 5 minutes at room temperature (RT) before a further 500µl of ACK buffer was added, after which samples were incubated at RT for an additional 5 minutes. The blood samples were then washed with cold (4°C) 1x PBS, resuspended in 1ml ACK buffer and incubated for a further 5 minutes at RT. Blood samples were then washed twice more with cold (4°C) 1x PBS before being resuspended in complete RPMI medium (Table 2.6) prior to downstream analysis.

(II) Spleens

At the termination of experiments, mice were sacrificed via cervical dislocation. Spleens were removed via surgical excision and transferred to 1.5ml Eppendorfs

containing 1ml of 1x PBS and kept on ice. Spleens were then processed to obtain single cell suspensions of splenocytes to evaluate antigen-specific immune responses. Initially, spleens were mashed between two glass slides then passed through a 70µm cell strainer into a 50ml Falcon tube and washed with 15ml of cold (4°C) 1x PBS. Cells were then pelleted by spinning the samples at 500g for 5 minutes. Cell pellets were then resuspended in 1ml of ACK buffer (Gibco) to lyse red blood cells. The lysis reaction was stopped by adding 29ml of cold (4°C) 1x PBS after which each cell samples was passed again through a 70µm cell strainer. The samples were then centrifuged at 500g for 5 minutes to pellet the cells before being resuspended in complete RPMI medium (Table 2.6) prior to downstream analysis. Total cell numbers and concentrations were determined by counting with an automated Countess II cell counter.

(III) Tumours

To analyse the immune infiltrate in 15V4T3 tumours, tumours were harvested into 1ml of RPMI 1640 medium in 1.5ml Eppendorf tubes. Tumours were then transferred into gentleMACS C-tubes containing 5ml of tumour dissociation buffer (Table 2.5). To obtain single cell suspensions, tumours were dissociated using programme m_impTumor_01 of the gentleMACS dissociator instrument (Miltenyi Biotec) and incubated for 45 minutes in tumour dissociation buffer at 37°C and 5% CO_2. Following incubation cell suspensions were passed through a 70µm cell strainer and washed with 15ml of PBS to remove fat and debris. Any remaining pieces of tumour tissue were dissociated by mashing through the cell strainer with the end of the plunger of a 5ml syringe. Each cell suspension was

passed a second time through a 70µm cell strainer and washed with PBS before being resuspended in FACS buffer (Table 2.9) for downstream analysis. Total cell number and concentration was then determined via manual counting using a haemocytometer and cell viability assessed through trypan blue staining.

2.2.5.2 Measurement of antigen-specific T-cell responses

(I) Ex vivo peptide stimulation

To detect antigen-specific T-cells induced by vaccination via cytokine production, PBMCs or splenocytes isolated from mice were transferred to 96-well V-bottom plates and stimulated with 4µg/ml of MAGE-A3, NY-ESO-1 or P1A peptides (pools or individual peptides) at 37°C and 5% CO_2 for 5 hours. Stimulations were carried out in a total volume of 200µl in complete RMPI 1640 medium supplemented with DNaseI (20µg/ml, Roche) and anti-mouse CD28 (2µg/ml, Tonbo Biosciences). For every sample an equivalent volume of DMSO (peptide diluent) was used in place of peptides as a negative unstimulated control to establish levels of background cytokine production. To inhibit cell secretion and promote intracellular cytokine accumulation, cells were stimulated for the final 4 hours in the presence of brefeldin A, with 2µl of 100x brefeldin A added to every well (10µg/ml final working concentration) after the first hour of stimulation.

(II) Intracellular cytokine staining assay (ICS)

Immediately following stimulation, cells were stained with fluorescently-conjugated antibodies against surface and intracellular markers. All staining steps were carried out in a 96-well V-bottom plate. Samples were kept cold on ice during processing and centrifugations were performed at 4°C.

Initially, cells were washed with 200µl PBS and then Fc receptors blocked via incubation in 50ul anti-mouse CD16/CD32 antibody (5µg/ml) diluted in 1x PBS for 10 minutes at 4°C. Cells were then washed again with 200µl PBS and staining

for surface markers was performed. Cells were stained via incubation with 50µl of fluorochrome-conjugated antibodies (anti-CD8-FITC, anti-CD4-BV421) and viability dye (LIVE/DEAD Aqua, Invitrogen) diluted in 1x PBS for 20 minutes at 4°C. After surface staining cells were washed twice with 200µl PBS and then fixed and permeabilized by incubation in 100µl of CytoFix/CytoPerm buffer (BD Biosciences) for 20 minutes at 4°C. Following fixation/permeabilization cells were washed twice with 1x Perm/Wash buffer (BD Biosciences) and then stained for intracellularly for the cytokines IFN-γ, IL-2 and TNF-α. Cells were stained with 50ul fluorochrome-conjugated antibodies (anti-IFN-γ-APC, anti-IL-2-PE, anti-TNF-α-BV650) diluted in 1x Perm/Wash buffer for 20 minutes at 4°C. After staining cells were washed twice more with 1x Perm/Wash buffer and then resuspended in 120ul of 1x Perm/Wash buffer. Cells were then acquired and analyzed using a Fortessa flow cytometer (BD Biosciences).

(III) MHC-class I multimer and surface antigen staining

Following processing, PBMCs, splenocytes or tumour cells were transferred to 5ml FACS tubes for detection and phenotyping of antigen-specific T-cells via staining with MHC-class I multimers and antibodies against surface markers. Samples were kept cold on ice during processing and all centrifugations were performed at 4°C. Cells were first washed with 3ml of cold (4°C) PBS and then Fc receptors blocked via incubation in 50µl anti-mouse CD16/CD32 antibody (5µg/ml) diluted in 1x PBS for 10 minutes at 4°C. Cells were then washed again with 3ml cold (4°C) PBS and stained with 50µl of PE-conjugated P1A-specific multimer diluted 1:250 in PBS for 30 minutes at 4°C. H-2L^{d}/P1A$_{35-43}$-

LPYLGWLVF was used for samples from DBA/2 mice whilst H-2D^b/P1A$_{43\text{-}51}$ FAVVTTSFL was used for samples from C57BL/6 mice. Following multimer staining, samples were washed with 3ml PBS and then stained for cell surface markers. Cells were stained via incubation with 50µl of fluorochrome-conjugated antibodies (anti-CD3-APC, anti-CD8-FITC, anti-CD4-Alexaflour-700, anti-CD44-BV650, anti-CD62L-APC-Cy7, anti-CXCR3-BV421 and anti-PD-1-PE-Cy7) and viability dye (LIVE/DEAD Aqua, Invitrogen) diluted in PBS for 20 minutes at 4°C. After surface marker staining cells were washed with 3ml PBS and resuspended in 100µl FACS buffer prior to sample acquisition using a Fortessa flow cytometer (BD Biosciences).

2.2.6 Flow cytometry data analysis

Flow cytometry data were analysed using FlowJo software version 10 (Tree Star, Ashland, OR). Representative diagrams of the gating strategies used for the different flow cytometry panels are shown and described in the following sections -- intracellular cytokine staining (Figure 2.2) and effector T-cells (Figure 2.3).

(I) Intracellular cytokine panel

Lymphocytes were gated on a forward scatter area (FSC-A) vs side scatter area (SSC-A) pseudocolour dot plot. Single cells were gated through a forward scatter-area (FSC-A) vs forward scatter-height (FSC-H) plot. Dead cells were excluded through the LIVE/DEAD Aqua staining. T-cells were gated on a CD4 vs CD8 plot. Antigen-specific T-cells responding to antigenic stimulation were enumerated by gating on IFN-γ+, TNF- α+, IL-2+ events in the CD8+ and CD4+ populations.

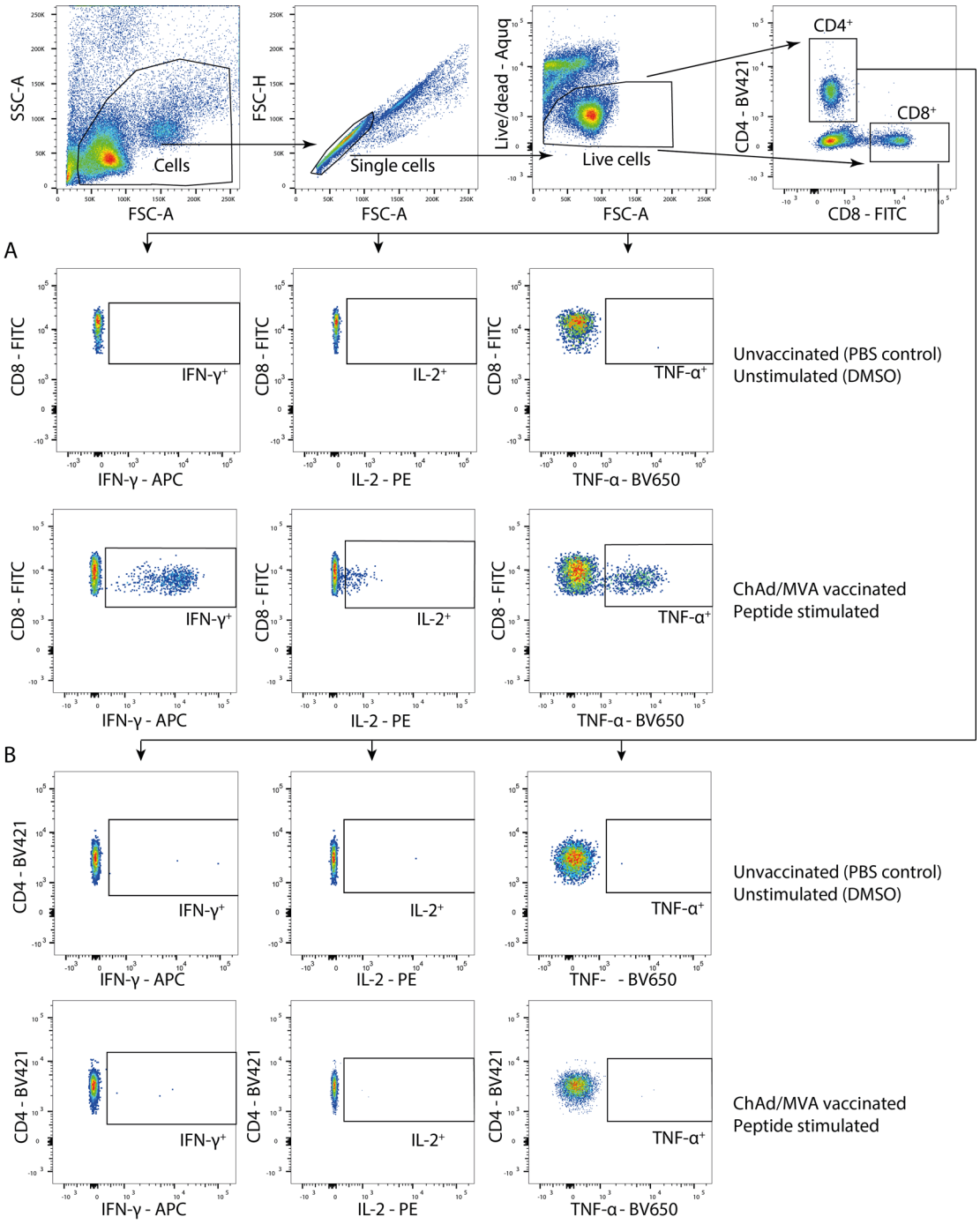


Figure 2.2. Flow cytometry intracellular cytokine staining gating strategy. Cells were first gated based on FSC-A and SSC-A properties to exclude debris. Single cells were then gated to exclude doublets and aggregates based on a FSC-H vs FSC-A plot. Live single cells were then gated based on staining with a LIVE/DEAD Aqua marker. CD8+ and CD4+ cells were then discriminated via a CD8 vs CD4 plot. Antigen-specific T-cells responding to antigenic stimulation were then identified by gating on IFN-γ+, TNF- α+, IL-2+ events in the CD8+ (A) and CD4+ (B) populations. The gates for the cytokine positive cells were set based on the staining signal observed in unstimulated cells taken from unvaccinated control animals.

(II) Tumour infiltrating lymphocyte / effector T-cell panel

Lymphocytes were gated on a FSC-A vs side scatter SSC-A pseudocolour dot plot. Single cells were gated through FSC-A vs FSC-H plot. Dead cells were excluded through the LIVE/DEAD Aqua staining. T-cells were identified as CD3+ and then further discriminated by gating on a CD4 vs CD8 plot. Naïve, effector/effector memory (T_{EM}) and central memory (T_{CM}) T-cells were identified by gating on CD62L vs CD44 within the CD8+ or CD4+ populations. P1A-specific CD8+ T-cells were identified by tetramer+ cells within the CD8+ T-cell population. CD8+ and CD4+ T-cells were further assessed for expression of CXCR3 and PD-1. Manual gates were drawn for all non-lineage markers based on the staining observed in florescence minus one (FMO) controls.

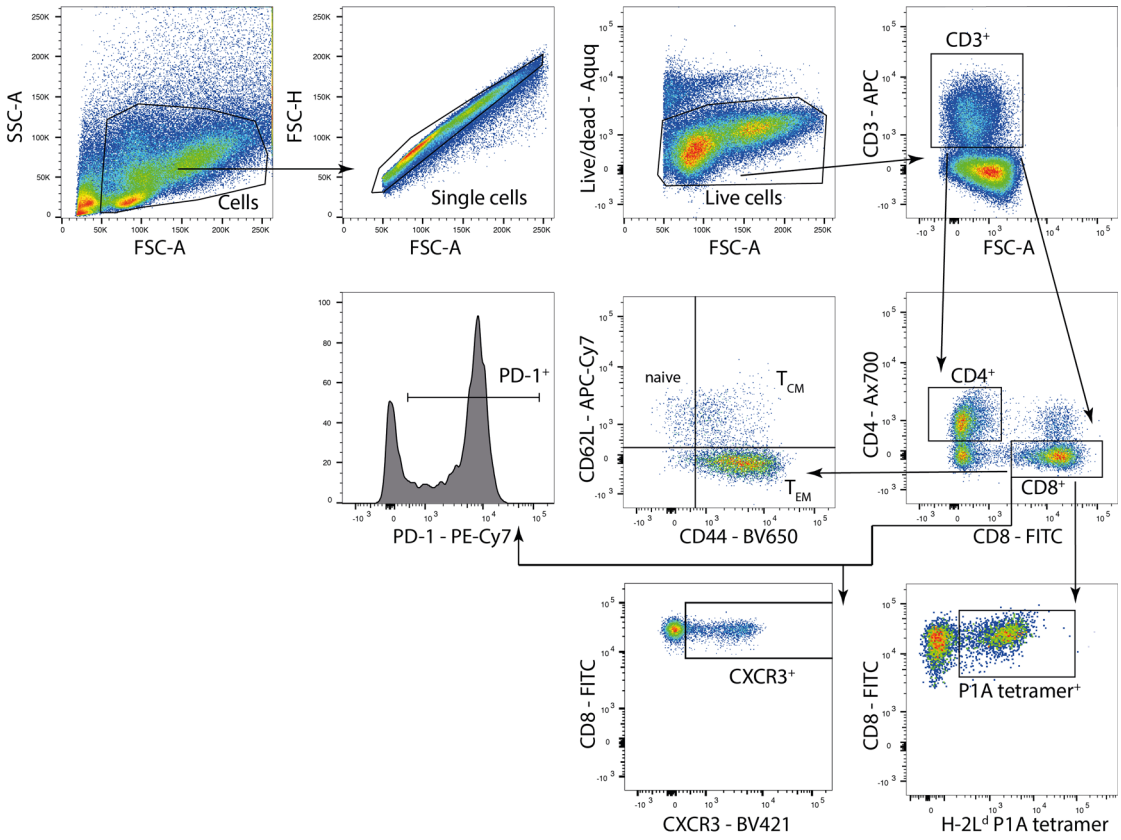


Figure 2.3. Flow cytometry effector T-cell / P1A tetramer panel staining gating strategy. Cells were first gated based on FSC-A and SSC-A properties to exclude debris. Single cells were then gated to exclude doublets and aggregates based on a FSC-H vs FSC-A plot. Live single cells were then gated based on staining with a LIVE/DEAD Aqua marker. T-cells were then identified based on CD3+ expression and further discriminated by CD8 vs CD4 expression. CD8+ T-cells were then further characterized as naïve, effector/effector memory (T_{EM}) and central memory (T_{CM}) T-cells using CD44 vs CD62L expression. Expression of PD-1, CXCR3 by CD8+ T-cells and the proportion of P1A-specific tetramer+ CD8+ T-cells were also determined. Gates for positive staining for all activation (non-lineage) markers (CD44, CD62L, PD-1 and CXCR3) and the P1A-specific tetramer were set using the signal observed from tissue-specific FMOs.

To calculate absolute numbers of a particular cell population in a harvested tissue sample, the total number of live cells isolated from the tissue was multiplied by the proportion of that particular population in the sample (of total live cells) as determined by flow cytometry. This was then normalized to the mass of tissue harvested to determine cell number per mg of tissue.

$$\text{Total cell number (subset X) per mg} = \frac{\left(\text{total number live cells harvested}\right) \times (\%\ \text{of cell subset X in sample})}{\text{Total mass of tissue harvested (mg)}}$$

(III) T-cell polyfunctionality analysis

Analysis of multifunctional CD8+ T-cell responses was performed by carrying out a Boolean analysis of IFN-γ+, TNF- α+, IL-2+ events in the CD8+ gate in FlowJo software. Pestle (NIH, Bethesda) and SPICE (Vaccine Research Centre, NIH, Bethesda) software were then used to further analyse these data and generate graphical representations of the proportion of T-cells expressing either 1, 2 or all 3 cytokines.

2.2.7 Gene expression analysis

Gene expression was quantified at the transcriptional level for various target genes – *P1A, Ccl5*, *Cxcl9*, *Cxcl10*, *Cd274*, *Gzmb* and *Ifng*.

(I) RNA extraction from cell culture

Cells were harvested directly from tissue culture dishes and then centrifuged at 500g to pellet cells, and lysed using 350µl RLT lysis buffer (Qiagen). Total cellular RNA was then isolated using an RNeasy mini kit (Qiagen) according to the manufacturer's instructions, incorporating on column RNase-free DNase I (Qiagen) digestion to remove genomic DNA. RNA was eluted in 30µl nuclease-free H_2O. RNA concentration was determined using a NanoDrop 2000 spectrophotometer (ThermoFisher Scientific).

(II) RNA extraction from murine tumours

Snapfrozen tumour samples were placed into 2ml Eppendorf tubes and homogenised using a mechanical tissue disruptor into 650µl RLT lysis buffer

(Qiagen). Total cellular RNA was isolated using an RNeasy mini kit (Qiagen) with on column RNase-free DNase I (Qiagen) digestion to remove genomic DNA. RNA was eluted in 30µl nuclease-free H_2O. RNA concentration was determined using a NanoDrop 2000 spectrophotometer (ThermoFisher Scientific).

(III) Reverse transcription RNA to cDNA conversion

A total of 0.5µg RNA was used to synthesize first single-strand cDNA using the SuperScript III First-Strand Synthesis kit (Thermo Fisher). Reactions were performed according to the manufacturer's protocol.

(IV) Real-time quantitative polymerase chain reaction (RT-qPCR)

For quantification of mRNA expression by rt-qPCR, the QuantiTect SYBR Green PCR kit (Qiagen) was used and reactions set up according to the manufacturer's instructions. Reactions were run on the StepOnePlus™ Real-Time PCR System (Applied Biosystems) at the following conditions - 95°C - 15 minutes, (94°C 15s + 60°C 30s + 72°C 30s) x 40 cycles. Gene expression at the mRNA level for each target gene assayed was quantified relative to an internal housekeeping gene control. The housekeeping genes used were either *ActB* or *Hprt1*. To determine relative mRNA expression, the mean ΔCt (difference in cycle threshold number) was calculated for each target gene relative to *ActB* or *Hprt1*. ΔCt for a given target gene in each sample was therefore calculated according to the formula $\Delta Ct = Ct_{\text{Target gene}} - Ct_{\text{Housekeeping gene}}$. Relative mRNA expression data are shown as $2^{-\Delta Ct}$.

In chapter 3, P1A mRNA level was assessed by a Taqman-based rt-qPCR assay using Takyon ROX Probe Core Kit dTTP reagents (Eurogentec). Reactions were

set up according to the manufacturer's instructions. Reactions were run on the StepOnePlus™ Real-Time PCR System (Applied Biosystems) at the following conditions - 95°C - 3 minutes, (94°C 10s + 60°C 60s) x 40 cycles. To determine relative mRNA expression, the mean ΔCt was calculated for each target gene relative to *ActB* as previously described.

Table 2.17. List of primer sequences used in rt-qPCR assays

Primer/Probe	Sequence (5'-3')
Actb for	CCTTCAACACCCCAGCCATGTA
Actb rev	GGATGGCGTGAGGGAGAGCAT
Actb probe - 5'FAM – 3'TAM	CTG TCC CTG TAT GCC TCT GGT GCT ACC ACA G
P1A for	AGCTGAGGAAATGGGTGCTG
P1A rev	CAGCATTTTCACACCTACACTCCA
P1A probe – 5'FAM – 3'TAM	CCA TCA TTT AAG GAA GAA TGA AGT GAA GTG TAG GAT GA
Hprt1 for	AGTGTTGGATACAGGCCAGAC
Hprt1 rev	CGTGATTCAAATCCCTGAAGT
Cxcl9 for	GCCATGAAGTCCGCTGTTCT
Cxcl9 rev	GGGTTCCTCGAACTCCACACT
Cxcl10 for	GACGGTCCGCTGCAACTG
Cxcl10 rev	GCTTCCCTATGGCCCTCATT
Ccl5 for	GCAAGTGCTCCAATCTTGCA
Ccl5 rev	CTTCTCTGGGTTGGCACACA
Ifng for	CGGCACAGTCATTGAAAGCCTA
Ifng rev	GTTGCTGATGGCCTGATTGTC
Cd274 for	TGCTGCATAATCAGCTACGG
Cd274 rev	GCTGGTCACATTGAGAAGCA
Gzmb for	GAAGCCAGGAGATGTGTGCT
Gzmb rev	GCACGTTTGGTCTTTGGGTC

2.2.8 Statistical analysis

Statistical analyses were carried out using Prism 8.0 software (GraphPad). For immunogenicity study data, to determine significance when comparing responses between multiple groups a Kruskal-Wallis test with a Dunn's post hoc analysis for multiple comparisons was performed. To determine significance in the responses between different time-points within the same group a Wilcoxon matched-pairs signed rank tested was performed. For rt-qPCR gene expression studies, ordinary one-way ANOVA was performed followed by Tukey's post hoc to determine significance between individual groups. In murine tumour studies, statistically significant differences in tumour growth between different groups was determined by two-way ANOVA followed by Tukey's post hoc test. Survival curves for tumour studies were created using the Kaplan-Meier method and statistical significance in survival between different groups of mice was determined using the log-rank (Mantel-Cox) test. All P values < 0.05 were considered statistically significant.

Chapter 3. Immunogenicity of ChAdOx1/MVA prime-boost vaccination encoding MAGE-A3 and NY-ESO-1

3.1 Introduction

Much recent evidence from both pre-clinical and clinical studies has clearly demonstrated that tumour-antigen-specific CD8+ T-cells play a crucial and highly effective role in bringing about immune-mediated tumour rejection [93, 170, 172, 182]. Upon recognition of cognate tumour antigens presented via MHC-class I , tumour-specific CD8+ T-cells can mediate destruction of target tumour cells through production of cytotoxic molecules like perforin, Granzyme B and type I effector cytokines such as IFN-γ and TNF-α [69]. Anti-tumour CD8+ T-cells are necessary for the success of most recently developed immunotherapies such as immune checkpoint blockade [93]. However, spontaneously generated tumour-specific CD8+ T-cells are often lacking in many cancer patients. Therapeutic cancer vaccines therefore represent a strategy for inducing de novo or boosting levels of anti-tumour-specific CD8+ T-cell responses.

The MAGE-type antigen family are an attractive class of tumour-associated antigens to target with a therapeutic cancer vaccine based on the tumour-specificity of their expression profile and natural immunogenicity [158]. Many attempts have been made to develop successful cancer vaccines using MAGE-type antigens, but none so far have shown efficacy in clinical testing [198, 199]. A key reason underpinning the failure of these attempts is believed to be a shared ineffectiveness of the vaccine platforms used at inducing antigen-specific CD8+ T-cells in cancer patients [202, 204, 213]. Despite this track record, the development of an effective MAGE-targeting cancer vaccine based on a platform able to induce strong CD8+ T-cell responses in humans still has great potential as a cancer

immunotherapy. A heterologous prime-boost vaccination using two different recombinant viral vectors, ChAdOx1 and MVA, has been shown to induce some of the highest antigen-specific CD8+ T-cell responses to date in clinical trials in a range of infectious disease settings [151, 152]. In this study, it was therefore sought to utilize the ChAdOx1/MVA platform to induce T-cell responses against MAGE-type antigens, and to extend this strategy to the treatment of MAGE-expressing tumours. The MAGE-A3 and NY-ESO-1 proteins are some of the most widely expressed of the MAGE-family across a range of common solid tumour types, and have proven immunogenicity [174, 175]. A wide range of CTL epitopes from both proteins have been identified from CTL clones isolated from cancer patients [185]. On this basis, MAGE-A3 and NY-ESO-1 were selected as target antigens for the vaccination strategy. ChAdOx1 and MVA viral vectors encoding MAGE-A3 and NY-ESO-1 (Figure 3.1 and Figure 3.2) were therefore designed and constructed.

ChAdOx1 vectors were produced encoding a MAGE-A3-NY-ESO-1 fusion construct. The coding sequences of the two antigens were separated by the use of a short GGGPGGG polypeptide linker, with MAGE-A3 upstream and NY-ESO-1 following on from the 3' end of MAGE-A3 and the linker peptide. In addition molecular adjuvant sequences were also incorporated into the vectors. These molecular adjuvant sequences have been seen to increase the response generated against certain antigens by viral vectored vaccines when encoded in the vector via linkage to the antigen sequence.

One such approach is tethering of the recombinant antigen at its N-terminus to the MHC-class II invariant chain (Ii), which has been seen to enhance the magnitude, breadth and duration of the antigen-specific T-cell responses induced following adenoviral vaccination in a range of settings [214] [215] [156]. These improved responses have also been seen to enhance CD8+ T-cell mediated anti-tumour activity induced by adenoviral vector based vaccines in murine tumour models [216]. Additionally further studies have shown that a truncated Ii sequence corresponding to a 26 amino-acid peptide, GALYTGFSILVTLLLAGQATTAYFLY (G_{30}-Y_{55}), from the N-terminal transmembrane domain to be more efficient than the full length sequence at enhancing CD8+ T-cell responses [217].

Another approach that has been developed is fusion of the human tissue plasminogen activator (tPA) signal sequence to the N-terminus of the encoded recombinant target antigen. The tPA signal peptide is a 21 amino-acid sequence, DAMKRGLCCVLLLCGAVFVSP (D_1-P_{21}), that has been shown to increase the level of protein expression of the tethered antigen and induce its secretion from infected cells, increasing both humoural and cellular immune responses against certain antigens when incorporated into adenoviral and DNA plasmid based vaccines [218] [219].

In total therefore, three ChAdOx1 vectors were constructed encoding both MAGE-A3 and NY-ESO-1, containing either the antigen sequence alone (ChAdOx1-M-NY) or with the tPA DAMKRGLCCVLLLCGAVFVSP (D_1-P_{21}) or Ii GALYTGFSILVTLLLAGQATTAYFLY (G_{30}-Y_{55}) sequences tethered at the N-

terminal of the MAGE-A3 coding sequence (ChAdOx1-tPA-M-NY and ChAdOx1-Ii-M-NY respectively).

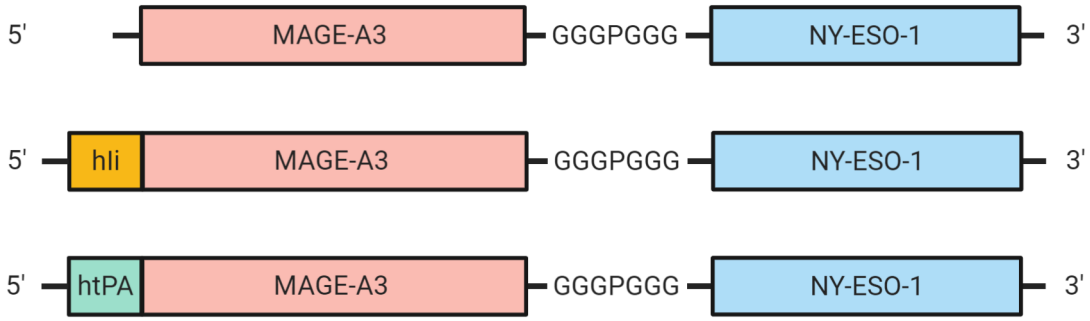


Figure 3.1 Schematic showing the design of ChAdOx1 viral vectors encoding the human MAGE-A3 and NY-ESO-1 antigens. Three ChAdOx1 viral vectors encoding both MAGE-A3 and NY-ESO-1 were constructed. MAGE-A3 and NY-ESO-1 were linked by a short polypeptide linker GGGPGGG. Either the transmembrane domain of human Ii or human tPA sequences were added to the N-terminal region of the MAGE-A3 coding sequence. Figure created with BioRender.

In addition four MVA vectors were constructed, each encoding only a single antigen - either MAGE-A3 or NY-ESO-1. Either the unmodified MAGE-A3 and NY-ESO-1 coding sequences were inserted into MVA vectors (MVA-M and MVA-NY) or MAGE-A3 and NY-ESO-1 sequences with the tPA sequence tethered to the N-terminus (MVA-tPA-M and MVA-tPA-NY). In the context of MVA vectored tuberculosis (TB) vaccines, the tPA signal peptide has been shown to increase the magnitude of the T-cell response against the encoded TB antigens when tested in murine models [220].

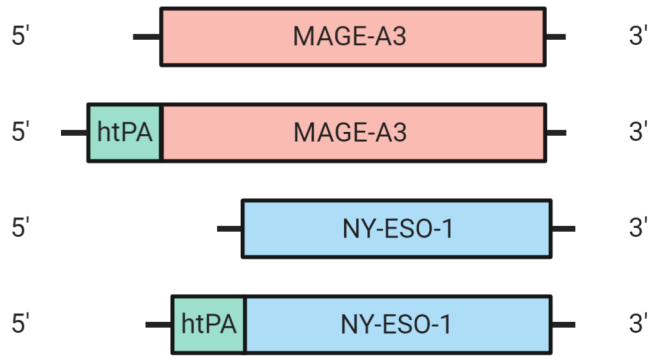


Figure 3.2. Schematic showing the design of MVA vectors encoding MAGE-A3 and NY-ESO-1 antigens. Four MVA vectors encoding either MAGE-A3 or NY-ESO-1 were constructed. The inserts were either only the unmodified antigen coding sequences or the human tPA sequences were added to the N-terminal region of the antigen coding sequence. Figure created with BioRender.

In this chapter the immunogenicity of these vectors was evaluated as part of a heterologous prime-boost vaccination scheme using CD1 mice, with a view to translation to clinical use. Although the most relevant setting to test these viral vectors is in humans, it was decided to first validate their potential using mice in a pre-clinical setting in order to identify the most promising approach in terms of vaccination schedule and incorporation of molecular adjuvant sequences. In particular, the ability of the vaccination strategy to induce CD8+ T-cell responses was assessed. IFN-γ, TNF-α and IL-2 are key effector cytokines produced by activated CD8+ T-cells. The magnitude and quality of an antigen-specific T-cell response elicited by a vaccine can therefore be assessed by measurement of the levels of these effector cytokines produced by T-cells following antigenic-stimulation [221] [222]. In this study, this readout was therefore used to evaluate antigen-specific T-cell responses. Outbred CD1 mice were used as they, like humans, have different MHC class I alleles and MHC-specificities and therefore

better reflect to some degree the challenges of inducing CD8+ T-cell responses to a given antigen across a variable population than inbred strains of mice.

3.2 Chapter aims

The specific aims of this chapter were:

1. To evaluate the immunogenicity of prime-boost vaccinations with ChAdOx1/MVA encoding MAGE-A3 and NY-ESO-1 in outbred CD1 mice.

2. To evaluate the potential of incorporating molecular adjuvant sequences encoded in the ChAdOx1/MVA viral vectors to enhance the level of any observed T-cell responses.

3. To investigate the kinetics of the prime-boost vaccination response to determine the most optimal combination and regime of vectors to induce high magnitude T-cell responses against both the MAGE-A3 and NY-ESO-1 antigens.

3.3 Results

3.3.1 Measuring T-cell responses induced by heterologous prime-boost vaccination with ChAdOx1/MVA vectors encoding MAGE-A3 and NY-ESO-1

To evaluate vaccine immunogenicity and identify the most promising vaccination schedules, CD1 mice were administered with different combinations of ChAdOx1 and MVA vectors encoding the MAGE-A3 and NY-ESO-1 antigens via intramuscular (i.m.) injection as part of a heterologous prime-boost vaccination regime (Figure 3.3), according to the experimental groupings shown in Table 3.1. To test antigen-specific T-cell responses induced by the vectors, blood was sampled from vaccinated mice around 2-weeks after each vaccination was given. PBMCs were obtained from the blood and stimulated ex vivo with overlapping pools of peptides spanning the whole length of either the MAGE-A3 or NY-ESO-1 protein sequences, and then stained intracellularly to detect the production of IFN-γ, TNF-α and IL-2 by activated T-cells. The level of response was evaluated in the blood as it contains recirculating antigen-specific T-cells induced by vaccination, and blood sampling is a readily tractable approach that allows serial measurements to be performed to monitor the immune response over time. Control mice received PBS sham vaccinations. ChAdOx/MVA vectors encoding irrelevant antigens were used to vaccinate control groups in pilot studies. This has the advantage of allowing the level of non-specific inflammation induced by vaccination to be assessed in T-cell assays. However, in these pilot studies irrelevant antigen vaccination was not found to induce levels of cytokine

production by T-cells above PBS sham vaccinations in stimulation assays and so PBS was used as a control vaccination.

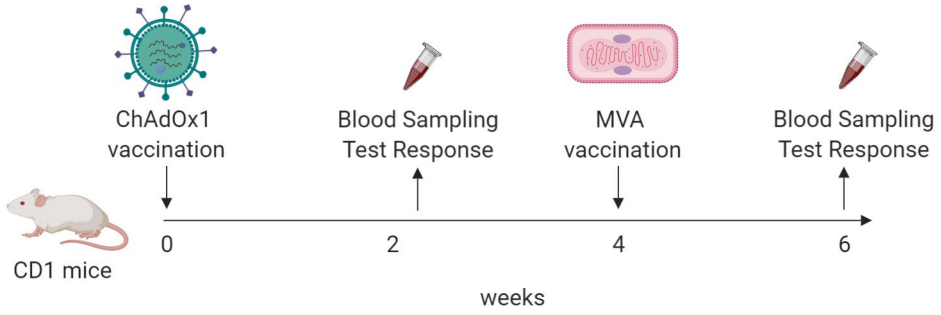


Figure 3.3. Timeline of ChAdOx1/MVA heterologous prime-boost vaccination scheme with vectors encoding MAGE-A3 and NY-ESO-1. CD1 outbred mice received a prime vaccination via intramuscular injection (i.m.) with 10^8 IU of ChAdOx1-M-NY (± Ii or tPA). or a PBS sham. 4 weeks after ChAdOx1-M-NY (± Ii or tPA) mice received a boost vaccination with 10^7 PFU of MVA-M or MVA-NY, or a PBS sham. Vaccinations were given according to the experimental groupings shown in Table 3.1. To test the response to vaccination, mice were bled 16 or 18 days after vaccination with ChAdOx1 and 14 days after vaccination with MVA. Figure created with BioRender.

Table 3.1 Combinations of ChAdOx1 and MVA viral vectors encoding MAGE-A3 and NY-ESO-1 tested in heterologous prime-boost vaccinations.

Group	ChAdOx1 prime vaccination	MVA boost vaccination
1	PBS	PBS
2	MAGE-A3_NY-ESO-1	MAGE-A3
3		NY-ESO-1
4	tPA_MAGE-A3_NY-ESO-1	MAGE-A3
5		NY-ESO-1
6	Ii_MAGE-A3_NY-ESO-1	MAGE-A3
7		NY-ESO-1

3.3.2 ChAdOx1-MAGE-A3-NY-ESO-1 vaccination primes a strong antigen-specific CD8+ T-cell response to both encoded antigens

Firstly, the magnitude of the CD8+ T-cell responses against both MAGE-A3 and NY-ESO-1 induced by vaccination with the ChAdOx1 vectors encoding the MAGE-A3-NY-ESO-1 fusion constructs (ChAdOx1-M-NY) with or without the addition of Ii or tPA (ChAdOx1-tPA-M-NY and ChAdOx1-Ii-M-NY) was assessed (Figure 3.4). Ex vivo peptide stimulation of PBMCs 2 weeks after vaccination demonstrated that all three vectors were capable of inducing a high magnitude CD8+ T-cell response specific to both MAGE-A3 and NY-ESO-1. Compared to the PBS sham vaccinated control group, there was a significant increase in IFN-γ producing CD8+ T-cells in the blood measured two weeks after vaccination with all three ChAdOx1 vectors (Figure 3.4 B). IFN-γ secreting CD8+ T-cells in the blood of PBS control mice were almost undetectable upon MAGE-A3 or NY-ESO-1 peptide stimulation. However, following vaccination with ChAdOx1-M-NY, ChAdOx1-tPA-M-NY or ChAdOx1-Ii-M-NY the percentage of CD8+ T-cells from the circulation producing IFN-γ in response to MAGE-A3 peptide stimulation was significantly increased (mean responses of 4.9%, 3.4% and 1.9% respectively). Likewise the frequencies of CD8+ T-cells secreting IFN-γ in response to NY-ESO-1 peptide stimulation was also significantly increased (mean responses of 1.3%, 1.7% and 2.1% respectively). Additionally, the production of TNF-α (Figure 3.4 C) and IL-2 (Figure 3.4 D) by CD8+ T-cells following peptide stimulation was also interrogated. TNF-α and IL-2 production was detectable in CD8+ T-cells from mice in all vaccinated groups. However, with the exception of IL-2 production by CD8+ T-cells in response to MAGE-A3 peptide stimulation in the ChAdOx1-M-

NY vaccinated group, this did not reach the classical threshold for significance. Having confirmed that vaccination with ChAdOx1 encoding the MAGE-A3-NY-ESO-1 fusion construct could generate CD8+ T-cell responses against both antigens, the question then arose of whether on an individual level, mice were mounting a response to both antigens, or whether the response in each individual mouse was biased entirely toward one or the other antigen. To determine this, the magnitude of the MAGE-A3 and NY-ESO-1 specific CD8+ T-cell responses mounted by each mouse in the vaccinated groups was correlated (Figure 3.4 E). This showed a weak but significant negative correlation (r= -0.3) between the magnitude of the CD8+ response mounted against NY-ESO-1 compared to the magnitude of response against MAGE-A3 by any given mouse. This relationship is only very weak however, indicating that a very large proportion of the mice mount CD8+ T-cell responses against both antigens. However, in some mice the response is biased towards one or the other encoded antigen, with high responses against MAGE-A3 or NY-ESO-1 typically correlating with low or no response against the other antigen.

3.3.3 Fusion of htPA or hIi sequences to the antigen coding sequence in the ChAdOx1 vector does not increase the magnitude of the MAGE-A3 or NY-ESO-1-specific CD8+ T-cell response

Next the effect on vaccine immunogenicity of incorporating the tPA or hIi molecular adjuvant sequences via linkage to the N-terminal region of the MAGE-A3-NY-ESO-1 fusion construct coding sequences was considered. The magnitude of IFN-γ, TNF-α or IL-2 producing CD8+ T-cells following vaccination with

ChAdOx1-M-NY was compared to that of the vectors incorporating tPA or Ii (Figure 3.4). By these three parameters measured, no benefit was identified for the inclusion of either tPA or Ii for increasing the level of the CD8+ response to MAGE-A3 or NY-ESO-1. The magnitudes of cytokine producing cells were comparable and not significantly different between any of the vaccinated groups (Figure 3.4).

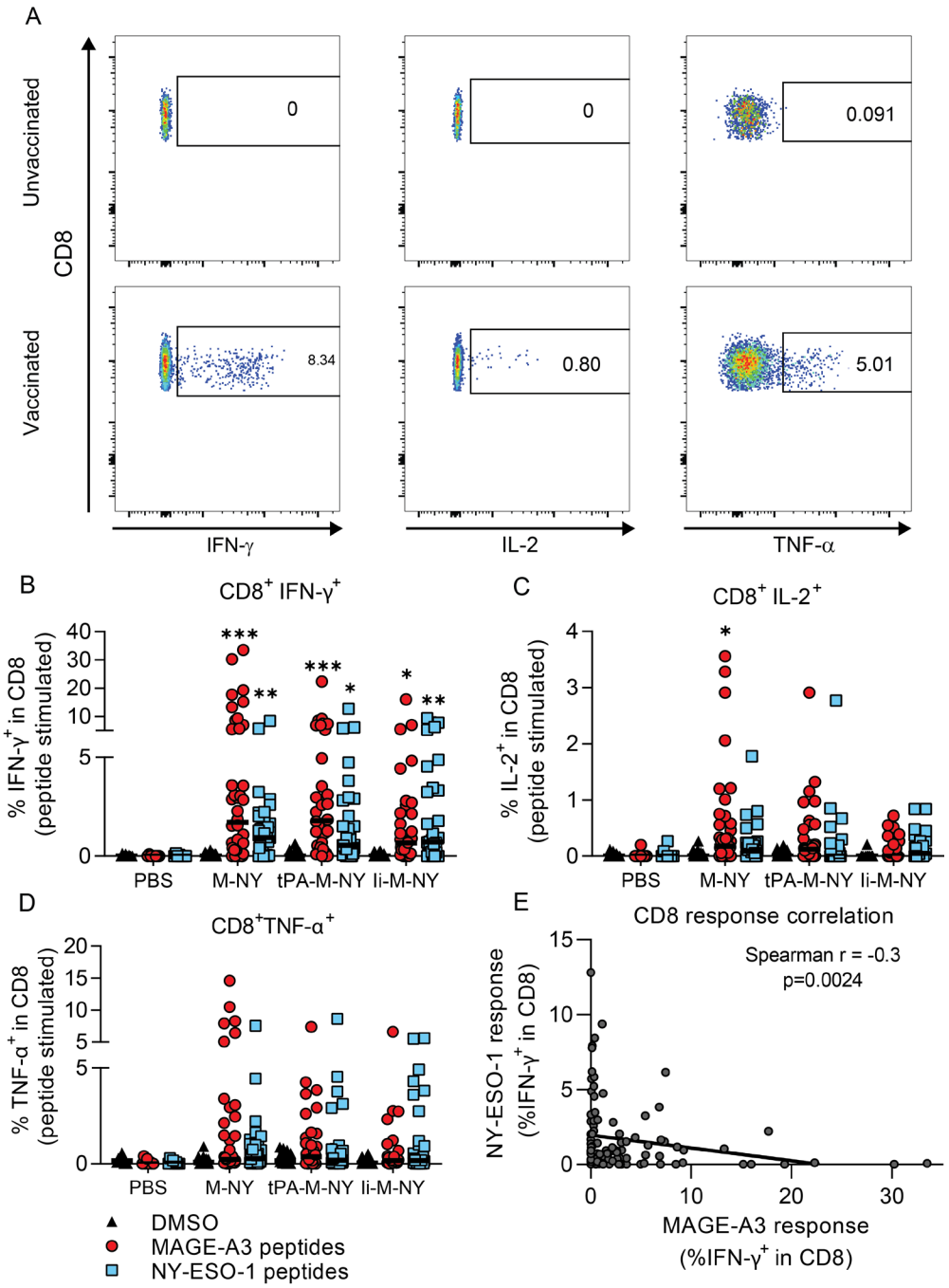


Figure 3.4. MAGE-A3 and NY-ESO-1-specific CD8+ T-cell response induced by ChAdOx1 prime vaccination. To evaluate the magnitude of antigen-specific T-cell responses induced by ChAdOx1-M-NY (± tPA or ± Ii) vaccination, blood was sampled 16-18 days after vaccination and PBMCs were stimulated ex vivo with 4µg/ml of either MAGE-A3 or NY-ESO-1 peptide pools, or a vehicle control (DMSO). The percentage of cytokine-producing antigen-specific CD8+ T-cells in the blood was determined by ICS and flow cytometry (gating strategy as described in Figure 2.2). Representative dot plots showing gating of IFN-γ, TNF-α and IL-2 expressing CD8+ T-cells (A). Percentage of IFN-γ+ (B), IL-2+ (C) and TNF-α+ (D) CD8+ T-cells in response to stimulation with MAGE-A3 peptides (red circles), NY-ESO-1 peptides (blue squares) or DMSO (black triangles). Data are shown as the median response of each group (horizontal lines). Each symbol represents an individual mouse, with 8 mice in the PBS group and 16 mice per ChAdOx1 vaccinated group, pooled from 2 independent experiments. Statistically significant difference is shown compared to the PBS group and was determined by a Kruskal-Wallis test with Dunn's multiple comparisons. *, p ≤ 0.05, **, p ≤ 0.01 ***, p ≤ 0.001. For each mouse, the magnitude of the CD8+ IFN-γ+ response to MAGE-A3 and NY-ESO-1 was correlated (E). Statistical significance was determined by a Spearman Rank correlation test.

3.3.4 Both MAGE-A3 and NY-ESO-1-specific CD8+ T-cell responses induced by ChAdOx1 vaccination are polyfunctional

T-cells producing multiple cytokines are considered to have a higher degree of functionality than those producing just one cytokine and have been associated with improved disease control in a range of settings [223]. Thus the proportion of T-cells producing multiple cytokines elicited by vaccination can be used as an indication of the quality of the induced response. For this reason, the proportion of antigen-specific CD8+ T-cells producing only a single cytokine - IFN-γ, TNF-α or IL-2, a combination of two, or all three cytokines after vaccination with ChAdOx1 vectors encoding MAGE-A3-NY-ESO-1 was determined (Figure 3.5). In all three vaccinated groups, MAGE-A3-specific CD8+ T-cells were found to be predominantly single producers of IFN-γ, with a minor proportion of approximately 25% of cells producing both IFN-γ and TNF-α and a smaller proportion still producing IFN-γ, TNF-α and IL-2 together (Figure 3.5 A). NY-ESO-1-specific CD8+ T-cells were found to be somewhat more polyfunctional (Figure 3.5 B). The largest proportion of cytokine producing CD8+ T-cells were still IFN-γ single producers, however a higher proportion of IFN-γ+ TNF-α+ double producers was present compared to the MAGE-A3-specific CD8+ T-cell population. Additionally, the incorporation of the tPA or Ii sequences did not impact on the degree of polyfunctionality of the T-cell response to either MAGE-A3 or NY-ESO-1, with almost identical distributions observed between the ChAdOx1-M-NY, ChAdOx1-tPA-M-NY and ChAdOx1-Ii-M-NY vaccinated groups.

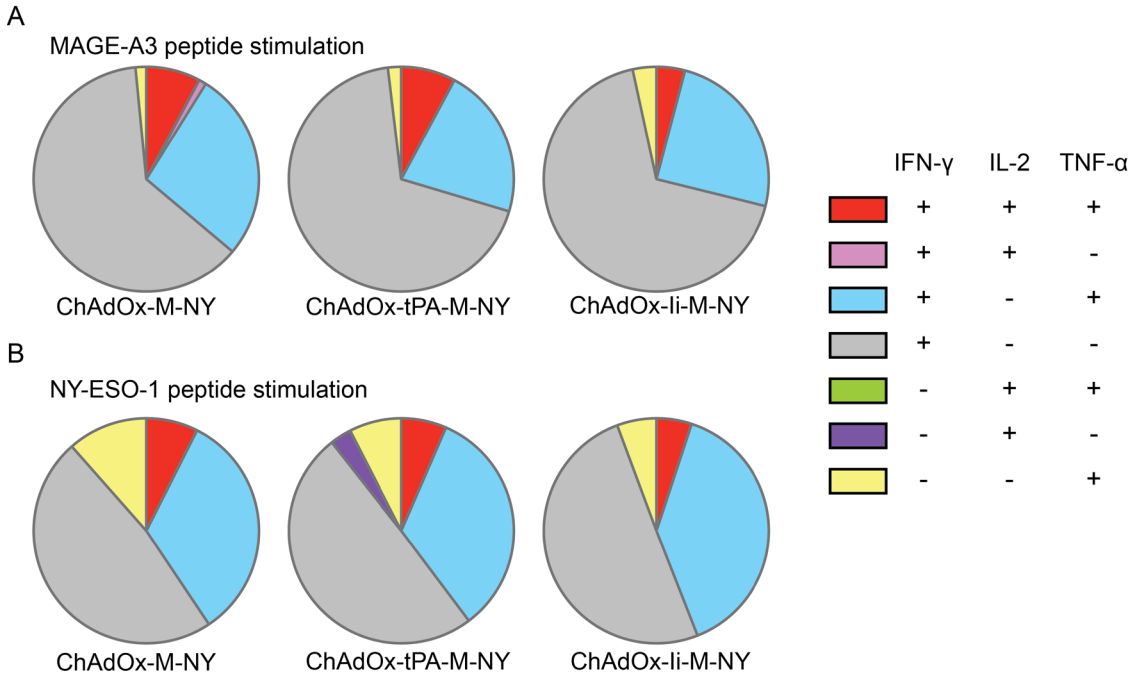


Figure 3.5 Cytokine profiles of antigen-specific CD8+ T-cells after ChAdOx1-M-NY prime vaccination. PBMCs were obtained 16-18 days after vaccination with ChAdOx1-M-NY (± tPA and ± Ii) and stimulated with MAGE-A3/NY-ESO-1 peptides as described in Figure 3.4. The multifunctionality of MAGE-A3-specific (A) and NY-ESO-1-specific (B) CD8+ T-cells was assessed. A Boolean analysis was performed in FlowJo software to calculate the percentage of CD8+ T-cells producing only one, a combination of two, or all three of the effector cytokines IFN-γ, IL-2 and TNF-α+. Pie charts show the mean relative proportion of each cytokine producing subset out of the total antigen-specific CD8+ T-cells.

3.3.5 ChAdOx1-MAGE-A3-NY-ESO-1 vaccination induces an antigen-specific CD4+ T-cell response

CD4+ T-cells represent an important part of an effective CD8+ T-cell mediated cellular immune response, helping to broaden, amplify and sustain the CD8+ response through the production inflammatory and effector cytokines. For this reason the magnitude of antigen-specific CD4+ T-cell response generated after ChAdOx1-M-NY vaccination was also analysed (Figure 3.6). Both MAGE-A3 and NY-ESO-1-specific CD4+ T-cells were induced in the CD1 mice by all three ChAdOx1 vectors. However, these responses were in general of quite low magnitude and the variability in the induction of a CD4 response was quite high, with only IFN-γ production in the CD4+ response to MAGE-A3 stimulation

significant compared to the control after ChAdOx1-M-NY and ChAdOx1-Ii-M-NY vaccinations (Figure 3.6 B). No significant differences were detected in the magnitude of the MAGE-A3 or NY-ESO-1 induced by ChAdOx1-M-NY vaccination, with or without incorporation of tPA or Ii. Due to the difficulty in assessing TNF-α production above background level in the CD4+ T-cell population, the polyfunctionality of the CD4 T-cell response was not calculated.

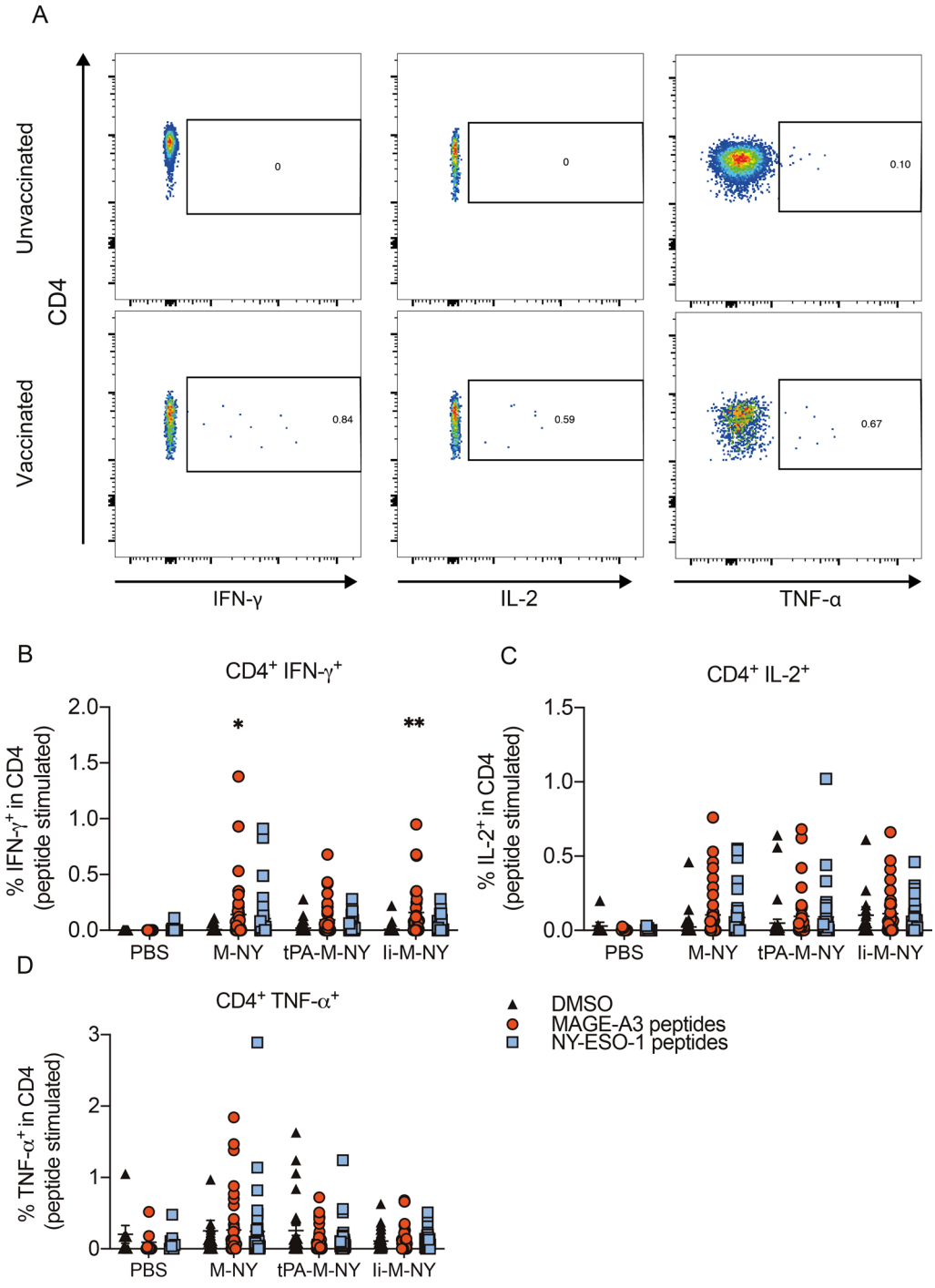


Figure 3.6. MAGE-A3 and NY-ESO-1-specific CD4+ T-cell responses after ChAdOx1 prime vaccination. CD1 mice were vaccinated and PBMCs isolated as described in Figure 3.4. To evaluate the magnitude of the antigen-specific T-cell response induced by vaccination, PBMCs were then stimulated ex vivo with either DMSO or with 4μg/ml of pools of either MAGE-A3 or NY-ESO-1 overlapping peptides. Following stimulation, the percentage of cytokine-producing antigen-specific CD4+ T-cells was determined by ICS combined with flow cytometry (gating strategy as described in Figure 2.2). Representative dot plots showing gating of IFN-γ, TNF-α and IL-2 positive cells in the CD4+ T-cell population (A). Percentage of IFN-γ (B), IL-2 (C) and TNF-α (D) expressing cells of total CD4+ PBMCs. Data are shown as the median response of each group (horizontal lines) and each symbol represents an individual mouse, with 8 mice in the PBS group and 16 mice per ChAdOx1 vaccinated group, pooled from 2 independent experiments. Statistical significance

between groups was determined by a Kruskal-Wallis test with Dunn's multiple comparisons test. *, $p \leq 0.05$, **, $p \leq 0.01$ ***, $p \leq 0.001$

3.3.6 Boost vaccination with either MVA-MAGE-A3 or MVA-NY-ESO-1 greatly increases the magnitude of the CD8+ response against either of the encoded antigens

Having confirmed that the ChAdOx1 prime vaccination could induce a high magnitude CD8+ T-cell response to both MAGE-A3 and NY-ESO-1 antigens encoded in the vector, it was then tested if the response could be boosted against either antigen individually with an MVA vaccination encoding only a single antigen. In a clinical setting, this would enable a tailoring of the specificity of the CD8+ T-cell response depending on patient tumour antigen expression. Mice primed with ChAdOx1-M-NY, ChAdOx1-tPA-M-NY or ChAdOx1-Ii-M-NY were distributed into experimental groupings based on the magnitude of CD8+ T-cell to both MAGE-A3 and NY-ESO-1 so as to ensure an equal level of antigen-specific response between groups prior to the boost vaccination . Mice then received a boost vaccination with MVA encoding either MAGE-A3 (MVA-M) or NY-ESO-1 (MVA-NY). The magnitude of the CD8+ T-cell response against each antigen in the blood was then evaluated. To investigate the kinetics of the response, the magnitude of the CD8+ T-cells in the circulation secreting IFN-γ in response to MAGE-A3 or NY-ESO-1 stimulation was compared before and after the boost (Figure 3.7). Firstly considering the response against MAGE-A3, this showed the MVA-M boost to be highly efficient, with almost all mice having higher MAGE-A3-specific CD8+ T-cell responses after as compared to before the boost vaccination (Figure 3.7 A). This increase in response following MVA vaccination was significant for the groups primed with ChAdOx1-tPA-M-NY or ChAdOx1-Ii-

M-NY, however for the group prime with ChAdOx1-M-NY this did not reach statistical significance despite following the same trend due to an extreme outlier that already had a very high response after prime vaccination. For those groups that did not receive an MVA boost encoding MAGE-A3, the magnitude of MAGE-A3-specific CD8+ T-cell response in the blood had significantly declined. The MVA-NY boost was similarly efficient at increasing the magnitude of NY-ESO-1-specific CD8+ T-cells response. Significantly higher frequencies of NY-ESO-1-specific CD8+ T-cells could be detected in the circulation of all groups after MVA-NY boost as compared to just after ChAdOx1 prime vaccination alone. Similar to the MAGE-A3-specfic CD8+ response, NY-ESO-1-specific CD8+ T-cell responses had declined in those groups that did not receive a vaccination with MVA encoding NY-ESO-1. Overall, the majority of mice that received a prime and a boost vaccination both encoding either MAGE-A3 or both encoding NY-ESO-1 generated a significant antigen-specific CD8+ T-cell response against that antigen (Table 3.2). However, a slightly higher proportion of mice were found to mount MAGE-A3-specific CD8+ T-cell responses after ChAdOx-M-NY/MVA-M vaccinations than the proportion that mounted NY-ESO-1-specific CD8+ T-cell responses after ChAdOx-M-NY/MVA-NY vaccinations.

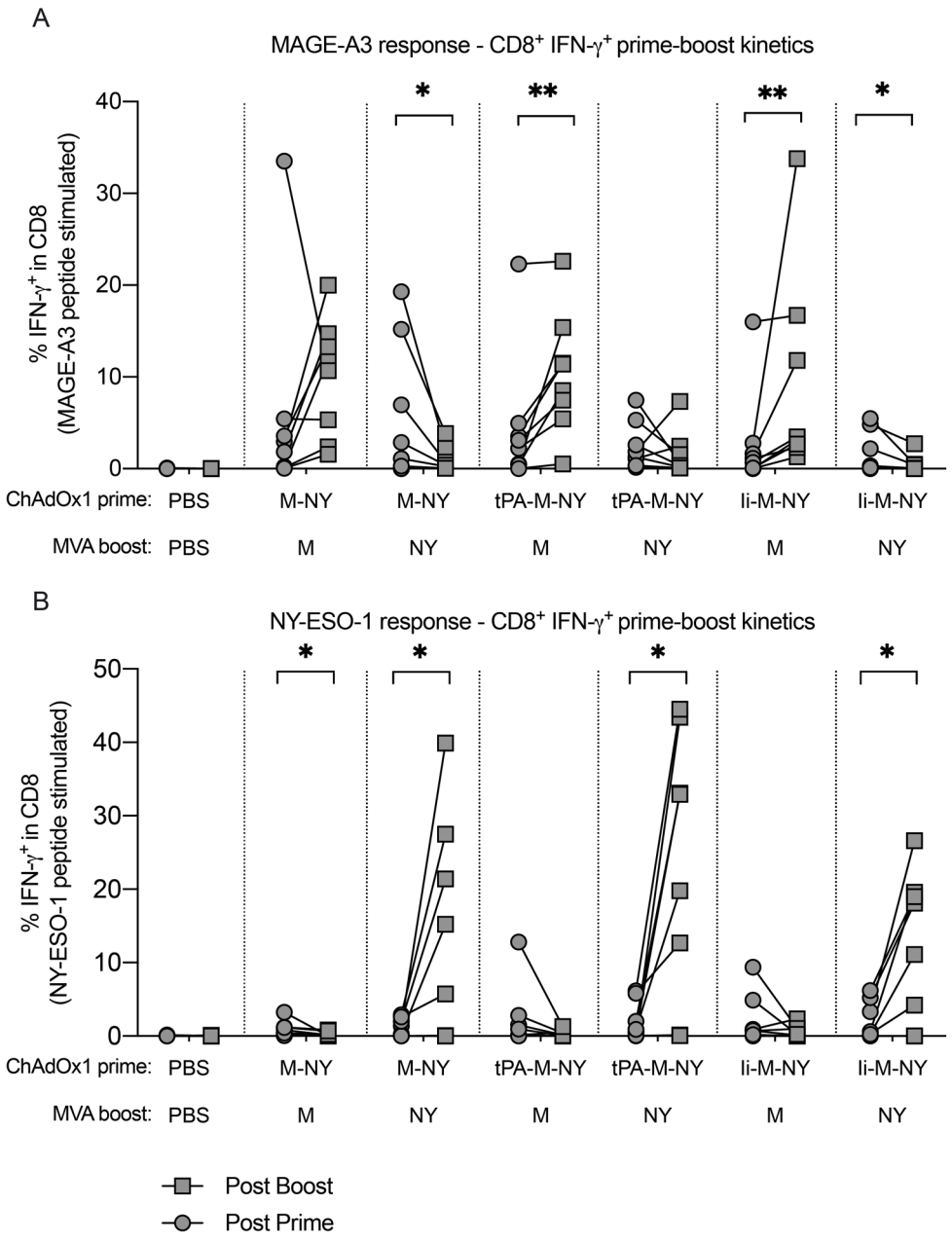


Figure 3.7. Kinetics of the MAGE-A3-specific and the NY-ESO-1-specific CD8+ T-cell response in the blood. CD1 mice received a prime vaccination with ChAdOx1-M-NY (± tPA or ± Ii) and a boost vaccination with either MVA-M or MVA-NY (or PBS sham vaccinations at identical time-points) and the antigen-specific T-cell response in the blood was assessed after each, as described Figure 3.3. The percentage of IFN-γ+ CD8+ T-cells in response to MAGE-A3 peptide stimulation (A) and NY-ESO-1 peptide stimulation (B) was determined by ICS and flow cytometry and compared after the prime (closed circles) and boost (closed squares). Each symbol represents an individual mouse with 8 mice per group, with data pooled from 2 independent experiments. Statistical significance between the post-prime and post-boost response in each group was determined by a Wilcoxon matched-pairs signed rank test. *, $p \leq 0.05$, **, $p \leq 0.01$.

The magnitude of MAGE-A3 and NY-ESO-1-specific CD8+ T-cell responses after the MVA boost were then compared head to head in an attempt to identify whether overall one of the vaccination regimes was more efficient at inducing a CD8+ T-cell responses against either antigen (Figure 3.8 and Figure 3.9). All groups however were found to be equally efficient at inducing both MAGE-A3-specific and NY-ESO-1-specific CD8+ T-cell responses, with no significance difference detected in the magnitude of the responses between the groups that received a prime vaccination with ChAdOx1-M-NY with or without the addition of Ii or tPA. Similarly no difference was detected in the proportion of mice mounting an antigen-specific CD8+ T-cell response after both prime and boost vaccination between any of the different schemes (Table 3.2).

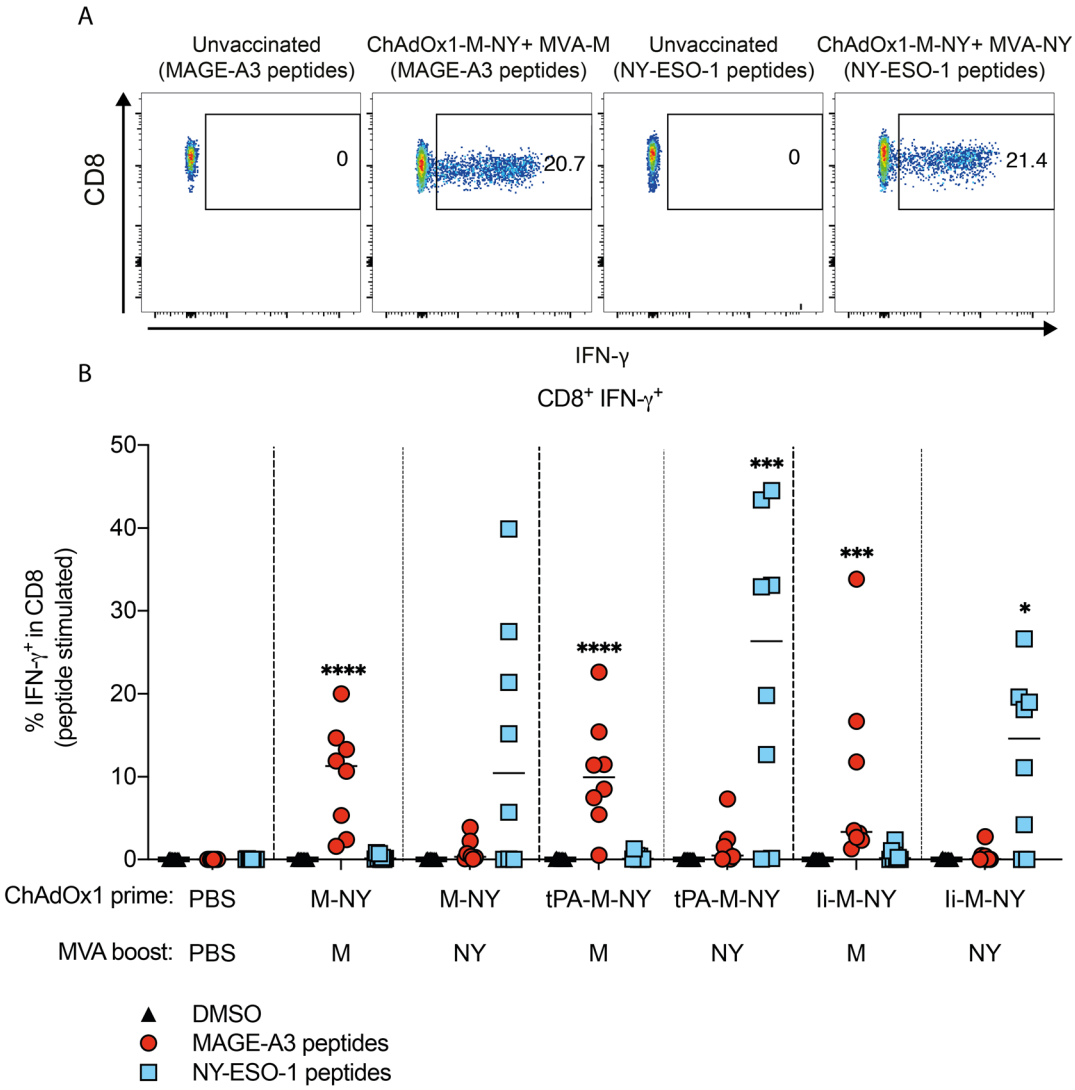


Figure 3.8. IFN-γ response by MAGE-A3-specific and NY-ESO-1-specific CD8+ T-cells after MVA boost vaccination. CD1 mice received a prime vaccination with ChAdOx1-M-NY (± tPA or ± Ii) and a boost vaccination with either MVA-M or MVA-NY (or PBS sham vaccinations at identical time-points). To measure the antigen-specific CD8+ T-cell response after the MVA boost, mice were bled 14 days after vaccination and PBMCs were stimulated ex vivo with 4μg/ml of pools of either MAGE-A3 or NY-ESO-1 overlapping peptides, or a vehicle control (DMSO). The percentage of cytokine-producing antigen-specific CD8+ T-cells in the blood was determined by ICS and flow cytometry (gating strategy as described in Figure 2.2). Representative dot plots showing gating of CD8+ IFN-γ+ T-cells (A). Percentage of IFN-γ+ CD8+ T-cells in response to stimulation with MAGE-A3 peptides (red circles), NY-ESO-1 peptides (blue squares) or DMSO (black triangles) (B). Data are shown as the median response of each group (horizontal lines). Each symbol represents an individual mouse, with 8 mice in the PBS group and 16 mice per ChAdOx1/MVA vaccinated group, pooled from 2 independent experiments. Statistically significant difference is shown compared to the PBS control group and was determined by a Kruskal-Wallis test with Dunn's multiple comparisons test. *, $p \leq 0.05$, ***, $p \leq 0.001$, ****, $p \leq 0.0001$.

Table 3.2. Proportion of mice that generated a positive MAGE-A3 or NY-ESO-1 specific CD8+ T-cell response following ChAdOx/MVA MAGE-A3/NY-ESO-1 prime-boost vaccination*.

	CD8+ T-cell response after boost	
Vaccine schedule	**Proportion of MAGE-A3 responders (%)**	**Proportion of NY-ESO-1 responders (%)**
C-M-NY+ MVA-M	**100**	NA
C-M-NY+ MVA-NY	NA	**62.5**
C-tPA-M-NY+ MVA-M	**87.5**	NA
C-tPA-M-NY+ MVA-NY	NA	**75**
C-Ii-M-NY+ MVA-M	**100**	NA
C-Ii-M-NY+ MVA-NY	NA	**75**

*A positive response was defined as a frequency of IFN-γ producing CD8+ T-cells in the blood after vaccination (in response to specific peptide stimulation) greater than 3 standard deviations above the mean of the response observed from unstimulated cells from unvaccinated mice.

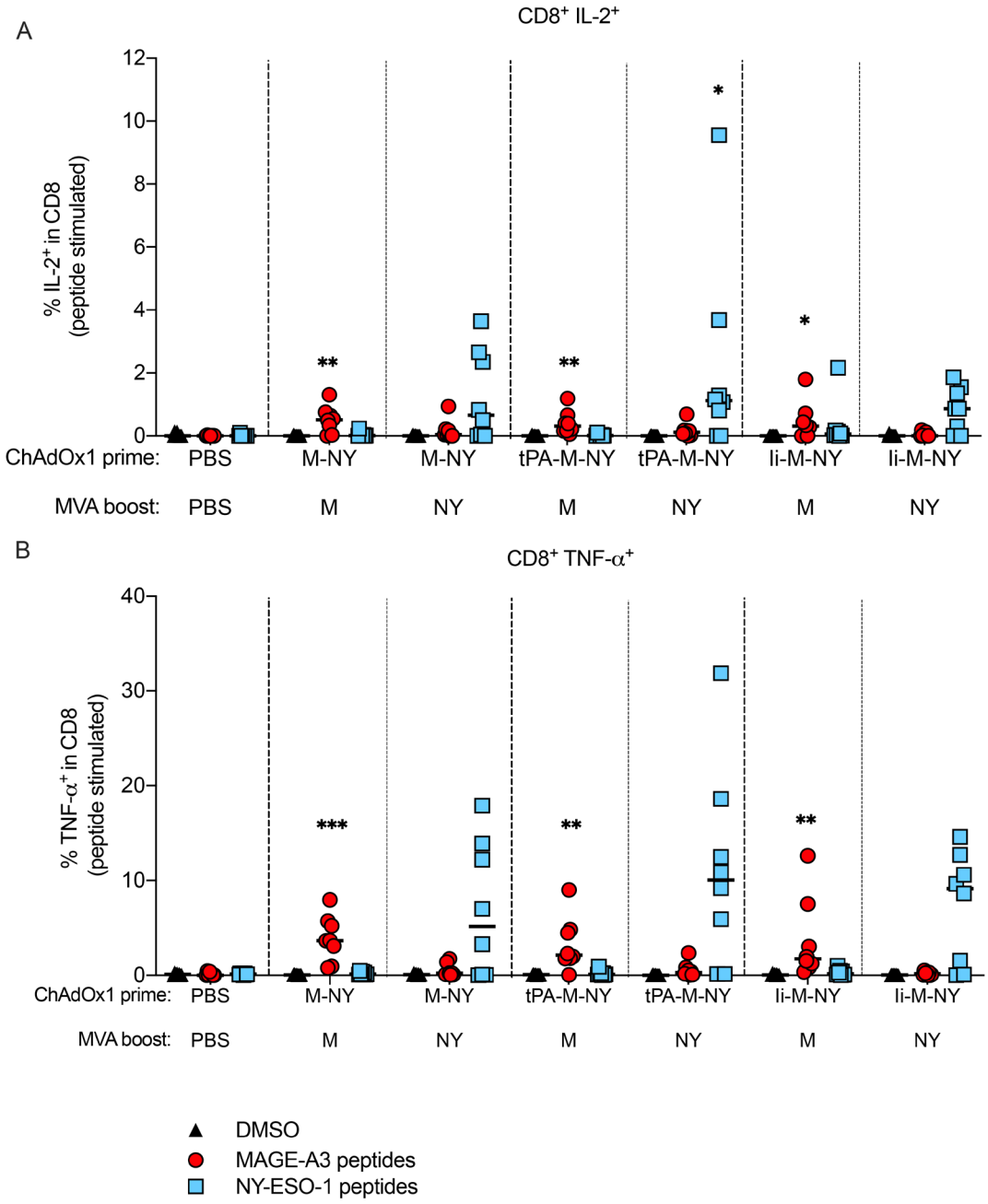


Figure 3.9. TNF-α and IL-2 response by MAGE-A3-specific and NY-ESO-1-specific CD8+ T-cells after MVA boost vaccination. CD1 mice were vaccinated, bled and PBMCs stimulated as described in Figure 3.8. Representative dot plots showing gating of TNF-α+ and IL-2+ CD8+ T-cells (A). Percentage of TNF-α+ (A) and IL-2+ (B) CD8+ T-cells in response to stimulation with MAGE-A3 peptides (red circles), NY-ESO-1 peptides (blue squares) or DMSO (black triangles). Gating strategy as described in Figure 2.2. Data are shown as the median response of each group (horizontal lines). Each symbol represents an individual mouse, with 8 mice in the PBS group and 16 mice per ChAdOx1/MVA vaccinated group, pooled from 2 independent experiments. Statistically significant difference is shown compared to the PBS control group and was determined by a Kruskal-Wallis test with Dunn's multiple comparisons test. *, $p \leq 0.05$, ***, $p \leq 0.001$, ****, $p \leq 0.0001$.

The cytokine profiles of the MAGE-A3 and NY-ESO-1-specific CD8+ T-cells were further assessed after the MVA boost vaccination to determine the degree of polyfunctionality of the response i.e. those producing multiple effector cytokines in addition to IFN-γ (Figure 3.10). The MAGE-A3-specific response was only considered for those groups that had received MVA encoding MAGE-A3 in the boost vaccination and the NY-ESO-1-specific response was only considered for those groups that received MVA encoding NY-ESO-1 in the boost vaccination. Similarly to after the prime, the NY-ESO-1-specific CD8+ T-cell response after the boost appeared to be more multifunctional than the MAGE-A3-specific CD8+ T-cell response. The majority of MAGE-A3 responding CD8+ T-cells were IFN-γ single-producers, with around 1/3 being IFN-γ and TNF-α double producers, and a minor population producing all 3 cytokines. The NY-ESO-1 responding CD8+ T-cells were around ½ IFN-γ single-producers, with the other half comprised of IFN-γ and TNF-α double producers, or CD8+ T-cells producing all 3 cytokines.

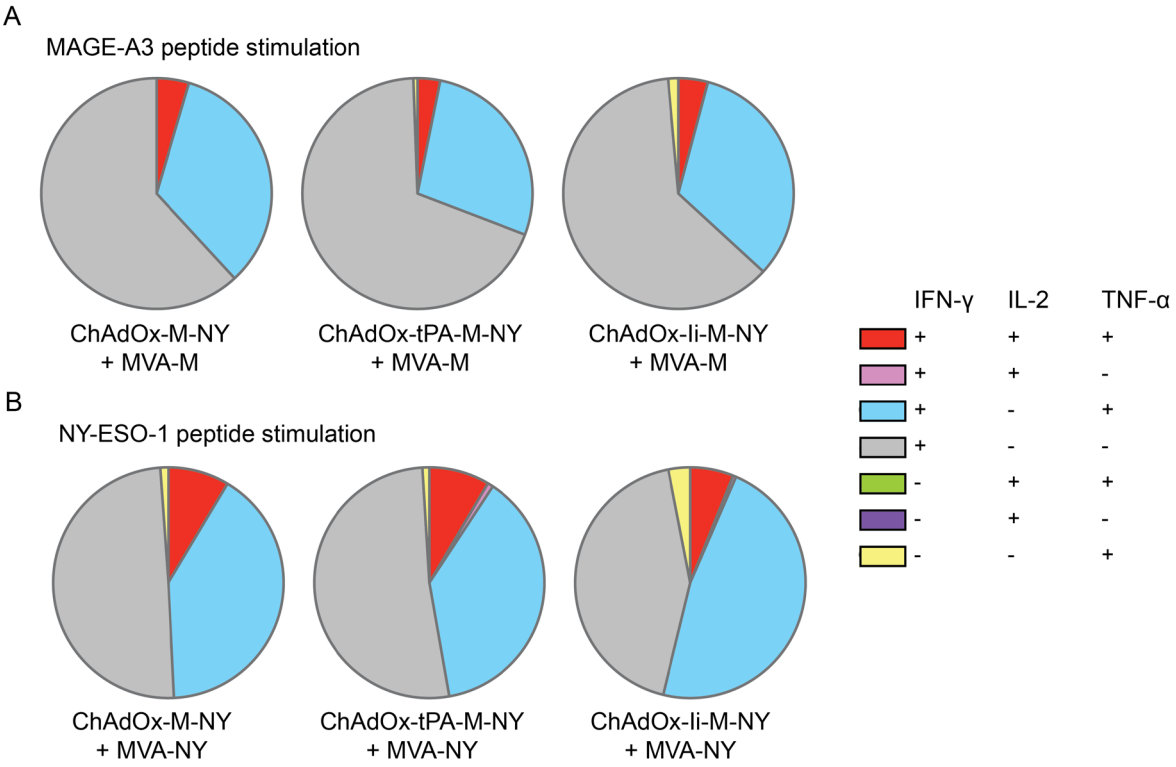


Figure 3.10. Cytokine profiles of CD8+ T-cells after heterologous prime-boost vaccination with ChAdOx1/MVA encoding MAGE-A3 and NY-ESO-1. PBMCs were obtained 14 days after a boost vaccination with either MVA-M or MVA-NY as described in Figure 3.8 and the multifunctionality of MAGE-A3-specific (A) and NY-ESO-1-specific (B) CD8+ T-cells was assessed. A Boolean analysis was performed in FlowJo software to calculate the percentage of CD8+ T-cells producing only one, a combination of two, or all three of the effector cytokines IFN-γ, IL-2 and TNF-α+. Pie charts show the mean relative proportion of each cytokine producing subset out of the total antigen-specific CD8+ T-cells

3.3.7 MAGE-A3 and NY-ESO-1-specific CD4+ T-cell responses after MVA boost vaccination

The effect of MVA vaccination on the MAGE-A3 and NY-ESO-1-specific CD4+ T-cell response was also evaluated (Figure 3.11). A boost vaccination with MVA encoding MAGE-A3 was found not to be efficient at boosting the level of the MAGE-A3-specific CD4+ T-cell response, although CD4+ T-cells secreting IFN-γ in response to MAGE-A3 peptide stimulation were detectable in the blood 2 weeks after MVA vaccination (Figure 3.11 A). However conversely for mice that received a prime vaccination of ChAdOx1-tPA-M-NY or ChAdOx1-Ii-M-NY, a vaccination with MVA encoding NY-ESO-1 was found to significantly boost the

level of IFN-γ secreting NY-ESO-1-specific CD4+ T-cells (Figure 3.11 B). Compared to the PBS control, a significant increase in MAGE-A3-specific CD4+ T-cells was detected after ChAdOx1-M-NY + MVA-M and ChAdOx1-Ii-M-NY + MVA-M vaccinations, and a significant increase in NY-ESO-1-specific CD4+ T-cells was detected after ChAdOx1-M-NY + MVA-NY and ChAdOx1-tPA-M-NY + MVA-NY vaccinations (Figure 3.12). However when comparing between groups that received different ChAdOx1-M-NY prime vaccinations with or without the addition of tPA or Ii, none were found to be more effective at inducing antigen-specific CD4+ T-cell responses than the other.

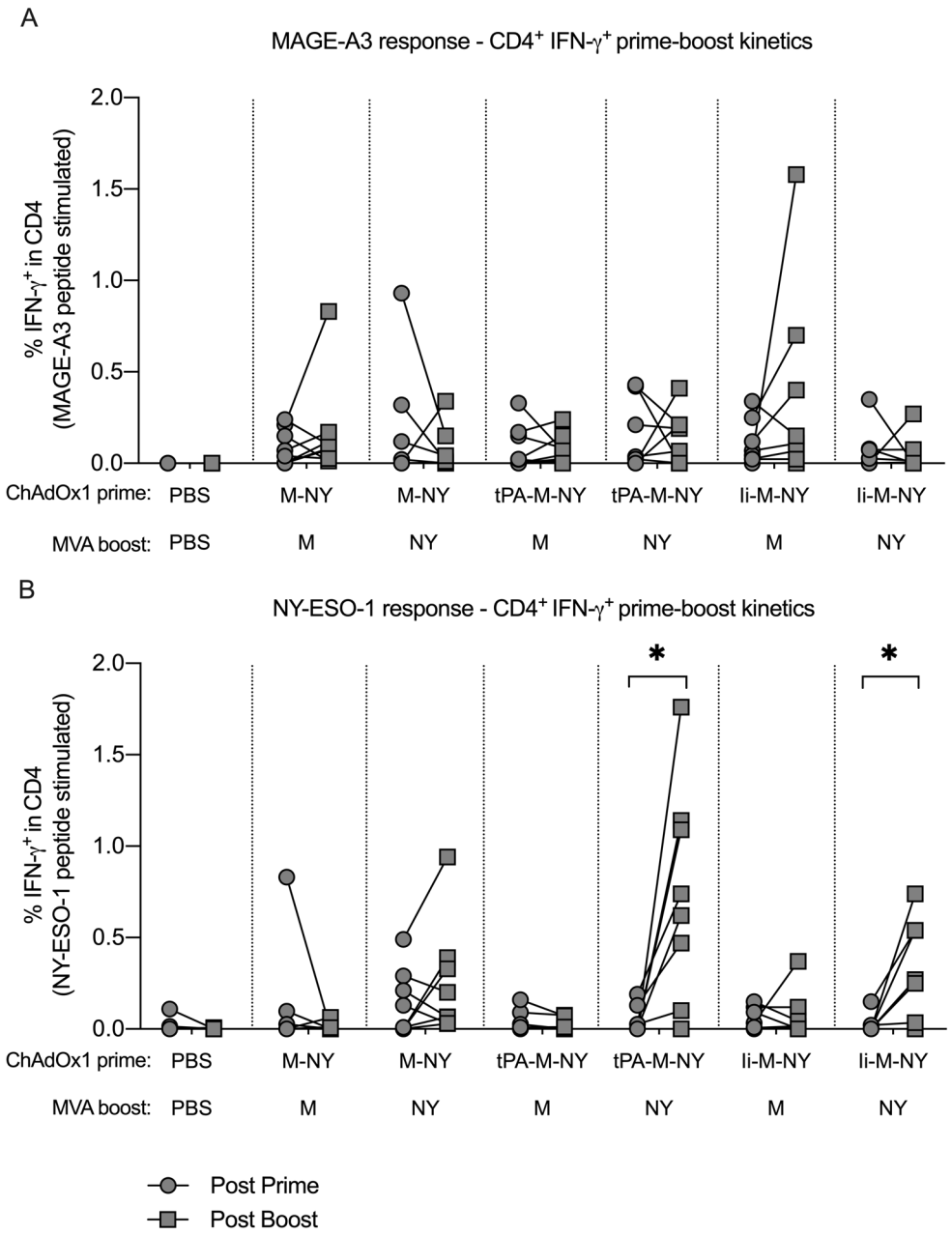


Figure 3.11. Kinetics of the MAGE-A3-specific and the NY-ESO-1-specific CD4+ T-cell response in the blood. CD1 mice received a prime vaccination with ChAdOx1-M-NY (± tPA or ± Ii) and a boost vaccination with either MVA-M or MVA-NY (or PBS sham vaccinations at identical time-points) and the antigen-specific T-cell response in the blood was assessed after each, as described Figure 3.3. The percentage of IFN-γ+ CD4+ T-cells in response to MAGE-A3 peptide stimulation (A) and NY-ESO-1 peptide stimulation (B) was compared after the prime (closed circles) and boost (closed squares). Each symbol represents an individual mouse with 8 mice per group, with data pooled from 2 independent experiments. Statistical significance between the post-prime and post-boost response in each group was determined by a Wilcoxon matched-pairs signed rank test. *, $p \leq 0.05$, **.

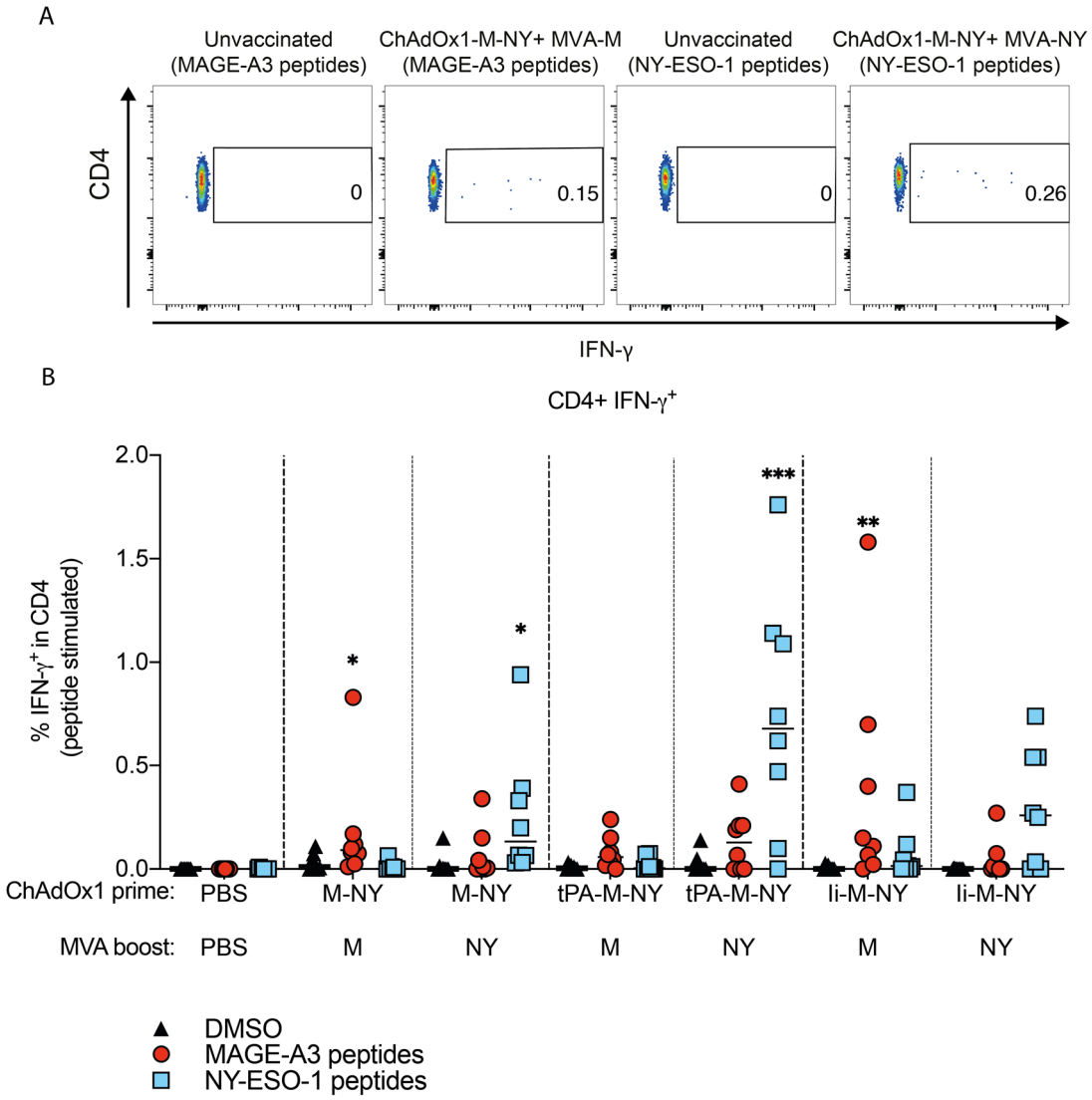


Figure 3.12. IFN-γ response by MAGE-A3-specific and NY-ESO-1-specific CD4+ T-cells after MVA boost vaccination. CD1 mice received a prime vaccination with ChAdOx1-M-NY (± tPA or ± Ii) and a boost vaccination 4 weeks later with either MVA-M or MVA-NY (or PBS sham vaccinations at identical time-points). To measure the antigen-specific CD4+ T-cell response after the MVA boost, mice were bled 14 days after vaccination and PBMCs were stimulated ex vivo with 4μg/ml of pools of either MAGE-A3 or NY-ESO-1 overlapping peptides, or a vehicle control (DMSO). The percentage of cytokine-producing antigen-specific CD4+ T-cells in the blood was determined by ICS and flow cytometry (gating strategy as described in Figure 2.2). Representative dot plots showing gating of CD4+ IFN-γ+ T-cells (A). Percentage of IFN-γ+ CD4+ T-cells in response to stimulation with MAGE-A3 peptides (red circles), NY-ESO-1 peptides (blue squares) or DMSO (black triangles) (B). Data are shown as the median response of each group (horizontal lines). Each symbol represents an individual mouse, with 8 mice in the PBS group and 16 mice per ChAdOx1 vaccinated group, pooled from 2 independent experiments. Statistically significant difference is shown compared to the PBS control group and was determined by a Kruskal-Wallis test with Dunn's multiple comparisons test. *, $p \leq 0.05$, ***, $p \leq 0.001$, ****, $p \leq 0.0001$.

3.3.8 Simultaneous vs alternate MVA boosts

Having evaluated and confirmed the ChAdOx1/MVA heterologous prime-boost vaccination strategy as an efficient means for inducing antigen-specific CD8 and CD4 T-cell responses to both MAGE-A3 and NY-ESO-1, some further aims were addressed. Firstly, whether the addition of an htPA signal sequence at the N-terminal region of the antigen encoded in MVA could increase the magnitude or further improve any aspect of the T-cell responses boosted after ChAdOx1 prime vaccination was assessed. Secondly, the tumours of some patients may express both MAGE-A3 and NY-ESO-1 simultaneously. Alternatively, tumours expressing only one antigen at the time of diagnosis or may progress to reactivate expression of the other antigen at a later time point throughout the course of tumour growth and evolution. It could therefore be advantageous in terms of anti-tumour efficacy to either boost the CD8+ T-cell response against both antigens simultaneously or alternately as part of a vaccination treatment schedule. With this scenario in mind, it was evaluated as to whether boosting the response against both MAGE-A3 and NY-ESO-1 with MVA vectors could be done more effectively with simultaneous dual MVA vaccinations or alternating MVA vaccinations.

From this point forward the ChAdOx1-Ii-M-NY vector incorporating the invariant chain sequence was used in all heterologous prime-boost vaccinations. This was chosen as although a clear benefit in terms of vaccine immunogenicity from the addition of the invariant chain could not be identified in this study, all ChAdOx1-M-NY vectors tested were seen to induce very strong CD8+ T-cell responses, and

the effect of fusing the invariant chain to the encoded antigen on enhancing T-cell responses has recently become well established using a range of adenoviral vaccine platforms and target antigens.

3.3.9 ChAdOx1 + MVA + MVA prime-boost-boost vaccinations

To address whether alternate or simultaneous MVA boosts would be a more efficient strategy for boosting CD8+ T-cell responses against both the MAGE-A3 and NY-ESO-1, a vaccination study was performed as shown according to the scheme in Figure 3.13 and the groupings in Table 3.3. CD1 mice were given a prime vaccination with ChAdOx1-Ii-M-NY and then 4 weeks later received either a single boost vaccination with MVA encoding MAGE-A3 or NY-ESO-1 or alternatively received two simultaneous boost vaccinations with two separate MVA vectors, one encoding MAGE-A3 and the other encoding NY-ESO-1. The mice then received a second set of MVA boost vaccinations a further 4 weeks after the first, with either an MVA vector encoding the alternate antigen to that contained in the first MVA boost, or again with two simultaneous vaccinations with an MVA vector encoding MAGE-A3 and an MVA vector encoding NY-ESO-1. Additionally groups were included to evaluate the effect on the antigen-specific T-cell response of incorporating the tPA sequence fused to the N-terminal region of the antigen encoded in the MVA. MVA vectors encoding the tPA sequence were only used once in the first boost vaccination, so as to avoid generating an antigen-specific response against tPA-derived sequences that might potentially divert the response away from the desired antigen sequence. As before, the

response to vaccination was tested in the blood 2 weeks after each vaccination via ex vivo stimulation of PBMCs with overlapping pools of MAGE-A3 and NY-ESO-1 peptides, followed by flow cytometry analysis of cytokine responses. The experiment was terminated one day after the final blood sampling, and the MAGE-A3 and NY-ESO-1-specific response was further tested in the spleen, as the spleen is an important secondary lymphoid organ for initiating immune responses.

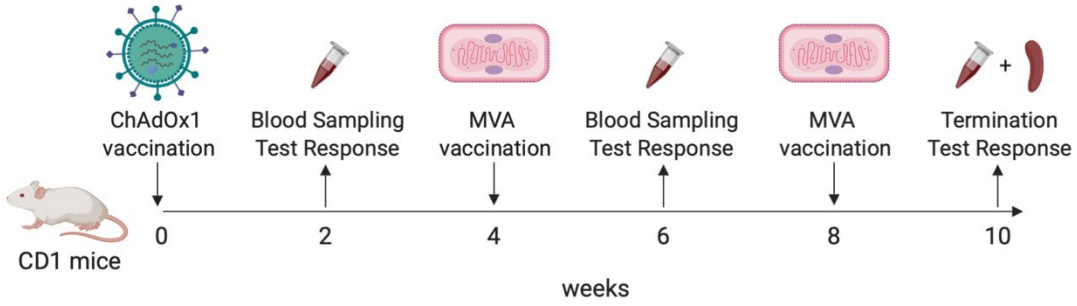


Figure 3.13. Timeline of the ChAdOx1-MVA-MVA prime-boost-boost vaccination scheme with vectors encoding MAGE-A3 and NY-ESO-1. CD1 outbred mice received a prime vaccination via intramuscular injection (i.m.) with 10^8 IU of ChAdOx1-Ii-M-NY. 4 weeks after ChAdOx1-M-NY mice received a boost vaccination via a single i.m injection with 10^7 PFU of either MVA-M (± tPA) or MVA-NY (± tPA), or two i.m injections – one with 10^7 PFU of MVA-M (± tPA) and the other 10^7 PFU of MVA-NY (± tPA). A further 4 weeks after the first MVA boost mice received another boost vaccination via i.m injection with 10^7 PFU of either MVA-M or MVA-NY, or again two i.m injections – one with 10^7 PFU of MVA-M and the other with 10^7 PFU of MVA-NY. I.m. injections were administered in the same site at each time point (right thigh muscle) with the exception of dual MVA boosts, where one MVA vaccination was administered in the right thigh and the other in the left thigh. Vaccinations were given according to the experimental groupings shown in Table 3.1. To test the response to vaccination, mice were bled 14 days after vaccination with ChAdOx1 and 14 days after each vaccination with MVA. On the day following the last bleed, mice were sacrificed and spleens harvested to obtain splenocytes to further test the response. Figure created with BioRender.

Table 3.3. Experimental groupings for ChAdOx1-MVA-MVA prime-boost-boost study

Group	ChAdOx1 Prime vaccination	MVA Boost 1 vaccination	MVA Boost 2 vaccination
1	PBS	PBS	PBS
2	Ii_MAGE-A3_NY-ESO-1	MAGE-A3	NY-ESO-1
3		NY-ESO-1	MAGE-A3
4		tPA_MAGE-A3	NY-ESO-1
5		tPA_NY-ESO-1	MAGE-A3
6		MAGE-A3 + NY-ESO-1	MAGE-A3 + NY-ESO-1
7		tPA-MAGE-A3 + tPA-NY-ESO-1	MAGE-A3 + NY-ESO-1

3.3.10 Antigen specific T-cell responses induced by ChAdOx1-Ii-M-NY prime vaccination

The induction of antigen-specific CD8+ and CD4+ T-cell responses by vaccination with ChAdOx1-Ii-M-NY in CD1 mice was again confirmed (Figure 3.14). In comparison to the PBS sham vaccinated group, statistically significant production of IFN-γ and IL-2 by CD8+ T-cells and IL-2 by CD4+ T-cells was detected in

response to MAGE-A3 and NY-ESO-1 peptide stimulation. As carried out previously, mice were then randomized into new experimental groupings based on their CD8 T-cell response to MAGE-A3 and NY-ESO-1 to ensure an equal distribution prior to MVA vaccination.

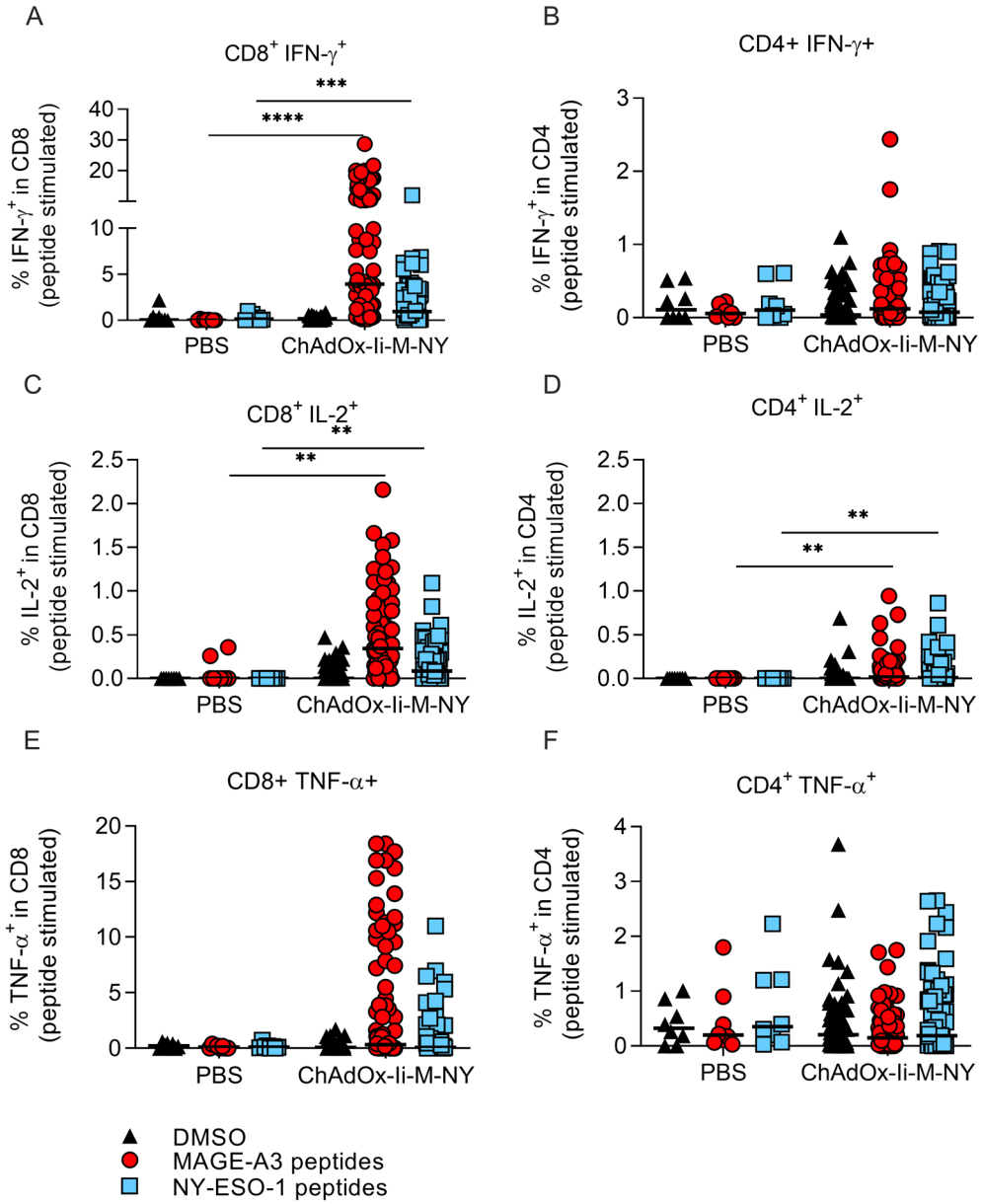


Figure 3.14. MAGE-A3 and NY-ESO-1-specific T-cell responses in the blood after ChAdOx1-Ii-M-NY vaccination. To evaluate the magnitude of antigen-specific T-cell responses induced by ChAdOx1-Ii-M-NY vaccination, blood was sampled 18 days after vaccination and PBMCs were stimulated ex vivo with 4μg/ml of either MAGE-A3 or NY-ESO-1 peptide pools, or a vehicle control (DMSO). The percentage of cytokine-producing antigen-specific CD8+ and CD4+ T-cells in the blood was determined by ICS and flow cytometry (gating strategy as described in Figure 2.2). Percentage of IFN-γ+ (A), IL-2+ (C) and TNF-α+ (E) CD8+ T-cells and IFN-γ+ (B), IL-2+ (D) and TNF-α+ (F) CD4+ T-cells in response to stimulation with MAGE-A3 peptides (red circles), NY-ESO-1 peptides (blue squares) or DMSO (black triangles). Data are shown as the median response of each group (horizontal lines). Each symbol represents an individual mouse, with 8 mice in the PBS group and 84 mice per ChAdOx1 vaccinated group, pooled from 2 independent experiments. Statistically significant differences between groups were determined by a Kruskal-Wallis test with Dunn's multiple comparisons test. *, $p \leq 0.05$, **, $p \leq 0.01$ ***, $p \leq 0.001$.

3.3.11 Fusion of the tPA signal sequence to the antigen in the MVA vector does not increase the magnitude of the antigen-specific CD8+ and CD4+ T-cell responses post-boost

The magnitude of MAGE-A3-specific and NY-ESO-1-specific CD8+ T-cell responses were again considered after the MVA boost vaccination. Firstly, the quesiton of whether incorporating the tPA sequence at the N-terminus of the MAGE-A3 or NY-ESO-1 antigen sequence encoded in MVA could increase the CD8+ T-cell response boosted by vaccination was addressed. Initially, just IFN-γ production in response to peptide stimulation was considered.

Compared to the PBS group, 2 weeks post MVA vaccination all groups that received MAGE-A3 encoded in the MVA antigen had significantly inreased high magnitude MAGE-A3-specific CD8+ T-cell responses (Figure 3.15). The boosting of the NY-ESO-1-specific CD8+ T-cell response however was slightly more variable than the MAGE-A3 response in this study. Only the group that received both MVA-tPA-M and MVA-tPA-NY vaccinations simultaneously had significantly increased NY-ESO-1 specifc CD8+ T-cells compared to the PBS (Figure 3.15). This is despite IFN-γ production by CD8+ T-cells in PBS sham vaccinated mice being almost undetectable and very high percentages of IFN-γ producing CD8+ T-cells being observed in over half of the mice in all of the groups that received an MVA vaccination encoding NY-ESO-1. Comparing groups that received a vaccination encoding tPA fused to the antigen with those that received a vaccination with no tPA showed that the tPA did not provide any increase to the magnitude of the CD8+ T-cell responses observed. The level of IFN-γ producing CD8+ T-cells in the MVA-M vaccinated group was broadly

similar to that in the MVA-tPA-M group and was not significantly different. This was true when comparing the NY-ESO-1-specific CD8+ T-cell response, with no significant difference being found between the level of IFN-γ producing CD8+ T-cells in the MVA-NY vaccinated group and the MVA-tPA-NY vaccinated group.

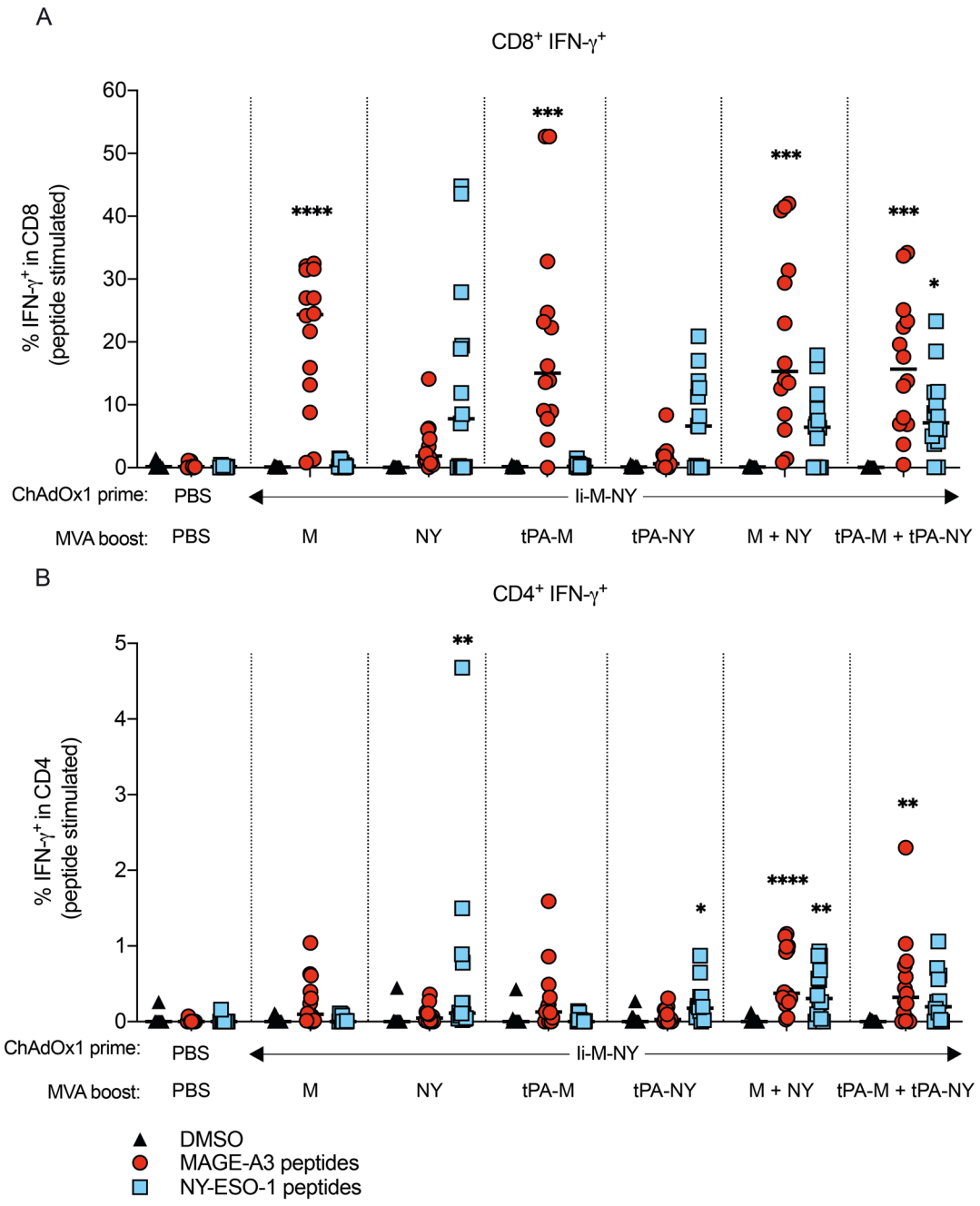


Figure 3.15. MAGE-A3 and NY-ESO-1-specific T-cell response in the blood after the first MVA boost vaccination. CD1 mice were vaccinated with ChAdOx1 and MVA vectors encoding MAGE-A3 and NY-ESO-1 as described in Figure 3.13. To measure the antigen-specific CD8+ and CD4+ T-cell response after the first MVA boost, mice were bled 14 days after vaccination and PBMCs were stimulated ex vivo with 4μg/ml of pools of either MAGE-A3 or NY-ESO-1 overlapping peptides, or a vehicle control (DMSO). The percentage of cytokine-producing antigen-specific CD8+ and CD4+ T-cells in the blood was determined by ICS and flow cytometry (gating strategy as described in Figure 2.2). Percentages of IFN-γ+ CD8+ T-cells (A) and IFN-γ+ CD4+ T-cells (B) in response to stimulation with MAGE-A3 peptides (red circles), NY-ESO-1 peptides (blue squares) or DMSO (black triangles) (B). Data are shown as the median response of each group (horizontal lines). Each symbol represents an individual mouse, with 8 mice in the PBS group and 14 mice per ChAdOx1/MVA vaccinated group, pooled from 2 independent experiments. Statistically significant difference is shown compared to the PBS control group and was determined by a Kruskal-Wallis test with Dunn's multiple comparisons test. *, $p \leq 0.05$, ***, $p \leq 0.001$, ****, $p \leq 0.0001$.

3.3.12 MAGE-A3 and NY-ESO-1-specific CD8+ T-cell responses can be boosted simultaneously or alternately with MVA vectors encoding a single antigen

Next it was evaluated whether alternate MVA vaccinations might be more efficient than simultaneous MVA vaccinations as a strategy for boosting the magnitude of the CD8+ T-cell response against both MAGE-A3 and NY-ESO-1. Firstly, the response after the first MVA boost vaccinations was considered. Both MAGE-A3 and NY-ESO-1-specific CD8+ T-cells were detected in the blood of mice that received simultaneous MVA-M and MVA-NY vaccinations, as well as in those that received simultaneous MVA-tPA-M and MVA-tPA-NY vaccinations (Figure 3.15). Compared to the PBS control, significantly higher frequencies of MAGE-A3-specific CD8+ T-cells were detected in the blood the MVA-M + MVA-NY and MVA-tPA-M + MVA-tPA-NY vaccinated groups (Figure 3.15). The magnitude of the NY-ESO-1-specific CD8+ T-cell response was significant for the MVA-tPA-M + MVA-tPA-NY vaccinated group but was slightly more variable in the MVA-M and MVA-NY vaccinated group, which just fell below the threshold of significance. Crucially, no significant difference was found in terms of level of either the MAGE-A3 and NY-ESO-1-specific CD8+ T-cell response between the groups that received two simultaneous MVA vaccinations against both antigens and those groups that received only a single MVA vaccination against one antigen (Figure 3.15). This suggests that there is no trade-off in terms of the magnitude of CD8+ T-cell response generated against either MAGE-A3 or NY-ESO-1 by boosting against both antigens simultaneously with two separate MVA vectors.

To determine whether alternately boosting the response against MAGE-A3 and NY-ESO-1 could be more effective than simultaneously boosting against both antigens, mice received a second round of MVA vaccinations 4 weeks after the first. The single MVA boosted groups received a vaccination with MVA encoding the alternate antigen to that received in the first boost, whilst the dual boosted groups again received dual vaccinations. The response was evaluated in the blood and spleen 2-weeks after vaccination (Figure 3.16 and Figure 3.17). At this time-point, in the blood and particularly the spleen, there was a trend towards higher frequency CD8+ T-cell responses to both MAGE-A3 and NY-ESO-1 in both dual MVA boosted groups, compared to the alternate MVA boosted groups, however this was not significant (Figure 3.16 A and Figure 3.17 A). This trend may indicate an advantage for boosting successively against both antigens simultaneously, rather than alternately if a response to both is desired.

For the alternately boosted groups, the timing of the MVA vaccination appears critical in terms of generating the highest possible magnitude response to a particular antigen. The kinetics of both the MAGE-A3 and NY-ESO-1 response in the blood at each time point are shown in Figure 3.18, to give a clearer visualization of how the CD8+ T-cell response to each antigen changes over time. A higher magnitude CD8+ T-cell response is generated against the antigen when it is given in the first MVA vaccination rather than the second. As previously observed, the level of antigen-specific CD8+ T-cells in the blood declines after the ChAdOx1 vaccination unless an MVA boost encoding that antigen is given. In the alternately boosted groups, when measuring the response 2-weeks after the first

MVA vaccination (corresponding to 6-weeks after the ChAdOx1), very few MAGE-A3-specific or NY-ESO-1 CD8+ T-cells can be detected in the blood if the response against the antigen was not boosted with MVA. When measuring the response 2-weeks after the second MVA vaccination (corresponding to 10-weeks after the ChAdOx1), the second of the two alternately given MVA vaccinations is able to boost the level of the response to the encoded antigen to a higher level than to which it has declined. However, the magnitude of the response is not boosted to the same peak magnitude as when the MVA is given at the time-point 4-weeks post ChAdOx1. This suggests that in such a vaccination strategy, it is critical to boost the response against either antigen with a 4-week interval between ChAdOx1 and MVA, in order to achieve the highest level antigen-specific response. However, comparing all the groups at the time-point 2 weeks after the second MVA boost is given, all of the alternately boosted groups have broadly equivalent levels of MAGE-A3 and NY-ESO-1-specific CD8+ T-cells in both the blood and the spleen, regardless of the order that the MVA vaccinations are given – MVA encoding MAGE-A3 first or MVA encoding NY-ESO-1 first (Figure 3.16 and Figure 3.17).

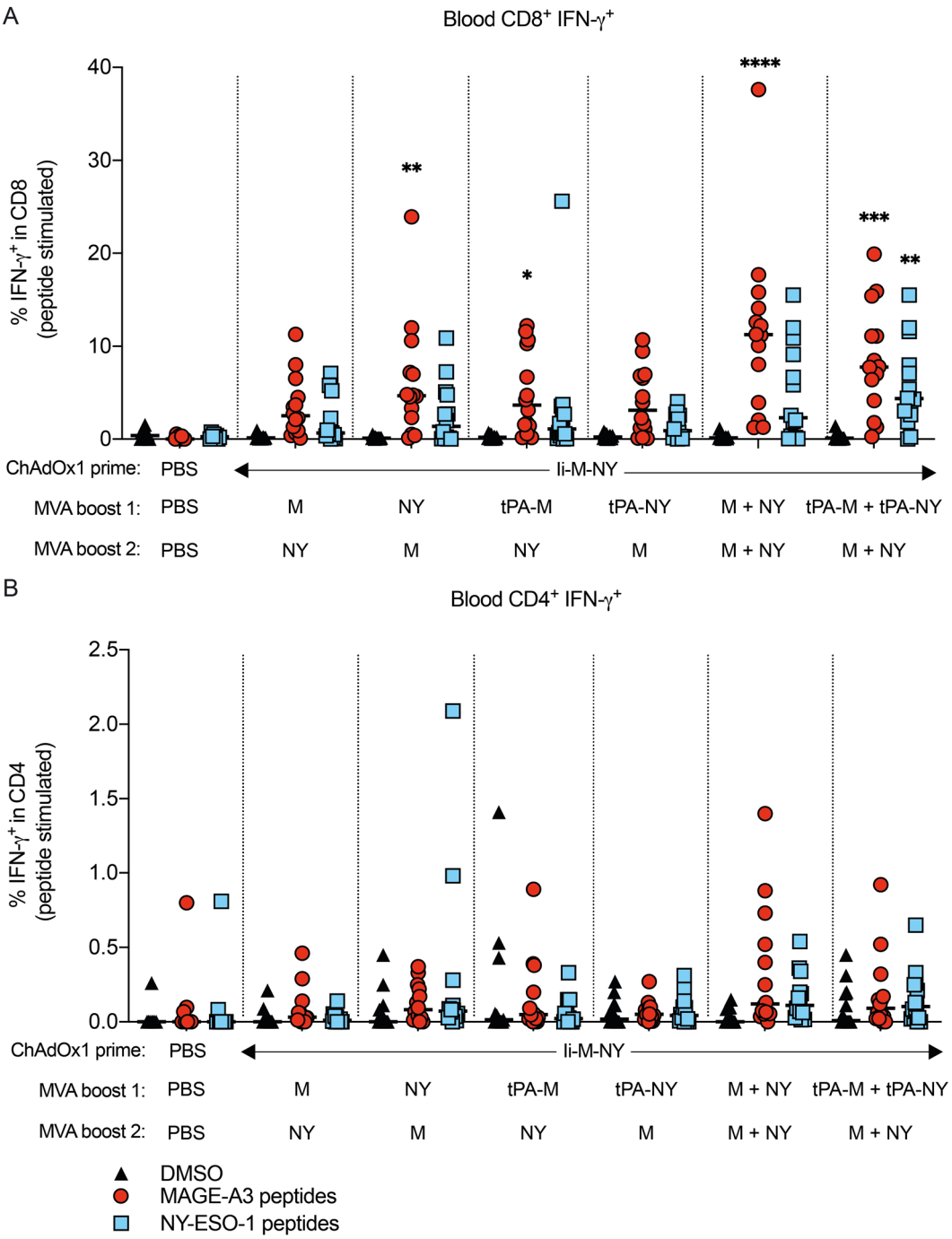


Figure 3.16. MAGE-A3 and NY-ESO-1-specific T-cell response in the blood after the second MVA boost vaccination. CD1 mice were vaccinated with ChAdOx1 and MVA vectors encoding MAGE-A3 and NY-ESO-1 as described in Figure 3.13. To measure the antigen-specific CD8+ and CD4+ T-cell response after the second MVA boost, mice were bled 14 days after vaccination and PBMCs were stimulated ex vivo with 4μg/ml of pools of either MAGE-A3 or NY-ESO-1 overlapping peptides, or a vehicle control (DMSO). The percentage of cytokine-producing antigen-specific CD8+ and CD4+ T-cells in the blood was determined by ICS and flow cytometry (gating strategy as described in Figure 2.2). Percentages of IFN-γ+ CD8+ T-cells (A) and IFN-γ+ CD4+ T-cells (B) in response to stimulation with MAGE-A3 peptides (red circles), NY-ESO-1 peptides (blue squares) or DMSO (black triangles) (B). Data are shown as the median response of each group (horizontal lines). Each symbol represents an individual mouse, with 8 mice in the PBS group and 14 mice per ChAdOx1/MVA vaccinated group, pooled from 2 independent experiments. Statistically significant difference is shown compared to the PBS control group and was determined by a Kruskal-Wallis test with Dunn's multiple comparisons test. *, $p \leq 0.05$, ***, $p \leq 0.001$, ****, $p \leq 0.00$

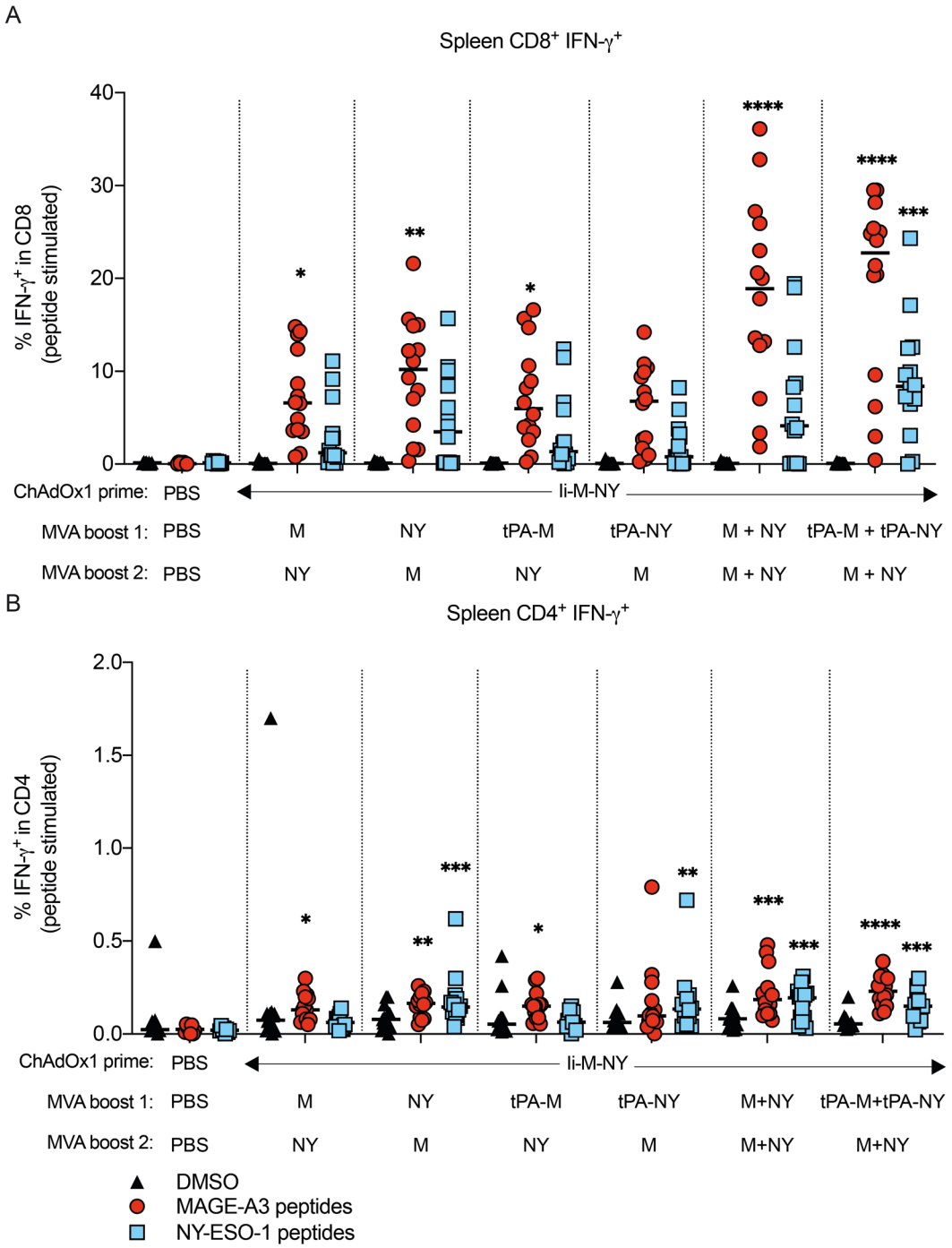


Figure 3.17. MAGE-A3 and NY-ESO-1-specific T-cell response in the spleen after second MVA vaccinations. CD1 mice were vaccinated with ChAdOx1 and MVA vectors encoding MAGE-A3 and NY-ESO-1 as described in Figure 3.13. Mice were sacrificed 15 days after last vaccination and splenocytes were stimulated ex vivo with 4μg/ml of pools of either MAGE-A3 or NY-ESO-1 overlapping peptides, or a vehicle control (DMSO). The percentage of cytokine-producing antigen-specific CD8+ and CD4+ T-cells in the spleen was determined by ICS and flow cytometry (gating strategy as described in Figure 2.2). Percentages of IFN-γ+ CD8+ T-cells (A) and IFN-γ+ CD4+ T-cells (B) in response to stimulation with MAGE-A3 peptides (red circles), NY-ESO-1 peptides (blue squares) or DMSO (black triangles) (B). Data are shown as the median response of each group (horizontal lines). Each symbol represents an individual mouse, with 8 mice in the PBS group and 14 mice per ChAdOx1/MVA vaccinated group, pooled from 2 independent experiments. Statistically significant difference is shown compared to the PBS control group and was determined by a Kruskal-Wallis test with Dunn's multiple comparisons test. *, $p \leq 0.05$, ***, $p \leq 0.001$, ****, $p \leq 0.0001$.

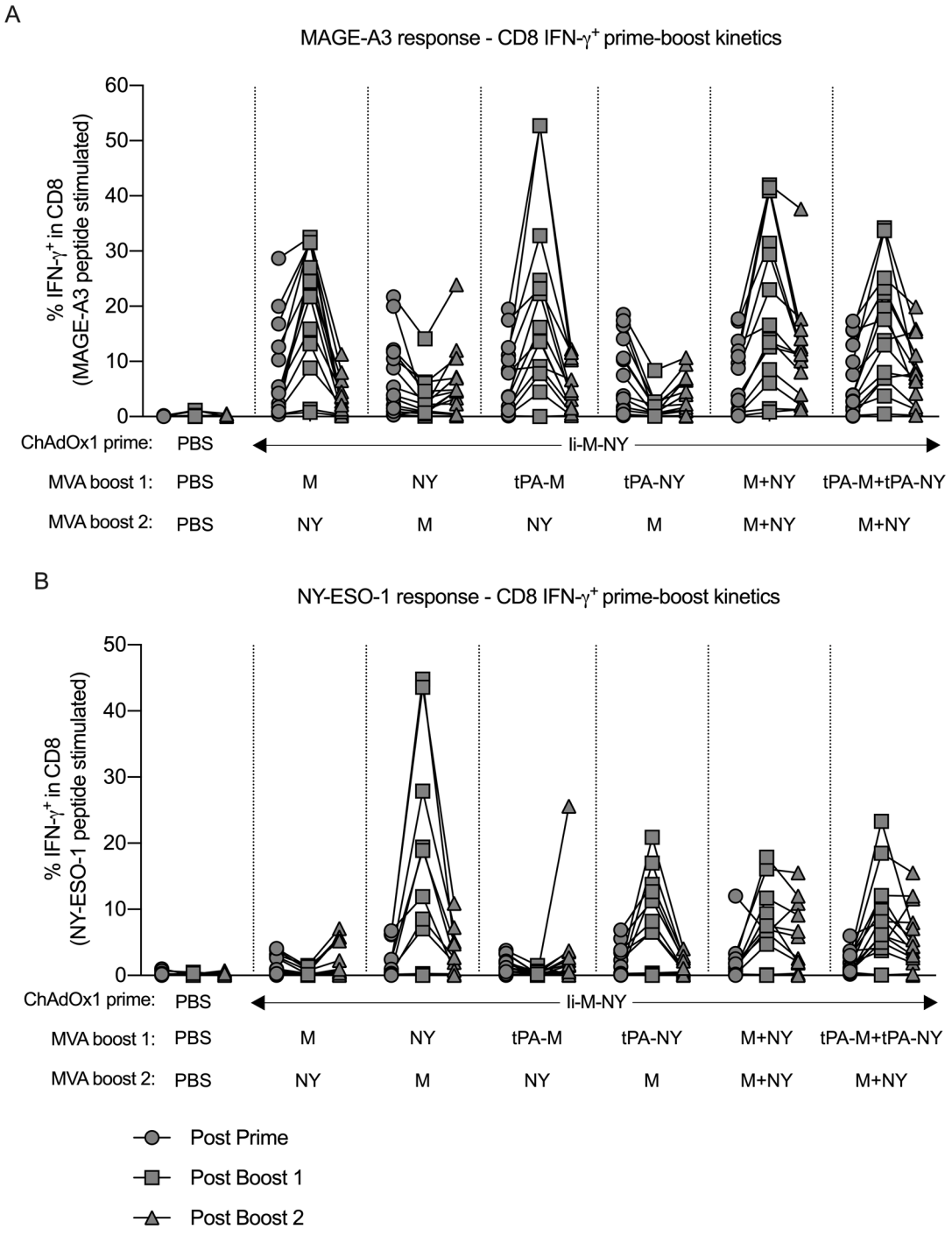


Figure 3.18. Kinetics of MAGE-A3 and NY-ESO-1-specific CD8+ T-cell response in the blood. CD1 mice were vaccinated with ChAdOx1 and MVA vectors encoding MAGE-A3 and NY-ESO-1 as and the antigen-specific T-cell response in the blood was assessed after each vaccination, as described in Figure 3.13 .The percentage of IFN-γ+ CD8+ T-cells in response to MAGE-A3 peptide stimulation (A) and NY-ESO-1 peptide stimulation (B) was compared after the prime (closed circles) and boost (closed squares) and second boost (closed triangles). Each symbol represents an individual mouse with 14 mice per group, with data pooled from 2 independent experiments. Statistical significance between the response from the previous time-point in each group was determined by a Wilcoxon matched-pairs signed rank test. *, $p \leq 0.05$, **.

3.3.13 Vaccination induces CD8+ T-cell responses against epitopes covering a broad range of sites in MAGE-A3 but against a narrow region of NY-ESO-1.

Vaccinations that induce a CD8+ T-cell response against a broad range of epitopes from the target antigen could be more efficacious than ones that induce a response against only a narrower range. This is particularly important in the setting of cancer, where certain regions of protein could either be lost or mutated. Although such an evaluation would be most relevant in the human setting and human HLA specificity, the breath of the response to MAGE-A3 and NY-ESO-1 was nonetheless tested to evaluate the capacity of the ChAdOx1/MVA vaccinations to induce a response against epitopes covering multiple regions of the encoded antigens. To test the breadth of the response, splenocytes from vaccinated mice were stimulated with a number of smaller pools of peptides each containing sequences spanning in total shorter regions of each protein. The level of IFN-γ production by CD8+ T-cells in response to stimulation with each pool was then assessed by a flow cytometry-based ICS assay (Figure 3.19). This was performed with six mice that had been vaccinated with a ChAdOx1-Ii-M-NY prime and two rounds of both MVA-M and MVA-NY boosts and found prior to have detectable responses against both MAGE-A3 and NY-ESO-1. Information on the protein sequences contained within each pool can be found within the appendix. The stimulation with peptides spanning the entire proteins confirmed that all mice had detectable CD8+ T-cell responses against both MAGE-A3 (Figure 3.19 A) and NY-ESO-1 (Figure 3.19 B) in the spleen. Dissecting the response to MAGE-A3 showed the CD8+ T-cell response to be quite broad and directed against epitopes from multiple regions of the protein (Figure 3.19 A). In three mice, CD8+ T-cells

producing IFN-γ were identified in response to stimulation with peptides of sequences found in both pools 7 and 8. Two mice showed a CD8+ T-cell response towards peptides in both pools 2 and 3, whilst one mouse showed a CD8+ T-cell response only in pool 3. The CD8+ T-cell response against NY-ESO-1 however was found to directed solely against a much smaller region of the protein (Figure 3.19 B). In all six mice IFN-γ production by CD8+ T-cells was detected only after stimulation with peptides from pool 3, and none of the other 4 sub-pools.

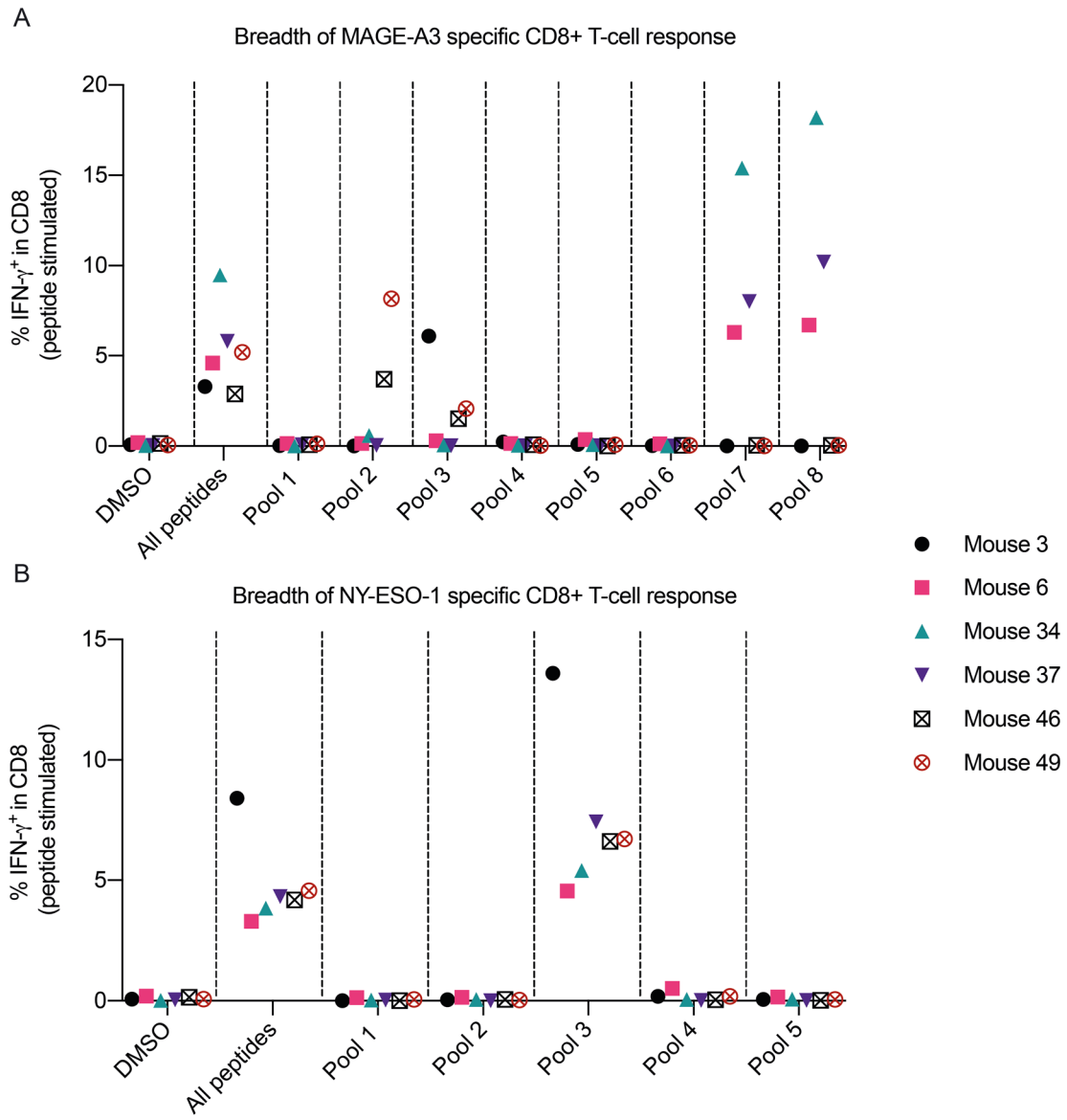


Figure 3.19. Breadth of the MAGE-A3 and NY-ESO-1-specific CD8+ T-cell responses induced by ChAdOx1/MVA/MVA vaccination. Six CD1 mice were vaccinated with ChAdOx1 and MVA vectors encoding MAGE-A3 and NY-ESO-1 as described in Figure 3.13. Mice were sacrificed 15 days after last vaccination and splenocytes were stimulated ex vivo with subpools of MAGE-A3 and NY-ESO-1 peptides, or DMSO. Percentages of IFN-γ+ CD8+ T-cells in response to stimulation with MAGE-A3 peptide subpools (A) and NY-ESO-1 peptide subpools (B). A positive response to stimulation with a pool was defined as a frequency of IFN-γ-producing CD8+ T-cells cells greater than 3 standard deviations above the mean of the signal from the unstimulated (DMSO) control samples.

3.4 Discussion

The human MAGE-type antigens MAGE-A3 and NY-ESO-1 are highly attractive targets for a therapeutic cancer vaccine based on their known immunogenicity, restricted healthy-tissue expression, and widespread expression in a range of cancers [174, 175]. A potent MAGE-type-antigen targeting therapeutic cancer vaccine could form the basis of a highly effective immunotherapeutic strategy. However despite many attempts, MAGE-targeting therapeutic cancer vaccines have so far not demonstrated significant clinical efficacy in cancer patients, very likely due to the inability of the platforms used to induce robust tumour-specific CD8+ T-cell responses in humans [198, 199]. Induction of strong antigen-specific CD8+ T-cell responses is one of the central requirements for a cancer vaccine to have effective anti-tumour activity.

This study therefore aimed to develop and evaluate in a pre-clinical setting a vaccination strategy based on a heterologous prime-boost with ChAdOx1/MVA viral vectors as a means to induce more potent CD8+ T-cell responses against MAGE-A3 and NY-ESO-1. The results presented in this chapter demonstrate that a heterologous prime-boost vaccination with ChAdOx1/MVA encoding MAGE-A3 and NY-ESO-1 has the capability to induce exceptionally high magnitude CD8+ T-cell responses against both antigens. In some mice frequencies of transgene-specific CD8+ T-cells approaching 50% (of total blood CD8+ T-cells) were observed after the boost. Even higher frequencies of specific T-cells than this may have been generated, given that the post boost response was measured 14 days after MVA vaccination, which may have been later than the peak of the

response. The CD8+ T-cell responses to both antigens were also to some degree multifunctional, with a proportion of CD8+ T-cells producing three type I cytokines - IFN-γ, TNF-α and IL-2.

Given that direct cell mediated cytotoxicity is a key effector function by which CTLs mediate killing against cancer cells, the results presented in this study could be enhanced by an investigation of the cytotoxic capability of the MAGE-antigen-specific CD8+ T-cells induced by ChAdOx1/MVA vaccination [69, 224]. This could be performed by also measuring expression of the cytotoxic mediators granzyme B and perforin by antigen-specific IFN-γ+ cells via flow cytometry, through the development of an expanded multi-colour flow antibody panel. Cytotoxicty could also be measured through a CD107a mobilisation assay [225, 226]. CD107a, or lysosomal associated membrane protein 1 (LAMP-1), is a protein present in the membranes of perforin/granzyme B containing granules in CTLs. During the process of CTL degranulation, granules are trafficked from the cytoplasm to the cell surface and fuse with the outer membrane. This leads to the transient localization of CD107a on the CTL surface. CD107a can therefore be used as a marker for degranulation, and monitoring of its mobilization to the cell surface by flow cytometry in response to peptide-specific stimulation enables T-cell cytotoxicity capacity to be assessed.

Although this initial evaluation was performed using human antigens in a murine setting, the positive results obtained here can be prospectively transferred to the human setting, given the well-established immunogenicity of both the

ChAdOx1/MVA platform and MAGE-A3 and NY-ESO-1 antigens in humans. Prime-boost vaccinations with recombinant ChAd/MVA vectors have been found to induce some of the highest recorded magnitude CD8+ T-cell response against antigens from a range of infectious disease settings [150-152]. Indeed comparing immunogenicity data from vaccine trials, as well as head-to-head comparisons with other antigen-delivery systems in mice have clearly shown the advantage of adenovirus/MVA prime-boost strategies for generating antigen specific CTL responses [138, 227]. Conversely, clinical studies of most MAGE-targeting vaccine candidates have reported the generation of CD4+ T-cell responses and humoural immunity, but little in the way of antigen-specific CTL responses [200, 201, 204, 209].

The pre-clinical setting was also used to investigate and inform as to the most promising strategy for inducing CD8+ T-cell responses in terms of combinations of vectors, vaccination schedule, and use of molecular adjuvants. These are questions that are difficult to address in the clinic given the length and expense of clinical trials, and often limited numbers of patients. A dual antigen prime single antigen boost vaccination approach was taken here, using a ChAdOx1 vector encoding a MAGE-A3 and NY-ESO-1 fusion construct for the prime and MVA encoding a single antigen, either MAGE-A3 or NY-ESO-1 for the boost. Vaccination with the ChAdOx1 vector alone encoding the fusion construct induced both CD8+ and CD4+ T-cell responses simultaneously against both MAGE-A3 and NY-ESO-1. The boost vaccination with MVA encoding a single antigen then afforded a high degree of selectivity for whichever of the two

antigens was desired to direct the response against. The magnitude of the CD8+ T-cell response could be greatly increased against either MAGE-A3 or NY-ESO-1, depending on which was encoded in the MVA vector. These results clearly demonstrate the fine control that the heterologous prime-boost ChAdOx1/MVA vaccine platform can exert over the nature and direction of the CD8+ T-cell response. This is an important feature in a clinical setting given that an individual patient may have a tumour expressing only one of either MAGE-A3 or NY-ESO-1. Coupled with molecular screening by a method such as rt-qPCR to determine the relative tumoural expression level of each antigen from patient biopsies, this would enable a personalized tailoring of the response in terms of choosing which antigen to predominantly direct the CD8+ T-cell response against. This versatility greatly improves the utility of the vaccine as it enables its use for both patients with tumours expressing only MAGE-A3 and patients with tumours expressing only NY-ESO-1.

A dual-antigen ChAdOx1 prime dual-antigen MVA boost approach was initially considered. However, the dual-antigen-prime single-antigen-boost approach was chosen due to concerns over potential immunodominance of NY-ESO-1. It was hypothesised that CD8+ T-cell responses against NY-ESO-1 may prove immunodominant in humans, given the frequency with which they are observed in patients bearing NY-ESO-1+ tumours [187, 189, 190]. In this scenario, when boosting against both antigens the response may be directed proportionally more against NY-ESO-1 than MAGE-A3. This would be problematic for treating patients with tumours positive for MAGE-A3 expression, but not NY-ESO-1. A

dual-prime dual-boost approach therefore would by nature not have permitted this degree of selectivity, and in cases of patients expressing only MAGE-A3 may possibly prevent the induction of good CTL responses against MAGE-A3.

Nonetheless, a strategy of boosting the response against both antigens was investigated here. In a therapeutic setting, targeting an immune response against two rather than a single antigen might produce a stronger more effective CD8+ T-cell response against a tumour, and could potentially decrease the likelihood of antigen-loss mediated tumour immune escape occurring. An approach of alternately boosting against MAGE-A3 and then NY-ESO-1 (or vice versa) with two successive MVA vaccinations was compared to boosting against both antigens simultaneously, with two MVA vaccinations, one against each antigen.

In the setting of alternate vaccinations, the order of the MVA boost vaccinations was crucial in order to achieve a maximum 'peak' response against a particular antigen. The CD8+ response against the recombinant antigen encoded in MVA was boosted most efficiently when administered at the time-point of 4-weeks after ChAdOx1, as opposed to 8-weeks. This could be due to 2 likely reasons; 1) it indicates that timing of the window between ChAdOx1 and MVA being given is critical, with 4-weeks between ChAdOx1 and MVA giving a more optimal boosting of the response than 8-weeks, or 2) that neutralizing antibodies could have developed against the MVA viral coat proteins blunting some of its infective capacity and making for a less effective boost of the CD8+ T-cell response. For a therapeutic cancer vaccine, the absolute magnitude of the peak CD8+ T-cell

response generated is likely to be key for anti-tumour efficacy, so these results suggest that it may be best to boost first against the antigen of highest priority if there is a preference e.g. expression of one antigen is higher than the other in a given patient's tumour. Despite this observation, a study investigating different vaccine schedules of a ChAd63/MVA vaccine encoding ME-TRAP in the clinic demonstrated that the interval between ChAd63and MVA may be flexible in humans, as MVA given both 4 or 8 weeks after ChAd63 generated equally high magnitude TRAP-specific CD8+ T-cell responses [228].

Boosting against both MAGE-A3 and NY-ESO-1 simultaneously however may be a superior approach than boosting alternately for generating a response against both antigens. There was a trend, although not significant, towards higher CD8+ and CD4+ T-cell responses against both MAGE-A3 and NY-ESO-1 in the blood and spleen when measured at week 10 after 2 rounds of MVA in the groups that had received two simultaneous boosts compared to those that had received alternate boosts. These results suggest that in practical terms a simultaneous boost against two given antigens with two MVA vaccinations after a ChAdOx1 prime encoding both is entirely feasible. No trade-off or partitioning of the response was observed when simultaneous boosts were given, as the magnitude of the response to each antigen was boosted to equivalent levels to that seen in mice from groups where a boost had been given against one antigen with a single MVA. However, for such an approach in the human setting this will depend on the exact identities of the two antigens chosen, their immunodominant properties, and the HLA haplotype of a particular patient, and therefore this question

regarding the specific combination of MAGE-A3 and NY-ESO-1 could only be answered in the clinic.

The use of Ii and tPA molecular adjuvants was also evaluated here as a means for increasing the magnitude of the responses against the antigens encoded in the viral vectors, as they have been seen to do so in studies testing responses against different antigens. However, in this setting, no benefit for their inclusion was identified. It was hypothesised that this may be due to a combination of the high variability of the magnitude of the T-cell responses observed in CD1 mice, and that the responses observed against the antigens were already at a very high level. Indeed, in CD1 mice, the vaccine induced CD8+ T-cell response to NY-ESO-1 was found to be more variable than against MAGE-A3, with slightly higher proportions of mice observed to mount a significant response to MAGE-A3 than NY-ESO-1.

This might be explained by an unequal translation efficiency of the MAGE-A3-NY-ESO-1 expression construct in the ChAdOx1 vector following vaccination. As MAGE-A3 precedes NY-ESO-1 in the construct, it may be expressed at a higher level, thus resulting in enhanced priming of MAGE-A3 specific CD8+ T-cell responses by ChAdOx1-M-NY vaccination. To test this, the relative translation efficiency could be tested in vitro, or the order of the antigens swapped in the construct to see if the same observation is made in reverse regarding T-cell responses to each antigen. This may also explain why the CD8+ T-cell response specific to NY-ESO-1 appeared somewhat more polyfunctional than that against

MAGE-A3. Levels of antigen exposure are tightly linked to T-cell exhaustion, where excessive or persistence antigenic stimulation causes T-cells to lose polyfunctionality in a progressive manner [229, 230]. More MAGE-A3 specific monofunctional IFN-γ producing CD8+ T-cells could therefore be linked to antigen expression.

This variation could also be explained by the observation that in CD1 mice NY-ESO-1-specific CD8+ T-cell responses were directed against epitopes from one dominant region of the protein. It is likely that this response is directed solely against one particular immuno-dominant epitope and therefore also likely that this epitope is restricted to a particular MHC-class I allele. Some mice in the CD1 population may lack this allele due to the fact that they are outbred and as such have a range of different haplotypes. This can likely explain some of the variability seen in the response to vaccination in CD1 mice. This variability reflects to some degree the challenges of vaccinating against a particular tumour-antigen in a population of human patients. An ideal tumour antigen for a cancer vaccine will ideally have multiple immunogenic epitopes presented by a range of MHC allele haplotypes. Both MAGE-A3 and NY-ESO-1 possess multiple confirmed CTL epitopes bound by different HLA types [165, 185, 231-235]. Viral vectored vaccine platforms have an advantage in this respect over for example peptide vaccines, in that they can encode the sequence for the entire antigen and require no prior choice or identification to be made about the most immunogenic peptide sequences to include. Choosing the wrong epitopes to vaccinate against has been

shown to have a negative effect on the tumour-reactivity of T-cells elicited by a vaccine, as has been found before with peptide based NY-ESO-1 vaccines [236].

An evaluation of a cancer vaccine would not be complete without the assessment of vaccine anti-tumour efficacy. However, as MAGE-A3 and NY-ESO-1 are humans MAGE-type antigens and thus foreign antigens to a mouse immune system, there is no truly relevant mouse tumour model to assess the anti-tumour efficacy of such vaccines. Human MAGE-type antigens such as MAGE-A3 and NY-ESO-1 are very likely to be more immunogenic in mice than a murine self-antigen counterpart, which may generate weaker immune responses due to partial expression in the thymus and subsequent deletion of T-cells bearing high affinity TCRs. Many published studies however have attempted to assess therapeutic efficacy of MAGE-targeting vaccines, frequently using syngeneic tumour models altered transgenically to express human MAGE-type antigens. This however is likely to generate misleading conclusions. For example, the rec-MAGE-A3 vaccine that has failed to demonstrate efficacy in the MAGRIT and DERMA trials was first evaluated in a pre-clinical setting using the TC-1 tumour model from BL/6 mice engineered to overexpress MAGE-A3 [237]. The results obtained here laid the groundwork for the subsequent clinical trials. The vaccine demonstrated good protective efficacy against tumour growth. Unusually however, this was found to be CD4+ T-cell mediated. CD4+ T-cell responses were also found to dominate in the human trials, but despite the promising pre-clinical results, the lack of CD8+ T-cell responses translated to little therapeutic efficacy in cancer patients, highlighting the limitations of conclusions that can be drawn from such an

approach. Therapeutic evaluation of the ChAdOx1/MVA vaccination encoding MAGE-type antigens is addressed in the following chapter where data is presented from studies that evaluate both ChAdOx1/MVA vaccine immunogenicity and anti-tumour activity using murine antigens in a setting more physiologically relevant to the mouse.

Chapter 4. Immunogenicity and anti-tumour therapeutic efficacy of ChAdOx1/MVA P1A vaccination

4.1 Introduction

The results presented in chapter 3 demonstrated that ChAdOx1/MVA prime-boost vaccination has the potential to induce high magnitude CD8+ T-cell responses against the human MAGE-type antigens MAGE-A3 and NY-ESO-1. However as these are xenogeneic antigens to a murine immune system, this setting does not reflect the challenges for a vaccine of inducing T-cell responses against self-antigens that arise due to mechanisms of central and peripheral immune tolerance. With this in mind it was decided to evaluate the ability of ChAdOx1/MVA vaccination to induce T-cell responses against MAGE-type antigens in a more immunologically relevant setting.

As there are no direct homologues in mouse of the human MAGE-A3 and NY-ESO-1 genes, the murine MAGE-type antigen P1A was used. P1A is a protein encoded by the murine cancer-germline gene Trap1a. A peptide derived from P1A is a tumour rejection antigen, termed P815A, and represents the best known murine equivalent of the human MAGE-type antigens [238]. Like the human cancer germline genes, the expression pattern of P1A in healthy tissue is limited to cells of the male germ-line, placenta and developing trophoblast, tissues with reduced expression of MHC-class I molecules (HLA-A and HLA-B downregulation) [239]. Its expression has however been observed in murine tumours, and like the human MAGE-type antigens its expression in tumour can induce spontaneous anti-tumour CD8+ T-cell responses. Indeed, P1A was the first described tumour rejection antigen, demonstrating that CD8+ T-cell responses against tumour-derived antigens can be sufficient to clear neoplastic growths

[172]. Studies have shown that P1A-specific CTL responses are directed solely against a 9-amino acid MHC-class I epitope, $P1A_{35\text{-}43}$LPYLGWLVF, restricted to H-2L^d [238]. The studies presented in this chapter were therefore performed using DBA/2 mice, which bear the H-2L^d MHC-class I allele and in which the majority of studies investigating anti-P1A responses have been carried out. Given that P1A is a non-mutated self-antigen it is likely to be only weakly immunogenic and is thus much more challenging to generate strong antigen-specific T-cell immunity against. On this basis, in this chapter the ability of the ChAdOx1/MVA platform to induce T-cell responses against P1A was therefore evaluated.

Furthermore, it was decided to use the P1A antigen setting to evaluate the anti-tumour efficacy of MAGE-antigen specific T-cell responses induced by ChAdOx1/MVA vaccination. P1A is spontaneously and constitutively expressed in a range of murine tumour models. P1A can therefore be used as a surrogate antigen to assess the anti-tumour efficacy of anti-P1A CTL responses induced by different vaccination strategies. P1A has been used previously as a model MAGE-type tumour antigen in other studies to evaluate the potential of cancer vaccines based on platforms such as other viral vectors and DNA plasmids, highlighting its suitability for this purpose [240] [241] [242].

Inducing high magnitude tumour-antigen-specific CD8+ T-cell responses is certainly a key determinant for a cancer vaccine platform to have effective anti-tumour activity. However, it is clear from recent studies that the this alone may not be sufficient to achieve the goal of effective tumour clearance. The TME of

established tumours is known to be highly immunosuppressive. Vaccine induced tumour-specific T-cells are therefore likely to become inhibited following migration to the tumour site.

Immune checkpoint inhibitors have shown great anti-tumour effect in the clinic by targeting these suppressive mechanisms that are operational in the TME to reinvigorate anti-tumour immune responses [11, 14, 243]. However, in most cancer types therapeutic response rates for CPIs are generally low and improved clinical outcomes are therefore currently limited to a minority of patients, indicating a need for improvement. Limited response rates are believed to be primarily due to the fact that CPIs are not effective in patients lacking spontaneously mounted tumour-specific CD8+ T-cell responses, and thereby have 'cold' tumours lacking the necessary antigen-specific T-cell infiltrate to be reactivated [7].

A combination therapy consisting of ChAdOx1/MVA vaccination against MAGE-type antigens and immune checkpoint blockade could therefore function in a highly complementary manner and synergize on two fronts to increase the therapeutic efficacy of either alone. In the first instance, through the de novo generation of tumour-specific CD8+ T-cells and enhancement of levels of tumour-specific T-cell infiltrate, therapeutic cancer vaccination could expand the proportion of individuals that respond to ICB. Indeed studies have shown strong correlations between patients who respond to treatment with CPIs and the detection of pre-existing MAGE-type antigen-specific CD8+ T-cell responses, for

example responses specific for NY-ESO-1-specific T-cell epitopes in the blood of melanoma patients in the context of anti-CTLA-4 blockade [196]. Looking at this from another angle, CPIs could enhance the anti-tumour activity of vaccine-induced CD8+ T-cells by eliminating T-cell suppressive mechanisms in the TME. Therefore, on this basis, a further aim of this chapter was to explore the potential of such an approach by evaluating the therapeutic efficacy of ChAdOx1/MVA vaccination targeting P1A in combination with CPIs in murine tumour models.

Therefore to test the anti-tumour efficacy of vaccination with ChAdOx1/MVA encoding MAGE-type antigens against MAGE-expressing tumours in a syngeneic tumour setting, ChAdOx1 and MVA vectors were constructed encoding P1A. Two ChAdOx1 vectors were designed and constructed, encoding either just the unmodified P1A coding sequence or with the sequence of the transmembrane domain of the murine MHC-class II invariant chain (mIi) fused to the N-terminus of the coding region (Figure 4.1).

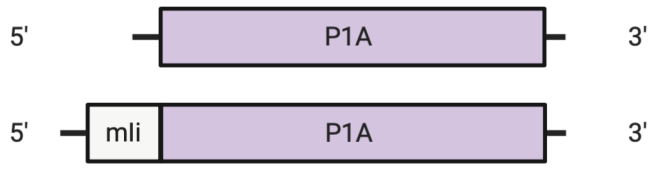


Figure 4.1. Schematic showing the design of ChAdOx1 viral vectors encoding P1A. Two ChAdOx1 viral vectors encoding P1A were constructed. Either the unmodified P1A coding sequence or the P1A coding sequence with the transmembrane domain of the murine MHC-class II invariant chain (mIi) fused to its N-terminus was inserted. Figure created with BioRender.

Additionally, two MVA vectors were designed and constructed, encoding either just the unmodified P1A coding sequence or with tPA fused to the N-terminus of the coding region (Figure 4.2).

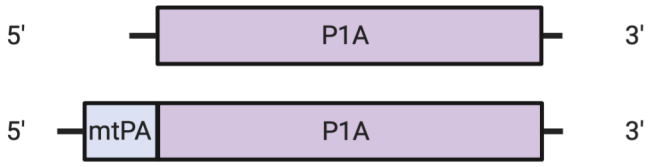


Figure 4.2. Schematic showing the design of MVA viral vectors encoding P1A.

Two MVA viral vectors encoding P1A were constructed. Either the unmodified P1A coding sequence or the P1A coding sequence with the signal peptide from the transmembrane domain of the murine tissue plasminogen activator (mtPA) fused to its N-terminus was inserted. Figure created with BioRender.

Despite an immunodominant minimal MHC-class I epitope from P1A having been already described, the ChAdOx1 and MVA vectors were designed to encode the full length of the P1A antigen rather than the minimal epitope. Studies evaluating P1A-specific T-cell responses induced by DNA vaccine platforms have shown that vectors encoding the full length antigen induce much more efficient P1A-specific CD8+T-cell responses than those encoding only the minimal epitope [241].

Two tumour models were employed in this chapter to evaluate the anti-tumour efficacy of the ChAdOx1/MVA vectors encoding P1A. P815 and 15V4T3 are two P1A-expressing mastocytomas, both syngeneic in mice of DBA/2 genetic background. The P815 tumour line was derived from tumours first induced by methylcholanthrene treatment of a DBA/2 mouse, and since has been widely studied, and was the model in which CD8+ T-cell responses against P1A were first described [244]. 15V4T3 is a tumour line previously derived from several successive in vitro oncogenic modifications of mast cells obtained from DBA/2 mice [181]. The precursor of 15V4T3 is a mast cell line, PB-3c, that was originally established by culturing bone-marrow cells from DBA/2 mice in the presence of

interleukin-3 (IL-3) [245] [246]. PB-3c mast cells were then infected with a retrovirus containing the *v-Ha-ras* gene to derive the cell line 15V4 expressing the *ras* p21 protein, the parental line of 15V4T3 [247] [248] [249]. The 15V4 cell line was found to be capable of forming tumours when injected into DBA/2 mice, from which four independent 15V4 tumours were isolated, termed 15V4T1-4 respectively. These isolated tumours were adapted to in vitro culture to generate four distinct mastocytoma tumour cell lines, all of which retained high tumourigenicity in DBA/2 mice [181]. Conversely compared to either of the P1A-negative parental lines PB-3c or 15V4, two of these cell lines, 15V4T1 and 15V4T3, were found to express high levels of P1A, demonstrating an association between the reactivation of P1A expression and oncogenesis.

The specific aims of this chapter were:

1. To evaluate the immunogenicity of a heterologous prime-boost vaccination regime with ChAdOx1/MVA vectors encoding the murine MAGE-type antigen, P1A. In particular the ability of the platform to induce a robust CD8+ T-cell response against P1A was investigated.

2. To assess the anti-tumour protective and therapeutic efficacy of ChAdOx1/MVA P1A vaccination using P1A-expressing syngeneic tumour models.

3. To evaluate the anti-tumour therapeutic potential of combining ChAdOx1/MVA P1A vaccination with immune checkpoint blockade.

4.2 Results

4.2.1 Evaluating T-cell responses induced by heterologous prime-boost vaccination with ChAdOx1/MVA vectors encoding P1A

Initially, the immunogenicity of ChAdOx1/MVA vectors encoding P1A were tested as part of a heterologous prime-boost using the same vaccination schedule as was used for the MAGE-A3/NY-ESO-1 vectors previously evaluated in chapter 3. DBA/2 mice received a prime vaccination with either 10^8 IU of ChAdOx1 encoding P1A ± Ii or a PBS sham vaccination and 4 weeks later were given a boost vaccination with 10^7 PFU MVA encoding P1A or a PBS sham vaccination (Figure 4.3, Table 4.1). The magnitude of P1A-specific T-cell responses against P1A were assessed via blood sampling of the mice after each vaccination, stimulating PBMCs with a pool of overlapping P1A peptides, and then cytokine producing T-cells were enumerated by ICS and flow cytometry.

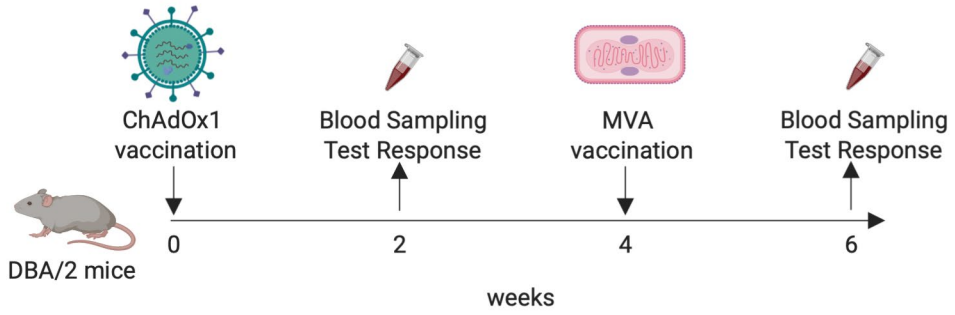


Figure 4.3 ChAdOx1/MVA heterologous prime-boost vaccination scheme with vectors encoding P1A. DBA/2 mice received a prime vaccination via intramuscular injection (i.m.) with 10^8 IU of ChAdOx1-P1A ± Ii or a sham vaccination with PBS. 4 weeks after ChAdOx1-P1A (±Ii) mice received a boost vaccination with 10^7 PFU of MVA-P1A. Vaccinations were performed according to the experimental groupings shown in Table 4.1. To test the response to vaccination, mice were bled 10-20 days after vaccination with ChAdOx1 and 9-14 days after vaccination with MVA. Image created with BioRender.

Table 4.1 Combinations of ChAdOx1 and MVA viral vectors encoding P1A tested in heterologous prime-boost vaccinations.

Group	ChAdOx1 prime vaccination	MVA boost vaccination
1	PBS	PBS
2	P1A	P1A
3	Ii-P1A	P1A

4.2.2 Heterologous prime-boost vaccination with ChAdOx1/MVA encoding P1A induces a high magnitude multifunctional P1A-specific CD8+ T-cell response

The prime-boost vaccination with ChAdOx1/MVA encoding P1A was found to generate a high magnitude P1A-specific CD8+ T-cell response. Evaluating the magnitude of cytokine producing CD8+ T-cells in the blood after the prime vaccination showed significant increases in P1A-specific CD8+ T-cells producing IFN-γ, IL-2 and TNF-α in both the ChAdOx1-P1A and ChAdOx1-Ii-P1A vaccinated groups compared to the PBS control group (Figure 4.4 B). The response was then further increased by the boost vaccination with MVA-P1A, with significantly higher levels of IFN-γ, IL-2 and TNF-α producing CD8+ T-cells detected in the blood after the boost than after prime vaccination (Figure 4.4 B). The quality of the induced CD8+ T-cell response was then assessed further in terms of the degree of multifunctionality of cytokine-producing T-cells. After the prime vaccination, the majority of CD8+ T-cells were found to be IFN-γ single producers, closely followed by a large proportion of IFN-γ/TNF-α double producers (Figure 4.5 A). After the boost vaccination, a small expansion of the IFN-γ/TNF-α double producing population was observed, becoming the largest proportion of cytokine producing CD8+ T-cells. A small expansion in the proportion of IFN-γ/TNF-α/IL-2 triple producing cells was also observed, indicating a move towards increased functionality after the boost (Figure 4.5 B).

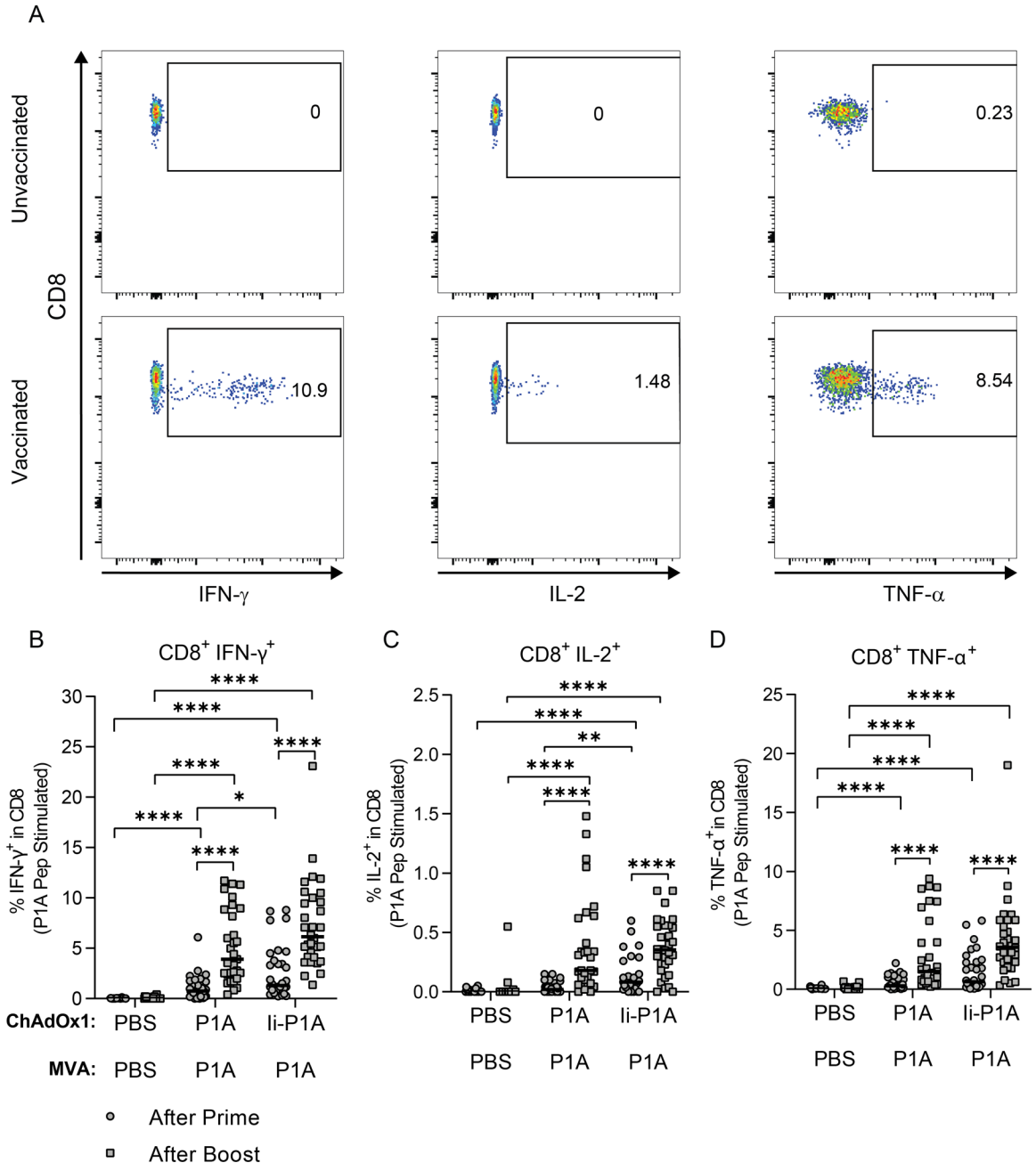


Figure 4.4. P1A-specific CD8+ T-cell response induced by prime-boost vaccination with ChAdOx1/MVA encoding P1A. DBA/2 mice were vaccinated as described in Figure 4.3 and bled 10-20 days after ChAdOx1 vaccination and 9-14 days after MVA vaccination. PBMCs were stimulated ex vivo with 4μg/ml of P1A peptide pools, or a vehicle control (DMSO). The percentage of cytokine-producing P1A-specific CD8+ T-cells in the blood after each vaccination was then determined by ICS and flow cytometry (gating as described in Figure 2.2). Representative dot plots showing gating of IFN-γ, TNF-α and IL-2 expressing CD8+ T-cells (A). Percentage of IFN-γ+ (B), IL-2+ (C) and TNF-α+ (D) CD8+ T-cells after prime (closed circles) and boost (closed squares) in response to stimulation with P1A peptides. Data are shown as the median response of each group (horizontal lines). Each symbol represents an individual mouse, with 24 mice in the PBS group, 31 mice in the ChAdOx1-P1A/MVA-P1A group and 32 mice in the ChAdOx1-Ii-P1A/MVA-P1A group, pooled from 4 independent experiments. Statistically significant differences between groups were determined by a Kruskal-Wallis test with Dunn's multiple comparisons test. *, $p \leq 0.05$, **, $p \leq 0.01$ ****, $p \leq 0.0001$.

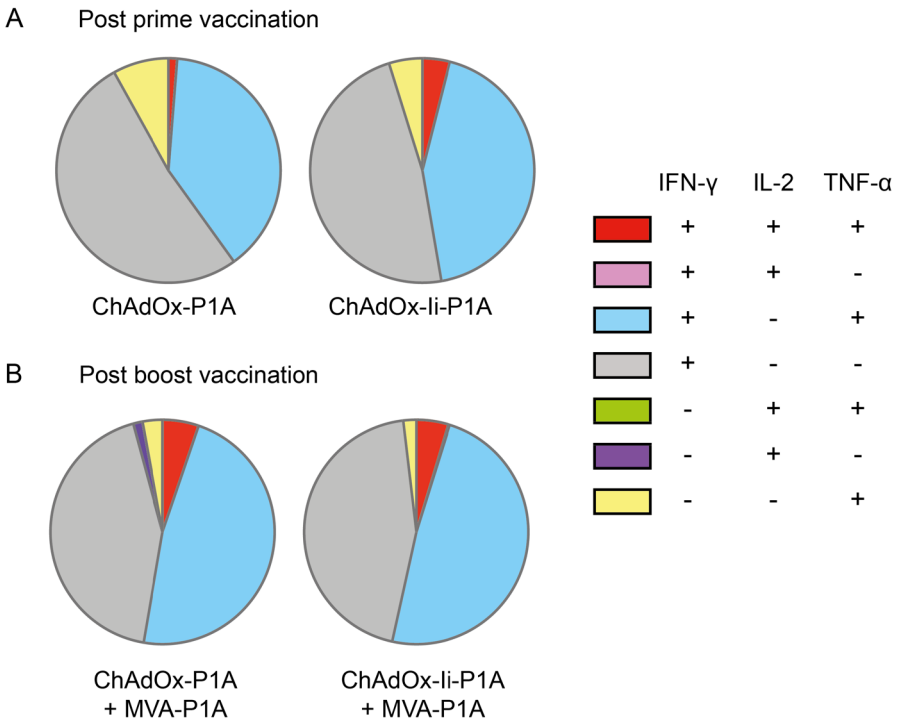


Figure 4.5. Cytokine profiles of P1A-specific CD8+ T-cells induced by prime-boost vaccination with ChAdOx1/MVA encoding P1A. DBA/2 mice were vaccinated as described in Figure 4.3 and blood sampled to assess the P1A-specific T-cell response as described in Figure 4.4. The multifunctionality of P1A-specific CD8+ T-cells was assessed after the prime vaccination (A) and after the boost vaccination (B). A Boolean analysis was performed in FlowJo software to calculate the percentage of CD8+ T-cells producing only one, a combination of two, or all three of the effector cytokines IFN-γ, IL-2 and TNF-α+. Pie charts show the mean relative proportion of each cytokine producing subset out of the total antigen-specific CD8+ T-cells.

4.2.3 Fusion of invariant chain to the P1A antigen sequence in the ChAdOx1 vector increases the magnitude of P1A-specific CD8+ T-cells induced by vaccination

The effect of incorporating the invariant chain TMD sequence via fusion to the antigen into the ChAdOx1 on vector immunogenicity was again investigated. Despite no significant improvement being detected in earlier evaluations of the ChAdOx1 vectors encoding MAGE-A3 and NY-ESO-1, it was hypothesised that any effect on immunogenicity might be more apparent for a weakly immunogenic self-antigen like P1A.

Considering the response after the prime-vaccination, fusion of the murine Ii sequence to the N-terminus of P1A was found to give a significant increase to the magnitude of the induced P1A-specific CD8+ T-cells (Figure 4.4 B). This was true in terms of both IFN-γ and IL-2 production, with significantly higher percentages of IFN-γ and IL-2 producing CD8+ T-cells detected in the blood. Whilst there was a trend after the MVA boost vaccination towards higher CD8+ responses being maintained in the group primed with the ChAdOx1-Ii-P1A vector, this was not significant when evaluated at this later time-point. Inclusion of the invariant chain did not seem however to have any impact on the quality of the observed CD8+ T-cell response after either prime or boost vaccination in terms of proportions multi-cytokine producing cells. The distribution of IFN-γ single producers and IFN-γ/TNF-α double producers was almost identical at each time-point considered for the groups vaccinated with or without the invariant chain encoded in the ChAdOx1 vector (Figure 4.5).

4.2.4 Heterologous prime-boost vaccination with ChAdOx1/MVA encoding P1A does not induce a P1A-specific CD4+ T-cell response

The induction of antigen-specific CD4+ T-cell responses after the prime and boost vaccination was also evaluated. However, no P1A-specific CD4+ T-cell response was detected after either vaccination. No significant increase in production of IFN-γ, IL-2 or TNF-α by blood CD4+ T-cells in response to P1A peptide stimulation compared to control mice was detected (Figure 4.6).

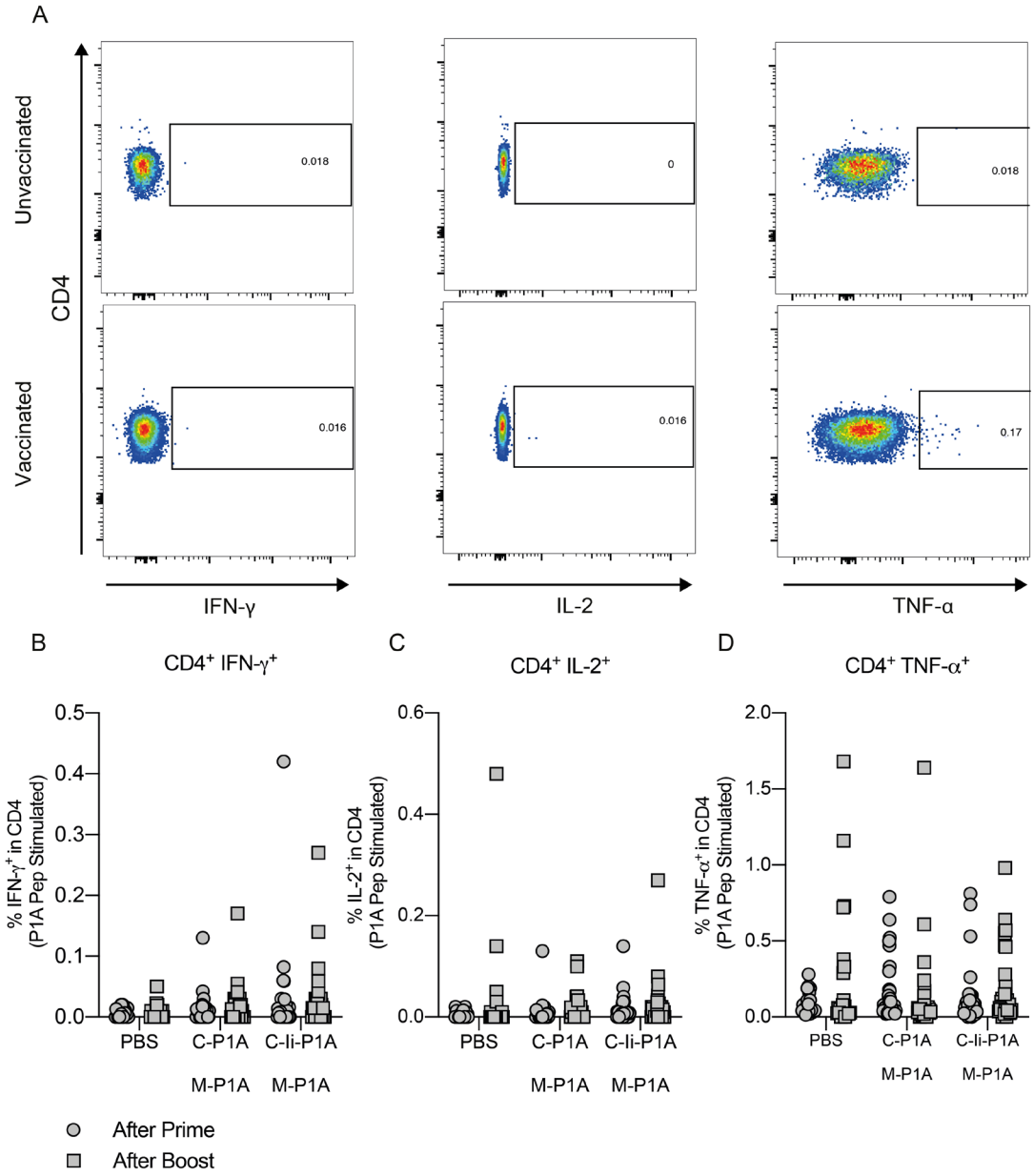


Figure 4.6. P1A-specific CD4+ T-cell response induced by prime-boost vaccination with ChAdOx1/MVA encoding P1A. DBA/2 mice were vaccinated as described in Figure 4.3 and bled 10-20 days after ChAdOx1 vaccination and 9-14 days after MVA vaccination. PBMCs were stimulated ex vivo with 4μg/ml of P1A peptide pools, or a vehicle control (DMSO). The percentage of cytokine-producing P1A-specific CD4+ T-cells in the blood after each vaccination was then determined by ICS and flow cytometry (gating as described in Figure 2.2). Representative dot plots showing gating of IFN-γ, TNF-α and IL-2 expressing CD4+ T-cells (A). Percentage of IFN-γ+ (B), IL-2+ (C) and TNF-α+ (D) CD4+ T-cells after prime (closed circles) and boost (closed squares) in response to stimulation with P1A peptides. Data are shown as the median response of each group (horizontal lines). Each symbol represents an individual mouse, with 24 mice in the PBS group, 31 mice in the ChAdOx1-P1A/MVA-P1A group and 32 mice in the ChAdOx1-Ii-P1A/MVA-P1A group, pooled from 4 independent experiments. Statistically significant differences between groups were determined by a Kruskal-Wallis test with Dunn's multiple comparisons test.

4.2.5 ChAdOx1/MVA P1A prime-boost vaccination confers good protection against P1A-expressing tumours in the prophylactic setting

Having confirmed that heterologous prime-boost vaccination with ChAdOx1/MVA encoding P1A could induce very high magnitude P1A-specific CD8+ T-cell responses, the anti-tumour efficacy of the vaccine induced response was then evaluated. This was first performed in the prophylactic setting, where mice are first vaccinated and then challenged with tumour cells around the peak of the vaccine induced response. Testing vaccine prophylactic protection against tumour challenge is commonly performed to evaluate the anti-tumour capacity of the immune response induced by vaccination. Initially the protection against tumour growth afforded by vaccination with the different ChAdOx1/MVA vectors encoding P1A was assessed in the P815 tumour model. DBA/2 mice received PBS sham vaccinations, or were vaccinated with ChAdOx1-P1A (± Ii) / MVA-P1A, 4 weeks apart (Figure 4.7). As a positive control, a fourth group were vaccinated with L1210.P1A.B7-1, a cellular-based vaccine, given via i.p. injection 5 days after the groups receiving ChAdOx1/MVA (Figure 4.7). L1210.P1A.B7-1 is derived from the L1210 murine leukaemia cell line, which does not naturally express P1A, and is stably transfected to overexpress both the P1A antigen and the T-cell costimulatory molecule B7-1 (CD80) [250]. L1210.P1A.B7-1 has been shown in other studies to be rejected by DBA/2 mice following inoculation rather than establish tumours, and to induce strong P1A-specific CD8+ T-cell immunity resulting in robust protection against P815 tumour growth [172]. As such it has been used a positive control to benchmark the level of protection against P815 afforded by other novel vaccination schemes [241] [242] [240]. Two weeks after the

last vaccination was given mice were challenged with P815 via a subcutaneous injection of $1.5x10^6$ cells in the right flank.

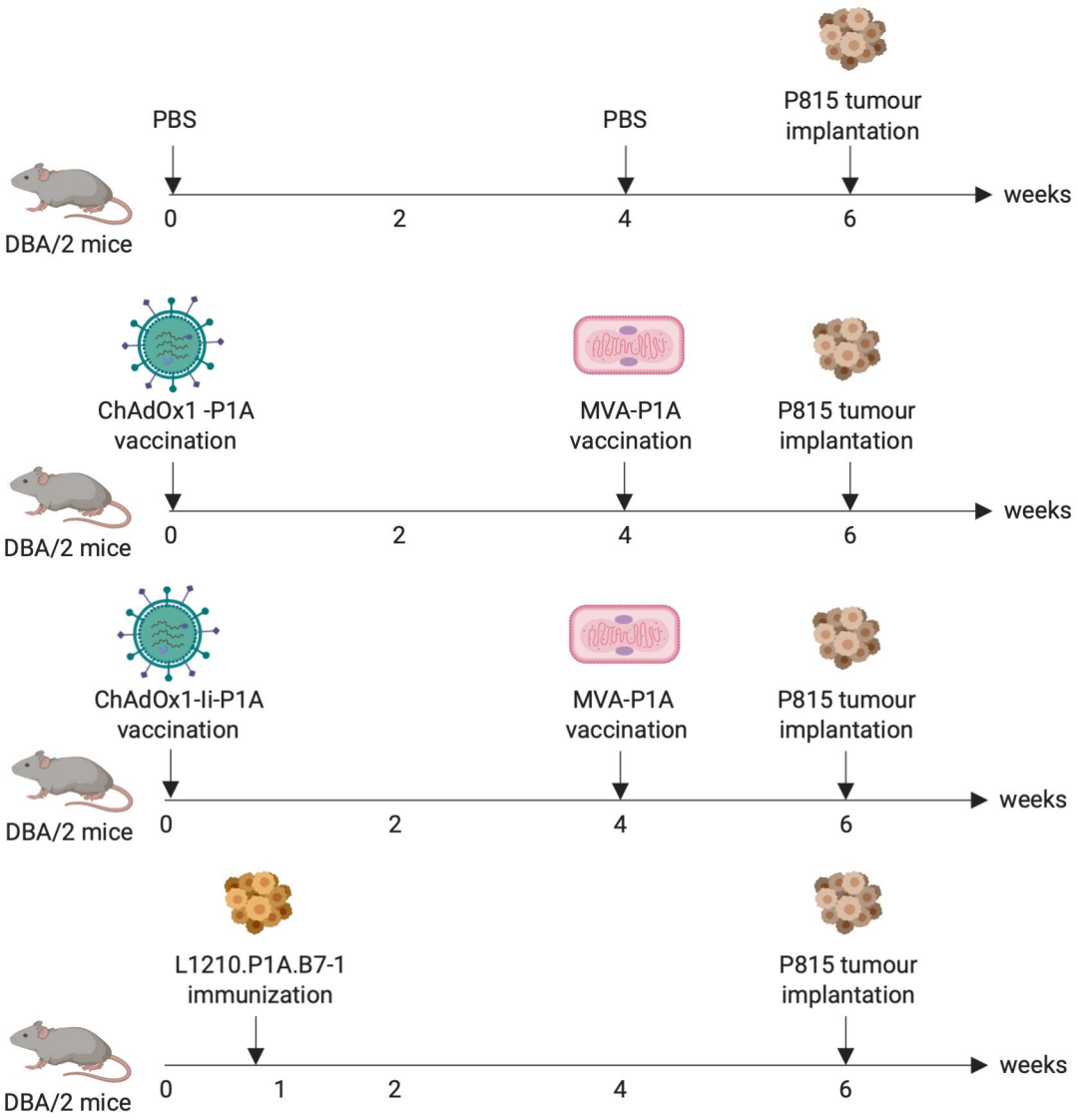


Figure 4.7. Timeline of vaccination followed by P815 tumour challenge. DBA/2 mice received a prime vaccination via intramuscular injection (i.m.) with 10^8 IU of ChAdOx1-P1A, ChAdOx1-li-P1A or a sham vaccination with PBS. A fourth control group received $1x10^6$ L1210.P1A.B7-1 cells via intraperitoneal injection (i.p.), 5 days after the other groups were vaccinated with ChAdOx1 (recommendation from author [172]). 4 weeks after ChAdOx1-P1A (± li) mice received a boost vaccination with 10^7 PFU of MVA-P1A. A further 2 weeks after the MVA boost vaccination, all mice were implanted with $1.5x10^6$ P815 cells in the right flank via subcutaneous injection. Tumour size was then measured every 3-4 days and mice were culled when tumour size reach 10mm length in any direction. Image created with BioRender.

Following implantation, tumour growth was monitored for 35 days (Figure 4.8). P815 is a fast-growing aggressive tumour, and most mice (7/9) in the PBS control

succumbed to tumour burden and had to be sacrificed around days 10-12 after implantation. However in contrast to the PBS control, tumour growth was significantly delayed in all vaccinated groups (Figure 4.8 A), with all mice in these groups remaining tumour-free until 3 weeks post-challenge, resulting in significantly increased survival (Figure 4.8 B). In the ChAdOx1-P1A/MVA-P1A, ChAdOx1-Ii-P1A/MVA-P1A and L1210.P1A.B7-1 vaccinated groups, 6/9, 9/10 and 8/10 mice respectively were still alive at the experiment termination (day 35), compared to 2/9 in the PBS control group. These 2 mice in the control group spontaneously rejected their tumours, a phenomenon that is well known with P815, likely due to naturally occurring immune responses induced by the tumour itself [251]. To further assess vaccine efficacy, an area under curve (AUC) analysis was performed at day 12 post tumour implantation when control mice started to be sacrificed (Figure 4.9 A). This showed highly significant reduction in tumour burden between all vaccinated groups and the PBS control. Both ChAdOx1/MVA P1A vaccinations provided comparable tumour protection to the L1210.P1A.B7-1 positive control vaccination, with no significant differences observed in either tumour growth or survival. The P1A-specific CD8+ T-cell response in the blood of each mouse was also assessed by ICS 3 days prior to P815 tumour challenge (corresponding to day 11 post boost vaccination in the ChAdOx1/MVA P1A vaccinated groups) and was compared with tumour burden on day 12 post implantation (Figure 4.9 B). What this analysis showed was a highly binary relationship where all mice with detectable P1A-specific IFN-γ secreting CD8+ T-cells in the blood were protected from tumour growth and were tumour free at

this time point. This observation strongly suggested that the P1A-specific CD8+ T-cell response induced by vaccination was responsible for the observed protection.

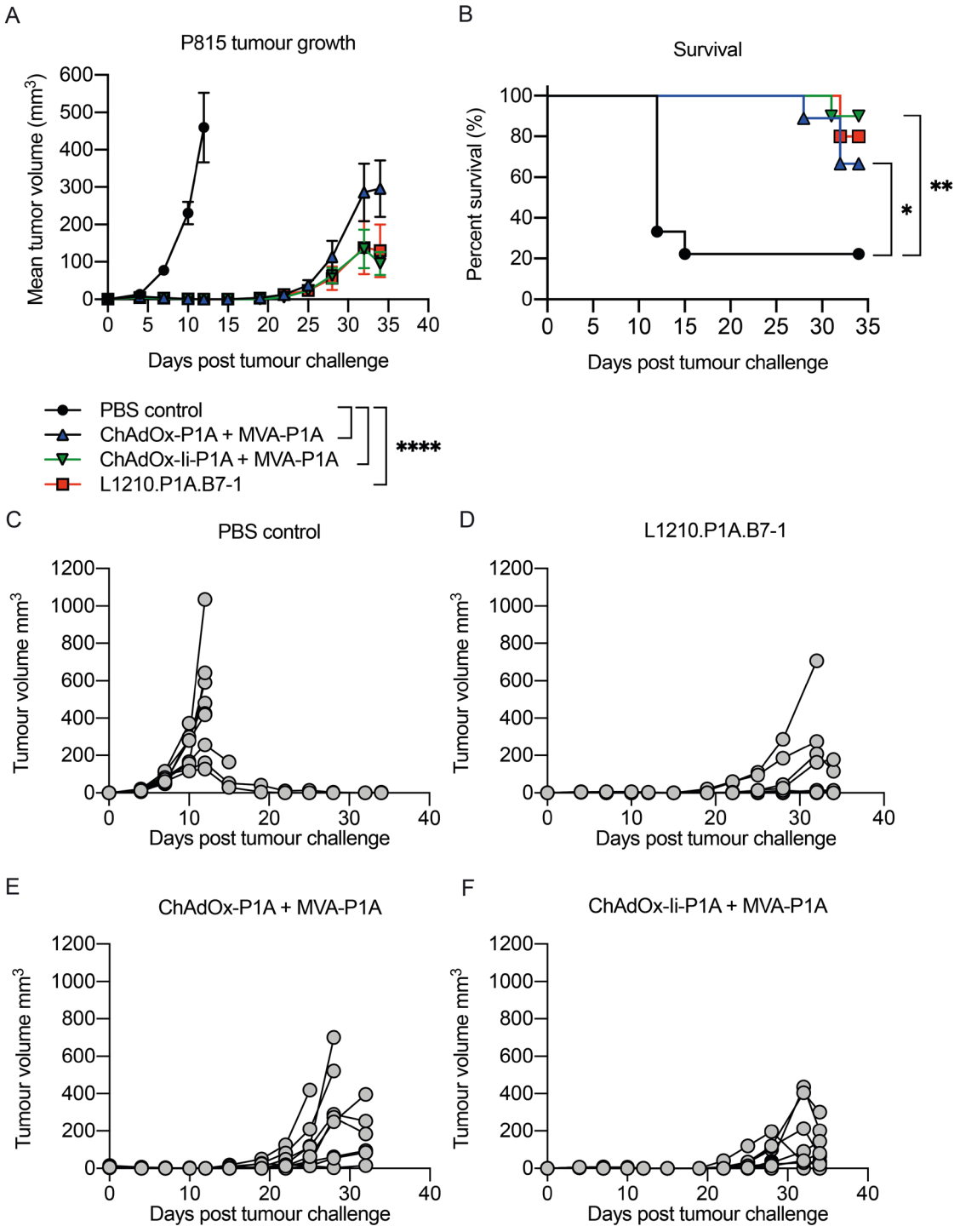


Figure 4.8. Protective efficacy of ChAdOx1/MVA P1A vaccination against P815 tumour growth in the prophylactic setting. DBA/2 mice were immunized with either PBS, live L1210.P1A.B7-1 cells or ChAdOx1-P1A (± Ii) and MVA-P1A as described in Figure 4.7 then challenged with $1.5x10^6$ P815 cells via subcutaneous injection. Mean tumour growth for each group (A), Survival curves (B) and individual tumour growth curves from each group - PBS (C), L1210.P1A.B7.1 (D), ChAdOx1-P1A/MVA-P1A (E), ChAdOx1-Ii-P1A/MVA-P1A (F) - are shown. Mean tumour growth data in (A) are presented as mean tumour volume (mm^3) ± SEM. Each group contained 9/10 mice, with data representative of 2 independent experiments. Statistically significant differences in mean tumour volume between groups were determined by a two-way ANOVA followed by Tukey's post hoc test and statistical differences in survival data were determined by a Log Rank test. *, $p \leq 0.05$, **, $p \leq 0.01$ ****, $p \leq 0.0001$.

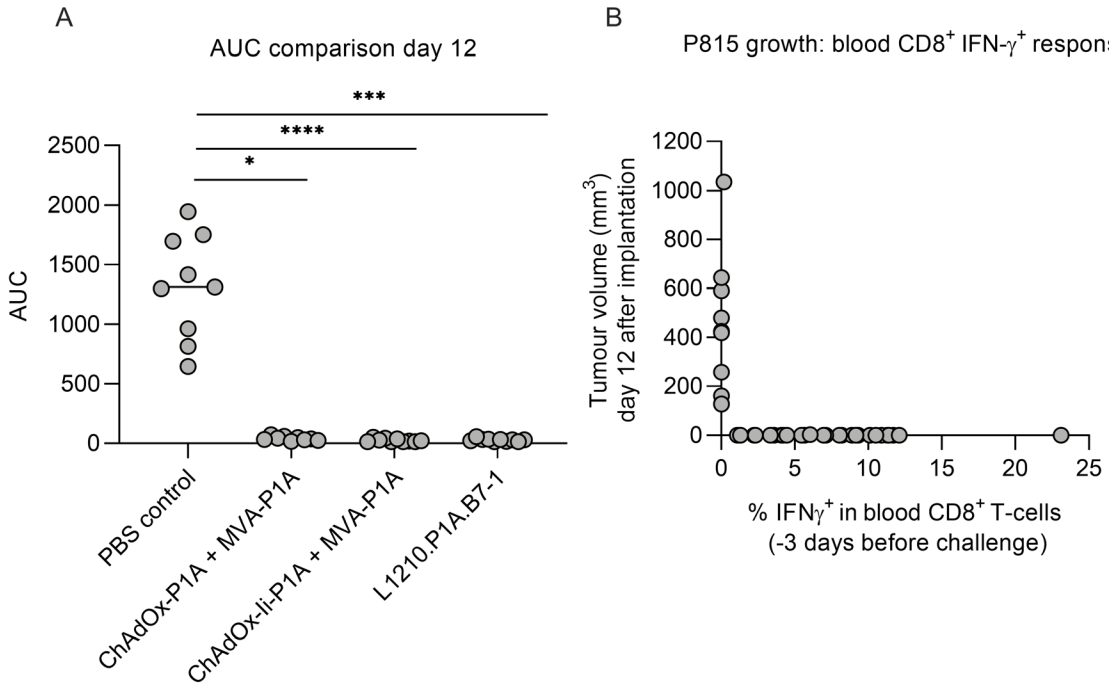


Figure 4.9. Assessment of ChAdOx1/MVA P1A vaccination protective efficacy against P815 tumour challenge. To measure vaccine protective efficacy, an area under curve analysis of tumour growth for mice in control and vaccinated groups was performed at day 12 post P815 challenge (A). Statistically significant differences between groups were determined by a Kruskal-Wallis test with Dunn's multiple comparisons test. *, $p \leq 0.05$, ***, $p \leq 0.001$ ****, $p \leq 0.0001$. Tumour size on day 12 after implantation was compared with the magnitude of IFN-γ producing P1A-specific CD8+ T-cells in the blood measured 3 days before implantation (B).

Having observed good protection against P815 tumour growth from ChAdOx1/MVA P1A vaccination, it was then decided to assess the protective anti-tumour efficacy in a second different P1A-expressing tumour model, 15V4T3, in order to further validate this result. As described previously, DBA/2 mice received PBS sham vaccinations, or were vaccinated with either ChAdOx1-P1A MVA-P1A, 4 weeks apart or with L1210.P1A.B7-1 (Figure 4.10). Two weeks after MVA vaccinations, mice were implanted with $1x10^6$ 15V4T3 cells in via a subcutaneous injection in the right flank.

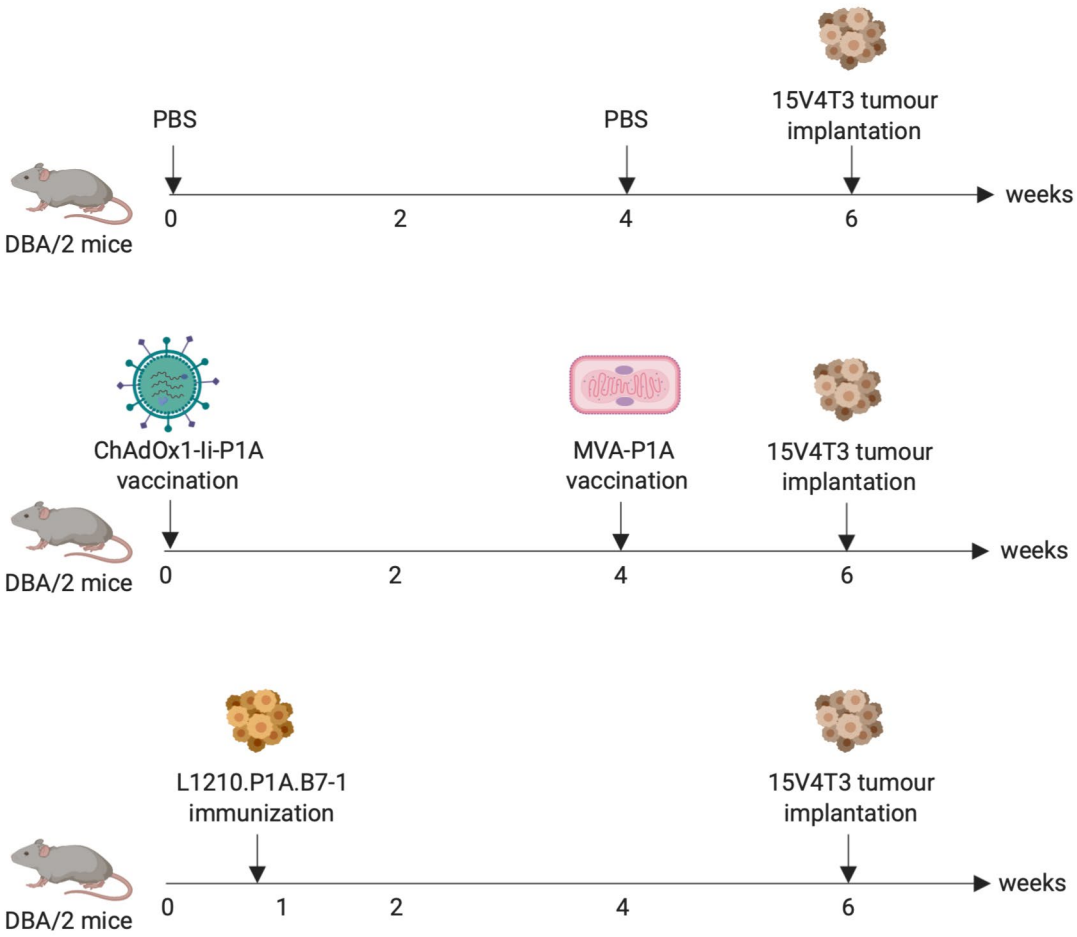


Figure 4.10. Timeline of vaccination followed by 15V4T3 tumour challenge. DBA/2 mice received a prime vaccination via intramuscular injection (i.m.) with 10^8 IU of ChAdOx1-li-P1A or a sham vaccination with PBS. A third received $1x10^6$ L1210.P1A.B7-1 cells via intraperitoneal injection (i.p.), 5 days after the group vaccinated with ChAdOx1. 4 weeks after ChAdOx1-li-P1A mice received a boost vaccination with 10^7 PFU of MVA-P1A. A further 2 weeks after the MVA boost vaccination, all mice were implanted with $1x10^6$ 15V4T3 cells in the right flank via subcutaneous injection. Tumour size was then measured every 3-4 days and mice were culled when tumour size reach 10mm length in any direction. Image drawn with BioRender.

Similarly to the results obtained with P815, ChAdOx1-Ii-P1A/MVA-P1A vaccination afforded strong protection against growth of 15V4T3 tumours. Tumour growth was significantly delayed in ChAdOx1-Ii-P1A/MVA-P1A vaccinated mice compared to the PBS control group (Figure 4.11 A), resulting in significantly improved survival (Figure 4.11 B). Indeed the majority of mice were completely protected from tumour growth (3/5) for the period monitored. Curiously, in this setting the ChAdOx1-Ii-P1A/MVA-P1A vaccination was significantly better than the L1210.P1A.B7-1 vaccination, which failed to give any protection against 15V4T3 tumour growth.

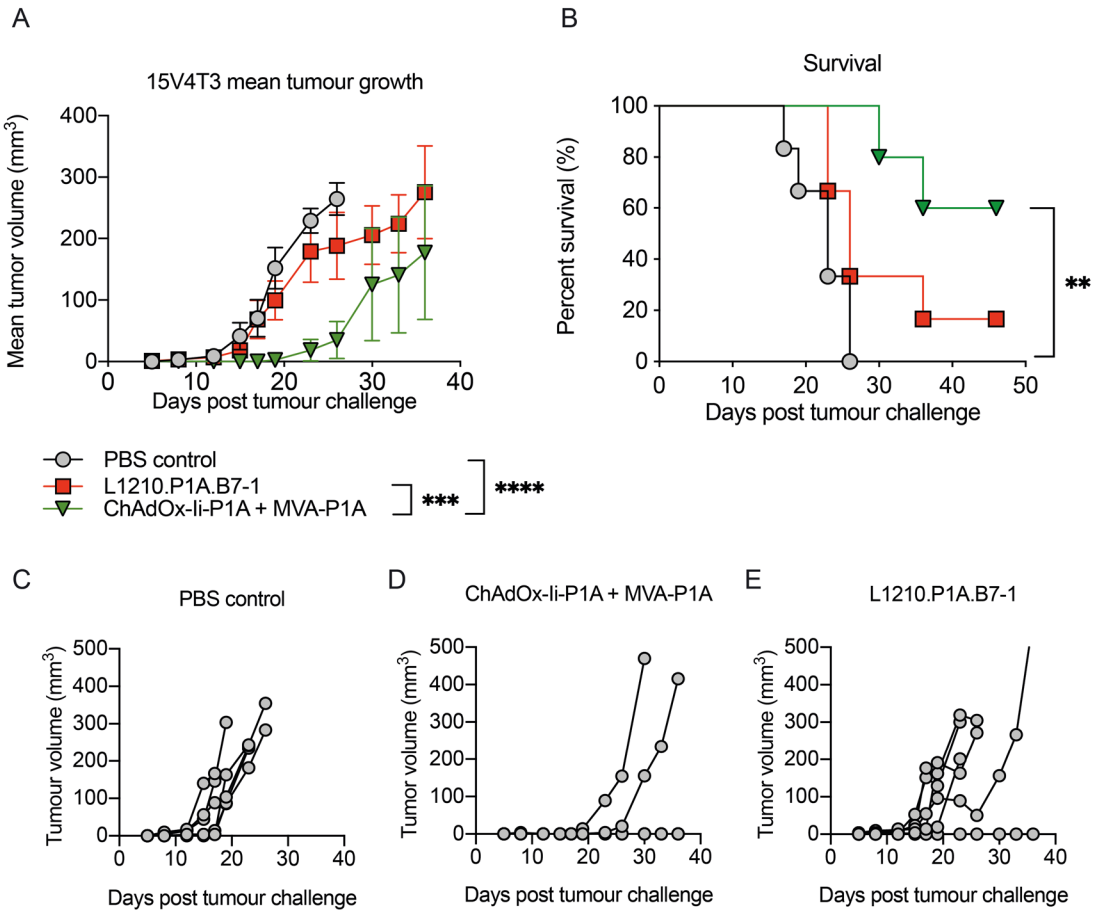


Figure 4.11. Protective efficacy of ChAdOx1/MVA P1A vaccination against 15V4T3 tumour challenge. DBA/2 mice were immunized with either PBS, live L1210.P1A.B7-1 cells or ChAdOx1-li-P1A/MVA-P1A as described in Figure 4.10 then challenged with $1x10^6$ 15V4T3 cells via subcutaneous injection. Mean tumour growth for each group (A), Survival curves (B) and individual tumour growth curves from each group - PBS (C), ChAdOx1-li-P1A /MVA-P1A (D), and L1210.P1A.B7.1 (E) are shown. Mean tumour growth data in (A) are presented as mean tumour volume (mm^3) ± SEM. Each group contained 5 mice, with data representative of 2 independent experiments. Statistically significant differences in mean tumour volume between groups were determined by a two-way ANOVA followed by Tukey's post hoc test and statistical differences in survival data were determined by a Log Rank test. *, $p \leq 0.05$, **, $p \leq 0.01$ ****, $p \leq 0.0001$.

4.2.6 Tumour immune escape in the P815 model results from loss of P1A antigen expression, but not in 15V4T3

The results of the tumour challenge studies showed that the P1A-specific CD8+ T-cell responses induced by vaccination of DBA/2 mice with ChAdOx1/MVA P1A afforded strong protection against growth of P1A-expressing P815 and 15V4T3 tumours compared to unvaccinated controls. However, in many mice after a tumour-free period of protection, a relapse occurred and outgrowth of tumours was observed. It was hypothesised that this escape from immune control may be due to either loss of P1A antigen expression, or otherwise the development of an immunosuppressive tumour microenvironment. To test the former, that this tumour outgrowth was due to loss of P1A expression, tumours were harvested from control or ChAdOx1/MVA P1A vaccinated mice once they reached size end-points for the study, and mRNA was extracted to evaluate tumoural P1A expression at the transcriptional level by rt-qPCR. It was found that all outgrowing P815 tumours from ChAdOx1-P1A (± Ii) / MVA-P1A and L1210.P1A.B7-1 vaccinated mice had significantly lower, almost undetectable, P1A expression compared to those harvested from PBS control mice. This strongly suggested that the loss of protection from vaccination and eventual tumour re-appearance was due to the outgrowth of P1A-antigen loss P815 variants. However, compared to the near total loss of P1A-expression in P815 tumours from vaccinated mice, 15V4T3 tumours did not show any difference in P1A expression between control and vaccinated groups, suggesting that immune escape by these tumours is likely due to an entirely different mechanism.

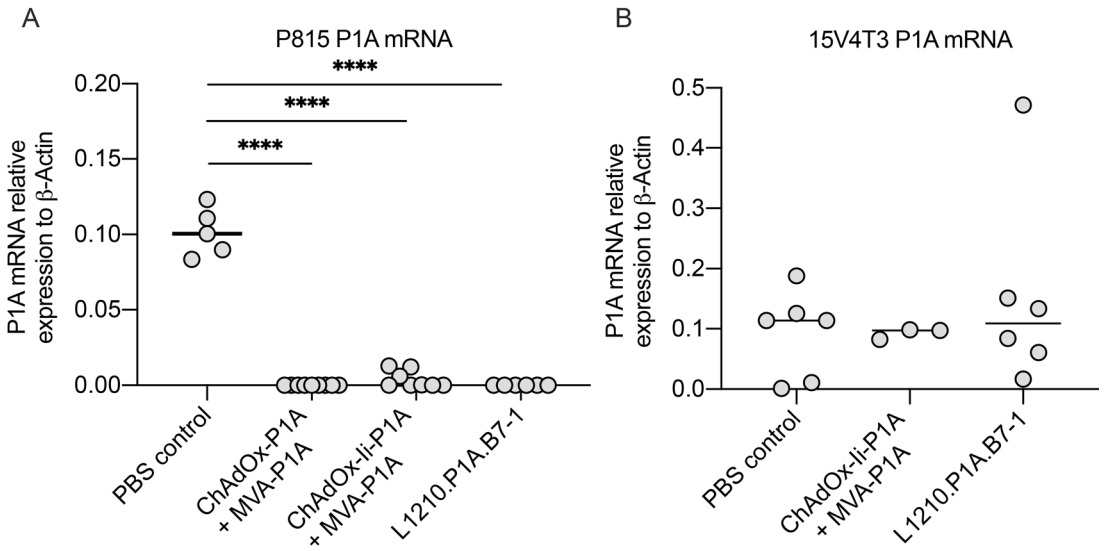


Figure 4.12. Tumour expression of P1A at the mRNA level in naive and vaccinated mice. P815 (A) or 15V4T3 (B) tumours were harvested from PBS control, ChAdOx1-P1A (± li) / MVA-P1A vaccinated or L1210.P1A.B7-1 vaccinated mice once they reached the size end points for the study. Tumours were processed to extract mRNA, and P1A gene expression at the transcriptional level was assessed by rt-qPCR. P1A expression was normalized to mRNA levels of β-Actin. Statistically significant differences in P1A mRNA expression between groups were determined by a one-way ANOVA followed by Tukey's post hoc test. ****, $p \leq 0.0001$.

4.2.7 Fusion of tPA to P1A in the MVA vector does not increase the magnitude or improve multifunctionality of the vaccine-induced P1A-specific CD8+ T-cell response

Having observed a clear increase in vaccine induced CD8+ T-cell responses from the incorporation of the Ii sequence into the ChAdOx1 vector in the setting of vaccination against P1A, the question was again considered of whether a similar increase in immunogenicity might be observed from the incorporation of the tPA signal sequence into the MVA vector. To address this, the effect of tPA on immunogenicity was tested in a range of different ChAdOx1/MVA P1A heterologous prime-boost vaccination schemes. Some mice received vaccinations with a conventional vaccination schedule of ChAdOx1 and MVA given 4-weeks apart, at a dose of 10^8 IU for ChAdOx1 and 10^7 PFU for MVA. However, it was hypothesised that lowering the dose of vaccine might facilitate a clearer detection of any effect on immunogenicity introduced by the addition of tPA, as the high P1A-specific CD8+ T-cell responses induced by the higher-dose might be masking the effect. Therefore, some groups were vaccinated with a reduced time-window between the ChAdOx1 and MVA, either 2 or 3 weeks, at a log fold reduced dose of 10^7 IU for ChAdOx1 and 10^6 PFU for MVA. For each vaccination schedule, the effect of including tPA on the vaccine induced P1A-specific CD8+ T-cell response was evaluated. An additional control group was vaccinated with ChAdOx1/MVA vectors encoding an irrelevant non-mouse non-tumour antigen, DPY-19 (DPY), a C-mannosyltransferase enzyme from Caenorhabditis elegans [252]. To measure the CD8+ T-cell response, mice were bled 3 days before and 14 days after the MVA boost, and the magnitude of cytokine producing P1A-specific CD8+ T-cells

was assessed by stimulation of PBMCs with overlapping P1A peptides and ICS. Comparing the responses after the MVA boost, very similar level responses were observed in terms of IFN-γ producing CD8+ T-cells, between mice given equivalent vaccination schedules receiving an MVA boost either with or without tPA fused to P1A in the MVA vector (Figure 4.13 A). Fusing tPA to the N-terminus of P1A therefore had no effect on the magnitude of the P1A-specific CD8+ T-cells induced after the MVA boost vaccination. The effect of tPA on the multifunctionality of the CD8+ T-cell responses after the MVA boost was also considered (Figure 4.13 B). As previously observed, the majority of cytokine producing P1A-specific CD8+ T-cells after the MVA boost were IFN-γ/TNF-α double-producers. However, the relative proportions of different cytokine-producing subsets were found to be the same between mice that had received tPA in the MVA or not, suggesting that the tPA does not have any effect on the degree of functionality of P1A-specific CD8+ T cells induced by ChAdOx1/MVA vaccination. From the metrics evaluated, no clear benefit from the use of tPA for improving the induced CD8+ responses could be derived, although the responses appeared to be at least equivalent whether or not the tPA sequence was included.

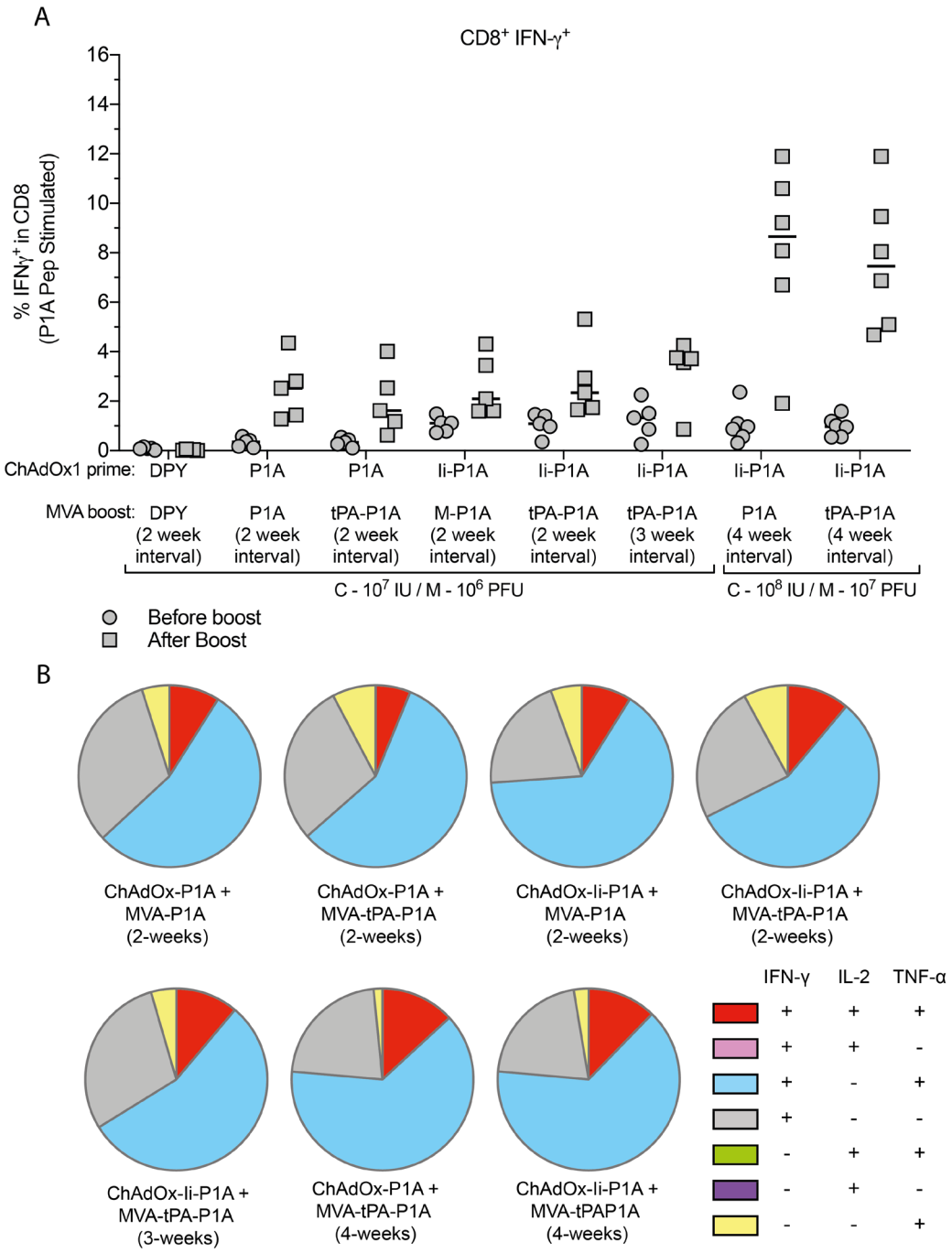


Figure 4.13. The effect of tPA linkage to P1A in MVA on P1A-specific CD8+ T-cell responses induced by ChAdOx1/MVA P1A vaccination. DBA/2 mice were vaccinated with different vaccination regimes and bled 3 days before and 14 days after the MVA vaccination. PBMCs were stimulated ex vivo with 4μg/ml of P1A peptide pools, or a vehicle control (DMSO). The percentage of cytokine-producing P1A-specific CD8+ T-cells in the blood after each vaccination was then determined by ICS and flow cytometry. Percentage of IFN-γ+ CD8+ T-cells after prime (closed circles) and boost (closed squares) in response to stimulation with P1A peptides are shown (A). Data are shown as the median response (horizontal lines). Each symbol represents an individual mouse, with 5 or 6 mice per group. The multifunctionality of P1A-specific CD8+ T-cells was assessed after the prime vaccination after the boost vaccination (B). A Boolean analysis was performed in FlowJo software to calculate the percentage of CD8+ T-cells producing one, a combination of two, or all three of IFN-γ, IL-2 and TNF-α. Pie charts show the mean relative proportion of each cytokine producing subset out of the total antigen-specific CD8+ T-cells. Statistically significant differences between groups were determined by a Kruskal-Wallis test with Dunn's multiple comparisons test. *, $p \leq 0.05$

4.2.8 Therapeutic ChAdOx1/MVA P1A vaccination exhibits moderate control of growth of established 15V4T3 tumours when administered at early time-points

The finding that ChAdOx1/MVA P1A vaccination could provide extremely good protection against tumour growth in the prophylactic setting in both the P815 and 15V4T3 P1A-expressing tumour models was encouraging, however, this is not how a therapeutic cancer vaccine would be used in a clinical setting. It was then decided to test the therapeutic efficacy of the ChAdOx1/MVA P1A prime-boost vaccination against established tumours. The 15V4T3 model was chosen to proceed with over P815 due to two findings; 1) lower rates of spontaneous tumour resolution than P815 and 2) a more favourable slower growth kinetics for vaccine evaluation in a therapeutic setting compared to P815, where most unvaccinated mice succumbed to tumour burden in around 10-12 days.

To assess the therapeutic efficacy of ChAdOx1/MVA P1A vaccination, DBA/2 mice were first implanted with 15V4T3 tumours via subcutaneous injection, and received ChAdOx1 prime vaccinations 5 days later when tumours first started to appear in some of the mice. Tumour growth was then monitored over a course of 50 days and survival curves generated. A range of different vaccination schemes with ChAdOx1/MVA encoding P1A were evaluated (Figure 4.14) - 10^8 IU of ChAdOx1 / 10^7 PFU MVA prime-boost given 3-weeks apart, an accelerated scheme of 10^7 IU ChAdOx1 / 10^6 PFU MVA given 1-week apart with a log-fold reduced dose, and weekly alternating vaccinations with 10^7 IU ChAdOx1 / 10^6 PFU MVA. Instead of PBS sham vaccinations, a control group received vaccination with ChAdOx1 and MVA encoding an irrelevant antigen, DPY, to

account for any effects of non-antigen-specific inflammation from viral vector infection on tumour growth. Additionally another group received vaccination with only ChAdOx1 at a dose of 10^7 IU to determine how important the MVA boost vaccination would be for any observed efficacy. In all schemes other than the DPY control, mice were primed with ChAdOx1-Ii-P1A, on the basis of prior results where a clear increase in P1A-specific CD8+ T-cell responses was observed from incorporating the invariant chain. Mice received a boost with MVA encoding P1A, with or without the incorporation or tPA, to determine if tPA might have any impact on therapeutic efficacy. The accelerated 1-week apart prime-boost scheme was included on the basis that vaccinations would need to be given more rapidly to induce a response to fit within the window of tumour growth and for a therapeutic effect to be observed. A weekly alternating vaccination scheme with ChAdOx1/MVA using different antigens had previously been evaluated by Cappuccini et al in a therapeutic cancer setting, with the rationale that a therapeutic setting might benefit from fresh supplies of effector CD8+ T-cells being generated due to exhaustion of those infiltrating into the tumour site [155]. In the setting of vaccinating against the STEAP-1 prostate cancer antigen TRAMP-C1 tumour model, this was found to have stronger anti-tumour therapeutic efficacy than a single prime-boost [155]. On the basis of these findings, the weekly alternating vaccination scheme was also further evaluated here.

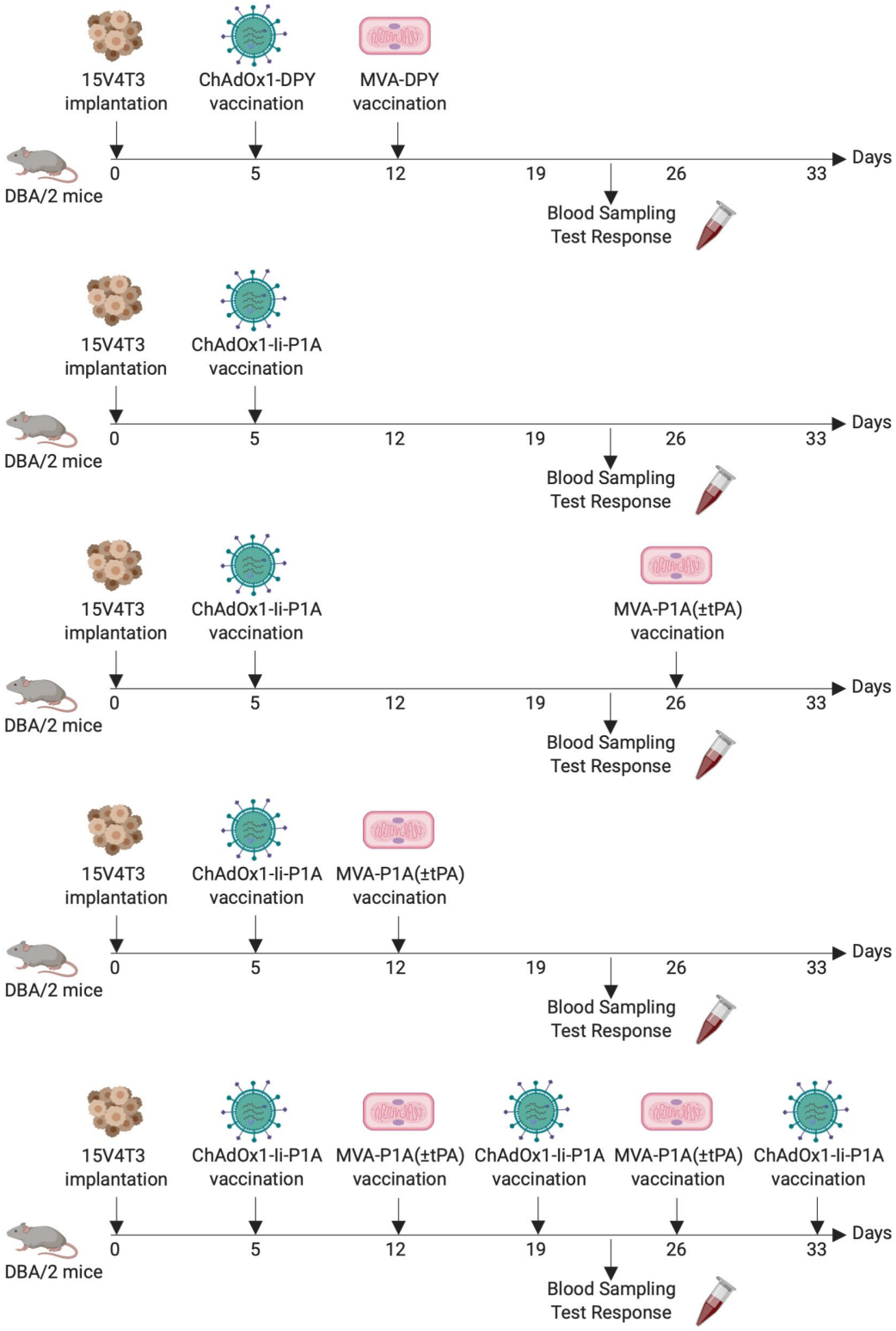


Figure 4.14. Timeline of therapeutic vaccination schedules following 15V4T3 tumour implantation. Mice were implanted with 1x10^6 15V4T3 cells via s.c. injection to initiate tumour growth. 5 days after tumour implantation, vaccinations were started. Mice received either 1-week apart prime boost vaccinations with 10^7 IU ChAdOx1-DPY / 10^6 PFU MVA-DPY, a single vaccination of 10^7 IU ChAdOx1-li-P1A, 3-week apart prime boost vaccinations with 10^8 IU ChAdOx1-li-P1A/ 10^7 PFU MVA-P1A (± tPA), 1-week apart prime boost vaccinations with 10^7 IU ChAdOx1-li-P1A/ 10^6 PFU MVA-P1A (± tPA), or weekly alternating 10^7 IU ChAdOx1-li-P1A/ 10^6 PFU MVA-P1A (± tPA) vaccinations. Tumour size was measured every 3-4 days and mice were culled when tumour size reach 12mm length in any direction.

Compared to the DPY control group, all groups vaccinated with ChAdOx1/MVA encoding P1A showed significantly improved control of 15V4T3 tumour growth (Figure 4.15 A). Mice in the control group had mostly succumbed to tumour burden within 24 days post tumour implantation. All mice receiving ChAdOx1/MVA P1A vaccinations however had significantly improved survival (Figure 4.15 B). This was most apparent in the groups receiving the weekly alternating vaccinations. A single vaccination with a log-fold reduced dose of 10^7 IU of ChAdOx1-Ii-P1A demonstrated no therapeutic effect, and tumour growth and survival in this group were not significantly different to the DPY control, and significantly worse than groups that received the boost vaccination with 10^6 PFU 1-week later. This indicated that the effect of the MVA boost on the P1A-specific CD8+ T-cell response was critical for therapeutic efficacy. This was clear from inspection of the individual growth curves, which revealed a markedly different trend in tumour growth between mice receiving only 10^7 IU of ChAdOx1-Ii-P1A, and those in weekly alternating ChAdOx1/MVA and 1-week apart prime-boost groups which all received a boost with 10^6 PFU MVA-P1A (±tPA) 1 week later (Figure 4.16). In mice in these groups where a therapeutic effect was observed, tumour growth peaked around day 16 after tumour implantation (day 4 post MVA), and was then followed by a clear tumour resolution phase where tumour volume decreased, beginning 5-6 days after MVA was given. Without the MVA, no such resolution occurred. Additionally, no significant effect was found from the incorporation of tPA via fusion to P1A in the MVA vectors. Vaccinated groups

with and without tPA had almost identical trends of tumour growth for each different scheme tested.

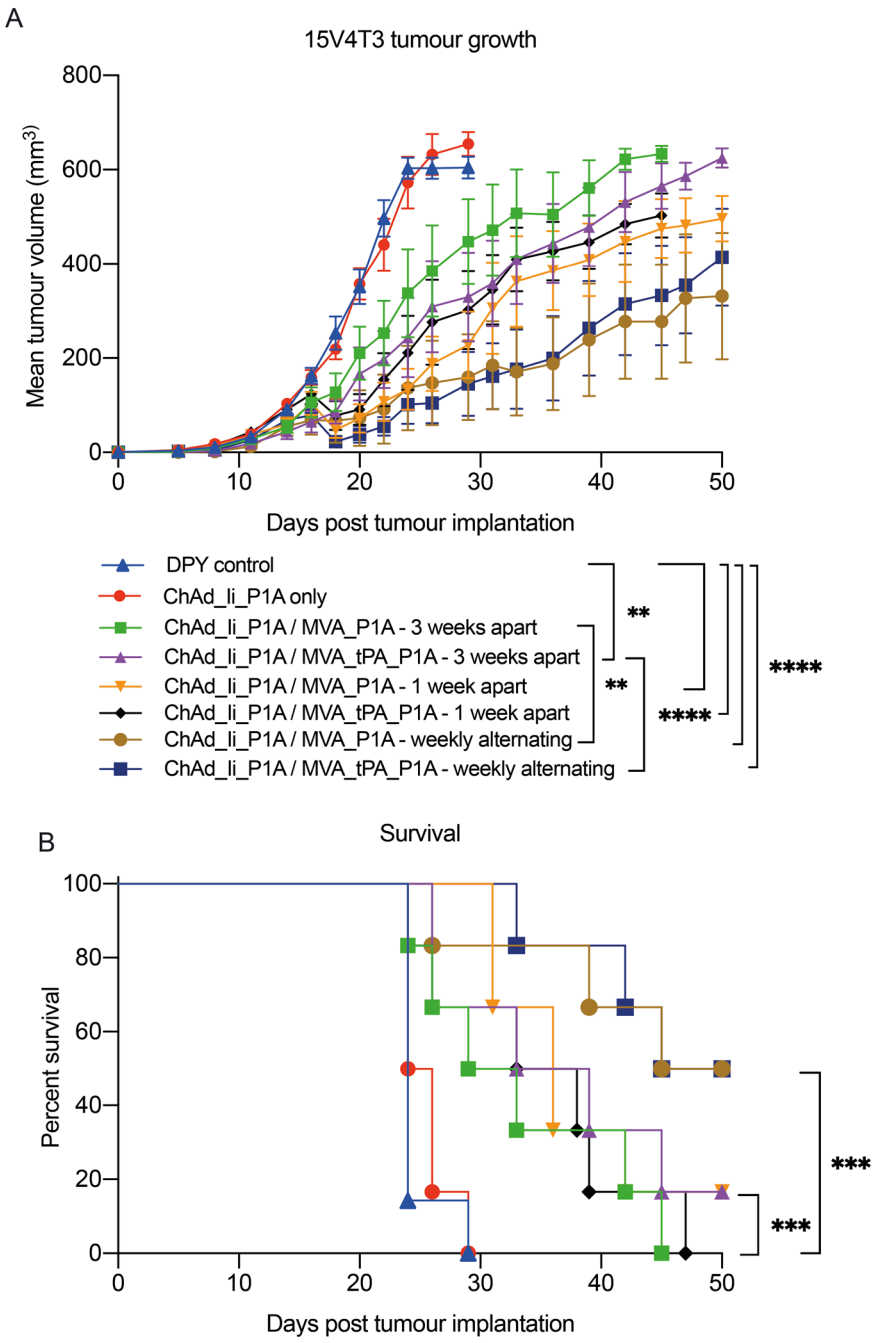


Figure 4.15. Therapeutic efficacy of ChAdOx1/MVA P1A vaccination against 15V4T3 tumours. DBA/2 mice were implanted with $1x10^6$ 15V4T3 cells via s.c. injection to initiate tumour growth. 5 days after tumour implantation, mice were vaccinated according to the schedules described in Figure 4.14. Tumour growth was followed for 50 days and mice were culled when tumour size reached 12mm in any direction. Mean tumour growth for each group (A) and survival curves (B) are shown. Mean tumour growth data in (A) are presented as mean tumour volume (mm^3) ± SEM. Each group contained 6 mice, with data representative of 2 independent experiments. Statistically significant differences in mean tumour volume between groups were determined by a two-way ANOVA followed by Tukey's post hoc test and statistical differences in survival data were determined by a Log Rank test. *, $p \leq 0.05$, **, $p \leq 0.01$ ****, $p \leq 0.0001$.

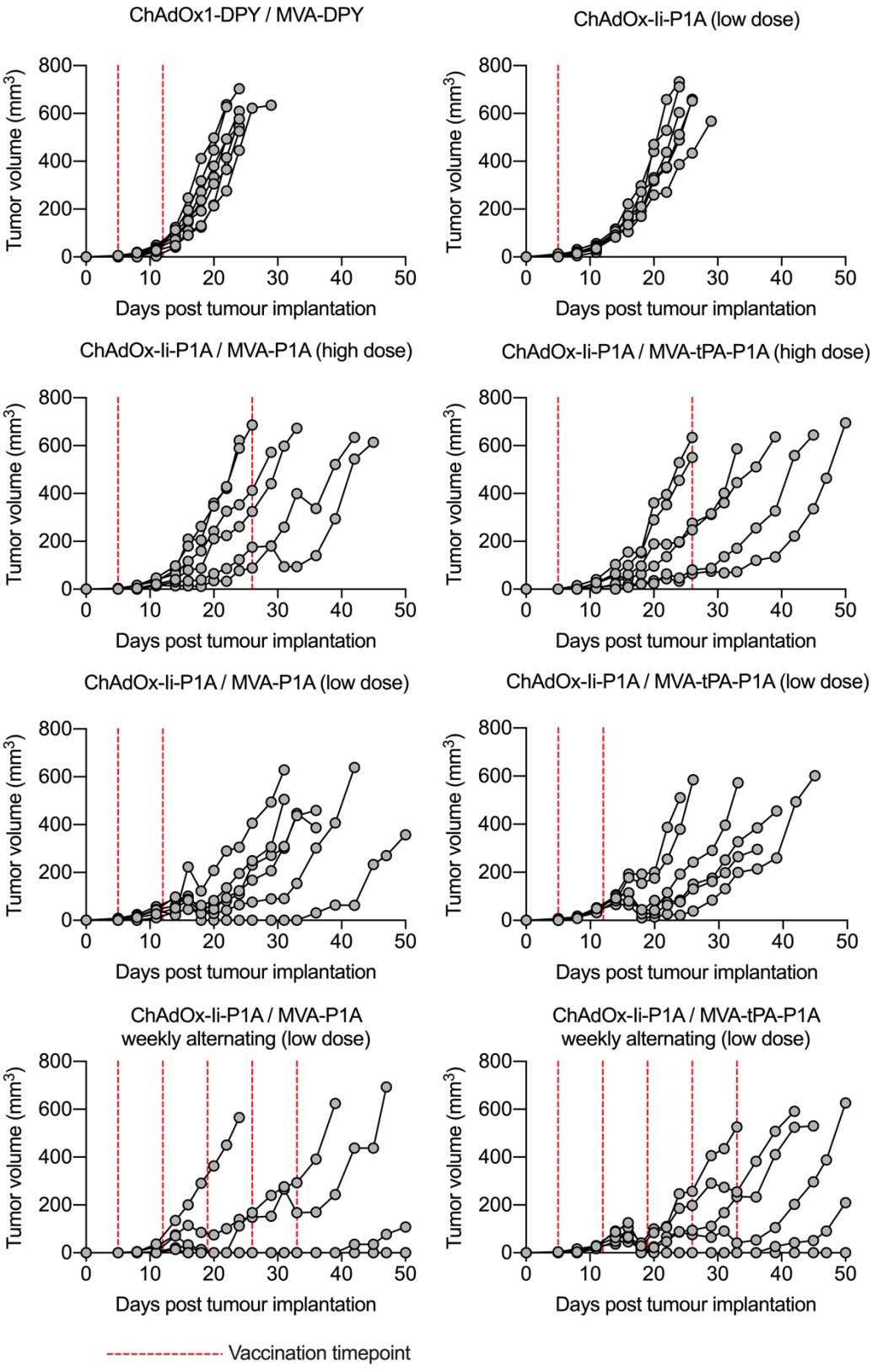


Figure 4.16. Individual 15V4T3 tumour growth curves for control and ChAdOx1/MVA P1A vaccinated mice.DBA/2 mice were implanted with 1x10^6 15V4T3 cells via s.c. injection to initiate tumour growth. 5 days after tumour implantation, mice were vaccinated according to the schedules described in Figure 4.14. Tumour growth was followed for 50 days and tumour volumes for individual mice in each vaccine treatment group are presented.

4.2.9 ChAdOx1/MVA P1A vaccine therapeutic efficacy correlates very strongly with the magnitude of vaccine induced P1A-specific CD8+ T-cell response

The CD8+ T-cell response induced by therapeutic ChAdOx1/MVA P1A vaccination in 15V4T3 tumour bearing mice was also assessed. Mice were bled 23 days after tumour implantation (corresponding to 18 days after the first ChAdOx1 vaccination), and the magnitude of the P1A-specific CD8+ T-cell response in the blood was measured via ex vivo stimulation of PBMCs with overlapping P1A peptides. P1A-specific IFN-γ producing CD8+ T-cells could be detected in all vaccinated mice with the exception of the DPY control, and those that received only a single vaccination of ChAdOx1-Ii-P1A (Figure 4.17 A). In line with the higher therapeutic efficacy observed in these groups, there was a trend toward higher magnitude P1A-specific CD8+ responses in the groups that received weekly alternating ChAdOx1/MVA P1A vaccinations, although this was not found to be significantly higher than other groups. For each mouse, the magnitude of P1A-specific IFN-γ producing CD8+ T-cells was correlated with tumour size on day 20 post tumour implantation, the time-point where partial or complete tumour resolution was observed in some vaccinated mice. A very strong and significant negative correlation was found between tumour burden in the mice and the magnitude of the P1A-specific CD8+ T-cell response in the blood (Figure 4.17 B), an observation which strongly implied that the observed tumour resolution was due to the response induced by ChAdOx1/MVA P1A vaccination.

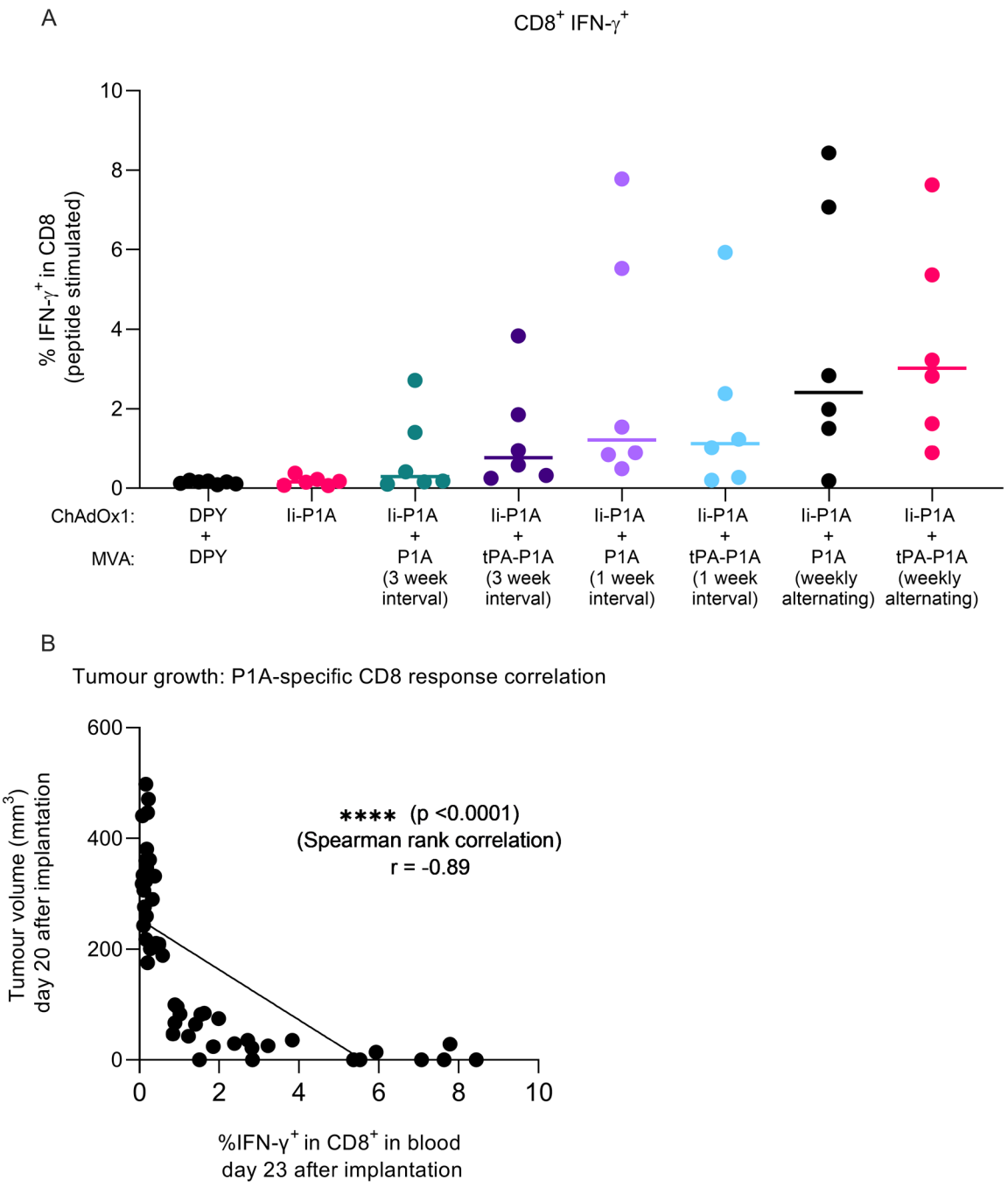


Figure 4.17. P1A-specific CD8+ T-cell responses in 15V4T3 tumour bearing mice following ChAdOx1/MVA P1A vaccination. DBA/2 mice were implanted with 1x10^6 15V4T3 cells via s.c. injection to initiate tumour growth. 5 days after tumour implantation, mice were vaccinated according to the schedules described in Figure 4.14. To determine the magnitude of vaccine induced P1A-specific CD8+ T-cell responses in 15V4T3 tumour-bearing mice, mice were bled 23 days after tumour implantation. PBMCs were stimulated ex vivo with 4μg/ml of P1A peptide pools and the percentage of cytokine-producing P1A-specific CD8+ T-cells in the blood was then determined by ICS and flow cytometry. Percentage of IFN-γ+ CD8+ T-cells in response to stimulation with P1A peptides are shown (A). Data are shown as the median response of each group (horizontal lines). Each symbol represents an individual mouse, with 6 mice per group. . Statistically significant differences between groups were determined by a Kruskal-Wallis test with Dunn's multiple comparisons test. *, p ≤ 0.05. Tumour size on day 20 after implantation was correlated with the magnitude of IFN-γ producing P1A-specific CD8+ T-cells in the blood measured 23 days after implantation (B). Significance was determined by a Spearman Rank correlation test.

4.2.10 15V4T3 tumours express surface PD-L1 which is further up-regulated by IFN-γ stimulation

Despite seeing good control of tumour growth from therapeutic ChAdOx1/MVA-P1A vaccination, this was often lost at later time-points in many mice after an initial regression in tumour size, and tumours were seen to grow out again. It was hypothesised that this may be due to T-cell exhaustion or immune-suppression present in the tumour microenvironment, or the combined effects of both. To combat this, combination of therapeutic vaccination with immune checkpoint blockade was then investigated.

In order to better inform a rational combination of vaccination with immune checkpoint blockade in the form of antibodies blocking the PD-L1/PD-1 axis, PD-L1 expression by 15V4T3 tumour cells was investigated, both constitutive and IFN-γ inducible. PD-L1 expression is known to be regulated by IFN-γ signalling and in vivo can be upregulated by tumour cells in response to IFN-γ secreted following T-cell recognition and activation. MC38, a murine colon carcinoma cell line, was used as a positive control, as it has been observed before in other studies that PD-L1 expression can be highly upregulated on this cell line in response to IFN-γ stimulation and mediate profound immunosuppression of T-cell responses targeting the tumour [253] [91]. 15V4T3 is however a relatively lesser studied cell line, and no literature could be found regarding its PD-L1 expression status.

15V4T3 and MC38 cells were treated with either 20 ng/ml or 100 ng/ml recombinant mouse IFN-γ in culture for 24 or 48 hours, or otherwise left

untreated. The level of surface PD-L1 expression on either unstimulated or IFN-γ treated cells was then evaluated by staining with fluorescent anti-PD-L1 antibodies and analysed by flow cytometry (Figure 4.18). The mean fluorescence intensity (MFI) of PD-L1 on cells from each condition was then determined. PD-L1 expression was found to be constitutively expressed by 15V4T3 cells, with significantly higher PD-L1 detected compared to the isotype control (Figure 4.18 A, C). However its expression level on the cell surface could also be further significantly increased by stimulation with IFN-γ (Figure 4.18 A, C). No significant differences in PD-L1 MFI were detected between either of the concentrations of IFN-γ tested or either of the treatment times (24 or 48 hours), suggesting that PD-L1 surface expression may be rapidly upregulated to a maximum level on 15V4T3 cells after an initial exposure to IFN-γ. MC38 cells were found to have much lower constitutive expression of PD-L1 when unstimulated, with only slight staining above the isotype control observed (Figure 4.18 B, D). However, similar to 15V4T3, PD-L1 surface expression was significantly upregulated to a maximum level by IFN-γ stimulation, independent of IFN-γ concentration or treatment time tested (Figure 4.18 B, D).

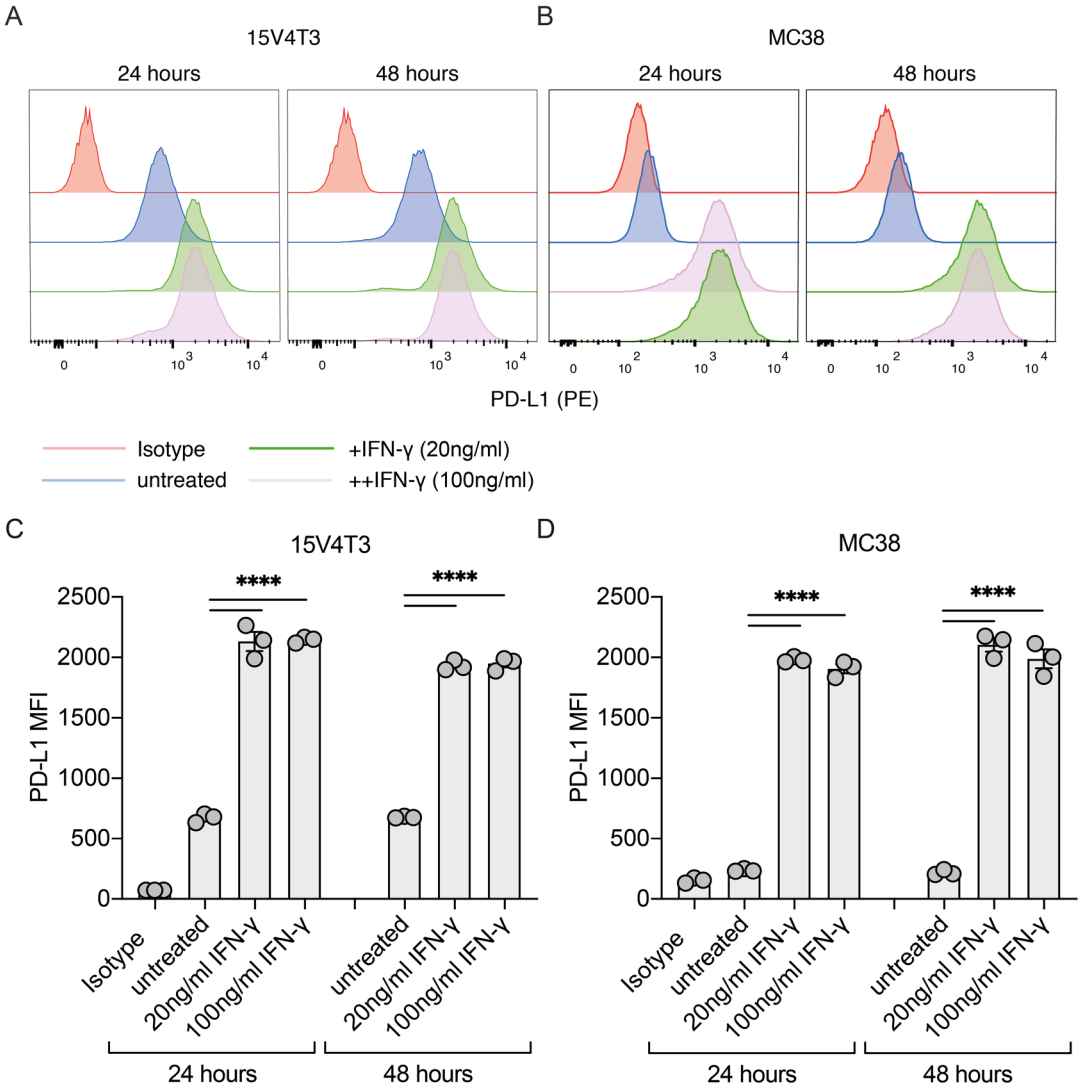


Figure 4.18. Surface PD-L1 expression on 15V4T3 cells. 15V4T3 and MC38 cells were cultured in vitro and stimulated with either 20ng/ml or 100ng/ml recombinant mouse IFN-γ for 24 or 48 hours. Cells were then surface stained with either PE-anti-PD-L1 or a PE-IgG2b isotype control and the level of surface PD-L1 expression was assessed on unstimulated and stimulated cells at each time point by flow cytometry. Representative flow cytometry histograms for PD-L1 expression level are shown for the different conditions for 15V4T3 (A) and MC38 (B). The signal for the isotype control staining is only shown for untreated cells, however no difference was observed in the isotype staining between untreated or stimulated cells. The PD-L1 mean fluorescence intensity (MFI) was calculated for each treatment condition for 15V4T3 (C) and MC38 (D). Each point shows an individual technical replicate and data are shown as mean ± SEM. Three technical replicates were performed per treatment group. Statistical differences between each group were calculated by an ordinary one-way ANOVA followed by a Tukey's post hoc test. ****, $p \leq 0.0001$.

4.2.11 Therapeutic ChAdOx1/MVA P1A vaccination treatment synergises with anti-PD-1 blockade to promote improved control of established 15V4T3 tumours and increased survival

Given that it was found that PD-L1 expression was observed on the surface of 15V4T3, and the finding that it was strongly upregulated by exposure to IFN-γ, combining therapeutic ChAdOx1/MVA P1A vaccinations with immune checkpoint blockade to combat tumour immunosuppression in the 15V4T3 model was then explored. The PD-L1/PD-1 axis can be targeted with either blocking antibodies against either the PD-L1 ligand or the PD-1 receptor. Those targeting the PD-1 receptor have been seen to be the most successful in recent clinical evaluations, and are currently approved for more cancer indications [8], and therefore anti-PD-1 blocking antibodies were chosen to test in combination with ChAdOx1/MVA P1A vaccination. The combination of ChAdOx1/MVA vaccination with anti-CTLA-4 blocking antibodies was also evaluated, as this has a different mechanism of action and is also approved for the treatment of some cancers..

To investigate the therapeutic efficacy of combining ChAdOx1/MVA P1A vaccinations with CPIs against established tumours, mice were implanted with 15V4T3 tumours via s.c. injection, and weekly alternating vaccinations with either ChAdOx1-Ii-P1A/MVA-P1A or a PBS control were given via i.m. injection and started on day 8 after implantation, when 90% of mice had developed palpable tumours (Figure 4.19). Three days after ChAdOx1-Ii-P1A vaccinations were administered, 3 doses of either αPD-1, αCTLA-4 or an isotype control antibody of irrelevant specificity were given via intraperitoneal (i.p.) injection, each 3 days

apart. Mice that received PBS control vaccinations also received 3 doses of either PBS, anti-PD-1, anti-CTLA-4 via i.p. injection at the same time-points to ChAdOx1-Ii-P1A/MVA-P1A vaccinated groups (termed PBS control, anti-PD-1 only and anti-CTLA-4 only groups respectively). Tumour growth in each group was monitored over the course of 50 days. The slightly later time-point of day 8 post tumour implantation to start vaccinations was chosen in this study to investigate the efficacy of different treatments against more evolved tumours of larger size. A schedule of weekly alternating ChAdOx1-Ii-P1A (10^7 IU) /MVA-P1A (10^6) vaccinations was opted for based on the superior therapeutic efficacy of this regime in comparison to others as determined in the previously presented findings (Figure 4.15).

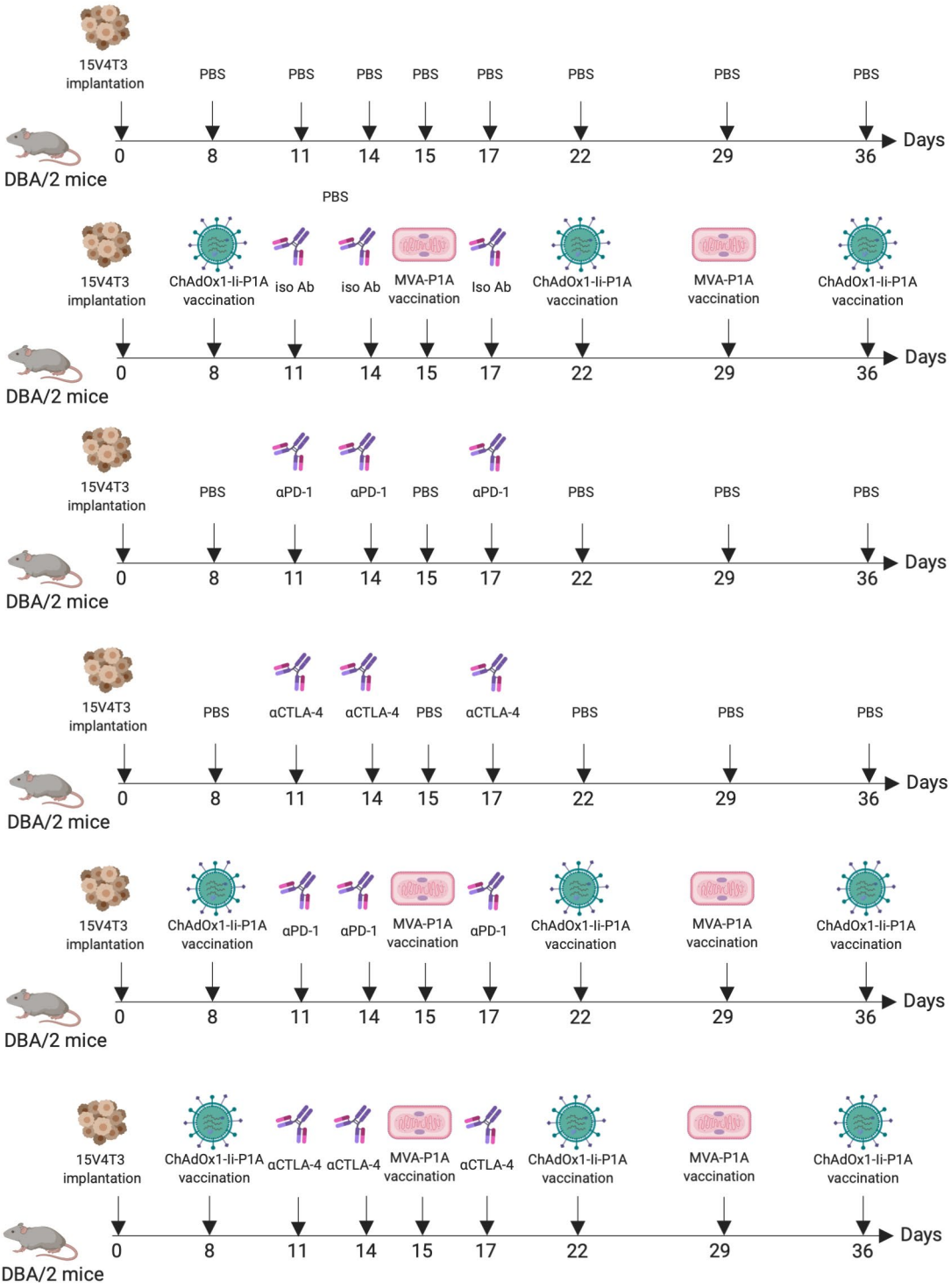


Figure 4.19. Timeline of therapeutic ChAdOx1-li-P1A/MVA-P1A vaccination in combination with CPI antibody treatment. DBA/2 mice were implanted with $1x10^6$ 15V4T3 cells via s.c. injection to initiate tumour growth. 8 days after tumour implantation, vaccinations were started and mice received either weekly alternating 10^7 IU ChAdOx1-li-P1A/ 10^6 PFU MVA-P1A or PBS sham vaccinations. Starting on day 11 after tumour implantation mice received 3 doses of 100μg of either αPD-1 or αCTLA-4, or PBS vehicle control via i.p. injection, 3 days apart. Tumour size was measured every 3-4 days and mice were culled when tumour size reached 10mm length in any direction.

In this later start setting with 15V4T3 tumours of larger size, ChAdOx1-Ii-P1A/MVA-P1A vaccinations were ineffective at providing any control of tumour growth (Figure 4.20). Compared to the PBS control group, tumour growth was not significantly delayed (Figure 4.20 A) and only a slight improvement in survival was observed (Figure 4.20 B). Similarly CPI treatment alone with either anti-PD-1 or anti-CTLA-4 was largely ineffective at controlling 15V4T3 tumours. There was only a slight delay in mean tumour growth in the anti-PD-1 only group compared to the PBS control (Figure 4.20 A) and slightly increased survival (Figure 4.20 B) . In the anti-CTLA-4 only group there was no overall delay in mean tumour growth across the group (Figure 4.20 A) and again only slightly increased survival (Figure 4.20 B) . However, the combination of ChAdOx1-Ii-P1A/MVA-P1A vaccination with either anti-PD-1 or anti-CTLA-4 improved tumour control compared over any modality given alone. There was significantly reduced tumour growth in the ChAdOx1-Ii-P1A/MVA-P1A + anti-PD-1 group compared to ChAdOx1-Ii-P1A/MVA-P1A only and anti-PD-1 only (Figure 4.20 A) and significantly improved survival (Figure 4.20 B). Indeed some mice in the ChAdOx1-Ii-P1A/MVA-P1A + anti-PD-1 group were able to completely resolve their tumours (Figure 4.20 C) and 50% of the mice were still surviving after 50 days (3/6). Similarly, in the ChAdOx1-Ii-P1A/MVA-P1A + anti-CTLA-4 group there was a significant reduction in mean tumour growth compared to either the ChAdOx1-Ii-P1A/MVA-P1A only or anti-CTLA-4 only groups, however survival was not significantly increased. Further still, the combination of ChAdOx1-Ii-P1A/MVA-P1A vaccination with anti-PD-1 was found to be more efficacious than with anti-

CTLA-4. Over the course of 50 days the mean tumour growth in the ChAdOx1-Ii-P1A / MVA-P1A + anti-PD-1 group was significantly less than the ChAdOx1-Ii-P1A / MVA-P1A + anti-CTLA-4 group.

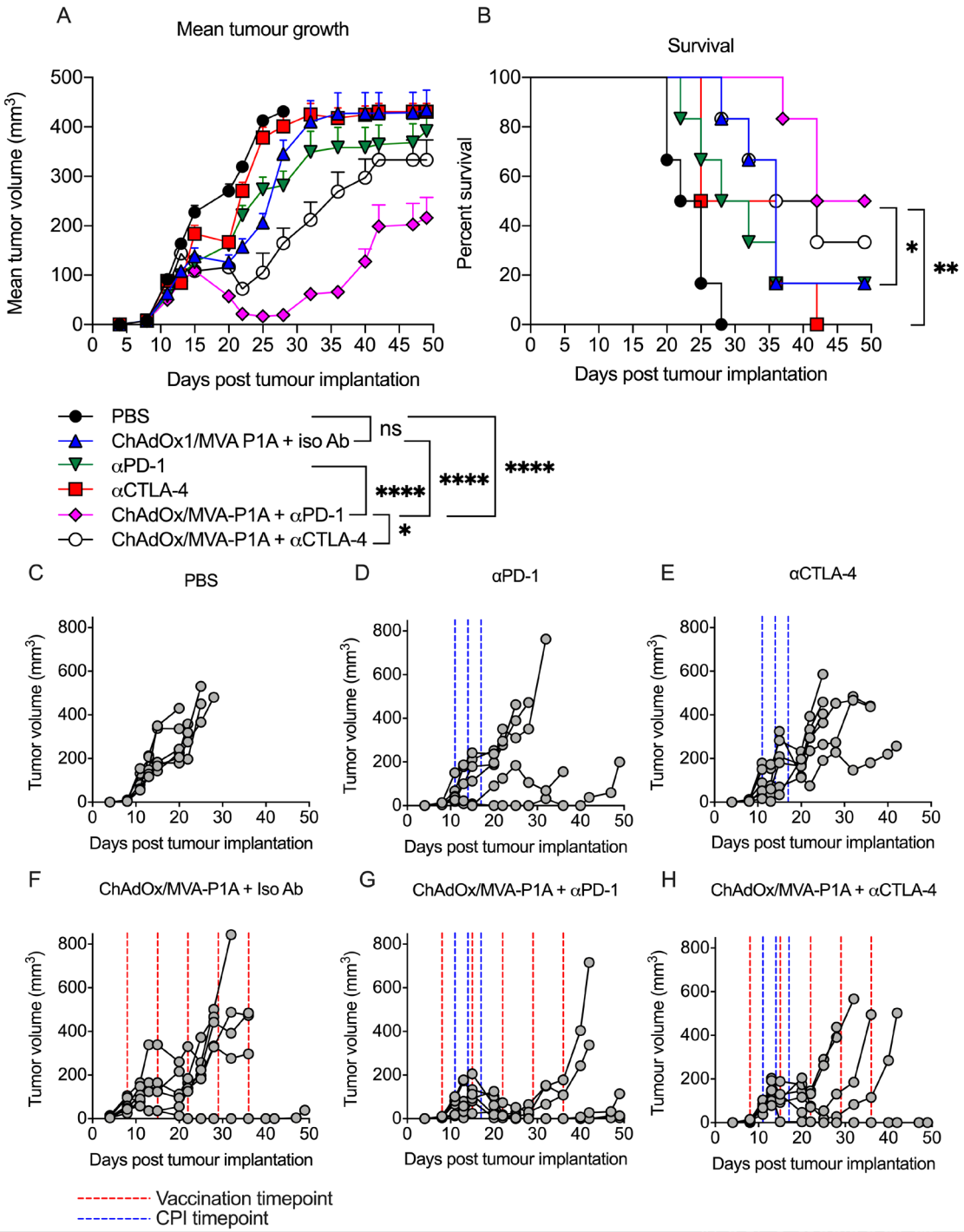


Figure 4.20. Therapeutic efficacy of ChAdOx1/MVA P1A vaccination in combination with immune checkpoint blockade in the 15V4T3 tumour model. DBA/2 mice were implanted with $1x10^6$ 15V4T3 cells via s.c. injection to initiate tumour growth. 8 days after tumour implantation, mice were vaccinated and treated with immune checkpoint inhibitors according to the schedules described in Figure 4.19. Tumour growth was followed for 50 days and mice were culled when tumour size reached 10mm in any direction. Mean tumour growth (A), survival curves (B) and individual tumour growth curves from each group - PBS control (C), αPD-1 only (D), αCTLA-4 only (E), ChAdOx1-li-P1A /MVA-P1A only (D) ChAdOx1-li-P1A /MVA-P1A + αPD-1 (F) and ChAdOx1-li-P1A /MVA-P1A + αCTLA-4 (G) are shown. Tumour growth data in (A) are presented as mean tumour volume (mm^3) ± SEM. Each group contained 6 mice, with data representative of at least 2 independent experiments. Statistically significant differences in tumour volume between groups were determined by a two-way ANOVA followed by Tukey's post hoc test and statistical differences in survival data were determined by a Log Rank test. *, $p \leq 0.05$, **, $p \leq 0.01$ ****, $p \leq 0.0001$.

4.2.12 Therapeutic ChAdOx1/MVA P1A vaccination increases P1A-specific CD8+ T-cell infiltration into the tumour

A central aim of an effective cancer vaccine is to generate a source tumour-antigen-specific T-cells and thereby to promote their intra-tumour accumulation. In this way the infiltrate of effector T-cells in the tumour can be increased. Having shown that ChAdOx1-Ii-P1A/MVA-P1A vaccination in combination with anti-PD-1 blockade could provide a strong therapeutic effect against established 15V4T3 tumours, the effect of the treatment on T-cell infiltration into 15V4T3 tumours was then considered. Mice were implanted with 15V4T3 tumours and treated with either anti-PD-1, ChAdOx1-Ii-P1A/MVA-tPA-P1A or with a combination of the two (Figure 4.21). Control mice received injections with PBS. Mice were bled on day 19 after tumour implantation to assess the immunogenicity of vaccination with and without anti-PD-1. Mice were sacrificed, spleens and tumours harvested, and the level of P1A-specific T-cell infiltrate assessed on day 20 after tumour implantation, immediately at the time-point where the beginning of tumour resolution had previously been seen in therapeutic studies.

Tumour growth was monitored over the course of the 20 days. At the harvest on day 20, a clear reduction in mean tumour volume was observed in the vaccinated groups compared to PBS control or anti-PD-1 alone treated groups (Figure 4.22 A) and a trend towards decreased tumour mass (Figure 4.22B). From inspection of the individual tumour growth curves, a clear inflection was observed in those from ChAdOx1-Ii-P1A/MVA-tPA-P1A tumours (± anti-PD-1) vaccinated mice, indicating that tumours were harvested at the beginning of the regression phase

(Figure 4.22 E and F). This was consistent with the timing of tumour regression observed in therapeutic studies.

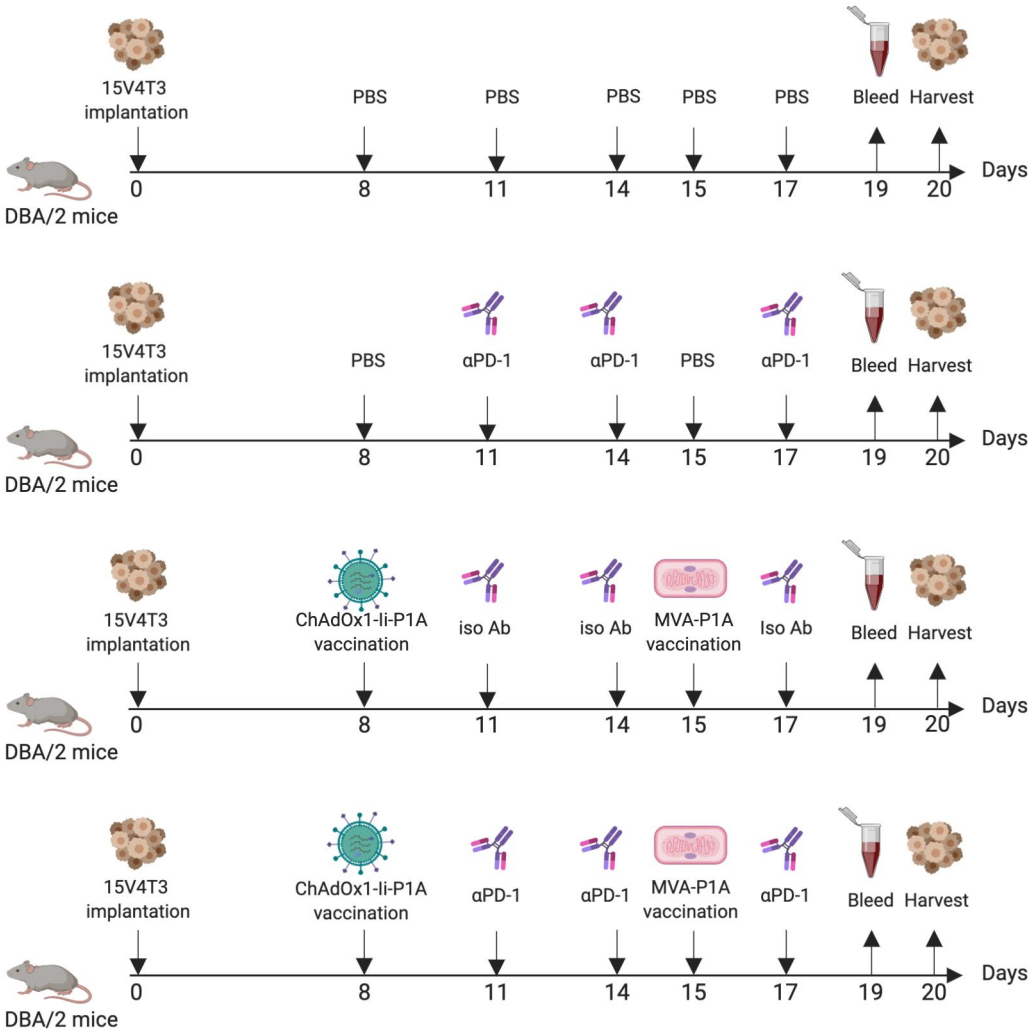


Figure 4.21. Timeline of 15V4T3 tumour harvest study to assess tumour T-cell infiltrate following ChAdOx1-li-P1A/MVA vaccination in combination with anti-PD-1 treatment. DBA/2 mice were implanted with $1x10^6$ 15V4T3 cells via s.c. injection to initiate tumour growth. 8 days after tumour implantation, mice received vaccinations of 10^7 IU ChAdOx1-li-P1A and 10^6 PFU MVA-tPA-P1A given 1-week apart or PBS sham vaccinations. Starting on day 11 after tumour implantation mice received 3 doses of 100μg of either αPD-1 or PBS vehicle via i.p. injection, 3 days apart. Mice were bled on day 19 for assessment of vaccine-induced P1A-specific CD8+ T-cell responses. Mice were sacrificed on day 20 after tumour implantation, and spleens and tumours surgically excised for analysis of effector T-cell infiltrate by flow cytometry and expression of inflammatory mediators by rt-qPCR.

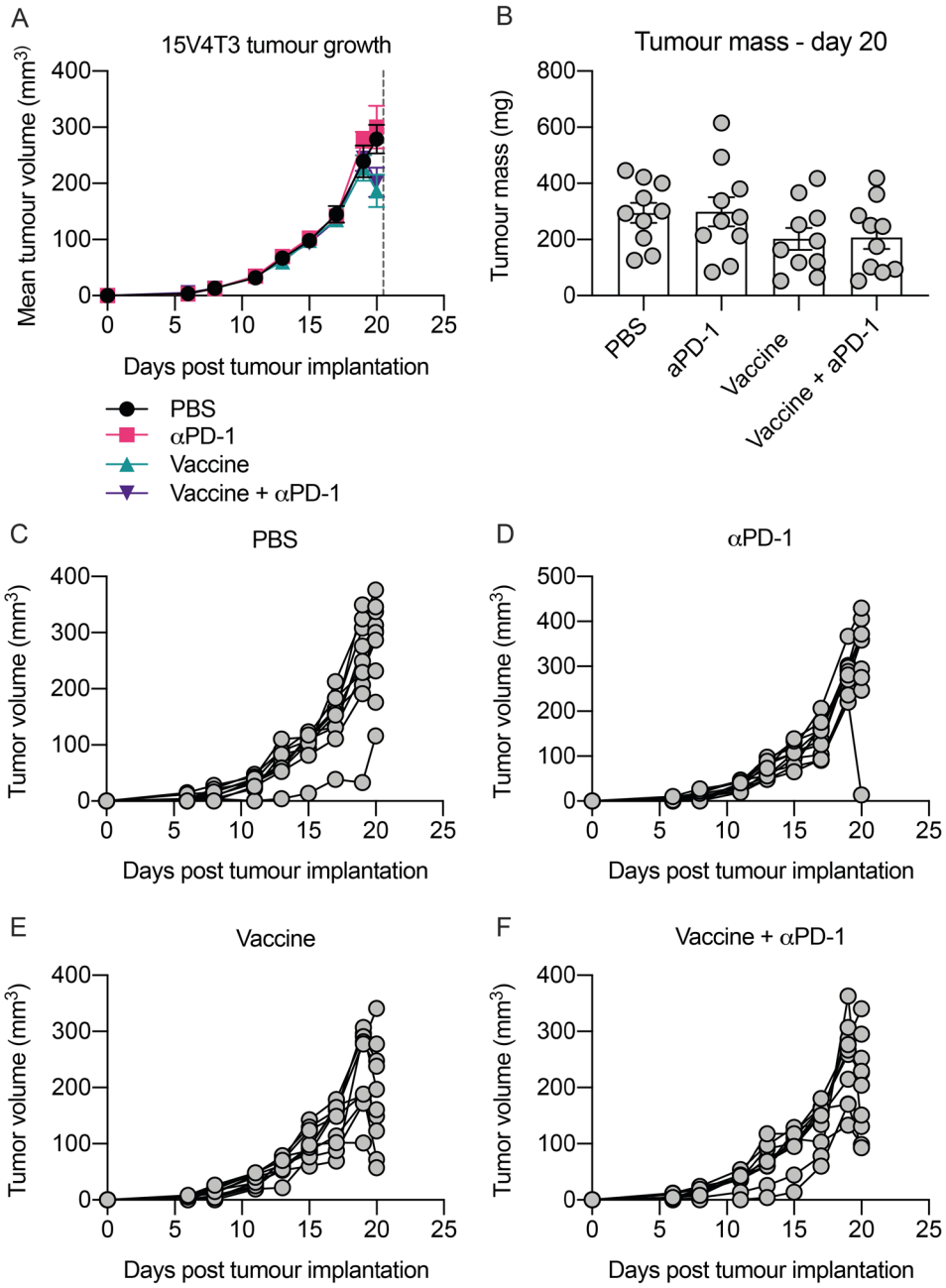


Figure 4.22. Harvesting 15V4T3 tumours for analysis of T-cell infiltrate. DBA/2 mice were implanted with 1x10^6 15V4T3 cells via s.c. injection to initiate tumour growth. 8 days after tumour implantation, mice were vaccinated and treated with immune checkpoint inhibitors according to the schedules described in Figure 4.21. Tumour growth was monitored and mice sacrificed on day 20 after implantation, prior to tumour regression. Tumours were excised for analysis of the T-cell infiltrate. Mean tumour growth (A), tumour mass on day 21 post implantation (B) and individual growth curves for each group - PBS control (C), αPD-1 only (D), ChAdOx1-Ii-P1A /MVA-tPA-P1A only (E) and ChAdOx1-Ii-P1A /MVA-tPA-P1A + αPD-1 (F) are shown.

The frequency of P1A-specific CD8+ T-cells induced by vaccination in the blood and the spleen was assessed. In the blood there were significantly increased levels of P1A-specific CD8+ T-cells in the vaccine + anti-PD-1 combination group, as assessed by IFN-γ production (Figure 4.23 A), compared to the PBS control and the anti-PD-1 only groups, and a trend towards an increase compared to the vaccine only group. Although there was a trend towards higher responses in the vaccine only group, this was not significantly higher than the PBS control and anti-PD-1 only groups. In the spleen there were significantly higher frequencies of IFN-γ producing CD8+ T-cells upon P1A peptide stimulation (Figure 4.23 C). It is known that P1A-specific CD8+ T-cells in DBA/2 mice recognize an H-2L^{d} restricted 9mer epitope P1A$_{35-43}$-LPYLGWLVF. P1A-specific CD8+ T-cells can therefore be labelled and detected with fluorescently labelled H-2L^{d} P1A$_{35-43}$ tetramers. Similarly to the pattern of IFN-γ producing CD8+ T-cells detected by ICS, there were significantly higher frequencies of P1A$_{35-43}$ tetramer+ CD8+ T-cells in in spleens of vaccine + anti-PD-1 treated mice compared to the PBS control and the anti-PD-1 only groups (Figure 4.23 D). Again by both of these metrics there was a trend towards an increase in the magnitude of the P1A-specific CD8+ T-cell response when anti-PD-1 was combined with vaccination compared to the vaccine only group, although this was not significant.

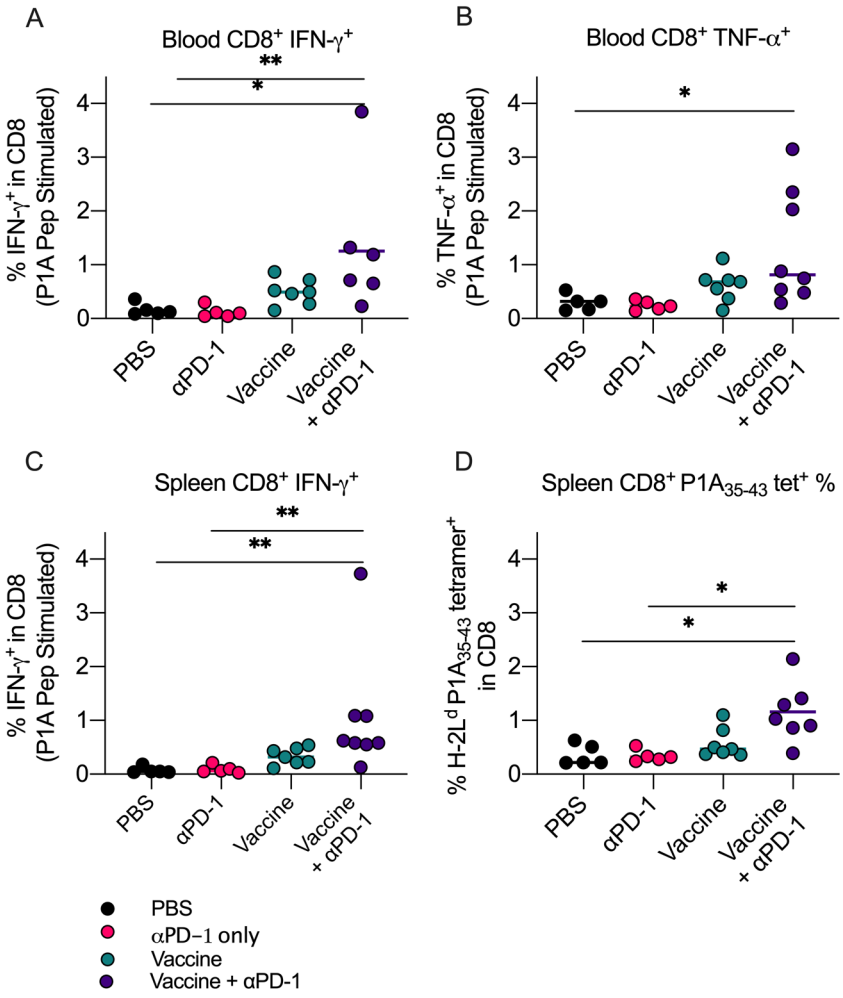


Figure 4.23. P1A-specific CD8+ T-cell responses induced in the blood and spleen of 15V4T3 tumour-bearing mice following treatment with ChAdOx1-li-P1A/MVA-tPA-P1A vaccination, with or without αPD-1. To determine the magnitude of vaccine induced P1A-specific CD8+ T-cell responses in 15V4T3 tumour-bearing mice treated with vaccine and/or αPD-1, mice were bled 19 days after tumour implantation. PBMCs or splenocytes were stimulated ex vivo with 4μg/ml of P1A peptide pools and the percentage of cytokine-producing P1A-specific CD8+ T-cells in the blood was then determined by ICS and flow cytometry. The percentage of IFN-γ+ (A) and TNF-α+ (B) blood CD8+ T-cells observed in response to stimulation with P1A peptides are shown. Mice were sacrificed on day 21 and splenocytes isolated to further evaluate P1A-specific CD8+ T-cell responses in the spleen. Splenocytes were stimulated with P1A-peptides according to the same protocol as PBMCs. The percentage of IFN-γ+ CD8+ T-cells from the spleen are shown (C). Unstimulated splenocytes were also stained ex vivo with H-2L^d P1A$_{35-43}$ tetramer and the percentage of tetramer+ CD8+ T-cells are shown (D). Data are shown as the median response of each group (horizontal lines). Each symbol represents an individual mouse, with 5-8 mice per group. Statistically significant differences between groups were determined by a Kruskal-Wallis test with Dunn's multiple comparisons test. *, $p \leq 0.05$, **, $p \leq 0.01$

Tumours from sacrificed mice were harvested, disaggregated and the T-cell infiltrate in the TME analysed by flow cytometry (Figure 4.24). Tumours from mice receiving either vaccine alone or vaccine combined with anti-PD-1 had significantly increased frequencies of CD8+ TILs as a proportion of total tumour cells compared to both the PBS control and anti-PD-1 only groups (Figure 4.24 B). Similarly tumours from both vaccinated groups had significantly higher total numbers of CD8+ TILs compared to tumours from unvaccinated mice (Figure 4.24 C). CD8+ T-cells were on average close to 10-fold higher in number in tumours from vaccinated mice compared to unvaccinated. Conversely, anti-PD-1 treatment given alone had no effect on CD8+ T-cell infiltration into the tumour, as tumours from mice treated with only anti-PD-1 had neither increased frequencies nor increased total numbers of CD8+ TILs compared to PBS control mice (Figure 4.24 B and C). Indeed tumours from unvaccinated mice appeared to be naturally very lowly infiltrated by CD8+ T-cells, with very few detectable CD8+ TILs present. Furthermore, the addition of anti-PD-1 to vaccination did not have any effect on the numbers of CD8+ TILs in the tumour, with roughly similar levels observed in tumours of mice from both groups. Neither vaccination nor anti-PD-1 significantly altered the numbers of CD4+ T-cells in the tumour (Figure 4.24 E). The increase in CD8+ T-cells in tumours from vaccinated mice also significantly altered the ratio of CD8+ T-cells to CD4+ T-cells (Figure 4.24 D). CD4+ T-cells far exceeded the amount of CD8+ T-cells as a proportion of total CD3+ T-cells in the tumours of PBS control and anti-PD-1 only treated mice. After vaccination however, the ratio of CD8+ T-cells: CD4+ T-cells in the tumour was roughly equal due to increased

numbers in the CD8+ T-cell compartment. Taken together this strongly suggests that ChAdOx1-Ii-P1A/MVA-tPA-P1A vaccination alone and combination with anti-PD-1 enhances CD8+ T-cell infiltration into the TME.

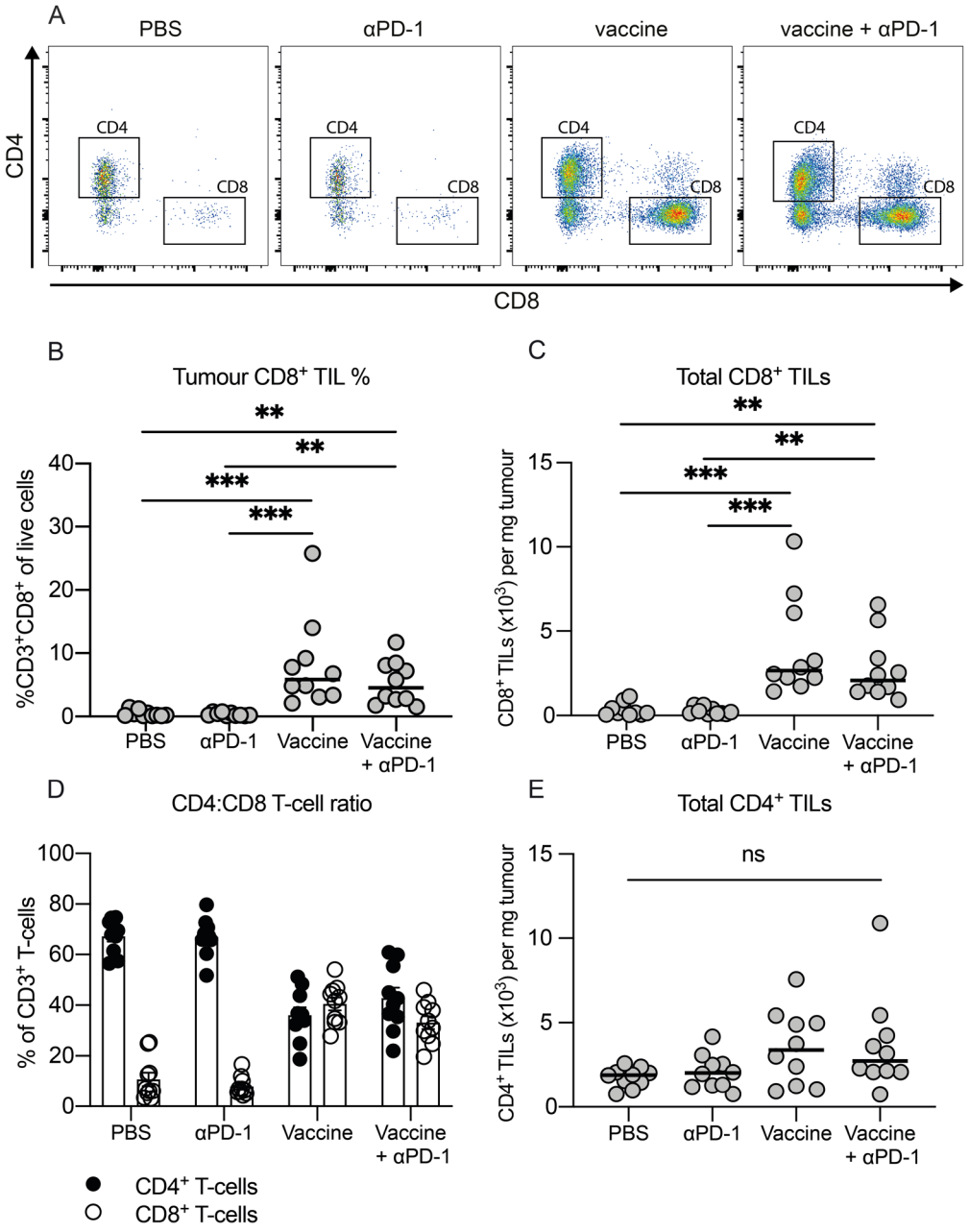


Figure 4.24 T-cell infiltrate in 15V4T3 tumours from mice treated with ChAdOx1-li-P1A/MVA-tPA-P1A and anti-PD-1 blockade. DBA/2 mice were implanted with 1x10^6 15V4T3 cells via s.c. injection to initiate tumour growth. 8 days after tumour implantation, mice were vaccinated and treated with immune checkpoint inhibitors according to the schedules described in Figure 4.21. Mice were sacrificed on day 20 post implantation, tumours excised and disaggregated, and the T-cell immune infiltrate profiled by flow cytometry (gating as described in Figure 2.3). Representative flow cytometry gating plots of CD8+ and CD4+ TILs from each group (A). The proportion of CD3+CD8+ TILs of total live cells in the tumour (B), the absolute number of CD3+CD8+ TILs per mg of tumour tissue (C) the ratio of CD4+:CD8+ TILs (D) and the absolute number of CD3+CD4+ TILs per mg of tumour tissue (E) are shown. Each symbol represents an individual mouse, with 10 mice per group. Representative of 2 independent experiments. Statistically significant differences between groups were determined by a Kruskal-Wallis test with Dunn's multiple comparisons test. *, $p \leq 0.05$, **, $p \leq 0.01$, ***, $p \leq 0.01$

The antigen-specificity of CD8+ TILs was further investigated. ChAdOx1-Ii-P1A/MVA-tPA-P1A vaccination significantly increased both the frequency and total number of P1A-specific CD8+ T-cells in the tumour (Figure 4.25). The frequency of $P1A_{35-43}$ tetramer+ CD8+ TILs was significantly higher in tumours from vaccinated mice or mice receiving vaccination combined with anti-PD-1 compared to those from mice in the PBS control or anti-PD-1 alone groups (Figure 4.25 B). Indeed a very high proportion of the CD8+ TILs in the tumours of vaccinated mice were observed to bind $P1A_{35-43}$ tetramer and therefore be P1A-specific. In line with this, the total numbers of $P1A_{35-43}$ tetramer+ cells were significantly increased in the tumours of vaccinated mice compared to those from unvaccinated (Figure 4.25 C). In numerical terms this represented an above 100-fold increase in mean numbers of $P1A_{35-43}$ tetramer+ CD8+ T-cells in the tumours of vaccinated mice compared to unvaccinated. Again anti-PD-1 alone had no effect on numbers of P1A-specific CD8+ TILs. Interestingly, despite the increased therapeutic efficacy observed from combining anti-PD-1 treatment with vaccination, the numbers of $P1A_{35-43}$ tetramer+ P1A-specific CD8+ T-cells were not significantly different between the vaccine only and vaccine + anti-PD-1 groups.

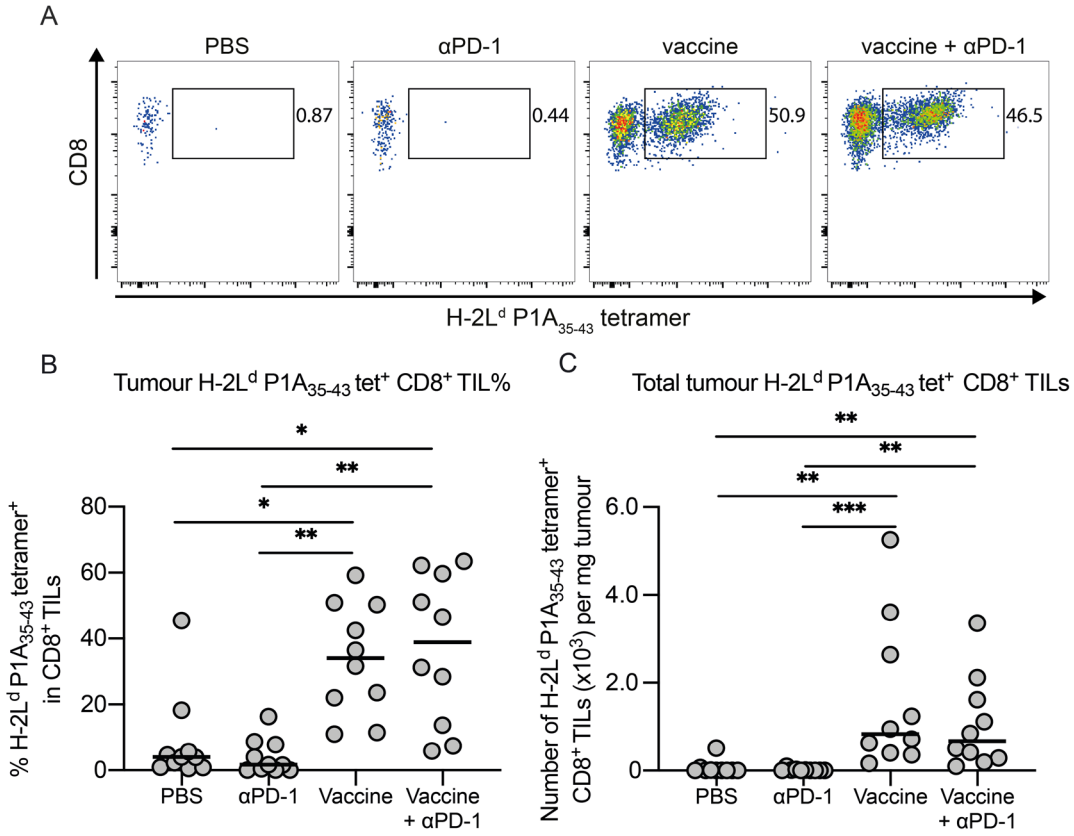


Figure 4.25. P1A-specific CD8+ T-cell infiltrate in 15V4T3 tumours from mice treated with ChAdOx1-li-P1A/MVA-tPA-P1A and anti-PD-1 blockade. DBA/2 mice were implanted with 1x10^6 15V4T3 cells via s.c. injection to initiate tumour growth. 8 days after tumour implantation, mice were vaccinated and treated with immune checkpoint inhibitors according to the schedules described in Figure 4.21. Mice were sacrificed on day 20 post implantation, tumours excised and disaggregated, and the T-cell immune infiltrate profiled by flow cytometry (gating as described in Figure 2.3). CD8+ TILs specific for P1A were enumerated by labelling cells ex vivo with an H-2L^d P1A$_{35-43}$ tetramer. Representative gating of H-2L^d P1A$_{35-43}$ tetramer+ CD8+ TILs from each group (A). The proportion of P1A$_{35-43}$-specific CD8+ TILs (B) and the absolute number of P1A$_{35-43}$ tetramer+ CD8+ TILs per mg of tumour tissue (C) are shown. Each symbol represents an individual mouse, with 10 mice per group. Representative of 2 independent experiments. Statistically significant differences between groups were determined by a Kruskal-Wallis test with Dunn's multiple comparisons test. *, $p \leq 0.05$, **, $p \leq 0.01$, ***, $p \leq 0.001$

Having observed increased numbers of CD8+ TILs in tumours of vaccinated mice, their functionality was then assessed. Tumour cell suspension was stimulated ex vivo with P1A peptides, and cytokine production detected by ICS to evaluate the activation of TILs in response to antigenic stimulation. Both significantly increased frequencies and total numbers of IFN-γ producing CD8+TILs were detected in the tumours of mice from the vaccine only or vaccine combined with anti-PD-1 groups compared to the PBS control or anti-PD-1 alone groups (Figure 4.26 B and C). Indeed a high proportion of CD8+ TILs in tumours from vaccinated mice were found to produce IFN-γ, indicating that the increased CD8+ T-cell infiltrate induced by vaccination also likely has effector functionality in the TME.

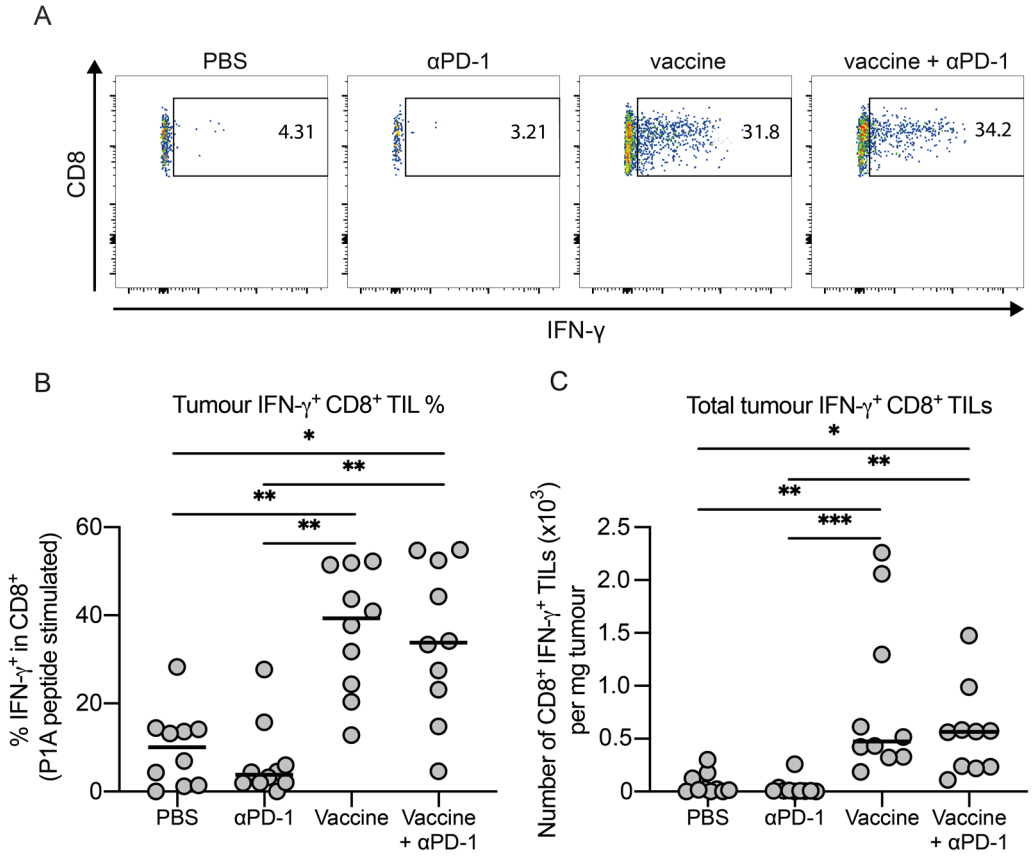


Figure 4.26. IFN-γ production by CD8+ TILs in 15V4T3 tumours from mice treated with ChAdOx1-li-P1A/MVA-tPA-P1A and anti-PD-1 blockade. DBA/2 mice were implanted with $1x10^6$ 15V4T3 cells via s.c. injection to initiate tumour growth. 8 days after tumour implantation, mice were vaccinated and treated with immune checkpoint inhibitors according to the schedules described in Figure 4.21. Mice were sacrificed on day 20 post implantation, tumours excised and disaggregated, and the T-cell immune infiltrate profiled by flow cytometry (gating as described in Figure 2.2). To detect IFN-γ production by CD8+ TILs, tumour cell suspension was stimulated ex vivo for 5 hours with overlapping P1A peptides (with brefeldin A added after 1 hour), combined with ICS. Representative gating of IFN-γ+ CD8+ TILs from each group (A). The proportion of IFN-γ+ CD8+ TILs (B) and the absolute number of IFN-γ+ CD8+ TILs per mg of tumour tissue (C) are shown. Each symbol represents an individual mouse, with 10 mice per group. Representative of 2 independent experiments. Statistically significant differences between groups were determined by a Kruskal-Wallis test with Dunn's multiple comparisons test. *, $p \leq 0.05$, **, $p \leq 0.01$, ***, $p \leq 0.001$

The phenotype of CD8+ TILs in each group was also assessed. The surface markers CD62L and CD44 can be used to identify and discriminate naïve T-cells, from antigen-experienced central memory (T_{CM}) and effector/effector memory T-cells (T_{EM}). The vast majority of CD8+ T-cells in the tumours of all mice were of the T_{EM} phenotype, which shows a marked change compared to those found in the spleen and blood which are predominantly either naïve or T_{CM} (Figure 4.27). This indicates that the CD8+ T-cells in the tumour are activated antigen-experienced cells. There was no significant difference however between the distribution of CD8+ T_{EM} and CD8+ T_{CM} in the tumour between any of the different treatment groups.

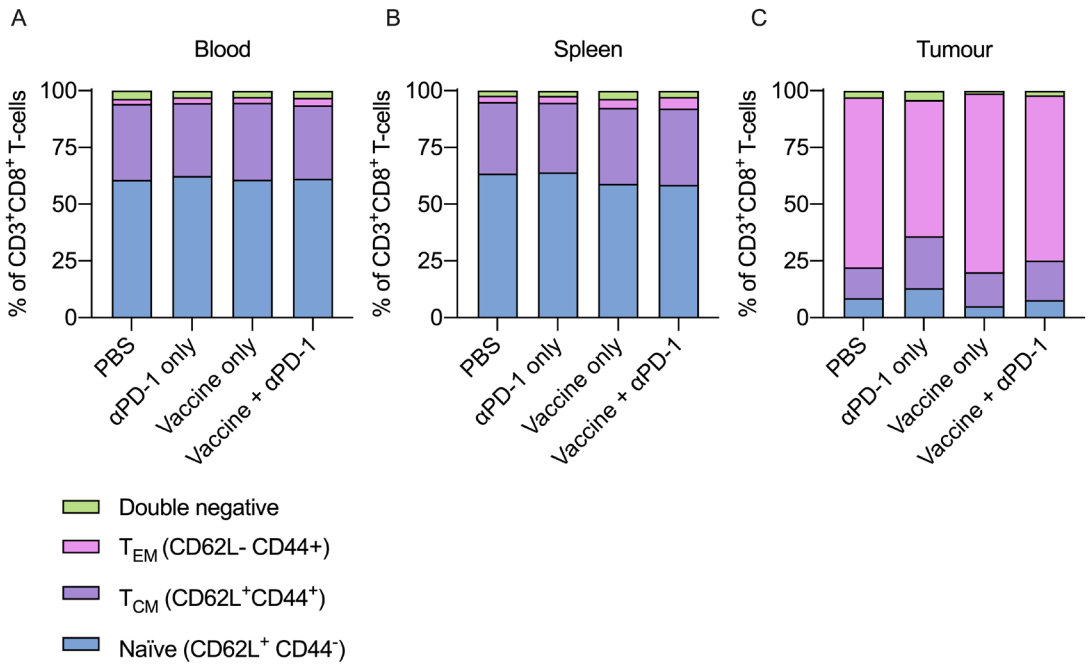


Figure 4.27. Central/effector memory phenotype of CD8+ T-cells in 15V4T3 tumour bearing mice. CD62L and CD44 expression on CD8+ T-cells in the blood (A), spleen (B) and tumour (C) of 15V4T3 bearing mice following treatment with ChAdOx1-Ii-P1A/MVA-tPA-P1A vaccination, with or without αPD-1 was analysed by flow cytometry to determine the proportions of naïve ($CD62L+CD44^-$), central memory (CD62L+CD44+) and effector/effector memory ($CD62L^-CD44+$) subsets (gating as described in Figure 2.3). Data are shown as the mean proportion of each cell subset of total CD8+ T-cells, representative of 2 independent experiments.

Furthermore, PD-1 expression on TILs was also assessed. The majority of CD8+ T-cells of any specificity in the tumour were PD-1+ (Figure 4.28 A). This is in contrast to the spleen and blood where the majority of CD8+ T-cells were found not to express PD-1. The expression of PD-1 is known to be upregulated on activated T-cells after antigen-exposure [90]. In both the spleen and tumour, the majority of the $P1A_{35-43}$ tetramer+ P1A-specific CD8+ T-cells expressed PD-1. However, the level of PD-1 expression on the surface of CD8+ T-cells in the tumour was far higher than those in the spleen or blood (Figure 4.28 B). Increased PD-1 expression on CD8+ TILs compared to peripheral T-cells is suggestive of increased activation status in response to antigen at an effector site, and likely renders these T-cells more susceptible to PD-L1 mediated suppression.

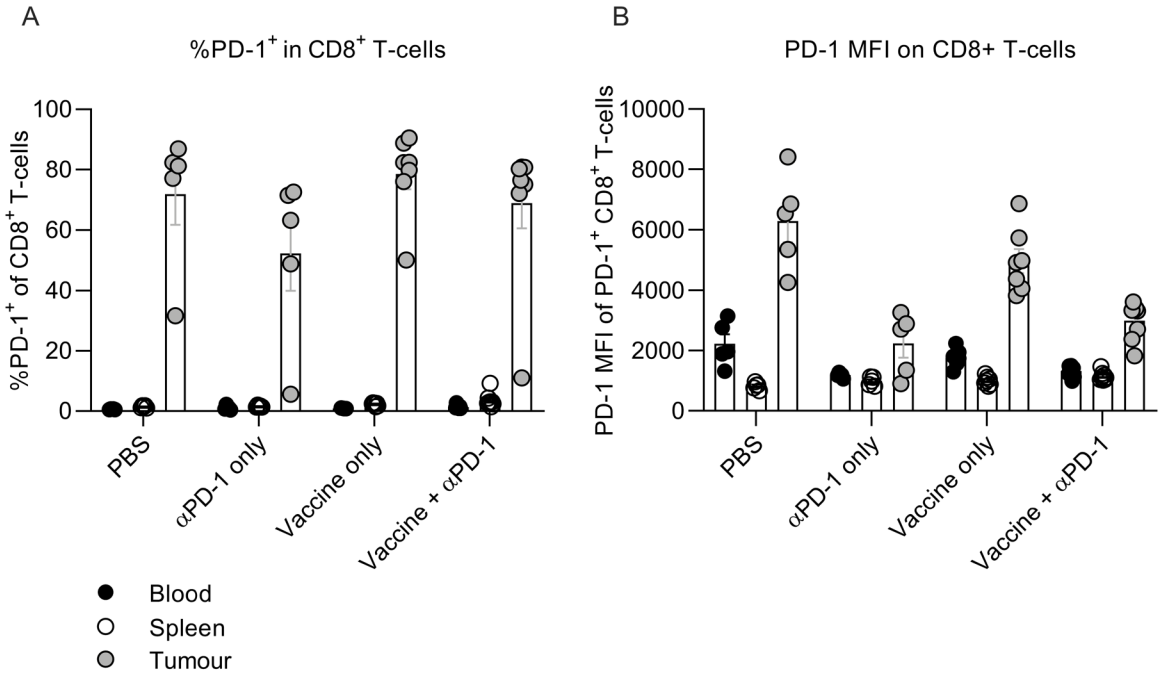


Figure 4.28. PD-1 expression on CD8+ T-cells in 15V4T3 tumour-bearing mice. PD-1 expression on CD8+ T-cells from 15V4T3 bearing DBA/2 mice following treatment with ChAdOx1-Ii-P1A/MVA-tPA-P1A vaccination, with or without αPD-1 was analysed by flow cytometry (gating as described in Figure 2.3). The percentage of PD-1+ CD8+ T-cells from total CD8+ T-cells in the blood, spleen and tumour was determined (A). The MFI of PD-1 on PD-1+ CD8+ T-cells was also calculated to determine relative levels of surface expression (B). (B). Data are shown as mean ± SEM, with each symbol representing an individual mouse, representative of 2 independent experiments.

4.2.13 Therapeutic ChAdOx1/MVA P1A vaccination promotes an increased inflammatory tumour microenvironment

T-cell trafficking to tumours is crucial for effective T-cell mediated tumour elimination to take place, however it is often impaired in many cancers. T-cell migration to inflammatory sites is governed by chemokines, in particular the CXCR3:CXCL9/CXCL10 axis, whereby activated effector T-cells expressing the cell surface receptor CXCR3 migrate to areas of inflammation where the chemokines CXCL9 and CXCL10 are produced [115]. CCL5 is another important cytokine in controlling T-cell migration [254]. To further characterise the inflammatory nature of the tumour microenvironment following ChAdOx1/MVA P1A vaccination, the production of cytokines that function as T-cell migratory

signals and effector molecules in the tumour was investigated by rt-qPCR (Figure 4.29).

Concurrent with the observed increase in T-cell numbers, a strong up-regulation in mRNA levels of T-cell chemoattractant cytokines was observed in the tumours of vaccinated mice. In the tumours of both vaccine and vaccine + anti-PD-1 treated groups, there was a significantly higher CXCL9 mRNA expression compared to tumours from both the PBS and anti-PD-1 only groups (Figure 4.29 A). In the vaccine + anti-PD-1 treated mice there was a significant upregulation of CXCL10 in tumours compared to the PBS and anti-PD-1 only groups, but not however in the vaccine only group (Figure 4.29 B). Tumour CCL5 expression was also significantly upregulated in the vaccine + anti-PD-1 treated group compared to the PBS control, anti-PD-1 only and vaccine only groups (Figure 4.29 C). This suggests that the vaccination, and in particular vaccine combined with anti-PD-1, or downstream events resulting from treatment, generates pro-inflammatory conditions in the tumour that result in increased T-cell migration.

The intra-tumoural expression at the mRNA level of T-cell effector molecules IFN-γ and granzyme B was also investigated. The expression of IFN-γ was significantly upregulated in the tumours of both vaccinated groups compared to the PBS control and anti-PD-1 only groups (Figure 4.29 D). The expression level of IFN-γ mRNA was significantly higher still in the vaccine + anti-PD-1 group compared to the vaccine only group. Unexpectedly however, granzyme B expression did not significantly differ between any of the groups (Figure 4.29 E). The expression of

PD-L1 mRNA in each of the tumours was also assessed. Concurrent with previous findings shown in this chapter about PD-L1 expression by 15V4T3 cells, and in line with the observed higher expression of IFN-γ in the tumours of vaccine + anti-PD-1 treated mice, PD-L1 mRNA expression was also significantly higher in the tumours of vaccine + anti-PD-1 treated mice compared to unvaccinated, anti-PD-1 alone and vaccine only treated mice (Figure 4.29 F).

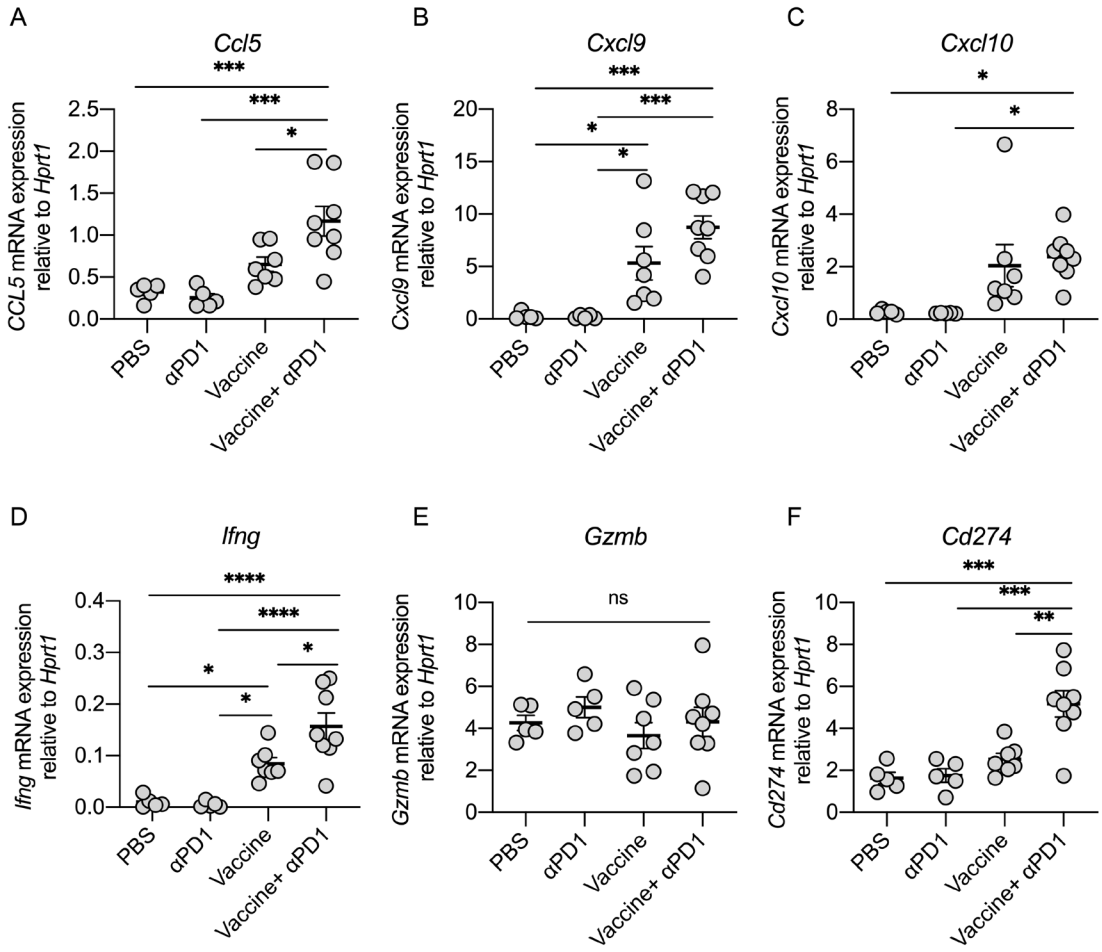


Figure 4.29. Expression or pro- and anti-inflammatory mediators in the 15V4T3 tumour microenvironment. 15V4T3 tumour-bearing DBA/2 mice received ChAdOx1-li-P1A/MVA-tPA-P1A or PBS sham vaccinations ± anti-PD-1 according to the schedules described in Figure 4.21. Mice were sacrificed on day 21 post implantation, tumours excised and mRNA extracted to analyse gene-expression at the transcriptional level of pro/anti inflammatory mediators. Expression of CCL5 (A), CXCL9 (B), CXCL10 (C), IFN-γ (D), Granzyme B (E) and PD-L1 (F) mRNA in the tumour was quantified by rt-qPCR. Target gene mRNA expression level was normalized relative to Hprt1 and is shown as $2^{-\Delta Ct}$. Data are presented as mean ± SEM and each symbol represents an individual mouse. Statistically significant differences between groups were determined by a one-way ANOVA followed by Tukey's post hoc test. *, $p \leq 0.05$, **, $p \leq 0.01$, *** $p \leq 0.001$ ****, $p \leq 0.0001$.

4.3 Discussion

The aim of this chapter was to evaluate in mice the immunogenicity of ChAdOx1/MVA prime-boost vaccination encoding the murine MAGE-type antigen, P1A, and the anti-tumour therapeutic efficacy of this vaccine using P1A-expressing syngeneic tumour models. Initially, the immunogenicity of this vaccination regime was evaluated in DBA/2 mice, in which an immunogenic H-2L^{d} restricted P1A CTL epitope has been defined – P1A$_{35-43}$. The results presented here demonstrate that a vaccination regime based on ChAdOx1 and MVA viral vectors encoding the murine MAGE-type antigen P1A has excellent immunogenicity and can induce very strong P1A-specific CD8+ T-cell responses. A single prime vaccination with ChAdOx1 encoding P1A was found to generate CD8+ T-cells producing all three of the type I cytokines IFN-γ, TNF-α and IL-2, and the magnitude and multifunctionality of the response was greatly increased by giving a boost vaccination with an MVA vector encoding P1A. The ability to prime the response with ChAdOx1 and then boost with MVA to generate high frequencies of antigen-specific CTLs mimics that seen with a wide range of different antigens.

Self-antigens such as those of the MAGE-type are weakly immunogenic relative to foreign antigens, and more challenging to induce CTL responses against with a vaccine. P1A is the best known murine equivalent of the human MAGE-type antigens, of which most do not have direct homologues in mouse, and is therefore an ideal target with which to evaluate the ability of a vaccine platform to induce MAGE-specific CTL responses. The high magnitude CTL responses against P1A

generated by ChAdOx1/MVA P1A vaccination observed here therefore demonstrate for the first time the suitability of the platform for inducing CD8+ T-cell responses against antigens from the MAGE-type family. Encouragingly the percentages of IFN-γ producing CD8+ T-cells detected was comparable to those elicited by ChAdOx1/MVA vaccines encoding infectious disease antigens [142], although technical variations in ICS methods used to assess vaccine-induced T-cell responses in other studies evaluating P1A-targeting vaccines precludes direct comparison with these studies.

P1A-specific CD4+ T-cell responses however were not detected following vaccination. This is perhaps not unsurprising, as no MHC-class II restricted CD4+ T-cell epitope has yet been described in mice of a DBA/2 genetic background. This may be due to either mechanisms of tolerance, where P1A-reactive CD4+ T-cells are deleted from the T-cell repertoire during T-cell development, or due to a lack of peptides encoded within the P1A sequence that are capable of binding to MHC-class II alleles. It is classically considered that antigen-specific CD4+ T_H cells are required to provide help to promote differentiation of naïve CD8+ T-cells into CTL effectors during T-cell activation, through the 'licensing' of DCs. This is mediated through the interaction of CD40L on T_H cells with CD40 receptor on DCs, which increases expression of costimulatory ligands and MHC molecules by DCs, thus enhancing their antigen-presentation capabilities and ability to prime CTLs [77, 255]. However, many recent studies have shown that CD4+ T_H may be dispensable for the maturation of CTLs and induction of effective CD8+ T-cell mediated immunity, as CD8+ T-cells can promote their own priming in a semi-

autocrine manner through their own CD40L expression [256-258]. This can explain the induction of high magnitude P1A-specific CD8+ T-cell responses here in the absence of a detectable CD4+ T-cell response.

A further aim was to again assess the use of molecular adjuvant sequences incorporated into the ChAdOx1 and MVA viral vectors, this time for enhancing the P1A-specific CD8+ T-cell response induced by vaccination. Here it was found that the incorporation of the murine invariant chain sequence via fusion to the N-terminus of P1A in the ChAdOx1 vector provided a significant increase to the level of the CD8+ T-cell response generated by ChAdOx1 vaccination, and this trend tended to maintain after MVA boost vaccination. The effects of tethering the invariant chain to the encoded antigen in ChAdOx1 were more apparent in the context of vaccinating against P1A than vaccinating against the human MAGE-type antigens, as detailed in the studies presented in chapter 3. That may be due to its relatively lower natural immunogenicity as a self-antigen compared to foreign antigens (which MAGE-A3 and NY-ESO-1 are to the mouse), and therefore strategies that enhance the level of specific CD8+ T-cell response may be more apparent in this setting. The beneficial effect on vaccine induced CD8+ T-cell responses of linking the Ii TMD sequence to the encoded antigen in adenoviral vectors has recently become quite established, having been demonstrated with several other antigens [214, 215, 217]. Similar findings here further confirm those made by others, and validates this as a strategy for enhancing CD8+ T-cell responses against MAGE-type antigens induced by ChAdOx1/MVA vaccination. Conversely however, beneficial effects of incorporating tPA into the MVA vector

via fusion to the N-terminus of the antigen were again not apparent, and no particular benefit was observed from the metrics measured here - magnitude of the CD8+ T-cell response or T-cell polyfunctionality. Alternatively, no downside was found, and there could be other potential benefits from the use of tPA that have not been identified here.

Having demonstrated that ChAdOx1/MVA P1A vaccination could induce high magnitude P1A-specific CD8+ T-cell responses, a central aim was to assess the anti-tumour activity of this vaccine strategy in murine tumour models, and whether the induced responses could mediate protection against growth of P1A-expressing tumours. In the prophylactic setting, ChAdOx1/MVA P1A vaccination was found to confer excellent protection against growth of two P1A-expressing syngeneic murine cancer lines, P815 and 15V4T3, where tumour growth was significantly delayed and survival significantly increased. ChAdOx1/MVA P1A vaccination performed as well as vaccination with L1210.P1A.B7-1, an autologous tumour-cell based vaccine which is known to generate very strong anti-P1A CD8+ T-cell immunity [172]. Although not how such a vaccination would be deployed in the clinic, these results are encouraging and confirm that the P1A-specific CD8+ T-cell responses induced by ChAdOx1/MVA vaccination have functional anti-tumour activity, and are capable of mediating tumour control.

In both models, many mice were protected for a period of time compared to control mice, before a relapse in tumour growth occurred. Gene expression analysis of outgrown tumours found this was due to near total loss of P1A

expression by the tumours from vaccinated mice in the P815 model. Loss of P1A expression in outgrowing P815 tumours strongly suggests that this event mediates immune escape of the tumours, as P1A-specific CTLs induced by vaccination would no longer be able to recognize tumour cells. On one hand, this demonstrates the efficacy of the vaccination, in that the vaccine induced CD8+ T-cell response is sufficiently strong to able to eliminate all P1A-expressing cancer cells, and that tumours are driven to the point of antigen loss before growing out again. However, antigen-loss mediated immune escape is a challenge that may need to be overcome by antigen-specific immunotherapeutic approaches for cancer. In practice this may be mitigated by the phenomenon of epitope spreading, whereby a CTL response generated against a single tumour-antigen mediates the destruction of cancer cells, releasing further immunogenic tumour antigens against which anti-tumour CTL responses can be mounted. Indeed it has shown before that the rejection of P1A-expressing P815 tumours by DBA/2 mice can lead to the generation of CTL responses against P1E, an alternative tumour-antigen expressed by P815, and that these mice are protected against subsequent challenge with tumours that express P1E, but not P1A [259]. This antigen-loss phenomenon was not observed in the 15V4T3 model however, where other mechanisms could perhaps underpin this immune-resistance. Other prior studies have shown that different P1A-expressing tumour models utilize different mechanisms of immune escape from P1A-specific T-cell responses [260]. In agreement with results obtained here, Bai and colleagues observed total loss of P1A expression in P815 tumours that recurred after therapy using adoptively

transferred $P1A_{35-43}$-specific CTLs [260]. However, MethA tumours, which also express P1A, were found to have intact P1A expression when recurring after adoptive transfer, and immune escape was found to be mediated by the ability of MethA tumours to induce apoptosis of TILs. This demonstrates the heterogeneity between different tumour types, and that different immune-evasion mechanisms are likely to be active in different tumours. Many tumours for example have been demonstrated to acquire resistance to adoptive T-cell therapy through loss of expression of surface MHC-class I molecules altogether, rendering them unable to be recognized by anti-tumour CTLs [111, 261]. Typically this is achieved by deletion of the gene encoding the β2-microglobulin subunit of the MHC-class I complex, which enables its surface localization. In such cases, immunotherapeutic approaches focused on enhancing NK-cell mediated immunity might be effective co-strategies alongside T-cell based therapies. Increased tumour T_{reg} recruitment in response to local inflammation induced by therapy can also underlie resistance. Further work should look to understand the mechanisms of immune escape most active in the 15V4T3 tumour model, to further enhance its use for studying novel combinatorial immunotherapy approaches. This could be achieved by comparing tumour immune infiltrate and gene expression patterns in tumours from control mice with relapsed tumours from treated mice, through methods such as flow cytometry and RNA-sequencing.

A further key aim of the study was to assess the therapeutic efficacy of ChAdOx1/MVA P1A vaccination and therefore to assess the potential of this approach for treating established tumours. ChAdOx1/MVA P1A vaccination was

found to have good therapeutic efficacy against established 15V4T3 tumours when vaccination was initiated at relatively early time points post tumour implantation. Compared to control groups, ChAdOx1/MVA P1A vaccination delayed tumour growth, improved mouse survival and in some mice complete tumour resolution was observed. Furthermore, the extent of tumour control was found to correlate very strongly with the magnitude of P1A-specific CD8+ T-cells in the blood producing IFN-γ. This indicates that the observed therapeutic efficacy was driven by the antigen-specific CD8+ T-cell response induced by vaccination, and could be confirmed in future by CD8+ T-cell depletion experiments. A vaccination regime consisting of weekly alternating vaccinations between ChAdOx1-Ii-P1A and MVA-P1A given a log-fold reduced dose was found to be particularly effective in the therapeutic setting. This is a deviation from the classical setting of ChAdOx1/MVA vaccination using higher virus doses and a longer interval between the prime and the boost, that was used to assess immunogenicity of the P1A encoding vectors. However, this agrees with the findings of Cappuccini et al, who also found a weekly alternating vaccinations with ChAdOx1/MVA encoding STEAP1 to provide superior control of STEAP1 expressing tumours [155]. The exact reason for the superiority of this regime scheme is unclear. Cappuccini et al postulated that in the therapeutic setting against tumours, weekly vaccination might be more effective by stimulating more frequent fresh supplies of effector CTLs, as effector CD8+ T-cells are likely to become exhausted or suppressed after arrival at the tumour site. The reason for

this warrants further investigation, as it may have implications for informing about the best vaccine schedules to use in cancer patients.

Another aim here was to investigate the combination of ChAdOx1/MVA P1A with different CPIs, to evaluate if the overall therapeutic efficacy of vaccination could be enhanced. By targeting immunosuppression in the TME, CPIs might improve the effect of vaccination by preventing the inhibition of the effector function of vaccine induced CD8+ T-cells. Indeed given that here it was observed that in many mice regrowth of tumours followed an initial vaccination induced tumour regression or clearance, it was postulated that P1A-specific CD8+ T-cells may indeed be being suppressed in the 15V4T3 TME. Combining vaccination with either PD-1 or CTLA-4 blocking antibodies significantly improved the therapeutic efficacy of ChAdOx1/MVA P1A vaccination against established 15V4T3 tumours, with by far the strongest effect coming from the combination of vaccination with anti-PD-1. Mice treated with ChAdOx1/MVA P1A and anti-PD-1 were able to better resolve tumours than mice receiving vaccination alone and had much improved survival. The particularly strong synergy with anti-PD-1 may be explained by the finding from in vitro study that 15V4T3 expresses PD-L1, which is further upregulated by IFN-γ stimulation. Studies in murine tumour models have shown mechanistically that PD-L1 expression by tumours alone is sufficient to exert a strong immunosuppressive role on tumour-antigen-specific TILs [91]. Indeed, in these combination experiments, vaccination was initiated at later time-points post tumour implantation, when tumours were slightly more established, and it was found that delaying the start of vaccination by even a short time was

enough to see an almost total loss of therapeutic efficacy from vaccination. It was observed that the ability of vaccination to regress larger tumours therefore required combination with anti-PD-1. These results confirm the notion that therapeutic ChAdOx1/MVA vaccination may require combination with anti-PD-1 for significant efficacy, and support similar findings made by a range of other pre-clinical studies [156, 262, 263]. A recent study evaluating therapeutic efficacy of great ape adenovirus (GAd) / MVA prime-boost vaccines encoding neoantigens in the CT26 and MC38 murine tumour models have also reported that the clearance of high tumour burden is dependent on combination with anti-PD-1 [264].

Interestingly, in the studies performed here there was also very little therapeutic effect from treatment with either anti-PD-1 or anti-CTLA-4 alone against 15V4T3 tumours. 15V4T3 tumours appear to be largely refractory to both anti-PD-1 and anti-CTLA-4. This mirrors a situation in the clinic, where PD-1 and CTLA-4 blocking antibodies as a monotherapy are an effective treatment in some cancers, but the positive effect on regressing tumours and increasing survival tends to be limited to a minority of patients. 15V4T3 would therefore appear to be a good model of tumours that are unresponsive to immune checkpoint blockade and for evaluating combinations with other agents such as vaccines for increasing CPI efficacy. The synergy observed between vaccine and anti-PD-1 treatment in this model, and that the therapeutic efficacy of the combination was stronger than either used alone therefore underlines complementarity of the two approaches. Overall this data lends further support to the idea of an effective therapeutic

vaccination as a strategy for sensitizing the tumour to CPIs and for increasing the proportion of individuals responding to CPIs. The promising results presented here with the 15V4T3 model suggest that a combination of a ChAdOx1/MVA vaccination targeting MAGE-type antigens with anti-PD-1 could be an effective means of regressing MAGE-expressing tumours.

Pivotal studies have shown that it is CD8+ T-cell mediated inflammation through the secretion of IFN-γ upon antigen-recognition in the TME that drives the upregulation of adaptive immune resistance mechanisms such as PD-L1 and IDO by tumours, rather than being tumour intrinsic [106]. This is due to the fact that expression of PD-L1 and IDO is IFN-γ inducible. Furthermore, gene expression studies have shown that the presence of CD8+ tumour-specific TILs and a T-cell inflamed IFN-γ related mRNA profile in tumours is necessary for and predicts effective clinical responses to anti-PD-1 [93, 105]. Indeed, that many patients have immunologically cold tumours lacking CD8+ T-cell infiltrate driven inflammation is believed to be the central reason for the lack of efficacy of checkpoint inhibitors in many cases. Why many tumours lack CD8+ TILs is still unclear. However, given that is has been shown that tumours lacking a T-cell inflamed mRNA profile frequently express at least as many immunogenic tumour antigens as T-cell inflamed counterparts [112], it is likely due to a failure either of priming, or T-cell recruitment. A central aim of using a therapeutic cancer vaccine therefore, either alone in combination with immune checkpoint blockade, is to generate a source of antigen-specific CD8+ T-cells that migrate into the tumour site. In this way, an immunologically 'cold' tumour lacking a sizeable T-cell infiltrate, could be turned

'hot'. On this basis the effect of ChAdOx1/MVA P1A vaccination alone and in combination with anti-PD-1 on the 15V4T3 TME was therefore explored here.

The data presented here clearly show that ChAdOx1/MVA P1A vaccination enhanced CD8+ T-cell mediated inflammation in the tumour. Therapeutic ChAdOx1/MVA P1A vaccination, either alone or in combination with anti-PD-1 was found to greatly increase both total CD8+ T-cell and P1A-specific CD8+ T-cell infiltration into 15V4T3 tumours. CD8+ T-cells in the tumours of vaccinated mice were also found to be functional, and produced IFN-γ upon antigen re-stimulation. Conversely 15V4T3 tumours from unvaccinated mice seemed to be poorly infiltrated, with very few detectable IFN-γ secreting CD8+ T-cells. Collectively, these results show that ChAdOx1/MVA vaccine induced CD8+ T-cells can effectively migrate into the tumour, and have effector function at the tumour site. In keeping with the observation that anti-PD-1 alone had no effect on growth of 15V4T3 tumours, anti-PD-1 alone also had no effect on CD8+ T-cell infiltration into the tumours. This observation is in contrast to anti-PD-1 responsive models such as P815, which may be more naturally inflamed, where studies have shown that anti-PD-1 treatment alone has significant therapeutic efficacy and induces CD8+ T-cell infiltration (or proliferation) in the tumour [265].

Furthermore, in line with the observed increase in IFN-γ-secreting P1A-specific CD8+ T-cells in 15V4T3 tumours from vaccinated mice, gene expression analysis by rt-qPCR demonstrated that these tumours also had higher levels of IFN-γ mRNA expression than tumours from either untreated, or anti-PD-1 monotherapy

treated mice. In agreement with the literature, some tumours from vaccinated mice with higher IFN-γ-producing CD8+ T-cell infiltrate, mostly those receiving vaccine in combination with anti-PD-1, had correspondingly higher levels of PD-L1 mRNA. The source of the increased expression of PD-L1 in these tumours is likely in part from tumour cells, as in vitro studies showed that 15V4T3 upregulates PD-L1 following IFN-γ stimulation. Interestingly, levels of granzyme B mRNA transcripts were not found to be any higher in the tumours of vaccinated mice compared to unvaccinated. However, this could very likely be because granzyme B enzymes along with perforin are stored in the cytoplasm of CTLs in pre-formed granules, which are released upon cell-cell engagement of activated effector CTLs with their targets [69]. Granzyme B expression at the mRNA level therefore does not necessarily have to be upregulated for CTL mediated cell lysis to take place. Taken together, these observations suggest that ChAdOx1/MVA P1A vaccination promotes CD8+ T-cell inflamed TME, and indicates that tumours from vaccinated mice bear a IFN-γ related gene-expression signature. RNA-sequencing could confirm this with a wider range of targets and also further delineate the effect of each treatment on the TME. Increased CD8+ T-cell driven inflammation at the tumour site induced by ChAdOx1/MVA vaccination strongly suggests why vaccinated mice are more responsive to anti-PD-1, and the synergy of the two treatments. Conversely, lack of significant CD8+ T-cell driven inflammation and resulting acquired adaptive immune resistance likely explains the unresponsiveness of 15V4T3 tumours from unvaccinated mice to PD-1 blockade. 15V4T3 may therefore be similar to models such as B16F10, which are

known to unresponsive to anti-PD-1, and be poorly infiltrated by CD8+ T-cells. As demonstrated here, this makes 15V4T3 model an appealing one in which to test combination therapies which seek to improve on the efficacy of CPI monotherapy.

Further supporting the observation that ChAdOx1/MVA can promote a T-cell inflamed TME, ChAdOx1/MVA P1A vaccination was observed to generate conditions in the tumour favourable for T-cell recruitment. CCL5, CXCL9, CXCL10 mRNA expression were all found to be particularly increased in tumours from mice treated with a combination of vaccine and anti-PD-1. Several studies have shown CCL5, CXCL9 and CXCL10 expression are key cytokines mediating T-cell infiltration into tumours, including those looking at melanoma biopsies showing that their presence correlates with a T-cell inflamed TME profile [115]. Furthermore, it has been shown recently that expression of CXCR3 on tumour-specific T-cells, the receptor for these chemokines, is necessary for their effective trafficking into tumours [116]. The observed increase in CXCL9/CXCL10 expression in tumours from vaccinated mice likely underlies the enhanced CD8+ infiltration also observed in these tumours.

The chemokines CXCL9 and CXCL10 are IFN-γ inducible and studies have shown that they are predominantly produced by CD8α+CD103+ cDC1s in the TME. In this way, these are the key cells that orchestrate CD8+ T-cell infiltration into the tumour and generation of the inflamed TME, and it has been shown that tumour T-cell engraftment does not occur in their absence [117]. Studies have also shown that CD8α+CD103+ cDC1 abundance within tumours is associated with immune-

mediated tumour rejection and their presence in the TME is necessary for response to immune checkpoint blockade. According to this literature, the increase in tumour CXCL9/CXCL10 expression in tumours from vaccinated mice is likely CD8α+CD103+ cDC1 mediated and suggests that therapeutic ChAdOx1/MVA P1A vaccination, or downstream events, may increase either CD8α+CD103+ cDC1s number or activation in the tumour. Supportive of this NK-cell derived CCL5 along with Xcl1 was recently shown to be a predominant chemokine underlying recruitment of CD8α+CD103+ cDC1s to tumours and here higher CCL5 expression was detected in tumours from vaccine + anti-PD-1 treated mice [84]. Overall this suggests NK cells and cDC1s may play a role in the therapeutic anti-tumour response to ChAdOx1/MVA P1A vaccination + anti-PD-1 in the 15V4T3 model and warrants further investigation.

Furthermore, Dangaj et al recently deciphered a step-wise model describing the cellular interplay underlying the generation of a "hot" T-cell inflamed TME using a combination of murine ovarian murine tumour models, ovarian-cancer patient tumour samples, and expression data from the TCGA [119]. They demonstrated that initial T-cell accumulation in tumours is driven by tumour-derived CCL5 expression. Recognition of cognate tumour antigen by infiltrating CD8+ T-cells promotes IFN-γ secretion, which in turn upregulates CXCL9 and CXCL10 expression by tumour CD103+ cDC1s. In turn, CXCL9 acts to further drive the recruitment of CXCR3 receptor bearing T-cells into the tumour in a positive feedback loop. A CCL5+CXCL9+ gene expression signature was found to be associated with response to anti-PD-1 in melanoma. Similarly, Chow et al

demonstrated using murine tumour models that CXCL9-CXCR3 signalling in tumours is actually required for the efficacy of anti-PD-1 blockade. They showed CXCL9 secreted by CD103+ cDC1s mediates cross-talk between the DCs and CXCR3+ tumour-specific CD8+ TILs in the TME, enabling their enhanced priming in the context of anti-PD-1 treatment. Lack of CXCL9 or CXCR3 abrogated anti-PD-1 efficacy and CXCL9 proved a useful biomarker for determining response in melanoma patients [118].

Results obtained from gene expression analysis of tumours from ChAdOx1/MVA P1A vaccinated mice are in full agreement with such a model of tumour T-cell infiltration regulation described by these recent studies. Hypothetically, the initial trafficking of vaccine induced P1A-specific CD8+ T-cells to the TME and killing of cancer cells might release inflammatory signals which recruit NK cells and cDC1s. In turn, IFN-γ produced by either CD8+ T-cells or NK cells activates cDC1s to secrete CXCL9/CXCL10, and recruit more P1A-specific CD8+ T-cells, enhancing and maintaining inflammation. Given the recently established role of cDC1s and the CXCL9/CXCR3 signalling axis in mediating effective responses to anti-PD-1, their enhancement in the tumour by the ChAdOx1/MVA induced CD8+ T-cell response might further explain how vaccination sensitizes normally unresponsive 15V4T3 tumours to anti-PD-1 blockade and the synergy between the two modalities. As an aside, although CXCR3 expression was not observed on CD8+ T-cells in 15V4T3 tumours, this may be due to the fact that CXCR3 undergoes ligand-induced downregulation upon binding. Chow et al. and other have showed that CXCR3 expression is rapidly lost on infiltrating CD8+ T-cells, and

therefore 15V4T3 tumours may have been harvested after the peak of expression [118, 266, 267]. Given the importance of CXCR3 expression for response to anti-PD-1, this has implications for timing of when anti-PD-1 should be given in relation to vaccination. Ideally, anti-PD-1 should be given early after vaccination during the initial effector phase and recruitment of CD8+ T-cells to the tumour.

Overall, such a detailed analysis of the effect of ChAdOx1/MVA vaccination against a MAGE-type antigen on the immune profile of the TME has been little explored. These results strongly suggest ChAdOx1/MVA is an efficient means for generating a CD8+ T-cell-inflamed TME, by promoting increased infiltration of functional tumour-antigen-specific CD8+ T-cells. An increase in P1A-specific T-cell infiltrate and activation of T-cell recruitment gene expression patterns induced by ChAdOx1/MVA vaccination could explain the increased responsiveness of 15V4T3 tumours to anti-PD-1 treatment, and explain the synergy between the two. The strong therapeutic efficacy from ChAdOx1/MVA vaccination combined with anti-PD-1 underlines complementarity of the two therapies strongly suggests that ChAdOx1/MVA encoding MAGE-type antigens combined with PD-1 blockade has strong potential for translation to the clinic.

A question raised here, is why, in a genetically identical cohort of mice, there is such a variation in responses generated by vaccination – i.e. why some individuals would generate very high antigen-specific CD8+ T-cell responses, whilst in others the response was comparatively small. It may be that in some individuals, the CD8+ T-cell response is directed proportionally more against other antigens in the

viral vaccine platform, rather than against the transgene product. Strategies to enhance the response directed against the transgene rather than other viral components may therefore represent a route to enhanced efficacy. Further elucidation of the determinants underlying this discrepancy in the efficacy of vaccine priming would have direct translational relevance to humans, in that it would better inform strategies to increase vaccine immunogenicity to ensure high responses are mounted in a wider range of patients. It is also not fully understood how anti-PD-1 acts on anti-tumour CD8+ TILs. For example does it have any direct effect or bearing on their phenotype. Improved knowledge of this would enable more rational timing of combination vaccine and anti-PD-1 therapy. Such questions could be addressed through single-cell RNA-seq studies. An additional question is how tumours acquire secondary adaptive resistance to combined therapy. Given that some tumours grow out again after initial regression, ChAdOx1/MVA P1A vaccination in 15V4T3 could be used to explore strategies to combat this.

Chapter 5. Investigating P1A-specific T-cell responses in the C57BL/6 mouse strain

5.1 Introduction

The P1A tumour antigen is the best known murine equivalent of the human-MAGE-type antigens [238, 244]. P1A-specific CD8+ T-cell responses can be monitored and studied in murine tumour models and this has been vital in expanding knowledge of how the immune system can reject tumours and for evaluating the potential of novel immunotherapeutic agents [172, 240, 242]. However, to date P1A-specific immune responses have only been studied in mice bearing the H-2L^d MHC-class I allele such as DBA/2 and BALB/c, where an H-2L^d-restricted immunogenic epitope, P1A$_{35-43}$, is known to be presented to CD8+ T-cells [238]. P1A-specific CD8+ T-cell responses have not been studied in mice of the H-2^b genetic background such as the C57BL/6 strain before. Given that C57BL/6 is one of the most commonly used strains in biological research, the majority of transgenic mouse models and many commonly used murine tumour models exist on this genetic background. Identifying new P1A-specific CTL epitopes in the C57BL/6 strain would open up additional avenues to explore P1A-specific T-cell responses in new settings, and allow more in depth mechanistic study of the nature of immune responses against MAGE-type antigens. In this chapter therefore, heterologous ChAdOx1/MVA P1A prime-boost vaccinations were further evaluated in C57BL/6 mice, and used as a means to characterise P1A-specific T-cells responses in the C57BL/6 genetic background.

Furthermore, in this chapter an additional strategy to increase the efficacy of ChAdOx1/MVA P1A vaccination was explored. A potential barrier to efficacy for a MAGE-targeting cancer vaccine is that expression of MAGE-type antigens is

characterized by both inter-tumour and intra-tumour heterogeneity. For example, in epithelial ovarian cancer (EOC) NY-ESO-1 is expressed variably. It has been shown that tumour expression of NY-ESO-1 can be detected in just under half of EOC patients [268]. Furthermore, there is often also intratumor heterogeneity, with the proportion of tumour cells expressing NY-ESO-1 also variable. In the context of therapeutic cancer vaccination targeting MAGE-type antigens such as MAGE-A3 and NY-ESO-1 this heterogeneity could limit efficacy on two fronts. In the first instance, lack of tumour antigen expression precludes the use of a therapeutic vaccination targeting that antigen. Secondly, low proportions of tumour cells expressing the target antigen may potentially limit the potency of the vaccine induced anti-tumour CD8+ T-cell response or allow immune evasion through expansion of antigen-loss tumour-cell variants.

This heterogeneity is explained by the biological mechanisms underpinning control of CG gene expression. It has been known for some time that CG gene expression is primarily regulated by epigenetic mechanisms via DNA methylation at CpG islands in the gene promoter region [166-168, 269, 270]. In most healthy tissues, promoter methylation represses CG gene expression. In tumours progressively aberrant DNA methylation develops as the cancer evolves and leads to the spontaneous re-expression of cancer-germline genes by cancer cells [168]. Studies of the clonality of MAGE-A3 expression in melanoma have demonstrated that intra-tumour heterogeneity of expression is linked to MAGE-A3 promoter methylation status [270]. Furthermore, one study analysing resected EOC tumours by combining IHC staining for NY-ESO-1 expression, microdissection techniques

and DNA methylation analysis has shown that the inter-tumour and intra-tumour heterogeneity of NY-ESO-1 expression is directly associated with the methylation status at the NY-ESO-1 promoter [271].

Based on this mechanism of regulation, it has been shown that expression of MAGE-type antigens by cancer cells can be manipulated by DNA-methyl transferase inhibitors (DNMTi). DNMTis are compounds that inhibit cellular DNA-methyl transferase enzymes that maintain patterns of DNA methylation, and thus result in DNA hypomethylation. One of the most widely used DNMTis is 5-aza-2'-deoxycytidine (5-aza-dC), also termed decitabine. It has been shown that MAGE gene expression can be upregulated in a wide range of previously negative cancer cells by treatment with DNMTis [270]. For example studies in melanoma have shown that MAGE-A3 can be induced in MAGE-A3 negative clones derived from patient tumours by 5-aza-dC treatment [270]. Furthermore, that this facilitates their recognition by CTLs specific for known MAGE-A3 peptides in ex vivo co-culture assays. Upregulation of MAGE-type antigens by 5-aza-dC has also been observed in vivo in the clinic using tumour samples from patients undergoing treatment. In a phase I clinical trial, using pre- and post-treatment biopsies, 5-aza-dC increased expression of MAGE-A3 and NY-ESO-1 in roughly one third of patients tested with cancers of the lung or oesophagus [272].

Due to their ability to upregulate MAGE-type antigen expression by cancer cells, DNMTi treatment therefore presents a pharmacological means for increasing MAGE-type antigen expression and increasing tumour immunogenicity. DNMTi

agents have recently been approved and introduced into the clinic for the treatment of certain haematological disorders and malignancies. These have demonstrated an anti-neoplastic effect in patients with myelodysplastic syndrome and acute myeloid leukaemia (AML). Several are currently in clinical trials for treatment of solid cancers, alone and in combination with immunotherapeutic agents such as checkpoint inhibitors. A combination of DNMTi with a vaccine inducing potent MAGE-type antigen-specific CTL responses represents a promising novel therapeutic combination. Such an approach could be particularly useful for increasing the therapeutic effect of vaccination where target antigen expression in a patient's tumour is either low or lacking [273]. In this chapter, the potential of this strategy was tested by evaluating the therapeutic efficacy of combining ChAdOx1/MVA P1A vaccination with the DNMTi 5-aza-dC in some commonly used murine tumour models from the C57BL/6 genetic background.

5.2 Aims

The specific aims of this chapter were therefore:

1. To use the ChAdOx1/MVA P1A vaccination platform to investigate and characterise P1A-specific T-cell responses in mice of the C57BL/6 genetic strain.

2. Investigate the therapeutic potential of combining ChAdOx1/MVA P1A vaccination with DNA methyl transferase inhibitors in syngeneic tumour models

5.3 Results

5.3.1 ChAdOx1/MVA P1A heterologous prime-boost vaccination induces a high magnitude P1A-specific CD8+ T-cell response in C57BL/6 mice

Having previously confirmed induction of strong P1A-specific CD8+ T-cell responses induced by ChAdOx1/MVA P1A vaccination in DBA/2 mice, this strategy was then further evaluated in a different genetic background using C57BL/6 mice. The question was asked firstly as to whether CD8+ T-cell responses against P1A could be induced by ChAdOx1/MVA P1A vaccination in C57BL/6 mice, and therefore whether C57BL/6 mice had an MHC-class I haplotype capable of presenting P1A-derived CTL epitopes. Furthermore if responses could be observed, whether the heterologous prime-boost vaccination with ChAdOx1/MVA P1A could induce similarly strong P1A-specific CD8+ T-cell responses in the C57BL/6 genetic strain as those observed in DBA/2 mice. To investigate this, C57BL/6 mice received a heterologous prime-boost vaccination with ChAdOx1/MVA vectors encoding P1A according to the scheme in Figure 5.1. Mice were bled after each vaccination, and PBMCs were stimulated ex vivo with overlapping P1A peptides and ICS performed to evaluate the magnitude of any induced P1A-specific T-cell response by flow cytometry.

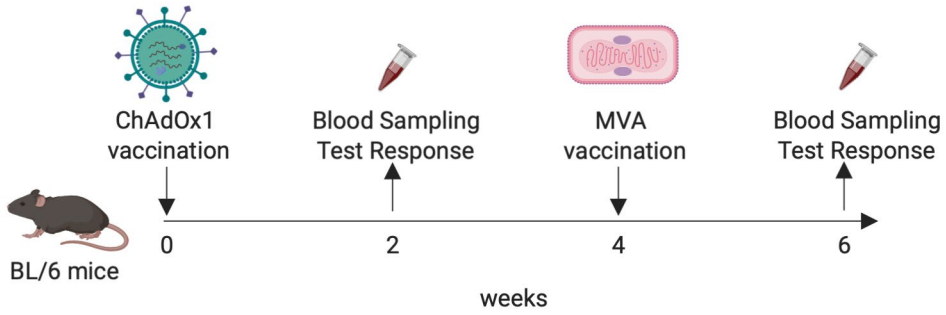


Figure 5.1. ChAdOx1/MVA heterologous prime-boost vaccination scheme with vectors encoding P1A. C57BL/6 mice received a prime vaccination via intramuscular injection (i.m.) with 10^8 IU of ChAdOx1-P1A ± Ii or a sham vaccination with PBS. 4 weeks after ChAdOx1-P1A (±Ii) mice received a boost vaccination with 10^7 PFU of MVA-P1A. Vaccinations were performed according to the experimental groupings shown in Table 5.1. To test the response to vaccination, mice were bled 18 days after vaccination with ChAdOx1 and 12-13 days after vaccination with MVA. Image created with BioRender.

Table 5.1 Combinations of ChAdOx1 and MVA viral vectors encoding P1A tested in heterologous prime-boost vaccinations.

Group	ChAdOx1 prime vaccination	MVA boost vaccination
1	PBS	PBS
2	P1A	P1A
3	Ii-P1A	P1A

Firstly, testing the response after vaccination, P1A-specific CD8+ T-cells were observed in the blood of vaccinated C57BL/6 mice, and significantly increased in frequency compared to control mice (Figure 5.2). Similar to the findings from the evaluation in the DBA/2 strain, CD8+ T-cells producing all 3 of the cytokines IFN-γ, TNF-α and IL-2 were observed after a single ChAdOx1 vaccination encoding P1A (± Ii) (Figure 5.2). The magnitude of the response was then increased greatly to significantly higher levels following boost vaccination with MVA encoding P1A, with significantly higher frequencies of CD8+ T-cells secreting IFN-γ, TNF-α

and IL-2 detected in the blood (Figure 5.2). Furthermore, as seen in DBA/2 there was a clear trend toward higher magnitude responses after both the prime and boost vaccinations in the group receiving ChAdOx1 encoding Ii fused to the N-terminus of P1A compared to the group with only the native antigen sequence, however this was not found to be significant. This observation confirmed therefore that P1A contains immunogenic epitope(s) that can be presented by MHC-class I alleles possessed by C57BL/6 mice to P1A-specific CD8+ T-cells.

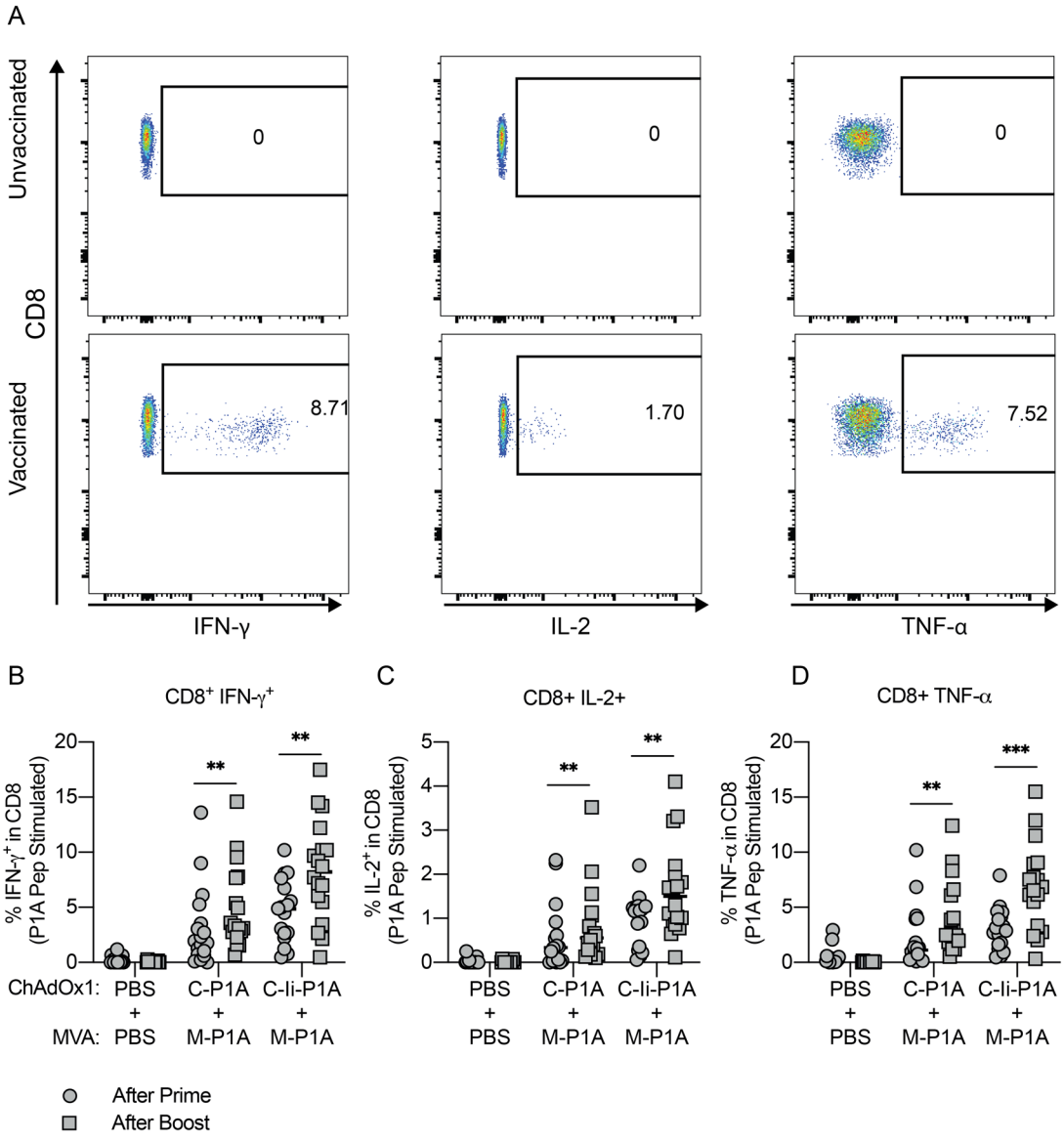


Figure 5.2. P1A-specific CD8+ T-cell response induced by prime-boost vaccination with ChAdOx1/MVA encoding P1A in C57BL/6 mice. C57BL/6 mice were vaccinated as described in Figure 5.1 and bled 18 days after ChAdOx1 vaccination and 12-13 days after MVA vaccination. PBMCs were stimulated ex vivo with 4μg/ml of P1A peptide pools, or a vehicle control (DMSO). The percentage of cytokine-producing P1A-specific CD8+ T-cells in the blood after each vaccination was then determined by ICS and flow cytometry (gating as described in Figure 2.2). Representative dot plots showing gating of IFN-γ, IL-2 and TNF-α expressing CD8+ T-cells (A). Percentage of IFN-γ+ (B), IL-2+ (C) and TNF-α+ (D) CD8+ T-cells after prime (closed circles) and boost (closed squares) in response to stimulation with P1A peptides. Data are shown as the median response of each group (horizontal lines). Each symbol represents an individual mouse, with 18 mice per group, pooled from 3 independent experiments. Statistically significant differences between groups were determined by a Kruskal-Wallis test with Dunn's multiple comparisons test. *, $p \leq 0.05$, **, $p \leq 0.01$ ****, $p \leq 0.0001$.

5.3.2 ChAdOx1/MVA P1A heterologous prime-boost vaccination does not induce a P1A-specific CD4+ T-cell response in C57BL/6 mice

The induction of P1A-specific CD4+ T-cell responses was also again tested in C57BL/6 mice following ChAdOx1/MVA P1A vaccination. However, no response was detected after either the ChAdOx1 or MVA vaccination – with no significant increase in cytokine producing cells detected in the blood of vaccinated groups compared to the PBS control group (Figure 5.3). This observation suggested that P1A does not contain any immunogenic MHC-class II epitopes presented to CD4+ T-cells in C57BL/6 mice.

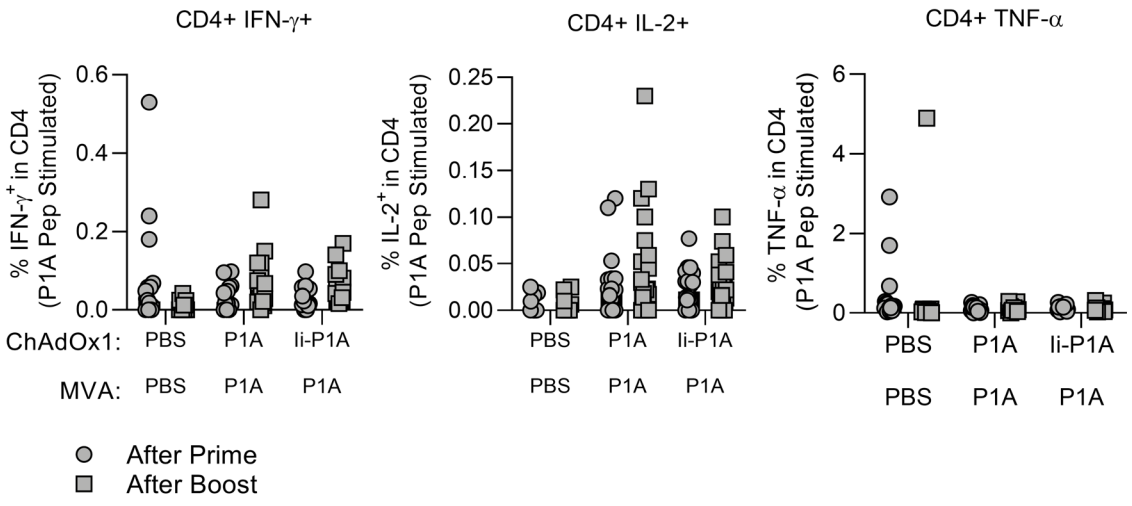


Figure 5.3. P1A-specific CD4+ T-cell response induced by prime-boost vaccination with ChAdOx1/MVA encoding P1A. BL6 mice were vaccinated as described in Figure 5.1 and bled 18 days after ChAdOx1 vaccination and 12-13 days after MVA vaccination. PBMCs were stimulated ex vivo with 4μg/ml of P1A peptide pools, or a vehicle control (DMSO). The percentage of cytokine-producing P1A-specific CD4+ T-cells in the blood after each vaccination was then determined by ICS and flow cytometry (gating as described in Figure 2.2). Percentage of IFN-γ+ (A), IL-2+ (B) and TNF-α+ (C) CD4+ T-cells after prime (closed circles) and boost (closed squares) in response to stimulation with P1A peptides. Data are shown as the median response of each group (horizontal lines). Each symbol represents an individual mouse, with 18 mice per group, pooled from 3 independent experiments. Statistically significant differences between groups were determined by a Kruskal-Wallis test with Dunn's multiple comparisons test.

5.3.3 P1A-specific CD8+ T-cells in C57BL/6 recognize a single immunogenic 9-amino acid MHC-class I restricted epitope – $P1A_{43-51}$ FAVVTTSFL

Having observed P1A-specific CD8+ T-cell responses in mice from the C57BL/6 genetic background for the first time, it was then decided to evaluate the breadth of the response, and to identify the sequences of the immunogenic epitope(s) recognized by P1A-specific CTLs. Identifying these epitopes would enable more in depth characterisation of the observed P1A-specific CD8+ T-cell responses. Peptide stimulation assays coupled with ICS can be performed in an iterative manner to narrow down and determine the exact sequences of MHC-class I epitopes recognized by CD8+ T-cells. This approach has been used in multiple other studies, for example with mapping epitopes from the respiratory syncytial virus (RSV) virus in C57BL/6 mice [274].

To determine the immunogenic P1A epitope sequence(s), splenocytes were isolated from C57BL/6 mice vaccinated with ChAdOx1/MVA vectors encoding P1A. Splenocytes were then stimulated ex vivo with pools of overlapping 15-amino-acid P1A peptides covering either the entire length of the P1A protein, or with one of 5 sub-pools, each containing peptides of sequences covering a short region of P1A. The peptide sequences contained within each subpool are listed in the appendix. The frequency of IFN-γ producing CD8+ T-cells in response to each stimulation was then determined by ICS and flow cytometry. As expected, a good magnitude CD8+IFN-γ+ response was observed following stimulation of splenocytes with the pool of peptides covering the entire length of P1A, and no

signal was observed from the unstimulated DMSO control samples (Figure 5.4 A). However, following stimulation with the sub-pools of peptides, by far the strongest response was observed from pool 1, where the frequency of IFN-γ producing splenocytes was higher in magnitude than that observed from the whole pool stimulation (Figure 5.4 A). This indicated that the majority of the P1A-specific response was directed against peptide(s) with sequences contained within this pool.

To further narrow down the identity of the immunogenic sequences contained within pool 1, ex vivo peptide stimulations were again performed using splenocytes from ChAdOx1/MVA P1A vaccinated mice, but this time stimulations were tested using each of the 11 peptides from pool 1 in isolation. Here it was found that the only immunogenic peptides from pool 1 that induced IFN-γ production by CD8+ T-cells were peptides 10 and 11 corresponding to sequences $P1A_{37-51}$-YLGWLVFAVVTTSFL and $P1A_{41-55}$-LVFAVVTTSFLALQM respectively (Figure 5.4 B).

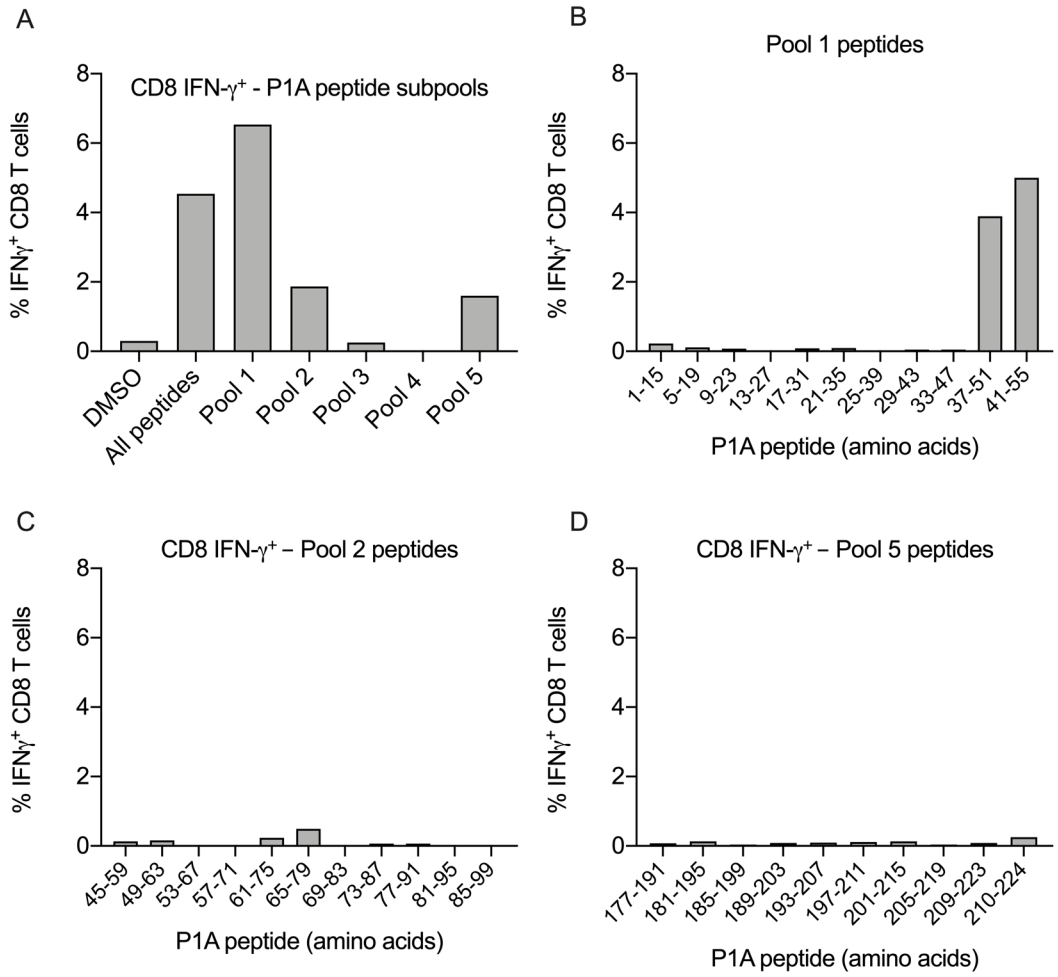


Figure 5.4. Identifying immunogenic P1A CTL epitopes in C57BL/6 mice. Splenocytes were harvested from C57BL/6 mice vaccinated with ChAdOx1-Ii-P1A/MVA-P1A. Splenocytes were stimulated with overlapping P1A peptides ex vivo and the percentage of CD8+IFN-γ+responding cells assessed by flow cytometry. A) CD8+IFN-γ+ response from stimulation with whole protein (all peptides) or from peptides divided into 5 smaller subpools. B) CD8+IFN-γ+ response from pool 1 peptides. C) CD8+IFN-γ+ response from pool 2 peptides. D) CD8+IFN-γ+ response from pool 5 peptides.

The canonical length of most MHC-class I peptide ligands is 9-10 amino acids, which is the optimal size for positioning within the MHC-class I binding groove, rather than the 15-amino-acid length used in the ex vivo overlapping peptide stimulation assay. The identity of the minimal MHC-class I restricted P1A peptide sequence was then further defined. In order to narrow down the identity of the most immunogenic 9-10 amino acid P1A epitope sequence binding to MHC-class I shared between the 15mer $P1A_{37-51}$ and $P1A_{41-55}$ peptides, Net-MHC 4.0 epitope

prediction software was used [275]. Net-MHC 4.0 is a machine learning algorithm designed to predict potential T-cell epitopes contained within a given peptide sequence by computationally estimating their affinity for different MHC molecules. Potential epitopes are also given a rank percentage score, by comparing their estimated binding affinity for a given MHC molecule with $4x10^5$ random peptides. True epitopes are likely to be those with a rank score <0.5% i.e. score higher for predicted binding affinity than 99.5% of random sequences. Mice from the C57BL/6 genetic background have MHC-class I alleles of the $H\text{-}2^b$ haplotype, and have two class I alleles – H-2K and H-2D. Net-MHC 4.0 software was used to predict the highest affinity canonical length peptide contained within the two immunogenic 15mers for either of the MHC-class I alleles possessed by C57BL/6 mice, and which allele this sequence was likely bound and presented by. The five sequences of 9 or 10 amino acids in length with the highest predicted binding affinity for either $H\text{-}2D^b$ and $H\text{-}2K^b$ from both $P1A_{37\text{-}51}$ and $P1A_{41\text{-}55}$ returned by the algorithm are presented here (Table 5.2 - Table 5.5).

The Net-MHC 4.0 algorithm returned a 9-amino acid sequence, $P1A_{43\text{-}51}$-FAVVTTSFL, as the sequence from both peptides 10 and 11 likely bound by the $H\text{-}2D^b$ MHC-class I allele with the highest affinity (Table 5.2). The sequence with the second highest binding affinity was a 9-amino acid sequence, $P1A_{45\text{-}53}$-VVTTSFLAL bound by $H\text{-}2K^b$ (Table 5.5).

Table 5.2. Highest affinity 9mer/10mer epitope sequences from P1A$_{37-51}$-YLGWLVFAVVTTSFL predicted by Net-MHC 4.0 algorithm for binding to H-2D^b

Peptide	Affinity (nM)	Rank (%)	Core
FAVVTTSFL	78.6	0.05	FAVVTTSFL
VFAVVTTSFL	1361.4	0.5	FAVVTTSFL
YLGWLVFAVV	18709.6	6	YLGWLFAVV
LGWLVFAVV	22549.7	8	LGWLVFAVV
YLGWLVFAV	23578.6	9	YLGWLVFAV

Table 5.3. Highest affinity 9mer/10mer epitope sequences from P1A$_{37-51}$-YLGWLVFAVVTTSFL predicted by Net-MHC 4.0 algorithm for binding to H-2K^b

Peptide	Affinity (nM)	Rank (%)	Core
LGWLVFAVV	1192.1	2.5	LGWLVFAVV
FAVVTTSFL	1685.3	3	FAVVTTSFL
VFAVVTTSF	2498.1	4	VFAVVTTSF
VFAVVTTSFL	5800.6	8	VAVVTTSFL
LVFAVVTTSF	7167	9.5	LVFVVTTSF

Table 5.4. Highest affinity 9mer/10mer epitope sequences from P1A$_{41-55}$-LVFAVVTTSFLALQM predicted by Net-MHC 4.0 algorithm for binding to H-2D^b

Peptide	Affinity (nM)	Rank (%)	Core
FAVVTTSFL	78.6	0.05	FAVVTTSFL
VFAVVTTSFL	1361.4	0.5	FAVVTTSFL
FAVVTTSFLA	3012.8	0.8	FAVVTTSFL
VVTTSFLAL	13550.8	4	VVTTSFLAL
AVVTTSFLAL	14109.3	4	AVVTSFLAL

Table 5.5. Highest affinity 9mer/10mer epitope sequences from P1A$_{41-55}$-LVFAVVTTSFLALQM predicted by Net-MHC 4.0 algorithm for binding to H-2K^b

Peptide	Affinity (nM)	Rank (%)	Core
VVTTSFLAL	242.5	0.6	VVTTSFLAL
VTTSFLALQM	527	1.1	VTTSFLAQM
FAVVTTSFL	1685.3	3	FAVVTTSFL
VTTSFLALQ	1934.1	3	VTTSFLALQ
VFAVVTTSF	2498.1	4	VFAVVTTSF

To confirm which of the sequences from the Net-MHC 4.0 predictions are recognized by P1A-specific CD8+ T-cells, synthetic peptides for $P1A_{43-51}$-FAVVTTSFL and $P1A_{45-53}$-VVTTSFLAL were produced and used to stimulate splenocytes isolated from ChAdOx1/MVA P1A vaccinated mice ex vivo. The P1A-specific response was again evaluated by ICS and measuring IFN-γ production by activated CD8+ T-cells. Stimulation with the $P1A_{43-51}$-FAVVTTSFL 9mer peptide was found to produce a high magnitude CD8+ IFN-γ+ response, similar in magnitude to that observed from stimulation with either peptides covering the whole pool of P1A peptides, the pool 1 peptides, or the $P1A_{37-51}$-YLGWLVFAVVTTSFL and $P1A_{41-55}$-LVFAVVTTSFLALQM individual 15mer peptides (Figure 5.5 A). Conversely no response was observed from stimulation with the $P1A_{45-53}$-VVTTSFLAL 9mer peptide. This confirmed that the highest affinity $P1A_{43-51}$-FAVVTTSFL sequence was the immunogenic MHC-class I restricted epitope recognized by P1A-specific CD8+ T-cells from C57BL/6 mice. To confirm that this 9mer sequence was the minimal core sequence bound by MHC-class I, two truncated 8mer peptides, removing a single amino-acid from either end of the FAVVTTSFL peptide were produced, corresponding to sequences $P1A_{44-51}$-AVVTTSFL and $P1A_{43-50}$-FAVVTTSF. PBMCs isolated from ChAdOx1/MVA P1A vaccinated mice were stimulated ex vivo either one of these peptides, or with the FAVVTTSFL peptide and IFN-γ production by CD8+ T-cells was measured by ICS and flow cytometry. As previously observed, the stimulation with the FAVVTTSFL peptide again produced a high magnitude CD8+ IFN-γ+ response (Figure 5.5 B). Conversely no response was detected from

stimulation with the P1A$_{43-50}$-FAVVTTSF 8mer, and a greatly reduced response was observed from P1A$_{44-51}$-AVVTTSFL stimulation (Figure 5.5 B). This confirmed P1A$_{43-51}$-FAVVTTSFL to be the minimal immunogenic sequence bound by MHC-class I.

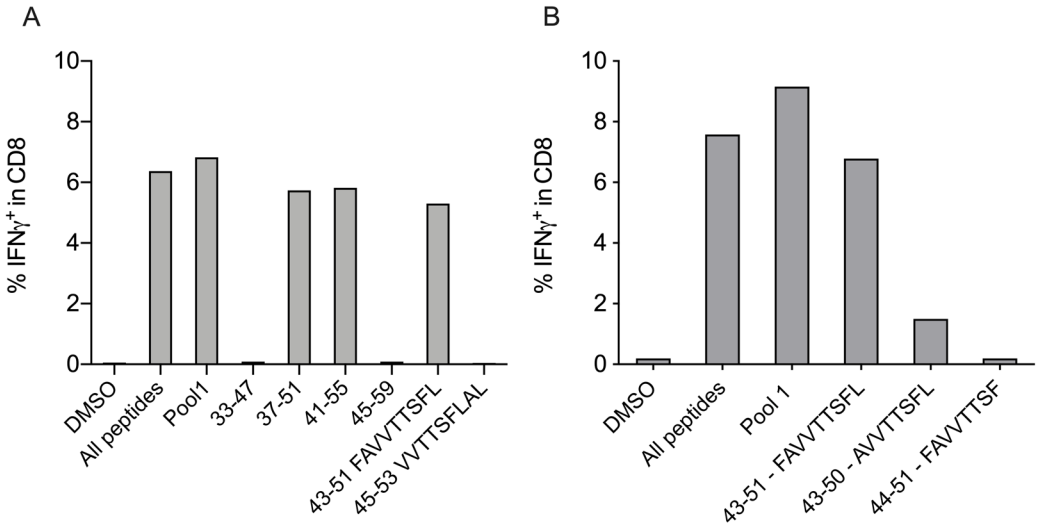


Figure 5.5 Characterization of the optimal 9-amino-acid P1A CTL epitope within the P1A$_{37-51}$ and P1A$_{41-55}$ peptides. Splenocytes were harvested from C57BL/6 mice vaccinated with ChAdOx1-Ii-P1A/MVA-P1A and stimulated with DMSO or P1A peptides and the percentage of CD8+IFN-γ+responding cells assessed by flow cytometry (A). PBMCs were harvested from C57BL/6 mice, vaccinated with ChAdOx1-Ii-P1A/MVA-P1A and stimulated with DMSO, all P1A peptides, P1A pool 1 peptides, FAVVTTSFL peptide, or truncated 8mer peptides and the percentage of CD8+IFN-γ+responding cells assessed by flow cytometry (B).

5.3.4 MHC-class I restriction of the P1A$_{43-51}$-FAVVTTSFL epitope

Having confirmed the minimal sequence of the immunogenic P1A epitope, attempts were then made to determine its MHC class I restriction by determining which allele it is presented by. The Net-MHC 4.0 algorithm predicted that the P1A $_{43-51}$-FAVVTTSFL epitope was likely bound by the H-2D^b allele. To confirm this, P1A$_{43-51}$-FAVVTTSFL peptides stimulations were performed combined with blocking antibodies specific for either of the two MHC-class I alleles from

C57BL/6 mice, H-2D^b and H-2K^b using splenocytes from two ChAdOx1/MVA P1A vaccinated mice. (Figure 5.6 A and B). The splenocytes were first incubated ex vivo with anti-H2D^b, anti-H-2K^b or anti-H-2D^b/H-2K^b prior to peptide stimulation, to block MHC-class I – TCR interactions and inhibit P1A-specific T-cell activation. CD8+ T-cell activation was then assessed via ICS for IFN-γ production. A slight reduction in the magnitude of IFN-γ-producing CD8+ T-cells compared to the positive control (FAVVTTSFL peptide stimulation with no blocking antibodies) was observed from incubation of splenocytes with anti-H-2D^b (Figure 5.6 B). However, with the exception of this, incubation of the splenocytes with blocking antibodies in any of the conditions tested did not greatly reduce the observed T-cell activation signal induced by FAVVTTSFL peptide stimulation. This assay therefore was unable to determine the exact MHC-class I restriction of the epitope.

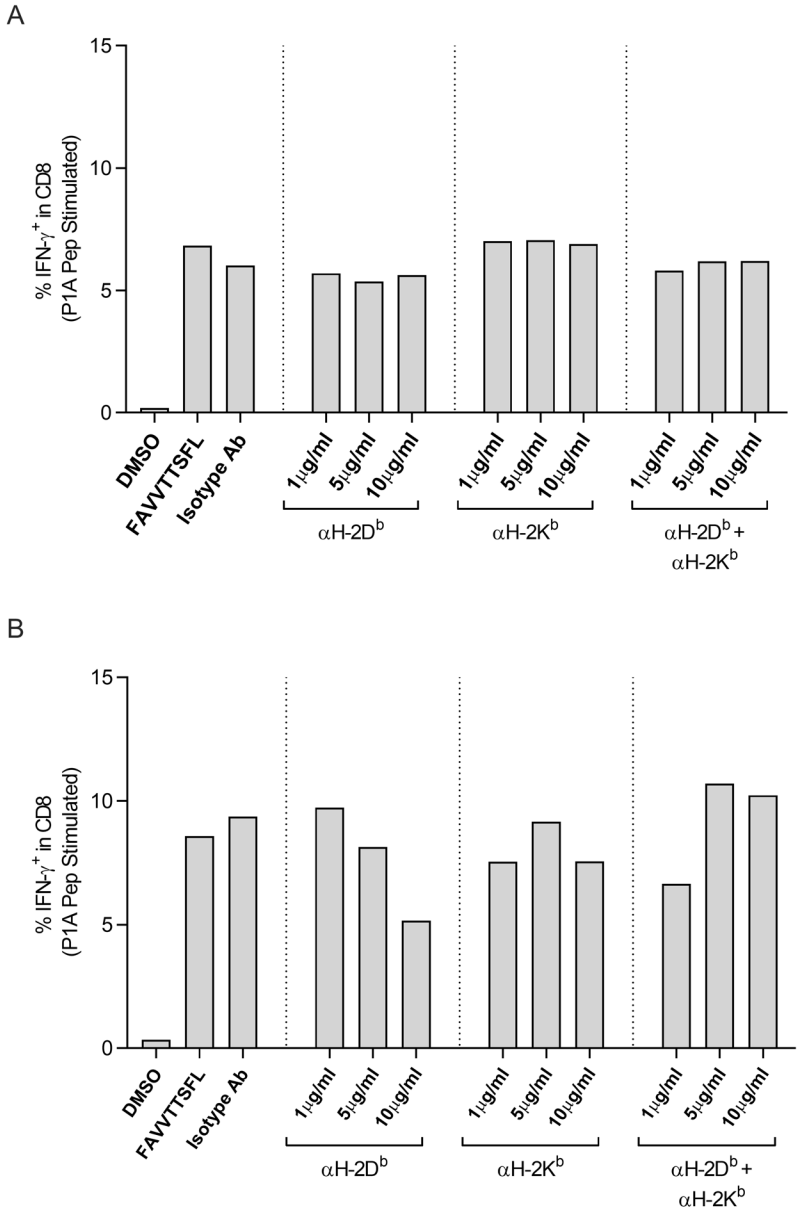


Figure 5.6. Validating the MHC-class I restriction of the P1A$_{43-51}$ epitope. Splenocytes were harvested from two C57BL/6 mice vaccinated with ChAdOx1-Ii-P1A/MVA-P1A ((A) and (B)) and stimulated ex vivo for 5 hours with 4μg/ml of either DMSO or FAVVTTSFL peptide. To determine the MHC-class I restriction of P1A$_{43-51}$, MHC-TCR interactions were blocked by pre-incubating splenocytes prior to stimulation with FAVVTTSFL peptide with different concentrations of anti-H-2D^b, anti-H-2K^b, anti-H-2D^b/anti-H-2K^b, an isotype control, or a no antibody control for 30 minutes. The percentage of CD8+IFN-γ+responding cells was assessed by ICS and flow cytometry.

5.3.6 P1A-specific CD8+ T-cell responses can be detected in C57BL/6 mice using a fluorescently labelled H-2D^b P1A$_{43-51}$-FAVVTTSFL multimer.

Despite not being able to confirm experimentally which MHC-class I allele the immunogenic FAVVTTSFL P1A peptide was presented by, a PE-labelled MHC-class I multimer binding this peptide was nonetheless produced on the basis of the results returned by the Net-MHC 4.0 epitope prediction algorithm. This indicated that the 9mer peptide had much higher affinity for H-2D^b binding than H-2K^b, therefore the tetramer was constructed from H-2D^b molecules. A multimer for the P1A$_{43-51}$ epitope would constitute a useful tool for monitoring P1A-specific CD8+ T-cells in C57BL/6 mice. To validate the ability of the tetramer to bind P1A-specific CD8+ T-cells, PBMCs and splenocytes were harvested from either mock treated or ChAdOx1-P1A (± Ii) / MVA-P1A vaccinated mice, stained with the tetramer, and analysed by flow cytometry. Significantly higher levels of H-2D^b P1A$_{43-51}$ tetramer positive CD8+ T-cells were detected by tetramer staining in the blood and spleen from ChAdOx1-Ii-P1A / MVA-P1A vaccinated mice compared to PBS control mice (Figure 5.7). No tetramer staining was observed in PBS control mice. Similar to the results obtained with ICS, a slightly higher level of tetramer staining was observed in the ChAdOx1-Ii-P1A/MVA-P1A vaccinated mice compared to ChAdOx1-P1A/MVA-P1A vaccinated mice, although not significant. This result indicated that P1A-specific CD8+ T-cells could be monitored in C57BL/6 mice through labelling with a fluorescently-conjugated H-2D^b P1A$_{43-51}$ tetramer. Furthermore, based on the results of the NET-MHC 4.0 prediction and the positive H-2D^b P1A$_{43-51}$ tetramer staining of CD8+ T-cells, this confirms that P1A$_{43-51}$ is presented via H-2D^b.

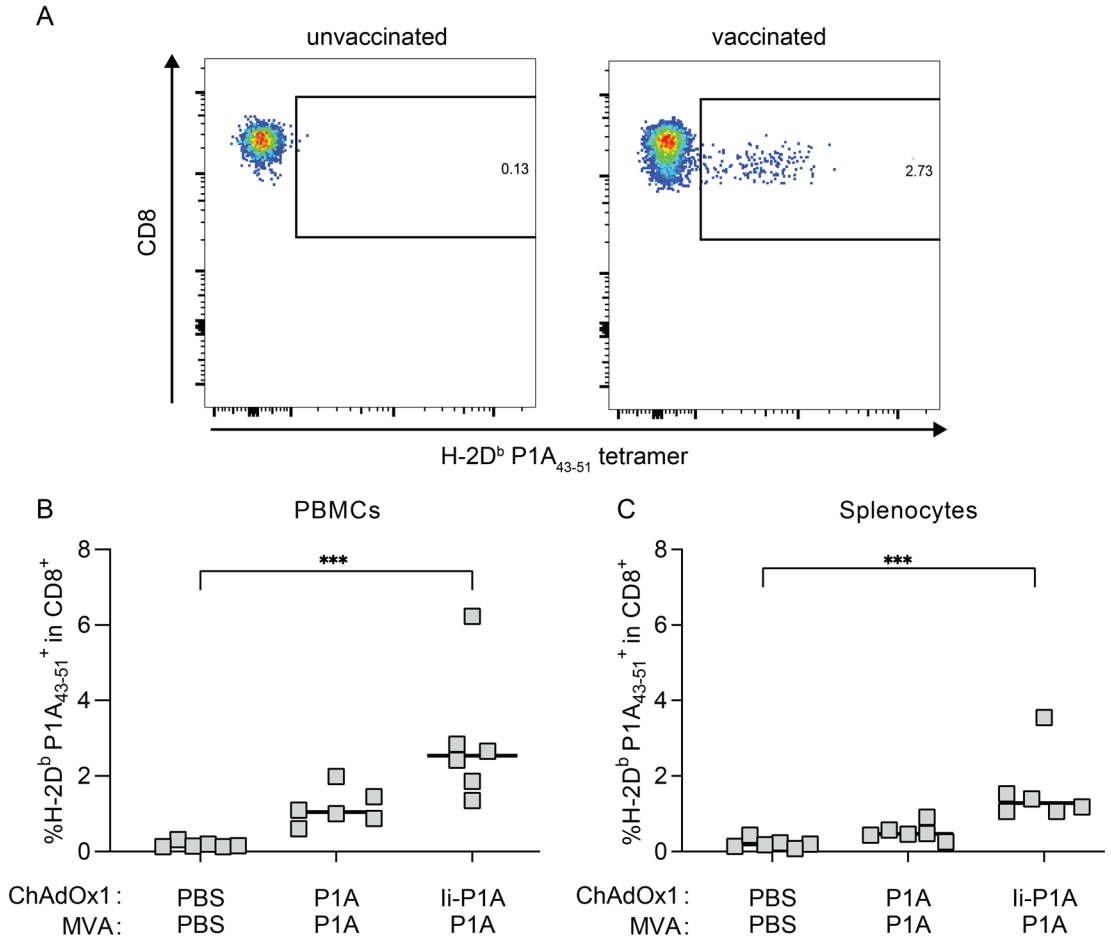


Figure 5.7 Detection of P1A-specific CD8+ T-cell responses in C57BL/6 mice via staining with a PE-labelled H-2D^b P1A$_{43-51}$ tetramer. Mice were vaccinated with either a PBS sham, or 10^8 IU ChAdOx1-P1A(± Ii) and 10^7 PFU MVA-P1A given 4 weeks apart. Mice were sacrificed 12 days after the MVA boost and PBMCs and splenocytes then harvested and stained with H-2D^b P1A$_{43-51}$ tetramer, and antibodies against surface T-cell markers. Representative gating for tetramer staining of CD8+ T-cells (A). The percentage of H-2D^b P1A$_{43-51}$ tetramer+ cells amongst total CD8+ T-cells from the blood (B) and spleen (C) are shown. Gating was performed as described in Figure 2.3. Data are shown as the median response of each group (horizontal lines). Each symbol represents an individual mouse, with 6 mice per group, representative of 2-independent experiments. Statistically significant differences between groups were determined by a Kruskal-Wallis test with Dunn's multiple comparisons test.

5.3.7 Determining the sequence of P1A-specific CD8+ T-cell TCRs recognizing the $P1A_{43-51}$-FAVVTTSFL epitope

Having defined the MHC-class I epitope recognized by CD8+ T-cells in C57BL/6 mice, it was then decided to determine the gene sequences of CD8+ T-cell receptors (TCRs) that are cognate for the $P1A_{43-51}$ epitope. Knowledge of the TCR sequence would enable the development of transgenic cell and mouse systems expressing P1A-specific TCRs to further study P1A-specific T-cell responses.

Having determined that P1A-specific CD8+ T-cells could be detected using a fluorescently-labelled H-$2D^b$ multimer binding the FAVVTTSFL epitope, it was then decided to use this facility to isolate P1A-specific CD8+ T-cells for TCR sequencing.

Initially, multiple attempts were made to clone P1A-specific CD8+ T-cells via single cell sorting of H-$2D^b$ $P1A_{35-43}$ tetramer+ CD8+ T-cells cells isolated from the spleens of ChAdOx1/MVA P1A vaccinated C57BL/6 mice, followed by in vitro expansion of isolated T-cells. Attempts at growing out murine CD8+ T-cells post single-cell sort were made using different culture methods, however, these were unsuccessful and will not be discussed further in this chapter.

TCRs are dimeric protein complexes formed from an alpha chain and beta chain subunit. The unique specificity of individual TCRs is determined from the recombination of V, D (for the β chain) and J gene segments that form the variable regions of both the TCR-α and TCR-β chains. Identifying the correct sequence for a productively rearranged TCR involves not only knowledge of the TCR-α and

TCR-β sequences, but also determining the pairing of TCR-α and TCR-β chain sequences. Unless a sample of isolated T-cells is truly 100% clonal, which is almost technically impossible to obtain, multiple TCR chain sequences are likely to be found within it. To determine P1A-specific TCR sequences, a single-cell V(D)J RNA sequencing platform developed by 10x Genomics was used, which uses molecular barcodes to identify individual cells and enables TCR-α and TCR-β chain sequences from each cell to be paired.

An experiment was carried out as depicted in Figure 5.8 A to determine P1A-specific CD8+ T-cell TCRs induced by ChAdOx1/MVA P1A vaccination. Splenocytes were isolated from vaccinated mice, labelled with H-2D^{b} P1A$_{43\text{-}51}$ tetramer and single-cell sorted to obtain a purified fraction of cells (Figure 5.8 B). Unique clonotypes were identified from the sequencing and defined as cells bearing alpha and beta chains with the same gene segment sequences that result in the same CDR3 region sequence.

Analysis of the distribution of different clonotypes contained within the sequenced sample showed a strong enrichment of particular clones, as would be expected for a sample of T-cells of a defined specificity (Figure 5.8 C). Several clonotypes occupied a significant proportion of the total sequenced cells (barcodes), indicating that they shared a common specificity.

The sequences of the most enriched clonotypes represent a promising avenue for further investigation of P1A$_{43\text{-}51}$ specific TCRs (Figure 5.8 D and E). The availability of the alpha and beta chain sequences of each these clonotypes permit

them to be cloned into expression vectors for the development of transgenic TCR systems. These sequences therefore warrant experimental validation for their ability to express productive P1A-specific TCRs.

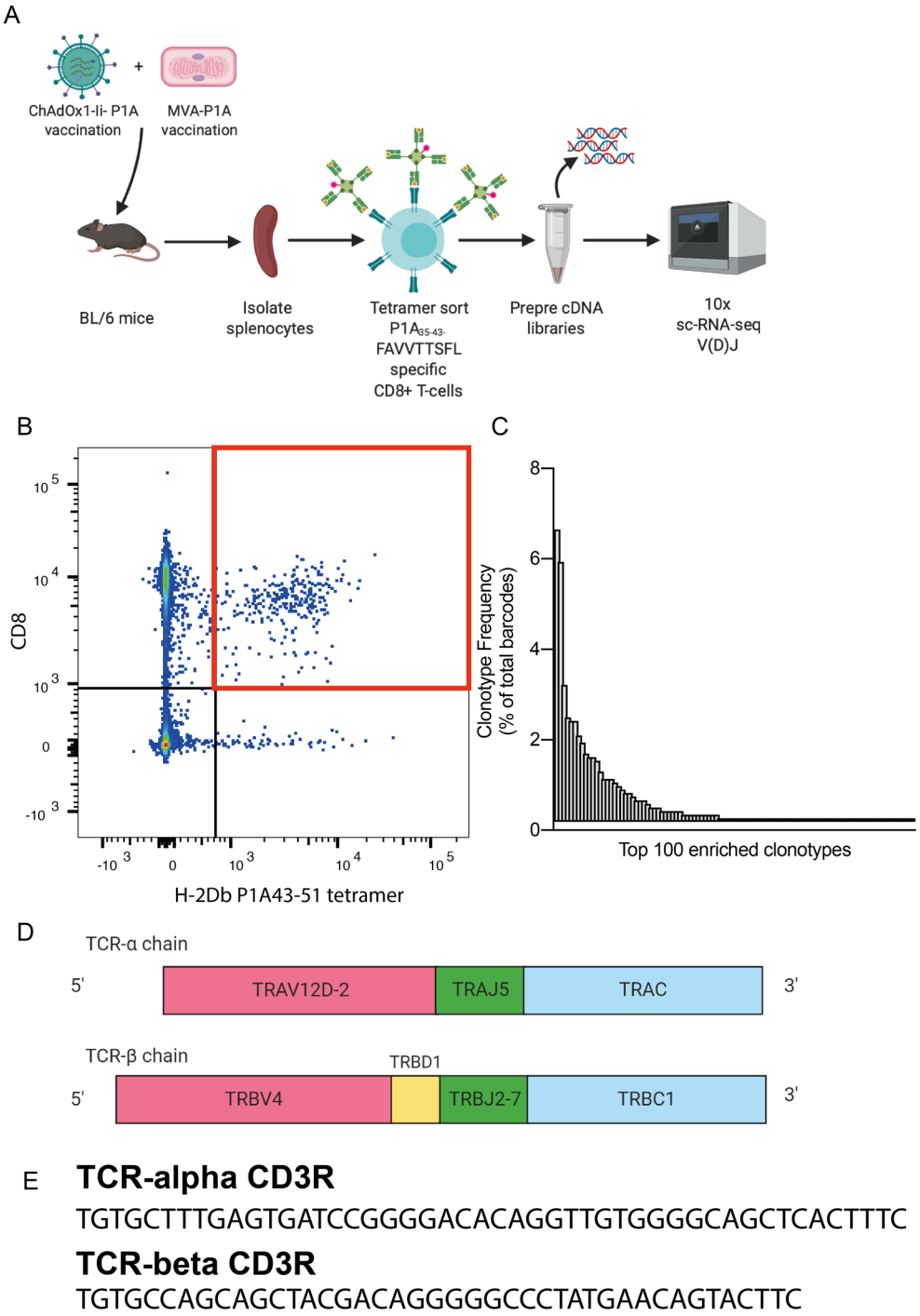


Figure 5.8. Determining P1A$_{43-51}$-specific TCR sequences from C57BL/6 mice. Experimental timeline (A) - Mice were vaccinated with 10^7 IU ChAdOx1-li-P1A and 10^6 PFU MVA-P1A given 1 week apart, splenocytes isolated 9 days after the MVA vaccination and P1A-specific CD8+ T-cells isolated by FACS sorting H-2D^b P1A$_{43-51}$ tetramer+ CD8+ T-cells. Single cell 10x barcoded cDNA libraries were then prepared from the RNA of isolated cells using a 10x Chromium Controller platform and sequencing data generated using an Illumina HiSeq-4000. RNA from a total of 1252 cells was sequenced. Representative flow cytometry plot for gating H-2D^b P1A$_{43-51}$ tetramer+ CD3+ CD8+ T-cells during single-cell sorting is shown (B). Gates were set for tetramer+ CD8+ T-cells based on the signal observed in a FMO control. V(D)J gene sequences for both the TCR alpha and TCR beta chain were determined for each cell in the dataset and used to define unique clonotypes. The frequency distribution of the 100 mostly highly represented clonotypes as a proportion of total sequenced cells (uniquely identified by 10x barcodes) is shown (C). V(D)J gene segment

combinations and CDR3 sequences of the TCR-alpha and TCR-beta chains of the most highly represented clonotype are shown (D) and (E).

5.3.8 Generating P1A-expressing C57BL/6 derived murine cancer cell lines

Having confirmed that high-magnitude P1A-specific CD8+ T-cells could be induced in C57BL/6 mice by ChAdOx1/MVA P1A vaccination, it was next sought to test their protective anti-tumour efficacy in additional murine tumour models. However, a search of available literature coupled with testing of available BL6 derived murine cancer lines was unable to reveal any that had constitutive P1A expression. Indeed endogenous P1A expression in murine cancer models has rarely been observed outside of mastocytoma cell lines. For this reason the decision was taken to develop P1A-expressing C57BL/6 derived murine tumour models.

Two murine tumour models were chosen – MC38 and B16F10. MC38 is a murine colon carcinoma cell line whilst B16F10 is a murine melanoma cell line. Both are commonly used models of solid tumours in a range of fields, including cancer vaccine development. MC38 and B16F10 expressing P1A were developed through a stable transfection method. Cells were transfected with a pEF4/V5 His A plasmid containing a P1A gene expression cassette with P1A under the control of a human elongation factor-1 alpha promoter (EF-1a). The plasmid also encoded a neomycin resistance gene, and stable transfectants were generated through continued culture with neomycin for 4 weeks.

Selected cells were then single cell sorted and individual clones were assessed for relative P1A expression levels by rt-qPCR (Figure 5.9). The clones with the highest expression level of those screened, MC38.E4.P1A and B16F10.C9.P1A, were selected and expanded in culture. The generation of these cell lines represents a useful tool for studying anti-tumour P1A-specific CD8+ T-cell responses in different settings. These therefore warrant testing in in vivo studies.

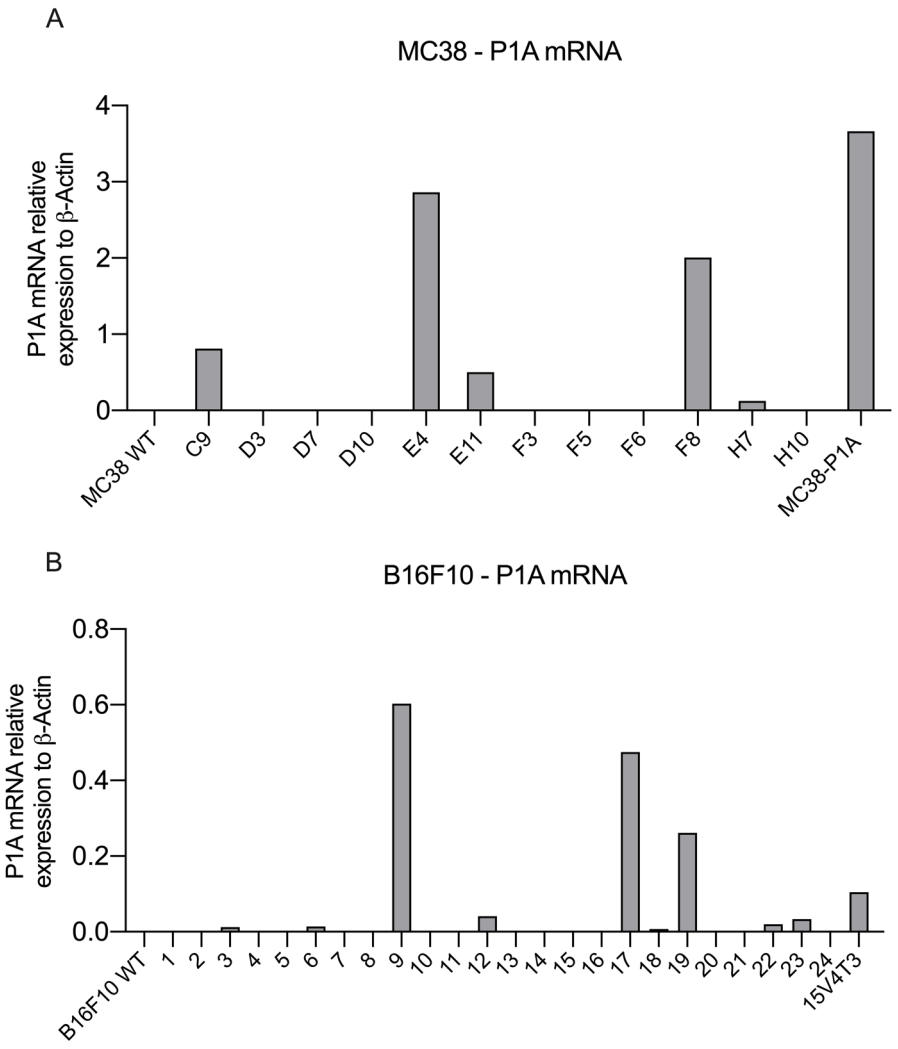


Figure 5.9. Screening of MC38 and B16F10 clones stably transfected with a P1A-expression plasmid for P1A mRNA expression by qPCR. MC38 and B16F10 cells were transfected with a pEF4/V5 His A plasmid containing a P1A gene expression cassette, and stable transfectants generated through selection with neomycin to generate polyclonal P1A-expressing cell lines. Clones were generated through singe-cell FACS sorting of stably transfected cell lines and then grown out in culture. A range of MC38-P1A (A) and B16F10-P1A (B) clones were screened for P1A expression level by determining P1A mRNA expression by rt-qPCR. Target gene mRNA expression level was normalized relative to β-Actin and is shown as $2^{-\Delta Ct}$.

5.3.9 P1A expression can be induced in a range of C57BL/6 cancer lines following treatment with the DNMTi, 5-aza-2'-deoxycytidine

The development of P1A-expressing murine tumours cell lines from the H-2^b genetic background represents a useful tool for studying the anti-tumour efficacy of P1A-specific CTL responses in novel settings. However, the forced overexpression of a tumour antigen is a somewhat artificial setting. Like other CG genes, P1A expression has been shown to be regulated by promoter sequence methylation at CpG islands and therefore able to be induced de novo in cancer cells by treatment with DNMTis such as 5-aza-dC [276]. The use of DNMTis represents a more physiological and clinically relevant means to induce P1A-expression in tumour cell lines of interest. 5-aza-dC for example already has regulatory approval for treatment of myeloproliferative blood disorders and acute myeloid leukaemia (AML). A combination of a viral vectored vaccine and DNMTi would also be a highly novel therapy, and could help overcome some of the potential limitations associated with a therapeutic cancer vaccine. On this basis, it was the tested whether 5-aza-dC treatment could induce P1A expression in cell lines of interest here for evaluating therapeutic efficacy of ChAdOx1/MVA P1A vaccination. Cells of three murine tumour lines, MC38, B16F10 and EL4, were treated in vitro with cell culture media supplemented with different concentrations of 5-aza-dC ranging from 0.1μM- 1μM for 48 hours. P1A expression at the mRNA level was then assessed by rt-qPCR (Figure 5.10). In the untreated state, all cell lines had scarcely detectable P1A mRNA expression. P1A expression was however readily upregulated in all 3 cell lines following treatment with 5-aza-dC. The cell lines were differentially responsive to the concentration

used, with MC38 (Figure 5.10 C) reaching a maximum expression level of P1A at 4μM, whereas B16F10 (Figure 5.10 A) and EL4 (Figure 5.10 B) reached a maximum expression level at 10μM. This likely reflects the different growth rates of the cells in culture, as due to its mechanism of action 5-aza-dC exerts the strongest effect on rapidly dividing cells.

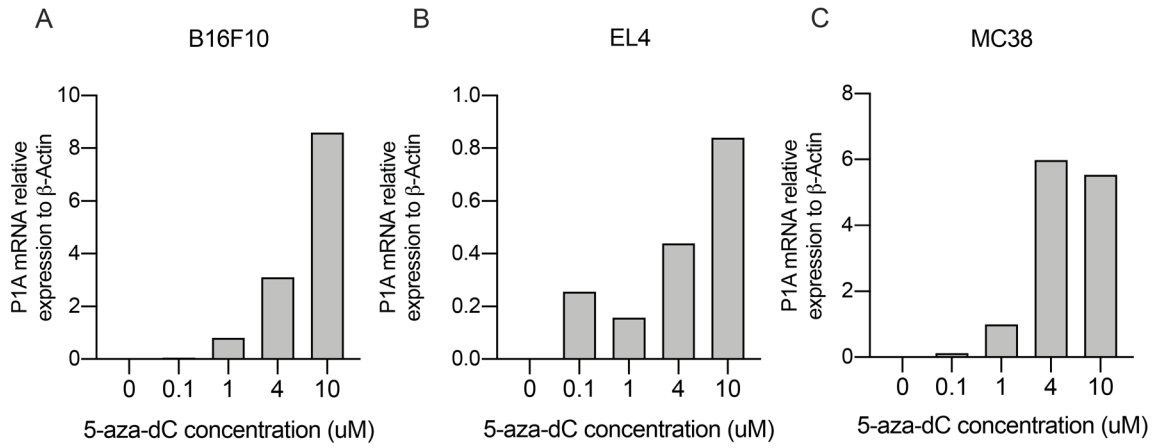


Figure 5.10. Assessing P1A expression in murine cancer cell lines following treatment with 5-aza-dC. Cells from three C57BL/6 cancer lines, B16F10 (A), EL4(B) and MC38 (C) were seeded in 6-well culture dishes at a density of 0.1 x 10^6 per well. Cells were then treated with different concentrations of 5-aza-2'- deoxycytidine ranging from 0.1μM- 10μM added to cell culture medium for 48 hours. Cells were then harvested, and P1A expression at the transcriptional level assessed by rt-qPCR. Target gene mRNA expression level was normalized relative to β-Actin and is shown as $2^{-\Delta Ct}$. Data are presented as mean ± SEM.

5.3.10 Tumour P1A expression can be induced in MC38 tumour-bearing C57BL/6 mice treated with 5-aza-2'-deoxycytidine.

Having confirmed that 5-aza-dC could induce P1A expression in vitro, its ability to induce expression in the tumours of tumour-bearing mice was then evaluated. Based on the finding that it exhibited higher sensitivity to lower doses of 5-aza-dC in terms of upregulation of P1A, MC38 was chosen to perform this study with. C57BL/6 mice were implanted with MC38 cells, and then treated for 5 days with 5-aza-dC once palpable tumours had developed. Tumours were harvested and P1A expression level was assessed by rt-qPCR. 5-aza-dC robustly upregulated P1A at the mRNA level, with detectable expression in the tumours of all treated mice (Figure 5.11 A). This was significantly increased compared to control treated mice, where very low – almost no P1A expression in the tumour was no detected. The effect of 5-aza-dC treatment on P1A expression in other healthy tissues was also considered, as upregulating P1A antigen expression in in non-tumour tissue

might lead to off target effects or toxicity if combined with ChAdOx1/MVA P1A vaccination. P1A expression was evaluated in a range of other tissues, but 5-aza-dC was only found to exert an effect on the bone marrow and spleen, where significantly increased P1A expression compared to vehicle control treated mice was detected (Figure 5.11 B). However, the size of the effect on these tissues was minimal when compared to the tumour, with orders of magnitude lower fold change in P1A mRNA expression observed between samples from control treated and 5-aza-dC treated mice.

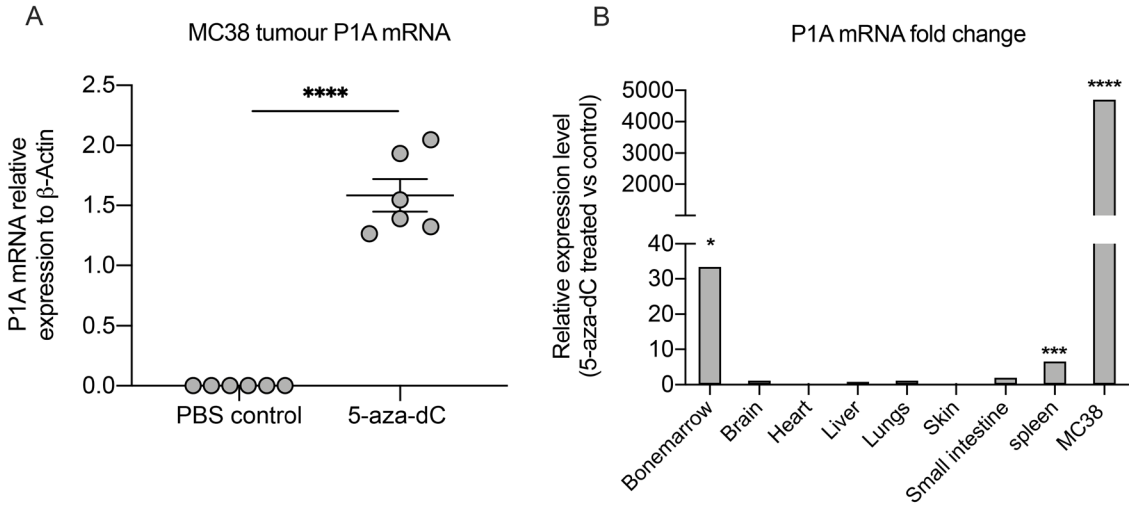


Figure 5.11 Assessing P1A expression level by rt-qPCR in tissues of MC38 tumour-bearing C57BL/6 mice following treatment with 5-aza-2'-deoxycytidine. C57BL/6 mice were implanted with $1x10^5$ MC38 cells via subcutaneous injection in the right flank. Following the development of palpable tumours, mice were treated with 5-aza-dC for 5 days given at a dose of 1mg/kg via i.p. injection per day or with PBS control injections. Two days after the last dose of 5-aza-dC was administered mice were sacrificed and tumours and a panel of healthy tissues were harvested for gene expression analysis. The effect of 5-aza-dC on P1A mRNA expression in tumour and healthy tissue was determined by rt-qPCR. P1A mRNA expression in MC38 tumours of control treated and 5-aza-dC treated mice (A). Data are analysed by the $2^{-\Delta Ct}$ method and P1A mRNA expression is shown as fold change relative to β-Actin. Mean ± SEM is shown and each symbol represents an individual mouse, with 6 mice per group. Representative of at least 2 individual experiments. P1A mRNA expression in healthy tissue (B). Data are analysed by the $2^{-\Delta\Delta Ct}$ and shown as mean fold change in P1A mRNA level between samples from 5-aza-dC treated mice vs control treated mice. Representative of at least 2 individual experiments. Statistically significant difference between groups was determined by a student's t-test. *, $p \leq 0.05$, ***, $p \leq 0.001$ ****, $p \leq 0.0001$

5.3.11 ChAdOx1/MVA P1A vaccination provides moderately improved control of growth of MC38 tumours formed from cells pre-treated in vitro with 5-aza-2'-deoxycytidine

Having observed that 5-aza-dC treatment could upregulate P1A expression in previously negative MC38 tumours, the question was asked whether this could enable their recognition by P1A-specific CD8+ T-cells generated by therapeutic ChAdOx1/MVA P1A vaccinations. MC38 cells were treated in vitro with 5-aza-dC to induce P1A expression, or otherwise with a vehicle only control, then injected subcutaneously into the flanks of C57BL/6 mice. Therapeutic ChAdOx1/MVA P1A vaccinations were then initiated and tumour growth monitored. As expected, therapeutic vaccination provided no control of growth of tumours formed from untreated MC38 cells, which do not express P1A (Figure 5.12). In addition 5-aza-dC treated cells alone were found to form significantly slower growing tumours than untreated cells in vivo (Figure 5.12). This could be due perhaps to either increased immunogenicity or the cytotoxic effect of the drug on the cells. However, therapeutic vaccination of mice bearing tumours formed from 5-aza-dC treated MC38 cells delayed tumour growth further still (Figure 5.12). This improved control of tumour growth suggested that the 5-aza-dC pre-treatment was sensitizing the tumours to recognition by the vaccine induced P1A-specific CD8+ T-cell response.

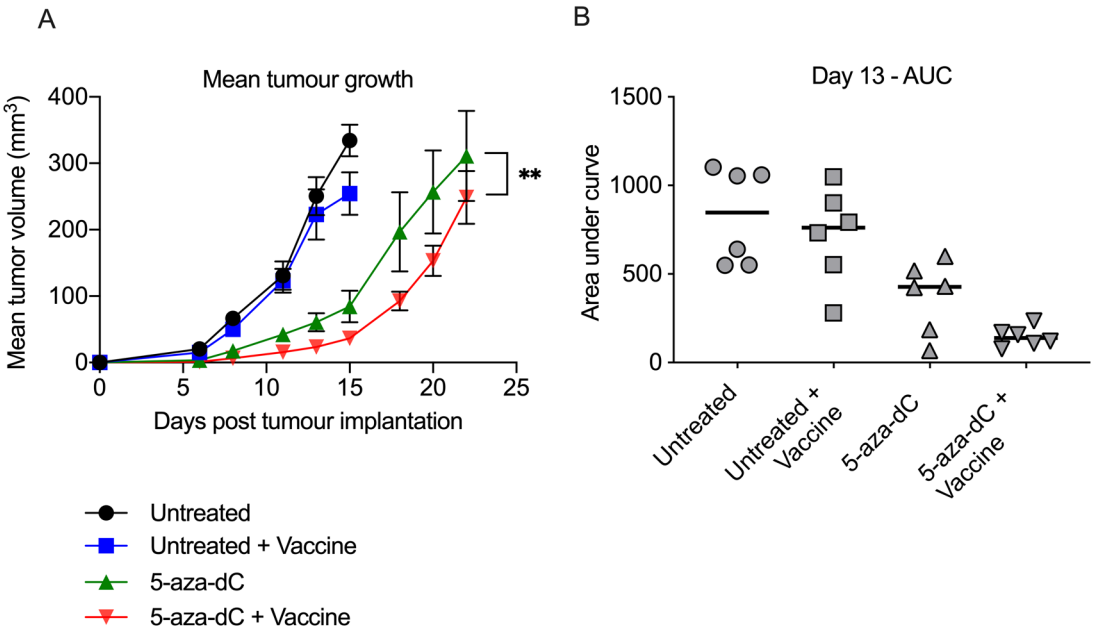


Figure 5.12 Therapeutic efficacy ChAdOx1-li-P1A/MVA-P1A againt tumours formed from 5-aza-2'-deoxycytidine pre-treated MC38 cells. MC38 cells were treated in vitro for 48 hours with either 1μM 5-aza-dC or a vehicle control, harvested, and then implanted in C57BL/6 mice via s.c. injection of $0.1x10^6$ cells in the right flank. Mice were then vaccinated with 10^7 IU ChAdOx1-li-P1A and 10^6 PFU MVA-P1A on days 1 and 8 post tumour implantation respectively, or otherwise were given PBS sham vaccinations. Tumour growth data is shown (A). Tumour growth data are presented as group mean ± SEM, with 6 mice per group, representative of 2-independent experiments. Statistically significant differences in mean tumour volume between groups were determined by a two-way ANOVA followed by Tukey's post hoc test and **, $p \leq 0.01$. An AUC analysis was performed on day 13 post tumour implantation to evaluate treatment therapeutic efficacy (B).

5.3.12 Combined 5-aza-2′-deoxycytidine treatment with ChAdOx1/MVA P1A vaccination is not sufficient to control tumour growth in mice bearing MC38 or EL4 tumours

As 5-aza-dC appeared to sensitize tumours to therapeutic vaccination, the anti-tumour efficacy of a combination of both treatments administered in vivo was then explored in two syngeneic tumour models. C57BL/6 mice were implanted with either MC38 or EL4 cells to initiate tumour growth, then received treatment with 5-aza-dC to induce tumour P1A expression, before receiving therapeutic vaccinations with ChAdOx1/MVA P1A. In both of these tumour models however, no significant control of tumour growth was observed from the combination therapy compared to the 5-aza-dC treatment alone or untreated control groups. Both tumour growth and overall survival were largely similar between different groups.

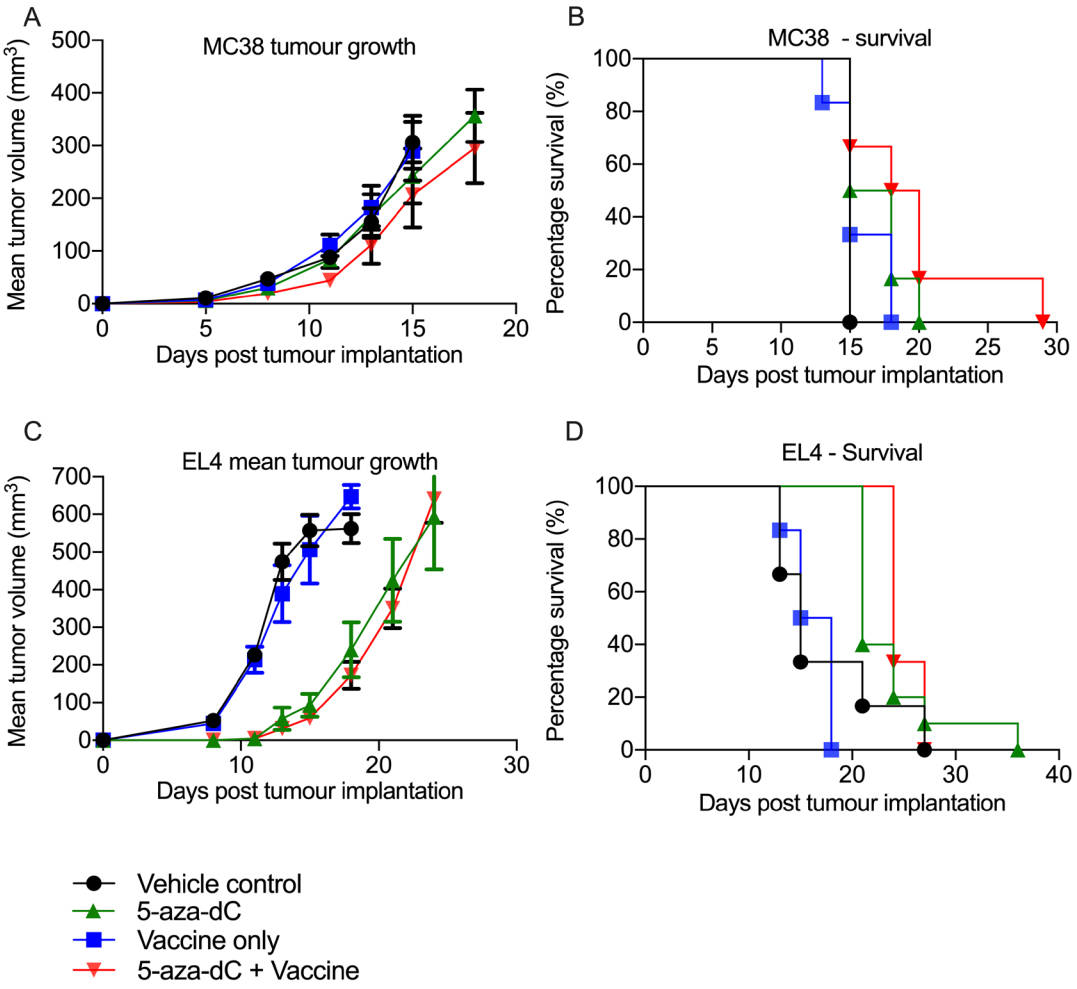


Figure 5.13 Threapeutic efficacy of 5-aza-2'-deoxycytidine treatment combined with ChAdOx1-li-P1A/MVA-P1A vaccination against MC38 and EL4 tumours. C57BL/6 mice were implanted with $0.1x10^6$ of either MC38 or EL4 cells via s.c. injection in the right flank to initiate tumour growth and were then treated with a dose of 0.5mg/kg of 5-aza-dC or a vehicle control given via i.p. injection once daily for a total of 3 days. Vehicle control and 5-aza-dC treated mice were then vaccinated with 10^7 IU ChAdOx1-li-P1A and 10^6 PFU MVA-P1A on days 4 and 11 post tumour implantation respectively, or otherwise were given PBS sham vaccinations. Tumour growth and survival are shown for MC38 tumour bearing mice (A and B) and EL4 tumour bearing mice (C and D). Tumour growth data are shown as group mean ± SEM, with 6 mice per group, representative of 2-independent experiments. Survival data are analysed according to the Kaplan-Meier method.

5.4 Discussion

In this study, vaccination with ChAdOx1/MVA vectors encoding P1A was used to investigate P1A-specific CD8+ T-cell responses in the C57BL/6 genetic background. To date, P1A-specific immune responses have only been studied in mice of H-2^d genetic background, such as the DBA/2 and BALB/c strains, where an H-$2L^d$-restrictred P1A CTL epitope has previously been defined. Here, a heterologous prime-boost vaccination with ChAdOx1/MVA P1A was found to induce high magnitude P1A-specific CD8+ T-cell responses in C57BL/6 mice. High frequencies of type-I cytokine-producing CD8+ T-cells were detected post vaccination by ex vivo stimulation of PBMCs with P1A peptide pools. This observation shows for the first time that P1A-specific T-cell responses can be induced in C57BL/6 mice of the H-2^b genetic background. These results also lend further support to those presented in chapter 4, and confirm the robustness of the ChAdOx1/MVA platform as a strategy for inducing high magnitude CD8+ T-cell responses against P1A, and therefore MAGE-type antigens. Indeed the magnitude of the P1A-specific CD8+ T-cell response induced by ChAdOx1/MVA P1A in C57BL/6 was comparable to that observed by the same vaccination scheme in DBA/2 mice.

The detection of P1A-specific CD8+ T-cells in BL/6 mice by ICS indicated that P1A contains immunogenic epitopes presented via H-2^b MHC molecules to CD8+ T-cells. To investigate this finding further it was sought to identify the immunogenic P1A CTL epitope(s) in C57BL/6 mice against which the CTL response is directed. Identifying MHC-class I restricted CTL epitopes is crucial for

fully characterizing CTL-responses against tumour-antigens such as P1A. The experiments performed here led to the discovery of a novel H-2^b restricted P1A-specific CTL epitope, corresponding to amino acids 43-51 (FAVVTTSFL). Interestingly, the P1A-specific CTL response in C57BL/6 was shown to be solely against the $P1A_{43-51}$-FAVVTTSFL epitope, with no other immunogenic epitopes in the protein detected. This is similar to DBA/2 mice, where it is directed solely against the $P1A_{35-43}$ epitope. Furthermore, the position of the H-2^b $P1A_{43-51}$ epitope is located very close to the H-$2L^d$ $P1A_{35-43}$ epitope, with the $P1A_{43}$ phenylalanine residue shared between the two. In this study, epitope identification was performed through a combination of empirical determination via iterative stimulations of splenocytes from ChAdOx1/MVA P1A vaccinated mice using pools of P1A peptides and bioinformatic predictions. This is similar to the methods used by other studies in defining T-cell epitopes from infectious disease agents such as RSV, and demonstrates the power of the approach for CTL epitope identification [274, 277]. MHC-binding prediction algorithms indicated that the epitope is restricted to the H-$2D^b$ MHC-class I allele rather than H-$2K^b$ based on its predicted binding affinity, however this could not be confirmed experimentally by the approach tested here. This therefore warrants further experimental validation, and a more promising approach may be to use P815 cells which naturally do not express H-2^b alleles, transfected to express either H-$2D^b$ or H-$2K^b$, pulsed with peptide, as antigen-presenting cells in a T-cell stimulation assay. This has been successfully carried out before in determining the restriction of novel RSV CTL epitopes in C57BL/6 mice [277]. Splenocytes from congenic mice could also be

used to achieve this aim. However, a $P1A_{43-51}$ MHC-class I tetramer based on H-$2D^b$ molecules was found to be able to label and identify P1A-specific CD8+ T-cells from ChAdOx1/MVA P1A vaccinated mice, strongly suggesting that H-$2D^b$ is indeed the restriction of the epitope.

This newly defined $P1A_{43-51}$-FAVVTTSFL epitope is the first P1A-specific CTL epitope identified in mice of the H-2^b genetic background, and the first in a strain other than DBA/2 or BALB/c of the H-2^d genetic background. The C57BL/6 mouse strain serves as the genetic background in which the majority of transgenic and knockout mouse models have been developed for the mechanistic investigation of immune responses. Additionally, P1A is the best known murine equivalent of the human MAGE-type antigens. Therefore, the identification of the H-2^b-restricted $P1A_{43-51}$ epitope opens up many additional avenues of research to gain further understanding of the immunology of MAGE-type antigen directed CTL responses and their role in anti-tumour immunity.

Given that P1A is a self-antigen in mice it allows MAGE-type antigen specific CD8+ T-cell responses to be studied using mouse models in a physiologically accurate setting. However, innumerable studies of antigen-specific T-cell responses against tumours in the H-2^b genetic background use OTI mice, a transgenic TCR stain bearing CD8+ T-cells with specificity for an epitope derived from the egg ovalbumin protein (OVA) - $OVA_{257-264}$-SIINFEKL, presented by H-$2K^b$ [278]. For the study of anti-tumour immune responses tumour models such as B16F10-OVA, MC38-OVA or other cells lines transfected to overexpress the OVA

antigen are frequently used. This has been useful in furthering understanding of antigen-specific CD8+ -cell responses, OVA is however a foreign antigen and therefore a very unphysiological setting to study anti-tumour immunity. OVA-specific immune responses are very unlikely to reflect the strength, magnitude and nature of T-cell responses against potentially less strongly immunogenic tumour antigens. Studying anti-tumour P1A responses in the H-2^b genetic background would represent an improvement. With this in mind, two C57BL/6 derived cancer cell lines frequently used in syngeneic tumour models, MC38 and B16F10, were modified to express P1A through stable transfection methods. The generation of these P1A-expresing cancer cell lines therefore represents a further tool to study P1A-specific CD8+ T-cell responses in C57BL/6 mice in an anti-tumour setting, to aid in the development of novel immunotherapeutic strategies. P1A-expression was confirmed in these cells by rt-qPCR. Further work however should first confirm whether P1A properly processed and the $P1A_{43-51}$ epitope presented in the context of MHC-class I in these particular cell lines, by determining whether they can be recognized by P1A-specific CD8+ T-cells in ex vivo assays.

This could be most optimally performed with a $P1A_{43-51}$-specific TCR T-cell line, generated through transgenic means with ex vivo primary cells or from transgenic TCR mice. To this end, P1A-specific CD8+ T-cells were isolated from ChAdOx1/MVA P1A vaccinated C57BL/6 mice via FACS sorting of H-$2D^b$ $P1A_{43-51}$ labelled CD8+ T-cells, and their TCR alpha and beta chain sequences determined via single-cell RNA-sequencing. The identification of these sequences

permits the development of transgenic TCR systems with specificity for the $P1A_{43-51}$ epitope. In future, these sequences should be validated, and their ability to generate expression of productive TCRs should be confirmed, alongside confirmation of their specificity. To achieve this, sequences of the most enriched T-cell clonotypes in the sequencing data set have been cloned into retroviral vectors. Retroviruses have been frequently used a means to transduce murine CD8+ T-cells to express transgenic TCRs. In particular, pMIG-II vectors, encoding a mouse stem cell virus (MSCV)-based retrovirus, have been successfully used to generate retrovirus to transduce cells to express OTI TCRs [279]. This involved the linkage of the TCR alpha and TCR beta chains via a cleavable 2A peptide sequence, to generate expression of both TCR subunits in a stoichiometric manner from the same vector. As such, this strategy has been adopted to validate the identified P1A-specific TCR sequences, which have been linked by a T2A peptide, and cloned into pMIG II vectors. These expression vectors require testing and may represent a means for transgenic P1A-specific TCR expression.

Whilst further development is required, taken together, the data presented here represent a useful platform and set of biological tools for further functional study of P1A-specific CD8+ T-cell responses in C57BL/6 mice. As P1A is the only available animal model system for MAGE-type tumour antigens and the majority of transgenic mouse model systems exist in the C57BL/6 background, the identification of immunogenic P1A CTL epitopes in C57BL/6 mice represents an important development for the study of immune responses against MAGE-type antigens.

The identification of P1A-specifc CD8+ T-cell responses in C57BL/6 mice was used as an opportunity to evaluate their anti-tumour capacity in syngeneic tumour models from the H-2^b background commonly used in tumour immunology studies. However, P1A has not been found to be widely endogenously expressed in many murine cancer cell lines [276]. This was confirmed here, as rt-qPCR of P1A expression showed that MC38, B16F10 and EL4 cell lines were found to be P1A-negative. This observation regarding the variable expression of P1A in murine tumour models mimics the situation regarding MAGE-type antigen expression in humans. MAGE-type antigen expression in cancers is characterized by heterogeneity – both between tumours of different patients and at the intra-tumour level regarding the proportion of tumour cells that express a given MAGE-type antigen.

Therefore a physiological and clinically relevant means of inducing P1A expression in tumours was explored, for combination with therapeutic ChAdOx1/MVA P1A vaccination. DNMTis have been shown in a wide range of studies to induce expression of human MAGE-type antigens in previously negative cancer cell lines. Combining DNMTi treatment with a MAGE-targeting ChAdOx1/MVA vaccine would be a highly novel therapy and could help overcome some of the potential limitations associated with a therapeutic cancer vaccine targeting MAGE-type antigens. In particular, it could serve as a means to increase MAGE-type antigen expression in tumours from patients where it is either not present or at a low level. In combination with a MAGE-targeting cancer vaccine, this could both increase the scope of its use by enabling more patients to

be eligible for treatment and to increase vaccine therapeutic potency through increasing the proportion of tumour cells expressing target antigens. This should facilitate more efficacious targeting by MAGE-specific T-cells.

The pre-clinical validation of such a strategy was explored here by evaluating the therapeutic efficacy of a combination of 5-aza-dC treatment and ChAdOx1/MVA P1A vaccination. Guo and colleagues have previously shown that like the human MAGE-type antigens, P1A expression can be induced in previously negative murine cancer lines by 5-aza-dC treatment, likely due to demethylation of the P1A promoter [276]. On this basis, the ability of 5-aza-dC to induce P1A expression in some cancer cell lines of interest for use in syngeneic tumour models that lack natural expression was evaluated. P1A was found to be upregulated in all cell lines tested, confirming the findings of Guo et al. Furthermore 5-aza-dC treatment of MC38 tumour bearing mice was found to strongly upregulate P1A-tumour-expression in vivo, with off-target effects limited to the spleen and bone-marrow. This confirmed this as a promising strategy to induce antigen-expression in P1A-negative tumours. 5-aza-dC has cytotoxic activity, and MC38 tumours formed from cells pre-treated with the compound were found to grow more slowly compared to untreated counterparts. Given DNMTi treatment has been shown to have wide ranging effects on the gene expression profiles of cancer cells, it is also possible that 5-aza-dC treatment alone increased the immunogenicity of MC38 cells, leading to constraint of their growth by T-cell responses. For example, 5-aza-dC treatment has been showing to upregulate expression of surface MHC-class I by cancer cells [280]. However, when 5-aza-dC pre-treated cells were implanted

into C57BL/6 mice, therapeutic ChAdOx1/MVA P1A vaccinations were found to provide a further delay of tumour growth compared to the effect of 5-aza-dC treatment alone. This suggested that the upregulation of antigen-expression in the tumour facilitates recognition by P1A-specific CD8+ T-cells induced by the ChAdOx1/MVA P1A vaccination. However, when 5-aza-dC and ChAdOx1/MVA P1A vaccination were combined together in vivo to treat mice bearing MC38 or EL4 tumours, no therapeutic efficacy was observed.

This could be due to the aggressive growth characteristics of these tumours, which develop very large tumour masses rapidly in a short space of time. This leaves a very short window for two successive therapeutic interventions to demonstrate an anti-tumour effect and halt growth. Particularly in a vaccination setting, where it is classically considered to take 7 days, or longer depending on the platform used, for an adaptive immune response to be generated. Furthermore the models used are known to be profoundly immunosuppressive, exhibiting expression of different suppressive mechanisms [91]. A combination with a third therapeutic intervention in the form of immune checkpoint inhibitors to target this suppression could therefore prove more effective. In the context of the cancer immunity cycle, the DNMTi and vaccine dual treatment only forms two parts of an effective anti-tumour immune response, which is 1) the induction antigen-expression in the tumour, and 2) the generation of antigen-specific CD8+ T-cell immunity. This alone may not be sufficient to achieve tumour regression, and the additional hurdle of tackling immunosuppression in the tumour is likely to have

to be cleared before efficacy is observed. Such an approach still bears much promise therefore, and further investigation is warranted.

Indeed an initial attempt has been made to test such an approach in the clinic, combining decitabine with an NY-ESO-1 vaccine. The only attempt so far has been a small phase I pilot study in EOC patients, using as previously described a poorly immunogenic recombinant NY-ESO-1 vaccine [281]. Induction of some NY-ESO-1 specific CD4+ and CD8+ T-cells were observed following treatment in some patients, although the relative effects of each therapy were not delineated, nor was the effect of treatment on tumour NY-ESO-1 expression. The combination of DNMTis and CPIs has also attracted interest recently, as a means for increasing the effectiveness and response rates of immune checkpoint blockade. As well as increasing expression of MAGE-type antigens, DNMTis have been observed to have other profound effects on gene expression by tumour cells, resulting in enhanced immunogenicity. Chiappinelli and colleagues have demonstrated the enhanced tumour cell immunogenicity by DNMTi treatment results from inducing a type I interferon response by cancer cells [282]. DNMTi treatment was found to hypomethylate endogeneous retroviral (ERV) elements present in the genome which are normally suppressed by methylation. ERV hypomethylation leads to the expression of double-stranded RNAs (dsRNA), which are sensed by cytosolic dsRNA PRRs driving expression of type-I IFNs. They further showed that in a mouse melanoma model, DNMTi treatment sensitized tumours to treatment with anti-CTLA-4 [282]. Amongst other targets, type-I IFN signalling increases the expression of MHC-class I pathway components by tumour cells. A

different study using a mouse colon cancer model demonstrated that decitabine can alter the make-up of the TME to enhance tumour immunogenicity, resulting in an improved therapeutic efficacy when combined with anti-PD-1 treatment compared to either therapeutic used alone [283]. In the clinic, a recent phase II trial in Hodgkin's lymphoma patients, addition of decitabine to anti-PD-1 treatment dramatically improved the complete response rate of patients to therapy compared to anti-PD-1 alone [284]. Furthermore, NSCLC patients who had undergone treatment with DNMTis in clinical trials have been observed to respond to anti-PD-1/anti-PD-L1 blockade at higher than expected rates when entered into subsequent clinical trials for these agents [285]. Tumours from these DNMTi treated patients who responded to anti-PD-L1/anti-PD-1 blockade had gene expression signatures indicating immune activation.

The results from these recent studies demonstrate that the combination of epigenetic and immunotherapy has great potential for improved cancer treatment, and combining therapeutic ChAdOx1/MVA vaccination targeting MAGE-type antigens with DNMTis warrants further investigation, particularly in combination with CPIs. Furthermore its effect on the nature of the tumour immune infiltrate should be explored, particularly whether treatment and subsequent P1A upregulation influences the recruitment of antigen-specific T-cells into the tumour. Another angle to consider is that 5-aza-dC acts systemically and therefore its administration may affect cells other than those of the tumour, such immune cell populations. The effect on the phenotype of ChAdOx1/MVA vaccine induced T-cell responses should also be evaluated.

Chapter 6. Conclusions and future work

6.1 Conclusions and future work

The primary aim of this study was to evaluate the potential of a novel MAGE-type-antigen targeting therapeutic cancer vaccine based on ChAdOx1/MVA in a pre-clinical setting. A therapeutic cancer vaccine targeting MAGE-type antigens has the potential to be an effective strategy for treating cancer patients bearing MAGE-expressing tumours. However, the clinical efficacy of previously developed MAGE-targeting cancer vaccines have been hampered by the use of vaccine platforms that do not readily induce antigen-specific CD8+ T-cell responses [198, 199]. CD8+ T-cells are the critical effectors for carrying out immune-mediated control of tumour growth. The presence of CD8+ TILs in tumours is a positive prognostic factor in many cancer types, and is necessary for the efficacy of recently developed immunotherapeutic approaches such as immune checkpoint blockade [93]. Recently, a vaccination strategy consisting of a heterologous prime-boost with recombinant ChAdOx1 and MVA viral vectors has emerged as a robust platform for inducing potent CD8+ T-cell responses against a wide range of antigens in humans. Therefore here the ChAdOx1/MVA platform was extended to the setting of MAGE-type antigens for the first time.

Immunogenicity studies demonstrated that a heterologous prime-boost with ChAdOx1/MVA encoding the murine MAGE-type antigen P1A was capable of generating very high-magnitude multifunctional P1A-specific CD8+ T-cell responses. The P1A antigen was utilized as it is the best-known murine equivalent of human MAGE-type antigens, most of which do not have direct mouse homologues. This observation was confirmed in two strains of mice tested –

DBA/2 and C57BL/6. These findings confirm for the first time that the ChAdOx1/MVA vaccination is an effective means for inducing MAGE-type antigen-specific CD8+ T-cell responses. Furthermore, fusion of the murine invariant chain (Ii) TMD sequence to the P1A encoded in the ChAdOx1 vector was found increase the magnitude of P1A-specific CD8+ T-cell response elicited by vaccination. This observation confirms findings by others of the positive effect of the Ii TMD sequence on enhancing CD8+ T-cell responses to transgenes encoded in viral vector vaccines, and extends it as a suitable strategy for enhancing MAGE-type antigen-specific CD8+ T-cell responses.

These results combined with the well demonstrated ability of ChAdOx1/MVA to induce CD8+ T-cell responses in humans suggests that this approach could be an improvement over previously developed MAGE-targeting cancer vaccines. The ChAdOx1/MVA platform has been demonstrated to induce some of the most potent CD8+ T-cell responses observed in humans to date against antigens from infectious disease agents and also against prostate cancer antigens [152, 157]. Conversely, most previous MAGE-targeting cancer vaccines have used classical technologies optimized for the infectious disease setting which generate CD4+ T_H and B-cell mediated neutralizing antibody responses, but little in the way of CD8+ cell-mediated immunity that is widely considered to be required for effective anti-tumour responses. Recombinant proteins in adjuvant formulations have been some of the most extensively tested, with an accumulated literature now clearly demonstrating their inability to consistently induce CD8+ T-cell responses in humans [199, 202-204].

In further support of this, therapeutic efficacy of ChAdOx1/MVA P1A vaccination was evaluated using the P1A-expressing 15V4T3 tumour model in DBA/2 mice and found to have potent anti-tumour activity. When administered at early stages of tumour growth, ChAdOx1/MVA P1A vaccination was able to greatly reduce disease progression. Anti-tumour therapeutic efficacy was further enhanced through combination with immune checkpoint inhibitors, with the strongest synergy observed through combination with PD1 blockade. Mice treated with combined ChAdOx1/MVA P1A and anti-PD-1 were better able to reject tumours and had improved survival compared to those receiving vaccine alone. Indeed the regression of larger tumours was found to be dependent on the addition of anti-PD-1, confirming findings from other recent pre-clinical studies that anti-PD-1 blockade is an efficient, and likely necessary, strategy to increase the anti-tumour activity of vaccination by targeting PD-L1 mediated immunosuppression in the TME [155, 156, 264].

Interestingly, ChAdOx1/MVA P1A combined with anti-PD-1 also had far superior therapeutic efficacy than anti-PD-1 used alone. Anti-PD-1 has proved highly effective in the clinic as a monotherapy for some individuals in a range of cancer types, although positive clinical responses are currently limited to a minority of patients. In this study 15V4T3 tumours were found to be largely refractory to anti-PD-1 alone, as monotherapy was rarely observed to delay tumour growth. On this basis, 15V4T3 therefore would appear to mirror the situation in cancer patients, and be a good model of tumours that do not respond to anti-PD-1 treatment. Therapeutic cancer vaccination has been proposed as a

potential strategy to increase the proportion of patients responding to immune-checkpoint blockade, by priming a tumour-specific CD8+ T-cell response. The synergistic effect observed from the combination of ChAdOx1/MVA P1A vaccination and anti-PD-1 treatment against 15V4T3 tumours supports this notion, and confirms that a MAGE-type antigen targeting ChAdOx1/MVA vaccination is a promising approach for enhancing response rates to anti-PD-1 treatment.

Response to anti-PD-1 treatment has become increasingly linked to tumours that have a 'hot' CD8+ T-cell inflamed phenotype. IFN-γ produced by activated CD8+ T-cells and CD8+ T-cell mediated inflammation in the TME has been shown to drive the upregulation of adaptive immune resistance mechanisms such as PD-L1 by tumours [106]. Studies have shown that a CD8+ T-cell driven IFN-γ-related gene expression profile is one of the strongest factors for predicting response to anti-PD-1 blockade [105]. Conversely tumours characterized by the absence of an IFN-γ-related gene expression profile are refractory to treatment. Therapeutic vaccination in this setting could be effective by promoting T-cell infiltration, reversing the non-inflamed 'cold' TME phenotype.

Immune profiling of the 15V4T3 TME revealed that therapeutic ChAdOx1/MVA P1A vaccination greatly increased total and P1A-specific CD8+ T-cell infiltration into the tumour compared to tumours from control mice. Tumours from unvaccinated mice appeared to be poorly infiltrated by CD8+ T-cells and anti-PD-1 treatment alone had no discernible effect on the T-cell profile of the tumour. Increased CD8+ TILs induced by ChAdOx1/MVA P1A vaccination were found to

be functional, with high frequencies of these producing effector cytokines such as IFN-γ. Correspondingly upregulation at the mRNA level of IFN-γ and IFN-γ inducible targets such as PD-L1 and the T-cell chemokine CXCL9 was also observed in tumours from vaccinated mice. Together these observations are highly indicative of a CD8+ T-cell inflamed TME, and suggest that tumours from vaccinated mice may acquire features of the IFN-γ-related gene expression profile defined by Ayers et al underlying responsiveness to anti-PD-1 [105]. Therefore the enhancement of CD8+ T-cell driven inflammation in the tumour by ChAdOx1/MVA P1A vaccination may explain why tumour-bearing vaccinated mice are more permissive to the effects of anti-PD-1 blockade, and the synergy observed between the two therapeutic agents. In future, RNA-sequencing studies of tumours from vaccinated mice might help further inform as to the effects of vaccination.

In further support of this idea, expression of CXCL9 in the TME has been shown to be critical for the recruitment of CD8+ T-cells and activity of the CXCL9/CXCR3 signalling axis in tumours has been shown to be essential for response to anti-PD-1 treatment [116, 118]. Therefore enhanced CD8+ T-cell infiltration and CXCL9 expression induced by ChAdOx1/MVA P1A vaccination may also explain the increased responsiveness of vaccinated mice to anti-PD-1 treatment in the 15V4T3 model. Furthermore, this increased expression of T-cell chemokines is indicative of many aspects of a model of tumour inflammation mediated by cDC1s and CD8+ T-cells and driven through CCL5/CXCL9 signalling that was recently mechanistically determined by Dangaj and colleagues

[119]. A great deal of evidence has recently accumulated showing that the CD8a+/CD103+ cDC1s are indispensable for mediating anti-tumour CD8+ T-cell responses, as they are the key cells producing the CXCR3 ligands CXCL9 and CXCL10 in the TME [117]. These cells likely therefore play a role in the anti-tumour therapeutic responses to vaccination. Further work could examine in in greater detail whether ChAdOx1/MVA P1A influences their recruitment to or activation in the TME.

Such an analysis as described here of the effect of ChAdOx1/MVA vaccination on the T-cell profile of the TME has not so far been performed. Overall, these results confirm a vaccination of ChAdOx1/MVA encoding a MAGE-type antigen is an effective strategy for enhancing CD8+T-cell driven inflammation in the tumour. Taken together with the strong anti-tumour effect observed from therapeutic evaluation of ChAdOx1/MVA P1A + anti-PD-1, these findings suggest that a combination of a ChAdOx1/MVA vaccine encoding a MAGE-type antigen with anti-PD-1 blockade has high potential for translation to a clinical setting.

It is to date unclear the precise mechanism of how PD-1 blockade enhances the effector function of tumour-specific TILs induced by therapeutic cancer vaccination. It is possible that it acts mechanically, to shield effector T-cells from PD-L1 interaction mediated inhibition. However, it may also have phenotypic effects on the responding T-cells. This a highly active area of research and warrants further investigation. A current focus of research in the field is determining the exact phenotype of tumour-specific CD8+ TILs that respond to

PD-1 blockade [286]. Pivotal recent studies have shown that the presence of a population of CD8+ T-cells expressing the transcription factor Tcf1 in tumours is necessary for response to PD-1 blockade [287, 288]. Tcf1+ CD8+ TILs have memory precursor/stem-cell like properties and undergo a proliferative burst in response to anti-PD-1. Future work on therapeutic ChAdOx1/MVA vaccination for treatment of solid tumours and optimization of vaccine design may wish to assess whether the vaccine is capable of inducing CD8+ T-cells of such a phenotype. Future work looking to improve anti-tumour efficacy of vaccination should investigate enhancing the generation of Tcf1+ CD8+ T-cells in the tumour, as this may further enhance the combination with anti-PD-1 blockade. It is also plausible that the anti-tumour effects of anti-PD-1 treatment are exerted in part through effects on other immune cell types such as myeloid cells or NK cells. For example, recent work using systemic and immune-cell constitutive PD-1 KO mice has shown that this may indeed be the case for myeloid cells [289]. Future research should focus on understanding the mechanisms through which anti-PD-1 enhances anti-tumour immunity to enable a more informed rational combination with therapeutic cancer vaccination.

Future pre-clinical work should also look at additional therapeutic combinations to improve ChAdOx1/MVA anti-tumour efficacy. Given the molecular and cellular heterogeneity of tumours, multiple non-redundant suppressive mechanisms are likely to be active in any given tumour. For example, in a clinical trial of anti-CTLA-4 for prostate cancer patients, it was found that expression of PD-L1 and another B7 checkpoint family ligand, VISTA, with T-cell inhibitory

function was upregulated in the tumours of patients post treatment [290]. This suggests therefore that tumours are likely to respond to the lone targeting of immune inhibitory mechanisms with the upregulation of compensatory strategies to acquire secondary adaptive immune resistance. The predominant immunosuppressive mechanisms are also likely to differ between patients. For this reason effective immunotherapeutic treatments will likely need to become increasingly combinatorial in nature, and there is unlikely to be a one-size-fits-all approach. One promising avenue to increasing the therapeutic efficacy of vaccination is through targeting of MDSCs. MDSCs are known to exert profound immunosuppressive effects in the TME [291]. Recently it was shown using a autochthonous murine tumour model that MDSCs expressing FasL can mediate resistance to diverse immunotherapies such as CPIs and vaccination by inducing apoptosis of tumour-specific TILs [292]. Strategies to deplete MDSCs may therefore be a route to increasing therapeutic vaccine efficacy. Indeed a recent study evaluated the combination of synthetic long peptide vaccine against HPV16 E6/E7 oncoantigens with CarboTaxel (carboplatin/paclitaxel) chemotherapy in mice, and found that the therapeutic efficacy of vaccination against E6/E7 expressing tumours was enhanced by the addition of chemotherapy [293]. This was linked to chemotherapy induced depletion of MDSCs from the tumour and blood. The addition of CarboTaxel, or other more targeted agents, may therefore increase the efficacy of MAGE-targeting cancer vaccines combined with anti-PD-1, and should be further explored. Combinations with multiple modalities may also need to be done in a highly timed manner, evolving to meet the most prominent

suppressive strategies active in a tumour as they arise. In support of this, Welters et al reported a key time-component to the enhanced anti-tumour efficacy combining CarboTaxel and vaccination, where vaccination was most effective when given after 2-cycles of chemotherapy. Furthermore, a recent report demonstrated that in anti-PD-1 resistant tumours, therapeutic vaccination may only synergize with anti-PD-1 when administered first. Anti-PD-1 was found to induce dysfunctional CD38+ CD8+ TIL, unless a response was primed first by vaccination [294]. Future work will therefore need to pay close attention to the relative timings of different immunomodulators in a multi-combinatorial therapy.

Intra-tumour heterogeneity of MAGE-type antigen expression is a further problem that may need to be overcome by MAGE-type antigen directed immunotherapies. Immunohistochemical (IHC) studies have shown that the proportion of cells expressing MAGE-type antigens at the protein level in tumours can be highly variable. Expression can be widespread, or limited to small foci. Limited numbers of tumour cells expressing the target antigen recognized by vaccine induced CD8+ T-cell effectors on their surface in the context of MHC-class I could conceivably limit therapeutic efficacy. Despite the variability of MAGE-type antigen expression within tumours, a MAGE-vaccine has been shown to induce regression of melanoma metastases in human patients through the phenomenon of antigen spreading [295]. However, the importance of clonal antigen expression for immunotherapy was demonstrated in a recent landmark study by McGranahan and colleagues. They demonstrate that clinical response to anti-PD-1 blockade and increased overall survival in NSCLC patients is

dependent on the presence of CD8+ TILs that recognize antigens expressed by cancer cells with a high degree of clonality throughout tumour [296]. Many studies have shown that DNMTis treatment can upregulate MAGE-type antigen expression by cancer cells. DNMTis therefore represent a highly promising strategy for increasing MAGE-targeting vaccine therapeutic efficacy by increasing antigen expression in patients with tumours where it is low or lacking altogether. Such a strategy would represent a highly novel approach, and one study has started to assess the possibility of this in the clinic [281].

Despite observing that 5-aza-dC treatment of MC38 tumour bearing mice could upregulate P1A expression in tumours, combination of ChAdOx1/MVA P1A vaccine with the DNMTi 5-aza-dC did not demonstrate a significant therapeutic effect. Further investigation is however needed. This may be due to the effects of immunosuppressive mechanisms present in the tumour. Given that PD-L1 is expressed in many murine tumours, including MC38, combination with CPIs would be warranted. Another possibility is that efficacy may also have been limited by 5-aza-dC treatment not acting effectively on all cells throughout the tumour. Most tumours develop a chaotic disorder vasculature and, given that 5-aza-dC was administered here systemically, delivery may have been limited to some areas of the tumour resulting in uneven exposure of tumours cells to the effects of drug treatment. Antigen expression therefore may not have been upregulated in all cells. Such a situation would leave cells not expressing the target antigen invisible to vaccine induced MAGE-antigen specific T-cells and thus resistant to vaccine-mediated anti-tumour control. It would be worth in future

work to examine the extent to which antigen expression is upregulated throughout the tumour, and to determine the proportion of antigen expressing cells by techniques such as IHC or RNA-scope. Intra-tumoural drug delivery methods could be explored if the degree of tumour antigen expression throughout the tumour is found to be less than desirable [297]. Further work should determine how such a combination of DNMTi and vaccination influences the immune profile of the TME. Such an approach of combined DNMTi, therapeutic ChAdOx/MVA vaccination and CPI could be highly effective, by targeting multiple steps of the 'cancer-immunity cycle'; 1) DNMTi could enhance tumour immunogenicity by upregulating tumour MAGE-type antigen-expression, 2) ChAdOx induce tumour-antigen-specific T-cell responses and 3) target immunosuppression in the tumour.

As demonstrated in this project, the P1A antigen is highly useful for the study of tumour-antigen specific CD8+ T-cell responses in murine models in an accurate physiological setting. In this study, P1A-specific CD8+ T-cell responses were studied in C57BL/6 mice for the first time, and a novel P1A CD8+ T-cell epitope, $P1A_{43-51}$, was identified. Translation of the P1A model antigen to the BL/6 setting will be an invaluable tool for investigating immune responses against self-antigens of the MAGE family. Given that the majority of transgenic mouse systems are available on the BL/6 genetic background, this opens up a wide array of avenues for further mechanistic study. This may provide additional tools with which to address some of the aims outlined previously. Further work needs to be

done to validate sequences corresponding to TCRs that recognize the $P1A_{43-51}$ epitope.

The most relevant application of these results is in the human setting. Despite the promising results obtained in mouse models, these can only truly be verified in clinical trials using cancer patients. With a view to clinical translation of the work, ChAdOx1 and MVA vectors encoding the human MAGE-type antigens MAGE-A3 and NY-ESO-1 were constructed. The ability of heterologous prime-boost vaccination with ChAdOx1 and MVA vectors encoding the human MAGE-type antigens MAGE-A3 and NY-ESO-1 to induce antigen-specific CD8+ T-cell responses was evaluated in CD1 mice. Although foreign antigens in a murine system, immunogenicity studies were conducted in a pre-clinical murine setting to evaluate functionality of the vectors and to inform key aspects about optimal vaccination regimen and schedule. A novel dual antigen-prime single-antigen boost strategy has been designed and evaluated. A prime vaccination with ChAdOx1 encoding a dual-antigen MAGE-A3-NY-ESO-1 fusion protein was observed to induce high-magnitude antigen-specific CD8+ and CD4+ T-cells against both MAGE-A3 and NY-ESO-1 simultaneously. It was found that the level of antigen-specific CD8+ T-cell responses primed by ChAdOx1 could then be further boosted against both MAGE-A3 and NY-ESO-1 again simultaneously, or specifically against either antigen of choice following a boost vaccination with MVA encoding either MAGE-A3 or NY-ESO-1 alone. As MAGE-type antigens exhibit both inter and intra tumour heterogeneity in their expression patterns, this capability greatly enhances the utility and scope of the vaccination, in that it

enables the vaccination regime to be tailored depending on the specific expression pattern of an individual's tumour. Theoretically it might enable additive efficacy in patients whose tumours express both antigens, by generating an anti-tumour CD8+ T-cell response on two distinct fronts, reducing the likelihood that a tumour might be able to acquire immune resistance through an antigen-loss mediated escape. These observations demonstrate the high flexibility and specificity of ChAdOx1/MVA prime-boost vaccination for inducing antigen-specific CD8+ T-cell responses. Furthermore, the confirmed expression of MAGE-A3 and NY-ESO-1 in a high proportion of tumours of several malignancies as well as their known CD8+ T-cell immunogenicity makes them highly suitable targets for a therapeutic cancer vaccine strategy. A large number of CTL epitopes from both proteins have been identified and defined covering different HLA class I alleles, and their ability to be naturally processed and presented on the surface of cancer cells resulting in recognition and killing by autologous specific T-cell clones has been experimentally confirmed.

On the basis of the highly positive results presented here from pre-clinical studies evaluating vaccine immunogenicity and therapeutic efficacy in tumour models, work is underway to translate ChAdOx1/MVA MAGE-A3-NY-ESO-1 vaccination into the clinic. At the time of writing, CRUK have agreed to support clinical development of this strategy, in partnership with Ludwig Institute for Cancer Research, and Vaccitech Oncology Limited (VOLT).Vaccination will be combined with anti-PD-1 treatment (pembrolizumab), supported by results from tumour studies presented in this study. The exact cancer indication in which this will be

tried is yet to be decided, but non-small cell lung cancer (NSCLC) is a likely setting. Expression of MAGE-A3 and NY-ESO-1 are both widely detected in tumours of NSCLC patients (Table 1.1). Furthermore, NSCLC is a highly prevalent cancer with low survival rates for which improved treatments are greatly needed [2]. Some, although a low proportion, of NSCLC patients have been seen to derive benefit from PD-1 blockade used a monotherapy [14]. In many countries, PD-1 in combination with carboplatin chemotherapy has already proceeded to become standard of care for the disease [298-300]. Therefore this represents an ideal indication to evaluate its therapeutic efficacy in combination with ChAdOx1/MVA MAGE-A3-NY-ESO-1 vaccination. On the basis of results presented here combination with vaccination has the potential to improve response rates to anti-PD-1 treatment, and improve patient outcomes. To maximise potential benefit from vaccination, patient enrolment will be on the basis of confirmed MAGE-A3 or NY-ESO-1 expression in tumour biopsies by rt-qPCR methods. Pre-GMP batches of virus have now been produced for the ChAdOx1-Ii-MAGE-A3-NY-ESO-1 and MVA-tPA-MAGE-A3 and MVA-tPA-NY-ESO-1 vectors ahead of a clinical trial. From an economic perspective, the cost of ChAdOx/MVA vaccines is lower than other immunotherapeutic approaches, such as adoptive T-cell transfer which requires highly technical personalized production procedures conforming to rigorous good manufacturing practice (GMP) standards making them expensive to perform. A therapeutic ChAdOx1/MVA vaccine targeting MAGE-A3 and NY-ESO-1 can offer a more cost

effective 'off the shelf' approach, making its applicability higher to a wider range of patients.

Translation of the work to the clinic will also give the opportunity to assess aspects of the ChAdOx1/MVA MAGE-A3-NY-ESO-1 vaccine response in the human setting using patient samples. Immunogenicity of the ChAdOx1/MVA MAGE-A3-NY-ESO-1 vaccine can be assessed in the human setting for the first time, to truly benchmark its ability to induce MAGE-A3 and NY-ESO-1 specific CD8+ T-cell responses. Furthermore, questions discussed in chapter 3 surrounding potential immunodominance of NY-ESO-1 directed CD8+ CTL responses over MAGE-A3 can be addressed to further inform future vaccination strategies.

References

1. Collaborators, G.C.o.D., *Global, regional, and national age-sex-specific mortality for 282 causes of death in 195 countries and territories, 1980-2017: a systematic analysis for the Global Burden of Disease Study 2017.* Lancet, 2018. **392**(10159): p. 1736-1788.
2. Bray, F., et al., *Global cancer statistics 2018: GLOBOCAN estimates of incidence and mortality worldwide for 36 cancers in 185 countries.* CA Cancer J Clin, 2018. **68**(6): p. 394-424.
3. Quaresma, M., M.P. Coleman, and B. Rachet, *40-year trends in an index of survival for all cancers combined and survival adjusted for age and sex for each cancer in England and Wales, 1971-2011: a population-based study.* Lancet, 2015. **385**(9974): p. 1206-18.
4. *CRUK RESEARCH STRATEGY: 2017 PROGRESS REPORT*.
5. Kruger, S., et al., *Advances in cancer immunotherapy 2019 - latest trends.* J Exp Clin Cancer Res, 2019. **38**(1): p. 268.
6. Hargadon, K.M., C.E. Johnson, and C.J. Williams, *Immune checkpoint blockade therapy for cancer: An overview of FDA-approved immune checkpoint inhibitors.* Int Immunopharmacol, 2018. **62**: p. 29-39.
7. Ribas, A. and J.D. Wolchok, *Cancer immunotherapy using checkpoint blockade.* Science, 2018. **359**(6382): p. 1350-1355.
8. Rotte, A., *Combination of CTLA-4 and PD-1 blockers for treatment of cancer.* J Exp Clin Cancer Res, 2019. **38**(1): p. 255.
9. Wolchok, J.D., et al., *Overall Survival with Combined Nivolumab and Ipilimumab in Advanced Melanoma.* N Engl J Med, 2017. **377**(14): p. 1345-1356.
10. Hodi, F.S., et al., *Nivolumab plus ipilimumab or nivolumab alone versus ipilimumab alone in advanced melanoma (CheckMate 067): 4-year outcomes of a multicentre, randomised, phase 3 trial.* Lancet Oncol, 2018. **19**(11): p. 1480-1492.
11. Larkin, J., et al., *Five-Year Survival with Combined Nivolumab and Ipilimumab in Advanced Melanoma.* N Engl J Med, 2019. **381**(16): p. 1535-1546.
12. Larkin, J. and M. Gore, *Malignant melanoma (metastatic).* BMJ Clin Evid, 2008. **2008**.
13. Hellmann, M.D., et al., *Nivolumab plus Ipilimumab in Lung Cancer with a High Tumor Mutational Burden.* N Engl J Med, 2018. **378**(22): p. 2093-2104.
14. Brahmer, J., et al., *Nivolumab versus Docetaxel in Advanced Squamous-Cell Non-Small-Cell Lung Cancer.* N Engl J Med, 2015. **373**(2): p. 123-35.
15. Motzer, R.J., et al., *Nivolumab plus Ipilimumab versus Sunitinib in Advanced Renal-Cell Carcinoma.* N Engl J Med, 2018. **378**(14): p. 1277-1290.
16. Overman, M.J., et al., *Nivolumab in patients with metastatic DNA mismatch repair-deficient or microsatellite instability-high colorectal cancer (CheckMate 142): an open-label, multicentre, phase 2 study.* Lancet Oncol, 2017. **18**(9): p. 1182-1191.

17. Overman, M.J., et al., *Durable Clinical Benefit With Nivolumab Plus Ipilimumab in DNA Mismatch Repair-Deficient/Microsatellite Instability-High Metastatic Colorectal Cancer.* J Clin Oncol, 2018. **36**(8): p. 773-779.
18. Qin, S., et al., *Novel immune checkpoint targets: moving beyond PD-1 and CTLA-4.* Mol Cancer, 2019. **18**(1): p. 155.
19. Marin-Acevedo, J.A., et al., *Next generation of immune checkpoint therapy in cancer: new developments and challenges.* J Hematol Oncol, 2018. **11**(1): p. 39.
20. Graham, C., et al., *Cancer immunotherapy with CAR-T cells - behold the future.* Clin Med (Lond), 2018. **18**(4): p. 324-328.
21. Majzner, R.G. and C.L. Mackall, *Clinical lessons learned from the first leg of the CAR T cell journey.* Nat Med, 2019. **25**(9): p. 1341-1355.
22. Guedan, S., et al., *Engineering and Design of Chimeric Antigen Receptors.* Mol Ther Methods Clin Dev, 2019. **12**: p. 145-156.
23. Maude, S.L., et al., *Sustained remissions with CD19-specific chimeric antigen receptor (CAR)-modified T cells in children with relapsed/refractory ALL.* Journal of Clinical Oncology, 2016. **34**(15_suppl): p. 3011-3011.
24. Maude, S.L., et al., *Chimeric antigen receptor T cells for sustained remissions in leukemia.* N Engl J Med, 2014. **371**(16): p. 1507-17.
25. Maude, S.L., et al., *Tisagenlecleucel in Children and Young Adults with B-Cell Lymphoblastic Leukemia.* N Engl J Med, 2018. **378**(5): p. 439-448.
26. Park, J.H., et al., *Long-Term Follow-up of CD19 CAR Therapy in Acute Lymphoblastic Leukemia.* N Engl J Med, 2018. **378**(5): p. 449-459.
27. Schuster, S.J., et al., *Chimeric Antigen Receptor T Cells in Refractory B-Cell Lymphomas.* N Engl J Med, 2017. **377**(26): p. 2545-2554.
28. Neelapu, S.S., et al., *Axicabtagene Ciloleucel CAR T-Cell Therapy in Refractory Large B-Cell Lymphoma.* N Engl J Med, 2017. **377**(26): p. 2531-2544.
29. Locke, F.L., et al., *Long-term safety and activity of axicabtagene ciloleucel in refractory large B-cell lymphoma (ZUMA-1): a single-arm, multicentre, phase 1-2 trial.* Lancet Oncol, 2019. **20**(1): p. 31-42.
30. O'Leary, M.C., et al., *FDA Approval Summary: Tisagenlecleucel for Treatment of Patients with Relapsed or Refractory B-cell Precursor Acute Lymphoblastic Leukemia.* Clin Cancer Res, 2019. **25**(4): p. 1142-1146.
31. Bouchkouj, N., et al., *FDA Approval Summary: Axicabtagene Ciloleucel for Relapsed or Refractory Large B-cell Lymphoma.* Clin Cancer Res, 2019. **25**(6): p. 1702-1708.
32. Larkin, J., et al., *Combined Nivolumab and Ipilimumab or Monotherapy in Untreated Melanoma.* N Engl J Med, 2015. **373**(1): p. 23-34.
33. Motzer, R.J., et al., *Nivolumab versus Everolimus in Advanced Renal-Cell Carcinoma.* N Engl J Med, 2015. **373**(19): p. 1803-13.
34. Postow, M.A., R. Sidlow, and M.D. Hellmann, *Immune-Related Adverse Events Associated with Immune Checkpoint Blockade.* N Engl J Med, 2018. **378**(2): p. 158-168.

35. Michot, J.M., et al., *Immune-related adverse events with immune checkpoint blockade: a comprehensive review.* Eur J Cancer, 2016. **54**: p. 139-148.
36. Neelapu, S.S., et al., *Chimeric antigen receptor T-cell therapy - assessment and management of toxicities.* Nat Rev Clin Oncol, 2018. **15**(1): p. 47-62.
37. Verma, V., et al., *A systematic review of the cost and cost-effectiveness studies of immune checkpoint inhibitors.* J Immunother Cancer, 2018. **6**(1): p. 128.
38. Haslam, A. and V. Prasad, *Estimation of the Percentage of US Patients With Cancer Who Are Eligible for and Respond to Checkpoint Inhibitor Immunotherapy Drugs.* JAMA Netw Open, 2019. **2**(5): p. e192535.
39. Lin, J.K., et al., *Cost Effectiveness of Chimeric Antigen Receptor T-Cell Therapy in Relapsed or Refractory Pediatric B-Cell Acute Lymphoblastic Leukemia.* J Clin Oncol, 2018: p. JCO2018790642.
40. Lin, J.K., et al., *Cost Effectiveness of Chimeric Antigen Receptor T-Cell Therapy in Multiply Relapsed or Refractory Adult Large B-Cell Lymphoma.* J Clin Oncol, 2019. **37**(24): p. 2105-2119.
41. Chen, D.S. and I. Mellman, *Oncology meets immunology: the cancer-immunity cycle.* Immunity, 2013. **39**(1): p. 1-10.
42. Banchereau, J. and R.M. Steinman, *Dendritic cells and the control of immunity.* Nature, 1998. **392**(6673): p. 245-52.
43. Embgenbroich, M. and S. Burgdorf, *Current Concepts of Antigen Cross-Presentation.* Front Immunol, 2018. **9**: p. 1643.
44. Mildner, A. and S. Jung, *Development and function of dendritic cell subsets.* Immunity, 2014. **40**(5): p. 642-56.
45. Böttcher, J.P. and C. Reis E Sousa, *The Role of Type 1 Conventional Dendritic Cells in Cancer Immunity.* Trends Cancer, 2018. **4**(11): p. 784-792.
46. Hildner, K., et al., *Batf3 deficiency reveals a critical role for CD8alpha+ dendritic cells in cytotoxic T cell immunity.* Science, 2008. **322**(5904): p. 1097-100.
47. Jongbloed, S.L., et al., *Human CD141+ (BDCA-3)+ dendritic cells (DCs) represent a unique myeloid DC subset that cross-presents necrotic cell antigens.* J Exp Med, 2010. **207**(6): p. 1247-60.
48. Bachem, A., et al., *Superior antigen cross-presentation and XCR1 expression define human CD11c+CD141+ cells as homologues of mouse CD8+ dendritic cells.* J Exp Med, 2010. **207**(6): p. 1273-81.
49. Sancho, D., et al., *Identification of a dendritic cell receptor that couples sensing of necrosis to immunity.* Nature, 2009. **458**(7240): p. 899-903.
50. Woo, S.R., et al., *STING-dependent cytosolic DNA sensing mediates innate immune recognition of immunogenic tumors.* Immunity, 2014. **41**(5): p. 830-42.
51. Corrales, L., et al., *Direct Activation of STING in the Tumor Microenvironment Leads to Potent and Systemic Tumor Regression and Immunity.* Cell Rep, 2015. **11**(7): p. 1018-30.
52. Broz, M.L., et al., *Dissecting the tumor myeloid compartment reveals rare activating antigen-presenting cells critical for T cell immunity.* Cancer Cell, 2014. **26**(5): p. 638-52.

53. Sánchez-Paulete, A.R., et al., *Cancer Immunotherapy with Immunomodulatory Anti-CD137 and Anti-PD-1 Monoclonal Antibodies Requires BATF3-Dependent Dendritic Cells.* Cancer Discov, 2016. **6**(1): p. 71-9.
54. Jenkins, M.K., et al., *CD28 delivers a costimulatory signal involved in antigen-specific IL-2 production by human T cells.* J Immunol, 1991. **147**(8): p. 2461-6.
55. Harding, F.A., et al., *CD28-mediated signalling co-stimulates murine T cells and prevents induction of anergy in T-cell clones.* Nature, 1992. **356**(6370): p. 607-9.
56. Curtsinger, J.M., et al., *Inflammatory cytokines provide a third signal for activation of naive CD4+ and CD8+ T cells.* J Immunol, 1999. **162**(6): p. 3256-62.
57. Curtsinger, J.M., D.C. Lins, and M.F. Mescher, *Signal 3 determines tolerance versus full activation of naive CD8 T cells: dissociating proliferation and development of effector function.* J Exp Med, 2003. **197**(9): p. 1141-51.
58. Henry, C.J., et al., *IL-12 produced by dendritic cells augments CD8+ T cell activation through the production of the chemokines CCL1 and CCL17.* J Immunol, 2008. **181**(12): p. 8576-84.
59. Díaz-Montero, C.M., et al., *Priming of naive CD8+ T cells in the presence of IL-12 selectively enhances the survival of CD8+CD62Lhi cells and results in superior anti-tumor activity in a tolerogenic murine model.* Cancer Immunol Immunother, 2008. **57**(4): p. 563-72.
60. Szabo, S.J., et al., *A novel transcription factor, T-bet, directs Th1 lineage commitment.* Cell, 2000. **100**(6): p. 655-69.
61. Sullivan, B.M., et al., *Antigen-driven effector CD8 T cell function regulated by T-bet.* Proc Natl Acad Sci U S A, 2003. **100**(26): p. 15818-23.
62. Szabo, S.J., et al., *Distinct effects of T-bet in TH1 lineage commitment and IFN-gamma production in CD4 and CD8 T cells.* Science, 2002. **295**(5553): p. 338-42.
63. Chen, A.I., et al., *Ox40-ligand has a critical costimulatory role in dendritic cell:T cell interactions.* Immunity, 1999. **11**(6): p. 689-98.
64. Gramaglia, I., et al., *Ox-40 ligand: a potent costimulatory molecule for sustaining primary CD4 T cell responses.* J Immunol, 1998. **161**(12): p. 6510-7.
65. De Smedt, T., et al., *Ox40 costimulation enhances the development of T cell responses induced by dendritic cells in vivo.* J Immunol, 2002. **168**(2): p. 661-70.
66. Bansal-Pakala, P., et al., *Costimulation of CD8 T cell responses by OX40.* J Immunol, 2004. **172**(8): p. 4821-5.
67. Shuford, W.W., et al., *4-1BB costimulatory signals preferentially induce CD8+ T cell proliferation and lead to the amplification in vivo of cytotoxic T cell responses.* J Exp Med, 1997. **186**(1): p. 47-55.
68. Taraban, V.Y., et al., *Expression and costimulatory effects of the TNF receptor superfamily members CD134 (OX40) and CD137 (4-1BB), and their role in the generation of anti-tumor immune responses.* Eur J Immunol, 2002. **32**(12): p. 3617-27.
69. Martínez-Lostao, L., A. Anel, and J. Pardo, *How Do Cytotoxic Lymphocytes Kill Cancer Cells?* Clin Cancer Res, 2015. **21**(22): p. 5047-56.

70. Böhm, W., et al., *T cell-mediated, IFN-gamma-facilitated rejection of murine B16 melanomas.* J Immunol, 1998. **161**(2): p. 897-908.
71. Tuttle, T.M., et al., *gamma-Interferon plays a key role in T-cell-induced tumor regression.* Cancer Res, 1993. **53**(4): p. 833-9.
72. Dobrzanski, M.J., J.B. Reome, and R.W. Dutton, *Immunopotentiating role of IFN-gamma in early and late stages of type 1 CD8 effector cell-mediated tumor rejection.* Clin Immunol, 2001. **98**(1): p. 70-84.
73. van den Broek, M.E., et al., *Decreased tumor surveillance in perforin-deficient mice.* J Exp Med, 1996. **184**(5): p. 1781-90.
74. Prévost-Blondel, A., et al., *Differential requirement of perforin and IFN-gamma in CD8 T cell-mediated immune responses against B16.F10 melanoma cells expressing a viral antigen.* Eur J Immunol, 2000. **30**(9): p. 2507-15.
75. Smyth, M.J., et al., *Perforin-mediated cytotoxicity is critical for surveillance of spontaneous lymphoma.* J Exp Med, 2000. **192**(5): p. 755-60.
76. Barth, R.J., et al., *Interferon gamma and tumor necrosis factor have a role in tumor regressions mediated by murine CD8+ tumor-infiltrating lymphocytes.* J Exp Med, 1991. **173**(3): p. 647-58.
77. Schoenberger, S.P., et al., *T-cell help for cytotoxic T lymphocytes is mediated by CD40-CD40L interactions.* Nature, 1998. **393**(6684): p. 480-3.
78. Paul, S. and G. Lal, *The Molecular Mechanism of Natural Killer Cells Function and Its Importance in Cancer Immunotherapy.* Front Immunol, 2017. **8**: p. 1124.
79. Chiossone, L., et al., *Natural killer cells and other innate lymphoid cells in cancer.* Nat Rev Immunol, 2018. **18**(11): p. 671-688.
80. Karlhofer, F.M., R.K. Ribaudo, and W.M. Yokoyama, *MHC class I alloantigen specificity of Ly-49+ IL-2-activated natural killer cells.* Nature, 1992. **358**(6381): p. 66-70.
81. Sivori, S., et al., *p46, a novel natural killer cell-specific surface molecule that mediates cell activation.* J Exp Med, 1997. **186**(7): p. 1129-36.
82. Bauer, S., et al., *Activation of NK cells and T cells by NKG2D, a receptor for stress-inducible MICA.* Science, 1999. **285**(5428): p. 727-9.
83. Li, Z., et al., *Cross-talk between T cells and innate immune cells is crucial for IFN-gamma-dependent tumor rejection.* J Immunol, 2007. **179**(3): p. 1568-76.
84. Böttcher, J.P., et al., *NK Cells Stimulate Recruitment of cDC1 into the Tumor Microenvironment Promoting Cancer Immune Control.* Cell, 2018. **172**(5): p. 1022-1037.e14.
85. Allen, F., et al., *CCL3 augments tumor rejection and enhances CD8+ T cell infiltration through NK and CD103+ dendritic cell recruitment via IFN γ.* Oncoimmunology, 2018. **7**(3): p. e1393598.
86. Gajewski, T.F., H. Schreiber, and Y.X. Fu, *Innate and adaptive immune cells in the tumor microenvironment.* Nat Immunol, 2013. **14**(10): p. 1014-22.
87. Spranger, S., *Mechanisms of tumor escape in the context of the T-cell-inflamed and the non-T-cell-inflamed tumor microenvironment.* Int Immunol, 2016. **28**(8): p. 383-91.

88. Freeman, G.J., et al., *Engagement of the PD-1 immunoinhibitory receptor by a novel B7 family member leads to negative regulation of lymphocyte activation.* J Exp Med, 2000. **192**(7): p. 1027-34.
89. Dong, H., et al., *Tumor-associated B7-H1 promotes T-cell apoptosis: a potential mechanism of immune evasion.* Nat Med, 2002. **8**(8): p. 793-800.
90. Ahmadzadeh, M., et al., *Tumor antigen-specific CD8 T cells infiltrating the tumor express high levels of PD-1 and are functionally impaired.* Blood, 2009. **114**(8): p. 1537-44.
91. Juneja, V.R., et al., *PD-L1 on tumor cells is sufficient for immune evasion in immunogenic tumors and inhibits CD8 T cell cytotoxicity.* J Exp Med, 2017. **214**(4): p. 895-904.
92. Krummel, M.F. and J.P. Allison, *CTLA-4 engagement inhibits IL-2 accumulation and cell cycle progression upon activation of resting T cells.* J Exp Med, 1996. **183**(6): p. 2533-40.
93. Tumeh, P.C., et al., *PD-1 blockade induces responses by inhibiting adaptive immune resistance.* Nature, 2014. **515**(7528): p. 568-71.
94. Spranger, S., et al., *Mechanism of tumor rejection with doublets of CTLA-4, PD-1/PD-L1, or IDO blockade involves restored IL-2 production and proliferation of CD8(+) T cells directly within the tumor microenvironment.* J Immunother Cancer, 2014. **2**: p. 3.
95. Uyttenhove, C., et al., *Evidence for a tumoral immune resistance mechanism based on tryptophan degradation by indoleamine 2,3-dioxygenase.* Nat Med, 2003. **9**(10): p. 1269-74.
96. Kumar, V. and D.I. Gabrilovich, *Hypoxia-inducible factors in regulation of immune responses in tumour microenvironment.* Immunology, 2014. **143**(4): p. 512-9.
97. Togashi, Y., K. Shitara, and H. Nishikawa, *Regulatory T cells in cancer immunosuppression - implications for anticancer therapy.* Nat Rev Clin Oncol, 2019. **16**(6): p. 356-371.
98. Chen, M.L., et al., *Regulatory T cells suppress tumor-specific CD8 T cell cytotoxicity through TGF-beta signals in vivo.* Proc Natl Acad Sci U S A, 2005. **102**(2): p. 419-24.
99. Raber, P.L., et al., *Subpopulations of myeloid-derived suppressor cells impair T cell responses through independent nitric oxide-related pathways.* Int J Cancer, 2014. **134**(12): p. 2853-64.
100. Selby, M.J., et al., *Anti-CTLA-4 antibodies of IgG2a isotype enhance antitumor activity through reduction of intratumoral regulatory T cells.* Cancer Immunol Res, 2013. **1**(1): p. 32-42.
101. Simpson, T.R., et al., *Fc-dependent depletion of tumor-infiltrating regulatory T cells co-defines the efficacy of anti-CTLA-4 therapy against melanoma.* J Exp Med, 2013. **210**(9): p. 1695-710.
102. Bonaventura, P., et al., *Cold Tumors: A Therapeutic Challenge for Immunotherapy.* Front Immunol, 2019. **10**: p. 168.

103. Danilova, L., et al., *Association of PD-1/PD-L axis expression with cytolytic activity, mutational load, and prognosis in melanoma and other solid tumors.* Proc Natl Acad Sci U S A, 2016. **113**(48): p. E7769-E7777.
104. Gajewski, T.F., et al., *Cancer Immunotherapy Targets Based on Understanding the T Cell-Inflamed Versus Non-T Cell-Inflamed Tumor Microenvironment.* Adv Exp Med Biol, 2017. **1036**: p. 19-31.
105. Ayers, M., et al., *IFN-γ-related mRNA profile predicts clinical response to PD-1 blockade.* J Clin Invest, 2017. **127**(8): p. 2930-2940.
106. Spranger, S., et al., *Up-regulation of PD-L1, IDO, and T(regs) in the melanoma tumor microenvironment is driven by CD8(+) T cells.* Sci Transl Med, 2013. **5**(200): p. 200ra116.
107. Ji, R.R., et al., *An immune-active tumor microenvironment favors clinical response to ipilimumab.* Cancer Immunol Immunother, 2012. **61**(7): p. 1019-31.
108. Dunn, G.P., L.J. Old, and R.D. Schreiber, *The three Es of cancer immunoediting.* Annu Rev Immunol, 2004. **22**: p. 329-60.
109. Bai, X.F., et al., *Antigenic drift as a mechanism for tumor evasion of destruction by cytolytic T lymphocytes.* J Clin Invest, 2003. **111**(10): p. 1487-96.
110. Uyttenhove, C., J. Maryanski, and T. Boon, *Escape of mouse mastocytoma P815 after nearly complete rejection is due to antigen-loss variants rather than immunosuppression.* J Exp Med, 1983. **157**(3): p. 1040-52.
111. Zheng, P., et al., *Two mechanisms for tumor evasion of preexisting cytotoxic T-cell responses: lessons from recurrent tumors.* Cancer Res, 1999. **59**(14): p. 3461-7.
112. Spranger, S., et al., *Density of immunogenic antigens does not explain the presence or absence of the T-cell-inflamed tumor microenvironment in melanoma.* Proc Natl Acad Sci U S A, 2016. **113**(48): p. E7759-E7768.
113. Pitt, J.M., G. Kroemer, and L. Zitvogel, *Immunogenic and Non-immunogenic Cell Death in the Tumor Microenvironment.* Adv Exp Med Biol, 2017. **1036**: p. 65-79.
114. Kunz, M., et al., *Strong expression of the lymphoattractant C-X-C chemokine Mig is associated with heavy infiltration of T cells in human malignant melanoma.* J Pathol, 1999. **189**(4): p. 552-8.
115. Harlin, H., et al., *Chemokine expression in melanoma metastases associated with CD8+ T-cell recruitment.* Cancer Res, 2009. **69**(7): p. 3077-85.
116. Mikucki, M.E., et al., *Non-redundant requirement for CXCR3 signalling during tumoricidal T-cell trafficking across tumour vascular checkpoints.* Nat Commun, 2015. **6**: p. 7458.
117. Spranger, S., et al., *Tumor-Residing Batf3 Dendritic Cells Are Required for Effector T Cell Trafficking and Adoptive T Cell Therapy.* Cancer Cell, 2017. **31**(5): p. 711-723.e4.

118. Chow, M.T., et al., *Intratumoral Activity of the CXCR3 Chemokine System Is Required for the Efficacy of Anti-PD-1 Therapy.* Immunity, 2019. **50**(6): p. 1498-1512.e5.
119. Dangaj, D., et al., *Cooperation between Constitutive and Inducible Chemokines Enables T Cell Engraftment and Immune Attack in Solid Tumors.* Cancer Cell, 2019. **35**(6): p. 885-900.e10.
120. Melief, C.J., et al., *Therapeutic cancer vaccines.* J Clin Invest, 2015. **125**(9): p. 3401-12.
121. Hollingsworth, R.E. and K. Jansen, *Turning the corner on therapeutic cancer vaccines.* NPJ Vaccines, 2019. **4**: p. 7.
122. Cheever, M.A. and C.S. Higano, *PROVENGE (Sipuleucel-T) in prostate cancer: the first FDA-approved therapeutic cancer vaccine.* Clin Cancer Res, 2011. **17**(11): p. 3520-6.
123. Kantoff, P.W., et al., *Sipuleucel-T immunotherapy for castration-resistant prostate cancer.* N Engl J Med, 2010. **363**(5): p. 411-22.
124. Kantoff, P.W., et al., *Overall survival analysis of a phase II randomized controlled trial of a Poxviral-based PSA-targeted immunotherapy in metastatic castration-resistant prostate cancer.* J Clin Oncol, 2010. **28**(7): p. 1099-105.
125. Gulley, J.L., et al., *Phase III Trial of PROSTVAC in Asymptomatic or Minimally Symptomatic Metastatic Castration-Resistant Prostate Cancer.* J Clin Oncol, 2019. **37**(13): p. 1051-1061.
126. *PROSTVAC in Combination With Nivolumab in Men With Prostate Cancer (NCT02933255).*
127. *Neoadjuvant PROSTVAC-VF With or Without Ipilimumab for Prostate Cancer (NCT02506114).* Available from: https://clinicaltrials.gov/ct2/show/NCT02506114.
128. Gilbert, S.C., *T-cell-inducing vaccines - what's the future.* Immunology, 2012. **135**(1): p. 19-26.
129. Rollier, C.S., et al., *Viral vectors as vaccine platforms: deployment in sight.* Curr Opin Immunol, 2011. **23**(3): p. 377-82.
130. van Montfoort, N., E. van der Aa, and A.M. Woltman, *Understanding MHC class I presentation of viral antigens by human dendritic cells as a basis for rational design of therapeutic vaccines.* Front Immunol, 2014. **5**: p. 182.
131. Albert, M.L., B. Sauter, and N. Bhardwaj, *Dendritic cells acquire antigen from apoptotic cells and induce class I-restricted CTLs.* Nature, 1998. **392**(6671): p. 86-9.
132. Subklewe, M., et al., *Dendritic cells cross-present latency gene products from Epstein-Barr virus-transformed B cells and expand tumor-reactive CD8(+) killer T cells.* J Exp Med, 2001. **193**(3): p. 405-11.
133. Dolan, B.P., K.D. Gibbs, and S. Ostrand-Rosenberg, *Dendritic cells cross-dressed with peptide MHC class I complexes prime CD8+ T cells.* J Immunol, 2006. **177**(9): p. 6018-24.

134. Bonaldo, M.C., et al., *Construction and characterization of recombinant flaviviruses bearing insertions between E and NS1 genes.* Virol J, 2007. **4**: p. 115.
135. Bonaldo, M.C., et al., *Recombinant yellow fever vaccine virus 17D expressing simian immunodeficiency virus SIVmac239 gag induces SIV-specific CD8+ T-cell responses in rhesus macaques.* J Virol, 2010. **84**(7): p. 3699-706.
136. Hansen, S.G., et al., *Effector memory T cell responses are associated with protection of rhesus monkeys from mucosal simian immunodeficiency virus challenge.* Nat Med, 2009. **15**(3): p. 293-9.
137. Larocca, C. and J. Schlom, *Viral vector-based therapeutic cancer vaccines.* Cancer J, 2011. **17**(5): p. 359-71.
138. Capone, S., et al., *Development of chimpanzee adenoviruses as vaccine vectors: challenges and successes emerging from clinical trials.* Expert Rev Vaccines, 2013. **12**(4): p. 379-93.
139. Gilbert, S.C., et al., *Enhanced CD8 T cell immunogenicity and protective efficacy in a mouse malaria model using a recombinant adenoviral vaccine in heterologous prime-boost immunisation regimes.* Vaccine, 2002. **20**(7-8): p. 1039-45.
140. Rodrigues, E.G., et al., *Single immunizing dose of recombinant adenovirus efficiently induces CD8+ T cell-mediated protective immunity against malaria.* J Immunol, 1997. **158**(3): p. 1268-74.
141. Shiver, J.W., et al., *Replication-incompetent adenoviral vaccine vector elicits effective anti-immunodeficiency-virus immunity.* Nature, 2002. **415**(6869): p. 331-5.
142. Reyes-Sandoval, A., et al., *Prime-boost immunization with adenoviral and modified vaccinia virus Ankara vectors enhances the durability and polyfunctionality of protective malaria CD8+ T-cell responses.* Infect Immun, 2010. **78**(1): p. 145-53.
143. Swadling, L., et al., *A human vaccine strategy based on chimpanzee adenoviral and MVA vectors that primes, boosts, and sustains functional HCV-specific T cell memory.* Sci Transl Med, 2014. **6**(261): p. 261ra153.
144. Nwanegbo, E., et al., *Prevalence of neutralizing antibodies to adenoviral serotypes 5 and 35 in the adult populations of The Gambia, South Africa, and the United States.* Clin Diagn Lab Immunol, 2004. **11**(2): p. 351-7.
145. Ersching, J., et al., *Neutralizing antibodies to human and simian adenoviruses in humans and New-World monkeys.* Virology, 2010. **407**(1): p. 1-6.
146. Dudareva, M., et al., *Prevalence of serum neutralizing antibodies against chimpanzee adenovirus 63 and human adenovirus 5 in Kenyan children, in the context of vaccine vector efficacy.* Vaccine, 2009. **27**(27): p. 3501-4.
147. Reyes-Sandoval, A., et al., *Single-dose immunogenicity and protective efficacy of simian adenoviral vectors against Plasmodium berghei.* Eur J Immunol, 2008. **38**(3): p. 732-41.
148. Sridhar, S., et al., *Single-dose protection against Plasmodium berghei by a simian adenovirus vector using a human cytomegalovirus promoter containing intron A.* J Virol, 2008. **82**(8): p. 3822-33.

149. Morris, S.J., et al., *Simian adenoviruses as vaccine vectors.* Future Virol, 2016. **11**(9): p. 649-659.
150. O'Hara, G.A., et al., *Clinical assessment of a recombinant simian adenovirus ChAd63: a potent new vaccine vector.* J Infect Dis, 2012. **205**(5): p. 772-81.
151. Sheehy, S.H., et al., *Phase Ia clinical evaluation of the Plasmodium falciparum blood-stage antigen MSP1 in ChAd63 and MVA vaccine vectors.* Mol Ther, 2011. **19**(12): p. 2269-76.
152. Ewer, K.J., et al., *Protective CD8+ T-cell immunity to human malaria induced by chimpanzee adenovirus-MVA immunisation.* Nat Commun, 2013. **4**: p. 2836.
153. Dicks, M.D., et al., *A novel chimpanzee adenovirus vector with low human seroprevalence: improved systems for vector derivation and comparative immunogenicity.* PLoS One, 2012. **7**(7): p. e40385.
154. Stylianou, E., et al., *Improvement of BCG protective efficacy with a novel chimpanzee adenovirus and a modified vaccinia Ankara virus both expressing Ag85A.* Vaccine, 2015. **33**(48): p. 6800-8.
155. Cappuccini, F., et al., *Immunogenicity and efficacy of the novel cancer vaccine based on simian adenovirus and MVA vectors alone and in combination with PD-1 mAb in a mouse model of prostate cancer.* Cancer Immunol Immunother, 2016. **65**(6): p. 701-13.
156. Cappuccini, F., et al., *5T4 oncofoetal glycoprotein: an old target for a novel prostate cancer immunotherapy.* Oncotarget, 2017. **8**(29): p. 47474-47489.
157. Redchenko, I., et al., *VANCE: First-in-human phase I study of a novel ChAdOx1-MVA 5T4 vaccine in low and intermediate risk prostate cancer.* Journal of Clinical Oncology, 2018. **36**(15_suppl): p. 3018-3018.
158. Coulie, P.G., et al., *Tumour antigens recognized by T lymphocytes: at the core of cancer immunotherapy.* Nat Rev Cancer, 2014. **14**(2): p. 135-46.
159. Ninkovic, T. and F.G. Hanisch, *O-glycosylated human MUC1 repeats are processed in vitro by immunoproteasomes.* J Immunol, 2007. **179**(4): p. 2380-8.
160. Stepensky, D., et al., *O-glycosylated versus non-glycosylated MUC1-derived peptides as potential targets for cytotoxic immunotherapy of carcinoma.* Clin Exp Immunol, 2006. **143**(1): p. 139-49.
161. Lakshminarayanan, V., et al., *Immune recognition of tumor-associated mucin MUC1 is achieved by a fully synthetic aberrantly glycosylated MUC1 tripartite vaccine.* Proc Natl Acad Sci U S A, 2012. **109**(1): p. 261-6.
162. Brentville, V.A., et al., *Citrullinated Vimentin Presented on MHC-II in Tumor Cells Is a Target for CD4+ T-Cell-Mediated Antitumor Immunity.* Cancer Res, 2016. **76**(3): p. 548-60.
163. Scanlan, M.J., et al., *Cancer/testis antigens: an expanding family of targets for cancer immunotherapy.* Immunol Rev, 2002. **188**: p. 22-32.
164. De Plaen, E., et al., *Structure, chromosomal localization, and expression of 12 genes of the MAGE family.* Immunogenetics, 1994. **40**(5): p. 360-9.

165. Almeida, L.G., et al., *CTdatabase: a knowledge-base of high-throughput and curated data on cancer-testis antigens.* Nucleic Acids Res, 2009. **37**(Database issue): p. D816-9.
166. De Smet, C., et al., *DNA methylation is the primary silencing mechanism for a set of germ line- and tumor-specific genes with a CpG-rich promoter.* Mol Cell Biol, 1999. **19**(11): p. 7327-35.
167. James, S.R., P.A. Link, and A.R. Karpf, *Epigenetic regulation of X-linked cancer/germline antigen genes by DNMT1 and DNMT3b.* Oncogene, 2006. **25**(52): p. 6975-85.
168. De Smet, C., et al., *The activation of human gene MAGE-1 in tumor cells is correlated with genome-wide demethylation.* Proc Natl Acad Sci U S A, 1996. **93**(14): p. 7149-53.
169. Gjerstorff, M.F., M.H. Andersen, and H.J. Ditzel, *Oncogenic cancer/testis antigens: prime candidates for immunotherapy.* Oncotarget, 2015. **6**(18): p. 15772-87.
170. Van den Eynde, B., et al., *Presence on a human melanoma of multiple antigens recognized by autologous CTL.* Int J Cancer, 1989. **44**(4): p. 634-40.
171. van der Bruggen, P., et al., *A gene encoding an antigen recognized by cytolytic T lymphocytes on a human melanoma.* Science, 1991. **254**(5038): p. 1643-7.
172. Brändle, D., et al., *The shared tumor-specific antigen encoded by mouse gene P1A is a target not only for cytolytic T lymphocytes but also for tumor rejection.* Eur J Immunol, 1998. **28**(12): p. 4010-9.
173. Vigneron, N., et al., *Database of T cell-defined human tumor antigens: the 2013 update.* Cancer Immun, 2013. **13**: p. 15.
174. Zajac, P., et al., *MAGE-A Antigens and Cancer Immunotherapy.* Front Med (Lausanne), 2017. **4**: p. 18.
175. Thomas, R., et al., *NY-ESO-1 Based Immunotherapy of Cancer: Current Perspectives.* Front Immunol, 2018. **9**: p. 947.
176. Gure, A.O., et al., *Cancer-testis genes are coordinately expressed and are markers of poor outcome in non-small cell lung cancer.* Clin Cancer Res, 2005. **11**(22): p. 8055-62.
177. Brisam, M., et al., *Expression of MAGE-A1-A12 subgroups in the invasive tumor front and tumor center in oral squamous cell carcinoma.* Oncol Rep, 2016. **35**(4): p. 1979-86.
178. Szender, J.B., et al., *NY-ESO-1 expression predicts an aggressive phenotype of ovarian cancer.* Gynecol Oncol, 2017. **145**(3): p. 420-425.
179. van Rhee, F., et al., *NY-ESO-1 is highly expressed in poor-prognosis multiple myeloma and induces spontaneous humoral and cellular immune responses.* Blood, 2005. **105**(10): p. 3939-44.
180. Grah, J., et al., *Immunohystochemical expression of cancer/testis antigens (MAGE-A3/4, NY-ESO-1) in non-small cell lung cancer: the relationship with clinical-pathological features.* Coll Antropol, 2008. **32**(3): p. 731-6.

181. Boon, T., et al., *Genes coding for tumor-specific rejection antigens.* Cold Spring Harb Symp Quant Biol, 1994. **59**: p. 617-22.
182. Gaugler, B., et al., *Human gene MAGE-3 codes for an antigen recognized on a melanoma by autologous cytolytic T lymphocytes.* J Exp Med, 1994. **179**(3): p. 921-30.
183. Scheibenbogen, C., et al., *Analysis of the T cell response to tumor and viral peptide antigens by an IFNgamma-ELISPOT assay.* Int J Cancer, 1997. **71**(6): p. 932-6.
184. *CTdatabase*. [cited 2019 September]; Available from: http://www.cta.lncc.br.
185. *Cancer Antigenic Peptide Database*. [cited 2019 September]; Available from: https://caped.icp.ucl.ac.be.
186. Chen, Y.T., et al., *A testicular antigen aberrantly expressed in human cancers detected by autologous antibody screening.* Proc Natl Acad Sci U S A, 1997. **94**(5): p. 1914-8.
187. Gnjatic, S., *Naturally occurring immunogenicity of NY-ESO-1 in cancer patients.* Cancer Immunity Archive, 2003. **3**(Suppl 2): p. 15.
188. Valmori, D., et al., *Naturally occurring human lymphocyte antigen-A2 restricted CD8+ T-cell response to the cancer testis antigen NY-ESO-1 in melanoma patients.* Cancer Res, 2000. **60**(16): p. 4499-506.
189. Gnjatic, S., et al., *NY-ESO-1: review of an immunogenic tumor antigen.* Adv Cancer Res, 2006. **95**: p. 1-30.
190. Jäger, E., et al., *Monitoring CD8 T cell responses to NY-ESO-1: correlation of humoral and cellular immune responses.* Proc Natl Acad Sci U S A, 2000. **97**(9): p. 4760-5.
191. Gnjatic, S., et al., *Survey of naturally occurring CD4+ T cell responses against NY-ESO-1 in cancer patients: correlation with antibody responses.* Proc Natl Acad Sci U S A, 2003. **100**(15): p. 8862-7.
192. Robbins, P.F., et al., *Tumor regression in patients with metastatic synovial cell sarcoma and melanoma using genetically engineered lymphocytes reactive with NY-ESO-1.* J Clin Oncol, 2011. **29**(7): p. 917-24.
193. Robbins, P.F., et al., *A pilot trial using lymphocytes genetically engineered with an NY-ESO-1-reactive T-cell receptor: long-term follow-up and correlates with response.* Clin Cancer Res, 2015. **21**(5): p. 1019-27.
194. Rapoport, A.P., et al., *NY-ESO-1-specific TCR-engineered T cells mediate sustained antigen-specific antitumor effects in myeloma.* Nat Med, 2015. **21**(8): p. 914-921.
195. Yuan, J., et al., *CTLA-4 blockade enhances polyfunctional NY-ESO-1 specific T cell responses in metastatic melanoma patients with clinical benefit.* Proc Natl Acad Sci U S A, 2008. **105**(51): p. 20410-5.
196. Yuan, J., et al., *Integrated NY-ESO-1 antibody and CD8+ T-cell responses correlate with clinical benefit in advanced melanoma patients treated with ipilimumab.* Proc Natl Acad Sci U S A, 2011. **108**(40): p. 16723-8.

197. Tyagi, P. and B. Mirakhur, *MAGRIT: the largest-ever phase III lung cancer trial aims to establish a novel tumor-specific approach to therapy.* Clin Lung Cancer, 2009. **10**(5): p. 371-4.
198. Dreno, B., et al., *MAGE-A3 immunotherapeutic as adjuvant therapy for patients with resected, MAGE-A3-positive, stage III melanoma (DERMA): a double-blind, randomised, placebo-controlled, phase 3 trial.* Lancet Oncol, 2018. **19**(7): p. 916-929.
199. Vansteenkiste, J.F., et al., *Efficacy of the MAGE-A3 cancer immunotherapeutic as adjuvant therapy in patients with resected MAGE-A3-positive non-small-cell lung cancer (MAGRIT): a randomised, double-blind, placebo-controlled, phase 3 trial.* Lancet Oncol, 2016. **17**(6): p. 822-835.
200. Kruit, W.H., et al., *Selection of immunostimulant AS15 for active immunization with MAGE-A3 protein: results of a randomized phase II study of the European Organisation for Research and Treatment of Cancer Melanoma Group in Metastatic Melanoma.* J Clin Oncol, 2013. **31**(19): p. 2413-20.
201. Vansteenkiste, J., et al., *Adjuvant MAGE-A3 immunotherapy in resected non-small-cell lung cancer: phase II randomized study results.* J Clin Oncol, 2013. **31**(19): p. 2396-403.
202. Atanackovic, D., et al., *Vaccine-induced CD4+ T cell responses to MAGE-3 protein in lung cancer patients.* J Immunol, 2004. **172**(5): p. 3289-96.
203. Valmori, D., et al., *Vaccination with NY-ESO-1 protein and CpG in Montanide induces integrated antibody/Th1 responses and CD8 T cells through cross-priming.* Proc Natl Acad Sci U S A, 2007. **104**(21): p. 8947-52.
204. Bioley, G., et al., *Vaccination with recombinant NY-ESO-1 protein elicits immunodominant HLA-DR52b-restricted CD4+ T cell responses with a conserved T cell receptor repertoire.* Clin Cancer Res, 2009. **15**(13): p. 4467-74.
205. Sharma, P., et al., *Immune responses detected in urothelial carcinoma patients after vaccination with NY-ESO-1 protein plus BCG and GM-CSF.* J Immunother, 2008. **31**(9): p. 849-57.
206. Diefenbach, C.S., et al., *Safety and immunogenicity study of NY-ESO-1b peptide and montanide ISA-51 vaccination of patients with epithelial ovarian cancer in high-risk first remission.* Clin Cancer Res, 2008. **14**(9): p. 2740-8.
207. Jäger, E., et al., *Recombinant vaccinia/fowlpox NY-ESO-1 vaccines induce both humoral and cellular NY-ESO-1-specific immune responses in cancer patients.* Proc Natl Acad Sci U S A, 2006. **103**(39): p. 14453-8.
208. Odunsi, K., et al., *Efficacy of vaccination with recombinant vaccinia and fowlpox vectors expressing NY-ESO-1 antigen in ovarian cancer and melanoma patients.* Proc Natl Acad Sci U S A, 2012. **109**(15): p. 5797-802.
209. Dhodapkar, M.V., et al., *Induction of antigen-specific immunity with a vaccine targeting NY-ESO-1 to the dendritic cell receptor DEC-205.* Sci Transl Med, 2014. **6**(232): p. 232ra51.
210. Daud, A.I., *Negative but not futile: MAGE-A3 immunotherapeutic for melanoma.* Lancet Oncol, 2018. **19**(7): p. 852-853.

211. Festing, M.F. and D.G. Altman, *Guidelines for the design and statistical analysis of experiments using laboratory animals.* ILAR J, 2002. **43**(4): p. 244-58.
212. Dell, R.B., S. Holleran, and R. Ramakrishnan, *Sample size determination.* ILAR J, 2002. **43**(4): p. 207-13.
213. Brichard, V.G. and Q. Godechal, *MAGE-A3-specific anticancer immunotherapy in the clinical practice.* Oncoimmunology, 2013. **2**(10): p. e25995.
214. Holst, P.J., et al., *MHC class II-associated invariant chain linkage of antigen dramatically improves cell-mediated immunity induced by adenovirus vaccines.* J Immunol, 2008. **180**(5): p. 3339-46.
215. Mikkelsen, M., et al., *Enhanced and sustained CD8+ T cell responses with an adenoviral vector-based hepatitis C virus vaccine encoding NS3 linked to the MHC class II chaperone protein invariant chain.* J Immunol, 2011. **186**(4): p. 2355-64.
216. Sorensen, M.R., et al., *Vaccination with an adenoviral vector encoding the tumor antigen directly linked to invariant chain induces potent CD4(+) T-cell-independent CD8(+) T-cell-mediated tumor control.* Eur J Immunol, 2009. **39**(10): p. 2725-36.
217. Halbroth, B.R., et al., *Development of a Molecular Adjuvant to Enhance Antigen-Specific CD8.* Sci Rep, 2018. **8**(1): p. 15020.
218. Biswas, S., et al., *Transgene optimization, immunogenicity and in vitro efficacy of viral vectored vaccines expressing two alleles of Plasmodium falciparum AMA1.* PLoS One, 2011. **6**(6): p. e20977.
219. Luo, M., et al., *Immunization with plasmid DNA encoding influenza A virus nucleoprotein fused to a tissue plasminogen activator signal sequence elicits strong immune responses and protection against H5N1 challenge in mice.* J Virol Methods, 2008. **154**(1-2): p. 121-7.
220. Kou, Y., et al., *Tissue plasminogen activator (tPA) signal sequence enhances immunogenicity of MVA-based vaccine against tuberculosis.* Immunol Lett, 2017. **190**: p. 51-57.
221. Seder, R.A., P.A. Darrah, and M. Roederer, *T-cell quality in memory and protection: implications for vaccine design.* Nat Rev Immunol, 2008. **8**(4): p. 247-58.
222. Badovinac, V.P. and J.T. Harty, *Intracellular staining for TNF and IFN-gamma detects different frequencies of antigen-specific CD8(+) T cells.* J Immunol Methods, 2000. **238**(1-2): p. 107-17.
223. Boyd, A., et al., *Pathogen-Specific T Cell Polyfunctionality Is a Correlate of T Cell Efficacy and Immune Protection.* PLoS One, 2015. **10**(6): p. e0128714.
224. Zaritskaya, L., et al., *New flow cytometric assays for monitoring cell-mediated cytotoxicity.* Expert Rev Vaccines, 2010. **9**(6): p. 601-16.
225. Rubio, V., et al., *Ex vivo identification, isolation and analysis of tumor-cytolytic T cells.* Nat Med, 2003. **9**(11): p. 1377-82.
226. Betts, M.R., et al., *Sensitive and viable identification of antigen-specific CD8+ T cells by a flow cytometric assay for degranulation.* J Immunol Methods, 2003. **281**(1-2): p. 65-78.

227. Rühl, J., et al., *Heterologous prime-boost vaccination protects against EBV antigen-expressing lymphomas.* J Clin Invest, 2019. **129**(5): p. 2071-2087.
228. Bliss, C.M., et al., *Assessment of novel vaccination regimens using viral vectored liver stage malaria vaccines encoding ME-TRAP.* Sci Rep, 2018. **8**(1): p. 3390.
229. Wherry, E.J. and M. Kurachi, *Molecular and cellular insights into T cell exhaustion.* Nat Rev Immunol, 2015. **15**(8): p. 486-99.
230. Wherry, E.J., et al., *Viral persistence alters CD8 T-cell immunodominance and tissue distribution and results in distinct stages of functional impairment.* J Virol, 2003. **77**(8): p. 4911-27.
231. Herman, J., et al., *A peptide encoded by the human MAGE3 gene and presented by HLA-B44 induces cytolytic T lymphocytes that recognize tumor cells expressing MAGE3.* Immunogenetics, 1996. **43**(6): p. 377-83.
232. Jäger, E., et al., *Simultaneous humoral and cellular immune response against cancer-testis antigen NY-ESO-1: definition of human histocompatibility leukocyte antigen (HLA)-A2-binding peptide epitopes.* J Exp Med, 1998. **187**(2): p. 265-70.
233. van der Bruggen, P., et al., *A peptide encoded by human gene MAGE-3 and presented by HLA-A2 induces cytolytic T lymphocytes that recognize tumor cells expressing MAGE-3.* Eur J Immunol, 1994. **24**(12): p. 3038-43.
234. Benlalam, H., et al., *Identification of five new HLA-B*3501-restricted epitopes derived from common melanoma-associated antigens, spontaneously recognized by tumor-infiltrating lymphocytes.* J Immunol, 2003. **171**(11): p. 6283-9.
235. Kawashima, I., et al., *The multi-epitope approach for immunotherapy for cancer: identification of several CTL epitopes from various tumor-associated antigens expressed on solid epithelial tumors.* Hum Immunol, 1998. **59**(1): p. 1-14.
236. Dutoit, V., et al., *Multiepitope CD8(+) T cell response to a NY-ESO-1 peptide vaccine results in imprecise tumor targeting.* J Clin Invest, 2002. **110**(12): p. 1813-22.
237. Gérard, C., et al., *Tumor mouse model confirms MAGE-A3 cancer immunotherapeutic as an efficient inducer of long-lasting anti-tumoral responses.* PLoS One, 2014. **9**(5): p. e94883.
238. Lethé, B., et al., *Mouse tumor rejection antigens P815A and P815B: two epitopes carried by a single peptide.* Eur J Immunol, 1992. **22**(9): p. 2283-8.
239. Uyttenhove, C., et al., *The expression of mouse gene P1A in testis does not prevent safe induction of cytolytic T cells against a P1A-encoded tumor antigen.* Int J Cancer, 1997. **70**(3): p. 349-56.
240. Näslund, T.I., et al., *Comparative prime-boost vaccinations using Semliki Forest virus, adenovirus, and ALVAC vectors demonstrate differences in the generation of a protective central memory CTL response against the P815 tumor.* J Immunol, 2007. **178**(11): p. 6761-9.
241. Vandermeulen, G., et al., *Intramuscular electroporation of a P1A-encoding plasmid vaccine delays P815 mastocytoma growth.* Bioelectrochemistry, 2014. **100**: p. 112-8.

242. Lopes, A., et al., *Codon-Optimized P1A-Encoding DNA Vaccine: Toward a Therapeutic Vaccination against P815 Mastocytoma.* Mol Ther Nucleic Acids, 2017. **8**: p. 404-415.
243. Hodi, F.S., et al., *Improved survival with ipilimumab in patients with metastatic melanoma.* N Engl J Med, 2010. **363**(8): p. 711-23.
244. Van den Eynde, B., et al., *The gene coding for a major tumor rejection antigen of tumor P815 is identical to the normal gene of syngeneic DBA/2 mice.* J Exp Med, 1991. **173**(6): p. 1373-84.
245. Ball, P.E., et al., *Spontaneous, in vitro, malignant transformation of a basophil/mast cell line.* Differentiation, 1983. **24**(1): p. 74-8.
246. Conscience, J.F. and F. Fischer, *Growth-factor-independent proliferation in vitro and tumorigenicity in vivo are associated in basophil/mast-cell lines and their somatic hybrids.* Differentiation, 1985. **28**(3): p. 291-5.
247. Nair, A.P., et al., *A v-H-ras-dependent hemopoietic tumor model involving progression from a clonal stage of transformation competence to autocrine interleukin 3 production.* Mol Cell Biol, 1989. **9**(3): p. 1183-90.
248. Nair, A.P., H.H. Hirsch, and C. Moroni, *Mast cells sensitive to v-H-ras transformation are hyperinducible for interleukin 3 expression and have lost tumor-suppressor activity.* Oncogene, 1992. **7**(10): p. 1963-72.
249. Hirsch, H.H., A.P. Nair, and C. Moroni, *Suppressible and nonsuppressible autocrine mast cell tumors are distinguished by insertion of an endogenous retroviral element (IAP) into the interleukin 3 gene.* J Exp Med, 1993. **178**(2): p. 403-11.
250. Gajewski, T.F., et al., *Costimulation with B7-1, IL-6, and IL-12 is sufficient for primary generation of murine antitumor cytolytic T lymphocytes in vitro.* J Immunol, 1995. **154**(11): p. 5637-48.
251. Gajewski, T.F., M.A. Markiewicz, and C. Uyttenhove, *The p815 mastocytoma tumor model.* Curr Protoc Immunol, 2001. **Chapter 20**: p. Unit 20.4.
252. Buettner, F.F., et al., *C. elegans DPY-19 is a C-mannosyltransferase glycosylating thrombospondin repeats.* Mol Cell, 2013. **50**(2): p. 295-302.
253. Lau, J., et al., *Tumour and host cell PD-L1 is required to mediate suppression of anti-tumour immunity in mice.* Nat Commun, 2017. **8**: p. 14572.
254. Lavergne, E., et al., *Intratumoral CC chemokine ligand 5 overexpression delays tumor growth and increases tumor cell infiltration.* J Immunol, 2004. **173**(6): p. 3755-62.
255. Bennett, S.R., et al., *Help for cytotoxic-T-cell responses is mediated by CD40 signalling.* Nature, 1998. **393**(6684): p. 478-80.
256. Tay, N.Q., et al., *CD40L Expression Allows CD8(+) T Cells to Promote Their Own Expansion and Differentiation through Dendritic Cells.* Frontiers in immunology, 2017. **8**: p. 1484-1484.
257. Shugart, J.A., et al., *A self-help program for memory CD8+ T cells: positive feedback via CD40-CD40L signaling as a critical determinant of secondary expansion.* PLoS One, 2013. **8**(5): p. e64878.

258. Wong, K.L., et al., *CD40L-expressing CD8 T cells prime CD8alpha(+) DC for IL-12p70 production.* Eur J Immunol, 2008. **38**(8): p. 2251-62.
259. Markiewicz, M.A., et al., *Epitope spreading upon P815 tumor rejection triggered by vaccination with the single class I MHC-restricted peptide P1A.* Int Immunol, 2001. **13**(5): p. 625-32.
260. Bai, X.F., et al., *Different lineages of P1A-expressing cancer cells use divergent modes of immune evasion for T-cell adoptive therapy.* Cancer Res, 2006. **66**(16): p. 8241-9.
261. Restifo, N.P., et al., *Loss of functional beta 2-microglobulin in metastatic melanomas from five patients receiving immunotherapy.* J Natl Cancer Inst, 1996. **88**(2): p. 100-8.
262. Xue, W., et al., *SCIB1, a huIgG1 antibody DNA vaccination, combined with PD-1 blockade induced efficient therapy of poorly immunogenic tumors.* Oncotarget, 2016. **7**(50): p. 83088-83100.
263. Xue, W., et al., *SCIB2, an antibody DNA vaccine encoding NY-ESO-1 epitopes, induces potent antitumor immunity which is further enhanced by checkpoint blockade.* Oncoimmunology, 2016. **5**(6): p. e1169353.
264. D'Alise, A.M., et al., *Adenoviral vaccine targeting multiple neoantigens as strategy to eradicate large tumors combined with checkpoint blockade.* Nat Commun, 2019. **10**(1): p. 2688.
265. Lopes, A., et al., *Combination of immune checkpoint blockade with DNA cancer vaccine induces potent antitumor immunity against P815 mastocytoma.* Sci Rep, 2018. **8**(1): p. 15732.
266. Meiser, A., et al., *The chemokine receptor CXCR3 is degraded following internalization and is replenished at the cell surface by de novo synthesis of receptor.* J Immunol, 2008. **180**(10): p. 6713-24.
267. Rahir, G., et al., *Cyclophosphamide treatment induces rejection of established P815 mastocytoma by enhancing CD4 priming and intratumoral infiltration of P1E/H-2K(d) -specific CD8+ T cells.* Int J Cancer, 2014. **134**(12): p. 2841-52.
268. Odunsi, K., et al., *NY-ESO-1 and LAGE-1 cancer-testis antigens are potential targets for immunotherapy in epithelial ovarian cancer.* Cancer Res, 2003. **63**(18): p. 6076-83.
269. Akers, S.N., K. Odunsi, and A.R. Karpf, *Regulation of cancer germline antigen gene expression: implications for cancer immunotherapy.* Future Oncol, 2010. **6**(5): p. 717-32.
270. Sigalotti, L., et al., *Intratumor heterogeneity of cancer/testis antigens expression in human cutaneous melanoma is methylation-regulated and functionally reverted by 5-aza-2'-deoxycytidine.* Cancer Res, 2004. **64**(24): p. 9167-71.
271. Woloszynska-Read, A., et al., *Intertumor and intratumor NY-ESO-1 expression heterogeneity is associated with promoter-specific and global DNA methylation status in ovarian cancer.* Clin Cancer Res, 2008. **14**(11): p. 3283-90.

272. Schrump, D.S., et al., *Phase I study of decitabine-mediated gene expression in patients with cancers involving the lungs, esophagus, or pleura.* Clin Cancer Res, 2006. **12**(19): p. 5777-85.
273. Karpf, A.R., *A potential role for epigenetic modulatory drugs in the enhancement of cancer/germ-line antigen vaccine efficacy.* Epigenetics, 2006. **1**(3): p. 116-20.
274. Rutigliano, J.A., et al., *Identification of an H-2D(b)-restricted CD8+ cytotoxic T lymphocyte epitope in the matrix protein of respiratory syncytial virus.* Virology, 2005. **337**(2): p. 335-43.
275. Andreatta, M. and M. Nielsen, *Gapped sequence alignment using artificial neural networks: application to the MHC class I system.* Bioinformatics, 2016. **32**(4): p. 511-7.
276. Guo, Z.S., et al., *De novo induction of a cancer/testis antigen by 5-aza-2'-deoxycytidine augments adoptive immunotherapy in a murine tumor model.* Cancer Res, 2006. **66**(2): p. 1105-13.
277. Schmidt, M.E. and S.M. Varga, *Identification of Novel Respiratory Syncytial Virus CD4+ and CD8+ T Cell Epitopes in C57BL/6 Mice.* ImmunoHorizons, 2019. **3**(1): p. 1.
278. Hogquist, K.A., et al., *T cell receptor antagonist peptides induce positive selection.* Cell, 1994. **76**(1): p. 17-27.
279. Holst, J., et al., *Generation of T-cell receptor retrogenic mice.* Nat Protoc, 2006. **1**(1): p. 406-17.
280. Siebenkäs, C., et al., *Inhibiting DNA methylation activates cancer testis antigens and expression of the antigen processing and presentation machinery in colon and ovarian cancer cells.* PLoS One, 2017. **12**(6): p. e0179501.
281. Odunsi, K., et al., *Epigenetic potentiation of NY-ESO-1 vaccine therapy in human ovarian cancer.* Cancer Immunol Res, 2014. **2**(1): p. 37-49.
282. Chiappinelli, K.B., et al., *Inhibiting DNA Methylation Causes an Interferon Response in Cancer via dsRNA Including Endogenous Retroviruses.* Cell, 2015. **162**(5): p. 974-86.
283. Yu, G., et al., *Low-dose decitabine enhances the effect of PD-1 blockade in colorectal cancer with microsatellite stability by re-modulating the tumor microenvironment.* Cell Mol Immunol, 2019. **16**(4): p. 401-409.
284. Nie, J., et al., *Addition of Low-Dose Decitabine to Anti-PD-1 Antibody Camrelizumab in Relapsed/Refractory Classical Hodgkin Lymphoma.* J Clin Oncol, 2019. **37**(17): p. 1479-1489.
285. Wrangle, J., et al., *Alterations of immune response of Non-Small Cell Lung Cancer with Azacytidine.* Oncotarget, 2013. **4**(11): p. 2067-79.
286. Im, S.J., et al., *Defining CD8+ T cells that provide the proliferative burst after PD-1 therapy.* Nature, 2016. **537**(7620): p. 417-421.
287. Siddiqui, I., et al., *Intratumoral Tcf1+PD-1+CD8+ T Cells with Stem-like Properties Promote Tumor Control in Response to Vaccination and Checkpoint Blockade Immunotherapy.* Immunity, 2019. **50**(1): p. 195-211.e10.

288. Kurtulus, S., et al., *Checkpoint Blockade Immunotherapy Induces Dynamic Changes in PD-1^{-}CD8^{+} Tumor-Infiltrating T Cells.* Immunity, 2019. **50**(1): p. 181-194.e6.
289. Strauss, L., et al., *Targeted deletion of PD-1 in myeloid cells induces antitumor immunity.* Sci Immunol, 2020. **5**(43).
290. Gao, J., et al., *VISTA is an inhibitory immune checkpoint that is increased after ipilimumab therapy in patients with prostate cancer.* Nat Med, 2017. **23**(5): p. 551-555.
291. Kumar, V., et al., *The Nature of Myeloid-Derived Suppressor Cells in the Tumor Microenvironment.* Trends Immunol, 2016. **37**(3): p. 208-220.
292. Zhu, J., et al., *Resistance to cancer immunotherapy mediated by apoptosis of tumor-infiltrating lymphocytes.* Nat Commun, 2017. **8**(1): p. 1404.
293. Welters, M.J., et al., *Vaccination during myeloid cell depletion by cancer chemotherapy fosters robust T cell responses.* Sci Transl Med, 2016. **8**(334): p. 334ra52.
294. Verma, V., et al., *PD-1 blockade in subprimed CD8 cells induces dysfunctional PD-1.* Nat Immunol, 2019. **20**(9): p. 1231-1243.
295. Corbière, V., et al., *Antigen spreading contributes to MAGE vaccination-induced regression of melanoma metastases.* Cancer Res, 2011. **71**(4): p. 1253-62.
296. McGranahan, N., et al., *Clonal neoantigens elicit T cell immunoreactivity and sensitivity to immune checkpoint blockade.* Science, 2016. **351**(6280): p. 1463-9.
297. Wolinsky, J.B., Y.L. Colson, and M.W. Grinstaff, *Local drug delivery strategies for cancer treatment: gels, nanoparticles, polymeric films, rods, and wafers.* J Control Release, 2012. **159**(1): p. 14-26.
298. *Lung cancer: diagnosis and management (NG122)*. 2019, National Institute of Health and Care Excellence (NICE).
299. Gandhi, L., et al., *Pembrolizumab plus Chemotherapy in Metastatic Non-Small-Cell Lung Cancer.* N Engl J Med, 2018. **378**(22): p. 2078-2092.
300. Schiller, J.H., *A New Standard of Care for Advanced Lung Cancer.* N Engl J Med, 2018. **378**(22): p. 2135-2137.

Appendix

Table 8.1. Peptide sequences in P1A Pepset library used for T-cell stimulation assays

Peptide No.	Pool	Amino Acids	Sequence
1	1	1-15	MSDNKKPDKAHSGSG
2		5-19	KKPDKAHSGSGGDGD
3		9-23	KAHSGSGGDGDGNRC
4		13-27	GSGGDGDGNRCNLLH
5		17-31	DGDGNRCNLLHRYSL
6		21-35	NRCNLLHRYSLEEIL
7		25-39	LLHRYSLEEILPYLG
8		29-43	YSLEEILPYLGWLVF
9		33-47	EILPYLGWLVFAVVT
10		37-51	YLGWLVFAVVTTSFL
11		41-55	LVFAVVTTSFLALQM
12	2	45-59	VVTTSFLALQMFIDA
13		49-63	SFLALQMFIDALYEE
14		53-67	LQMFIDALYEEQYER
15		57-71	IDALYEEQYERDVAW
16		61-75	YEEQYERDVAWIARQ
17		65-79	YERDVAWIARQSKRM
18		69-83	VAWIARQSKRMSSVD
19		73-87	ARQSKRMSSVDEDED
20		77-91	KRMSSVDEDEDDEDD
21		81-95	SVDEDEDDEDDEDDY
22		85-99	DEDDEDDEDDYYDDE
23	3	89-103	EDDEDDYYDDEDDDD
24		93-107	DDYYDDEDDDDDAFY
25		97-111	DDEDDDDDAFYDDED
26		101-115	DDDDAFYDDEDDEEE
27		105-119	AFYDDEDDEEEELEN
28		109-123	DEDDEEEELENLMDD
29		113-127	EEEELENLMDDESED
30		117-131	LENLMDDESEDEAEE
31		121-135	MDDESEDEAEEEMSV
32		125-139	SEDEAEEEMSVEMGA
33		129-143	AEEEMSVEMGAGAEE
34	4	133-147	MSVEMGAGAEEMGAG
35		137-151	MGAGAEEMGAGANCA
36		141-155	AEEMGAGANCACVPG
37		145-159	GAGANCACVPGHHLR
38		149-163	NCACVPGHHLRKNEV
39		153-167	VPGHHLRKNEVKCRM
40		157-171	HLRKNEVKCRMIYFF

41		161-175	NEVKCRMIYFFHDPN
42		165-179	CRMIYFFHDPNFLVS
43		169-183	YFFHDPNFLVSIPVN
44		173-187	DPNFLVSIPVNPKEQ
45	5	177-191	LVSIPVNPKEQMECR
46		181-195	PVNPKEQMECRCENA
47		185-199	KEQMECRCENADEEV
48		189-203	ECRCENADEEVAMEE
49		193-207	ENADEEVAMEEEEEE
50		197-211	EEVAMEEEEEEEEEE
51		201-215	MEEEEEEEEEEEEEE
52		205-219	EEEEEEEEEEEMGNP
53		209-223	EEEEEEEMGNPDGFS
54		210-224	EEEEEEMGNPDGFSP

Table 8.2. Peptide sequences in MAGE-A3 Pepset library used for T-cell stimulation assays

Peptide No	Pool	Amino Acids	Sequence
1	1	1-15	MPLEQRSQHCKPEEG
2		5-19	QRSQHCKPEEGLEAR
3		9-23	HCKPEEGLEARGEAL
4		13-27	EEGLEARGEALGLVG
5		17-31	EARGEALGLVGAQAP
6		21-35	EALGLVGAQAPATEE
7		25-39	LVGAQAPATEEQEAA
8		29-43	QAPATEEQEAASSSS
9		33-47	TEEQEAASSSSTLVE
10		37-51	EAASSSSTLVEVTLG
11	2	41-55	SSSTLVEVTLGEVPA
12		45-59	LVEVTLGEVPAAESP
13		49-63	TLGEVPAAESPDPPQ
14		53-67	VPAAESPDPPQSPQG
15		57-71	ESPDPPQSPQGASSL
16		61-75	PPQSPQGASSLPTTM
17		65-79	PQGASSLPTTMNYPL

18		69-83	SSLPTTMNYPLWSQS
19		73-87	TTMNYPLWSQSYEDS
20		77-91	YPLWSQSYEDSSNQE
21	3	81-95	SQSYEDSSNQEEEGP
22		85-99	EDSSNQEEEGPSTFP
23		89-103	NQEEEGPSTFPDLES
24		93-107	EGPSTFPDLESEFQA
25		97-111	TFPDLESEFQAALSR
26		101-115	LESEFQAALSRKVAE
27		105-119	FQAALSRKVAELVHF
28		109-123	LSRKVAELVHFLLLK
29		113-127	VAELVHFLLLKYRAR
30		117-131	VHFLLLKYRAREPVT
31	4	121-135	LLKYRAREPVTKAEM
32		125-139	RAREPVTKAEMLGSV
33		129-143	PVTKAEMLGSVVGNW
34		133-147	AEMLGSVVGNWQYFF
35		137-151	GSVVGNWQYFFPVIF
36		141-155	GNWQYFFPVIFSKAS
37		145-159	YFFPVIFSKASSSLQ
38		149-163	VIFSKASSSLQLVFG
39		153-167	KASSSLQLVFGIELM
40		157-171	SLQLVFGIELMEVDP
41	5	161-175	VFGIELMEVDPIGHL
42		165-179	ELMEVDPIGHLYIFA
43		169-183	VDPIGHLYIFATCLG
44		173-187	GHLYIFATCLGLSYD
45		177-191	IFATCLGLSYDGLLG
46		181-195	CLGLSYDGLLGDNQI
47		185-199	SYDGLLGDNQIMPKA
48		189-203	LLGDNQIMPKAGLLI
49		193-207	NQIMPKAGLLIIVLA
50		197-211	PKAGLLIIVLAIIAR
51	6	201-215	LLIIVLAIIAREGDC

52		205-219	VLAIIAREGDCAPEE
53		209-223	IAREGDCAPEEKIWE
54		213-227	GDCAPEEKIWEELSV
55		217-231	PEEKIWEELSVLEVF
56		221-235	IWEELSVLEVFEGRE
57		225-239	LSVLEVFEGREDSIL
58		229-243	EVFEGREDSILGDPK
59		233-247	GREDSILGDPKKLLT
60		237-251	SILGDPKKLLTQHFV
61	7	241-255	DPKKLLTQHFVQENY
62		245-259	LLTQHFVQENYLEYR
63		249-263	HFVQENYLEYRQVPG
64		253-267	ENYLEYRQVPGSDPA
65		257-271	EYRQVPGSDPACYEF
66		261-275	VPGSDPACYEFLWGP
67		265-279	DPACYEFLWGPRALV
68		269-283	YEFLWGPRALVETSY
69		273-289	WGPRALVETSYVKVL
70		277-293	ALVETSYVKVLHHMV
71	8	281-297	TSYVKVLHHMVKISG
72		285-301	KVLHHMVKISGGPHI
73		289-305	HMVKISGGPHISYPP
74		293-309	ISGGPHISYPPLHEW
75		397-313	PHISYPPLHEWVLRE
76		400-414	SYPPLHEWVLREGEE

Table 8.3. Peptide sequences in NY-ESO-1 Pepset library used for T-cell stimulation assays

Peptide No	Pool	Amino Acids	Sequence
1	1	1-15	MQAEGRGTGGSTGDA
2		5-19	GRGTGGSTGDADGPG
3		9-23	GGSTGDADGPGGPGI
4		13-27	GDADGPGGPGIPDGP
5		17-31	GPGGPGIPDGPGGNA
6		21-35	PGIPDGPGGNAGGPG
7		25-39	DGPGGNAGGPGEAGA
8		29-43	GNAGGPGEAGATGGR
9		33-47	GPGEAGATGGRGPRG
10	2	37-51	AGATGGRGPRGAGAA
11		41-55	GGRGPRGAGAARASG
12		45-59	PRGAGAARASGPGGG
13		49-63	GAARASGPGGGAPRG
14		53-67	ASGPGGGAPRGPHGG
15		57-71	GGGAPRGPHGGAASG
16		61-75	PRGPHGGAASGLNGC
17		65-79	HGGAASGLNGCCRCG
18		69-83	ASGLNGCCRCGARGP
19	3	73-87	NGCCRCGARGPESRL
20		77-91	RCGARGPESRLLEFY
21		81-95	RGPESRLLEFYLAMP
22		85-99	SRLLEFYLAMPFATP
23		89-103	EFYLAMPFATPMEAE
24		93-107	AMPFATPMEAELARR
25		97-111	ATPMEAELARRSLAQ
26		101-115	EAELARRSLAQDAPP
27		105-119	ARRSLAQDAPPLPVP
28	4	109-123	LAQDAPPLPVPGVLL
29		113-127	APPLPVPGVLLKEFT
30		117-131	PVPGVLLKEFTVSGN

31		121-135	VLLKEFTVSGNILTI
32		125-139	EFTVSGNILTIRLTA
33		129-143	SGNILTIRLTAADHR
34		133-147	LTIRLTAADHRQLQL
35		137-151	LTAADHRQLQLSISS
36		141-155	DHRQLQLSISSCLQQ
37	5	145-159	LQLSISSCLQQLSLL
38		149-163	ISSCLQQLSLLMWIT
39		153-167	LQQLSLLMWITQCFL
40		157-171	SLLMWITQCFLPVFL
41		161-175	WITQCFLPVFLAQPP
42		165-179	CFLPVFLAQPPSGQR
43		169-183	FLPVFLAQPPSGQRR